

2021

## Study on Energy Accumulation and Dissipation Associated with Coal Burst

Xiaohan Yang  
*University of Wollongong*

Follow this and additional works at: <https://ro.uow.edu.au/theses1>

### University of Wollongong

#### Copyright Warning

You may print or download ONE copy of this document for the purpose of your own research or study. The University does not authorise you to copy, communicate or otherwise make available electronically to any other person any copyright material contained on this site.

You are reminded of the following: This work is copyright. Apart from any use permitted under the Copyright Act 1968, no part of this work may be reproduced by any process, nor may any other exclusive right be exercised, without the permission of the author. Copyright owners are entitled to take legal action against persons who infringe their copyright. A reproduction of material that is protected by copyright may be a copyright infringement. A court may impose penalties and award damages in relation to offences and infringements relating to copyright material.

Higher penalties may apply, and higher damages may be awarded, for offences and infringements involving the conversion of material into digital or electronic form.

Unless otherwise indicated, the views expressed in this thesis are those of the author and do not necessarily represent the views of the University of Wollongong.

### Recommended Citation

Yang, Xiaohan, Study on Energy Accumulation and Dissipation Associated with Coal Burst, Doctor of Philosophy thesis, School of Civil, Mining and Environmental Engineering, University of Wollongong, 2021. <https://ro.uow.edu.au/theses1/1037>

Research Online is the open access institutional repository for the University of Wollongong. For further information contact the UOW Library: [research-pubs@uow.edu.au](mailto:research-pubs@uow.edu.au)



UNIVERSITY  
OF WOLLONGONG  
AUSTRALIA

**Faculty of Engineering & Information Sciences  
School of Civil, Mining and Environmental Engineering**

**Study on Energy Accumulation and Dissipation  
Associated with Coal Burst**

**A thesis submitted in fulfilment of the requirement for the  
award of the degree of Doctor of Philosophy  
of University of Wollongong**

**By**

**Xiaohan Yang**

**May 2021**

## **THESIS DECLARATION**

I, Xiaohan Yang, declare that this thesis, submitted in fulfilment of the requirements for the award of Doctor of Philosophy, in the School of Civil, Mining and Environmental Engineering, University of Wollongong, is wholly my own work unless otherwise referenced or acknowledged. This thesis contains no material that has been submitted previously, in whole or in part, for the award of any other academic degree or diploma.

Xiaohan Yang

May 2021

## ACKNOWLEDGEMENTS

I would like to express my deepest gratitude to my supervisors, Associate Professor Ting Ren and Prof Alex Remennikov, for their invaluable guidance and critical advice as well as consistent support throughout the study. Besides my academic research, Associate Professor Ren's considerate care in life has allowed me to enjoy my stay in Australia.

I am very grateful for the scholarship from the China Scholarship Council and the University of Wollongong for providing me living allowance and tuition fees, respectively.

I also feel indebted to the following staff and organisations:

- ❖ Mr Lihai Tan for his constant support with experimental processes and data collection.
- ❖ Professor Xueqiu He from the University of Science and Technology Beijing for his suggestions on the structure of this thesis.
- ❖ Professor Linming Dou, of China University of Mining and Technology (CUMT), for his advice and in-depth knowledge on coal burst for my study at UOW.
- ❖ Technical staff in the School of CME, especially Mr. Duncan Best and Mr. Travis Marshall for their assistance with laboratory work.
- ❖ Honorary fellow Mr. Kevin Marston for his proof reading which improves the quality of this thesis.
- ❖ Australian Research Council Nanocomm Hub for grant to perform this study.

I would also like to extend my gratitude to all our mining group members, especially Prof Jianming Wu, Prof Naj Aziz, Dr Jan Nemcik, Dr Patrick Booth, Dr Libin Gong, Dr Anxiu Liu, Dr Jia Lin, Dr Hongchao Zhao, Ms Justine Calleja and Mr Ming Qiao for their friendly support and motivation during my study.

I am thankful to my family, especially to my parents for encouraging me. I also would like to acknowledge the support from my parents-in-law.

Lastly, and most importantly, to my lovely and beautiful wife, Mrs Ivy Xu, the best gift that I received in my life. This study would not have been completed without her care, love, and encouragement.

## PUBLICATIONS

1. XH Yang, T Ren, LH Tan, AM Remennikov & XQ He, Developing coal burst propensity index method for Australian coal mines. *International Journal of Mining Science and Technology*, 2018, 28(5), 783-790.
2. XH Yang, T Ren, AM Remennikov, XQ He & LH Tan, Analysis of energy accumulation and dissipation of coal bursts. *Energies*, 2018, 11(7), 1816-1827.
3. LH Tan, T Ren, XH Yang & XQ He, A numerical simulation study on mechanical behaviour of coal with bedding planes under coupled static and dynamic load. *International Journal of Mining Science and Technology*, 2018, 28(5), 791-797.
4. XH Yang, T Ren, XQ He & LH Tan. A review of energy sources of coal burst in Australian coal mines. *Coal Operators' Conference*, January 2019, Wollongong, Australia.
5. LH Tan, T Ren & XH Yang. The development of a novel backfilling technology: concept and behaviour, *Coal Operators' Conference*, January 2019, Wollongong, Australia.
6. XH Yang, T Ren, AM Remennikov, XQ He & LH Tan. Fractal characteristics of temporal-spatial distribution of acoustic emission during coal bursts, *38th International Conference on Ground Control in Mining*, July 2019, Morgantown, U.S.
7. L Zhang, XC Li, JX Gao, ZX An, XH Yang, & BS Nie, Creep characteristics and constitutive model of coal under triaxial stress and gas pressure. *Energy Science & Engineering*, 2020, 8(2), 501-514.
8. XH Yang, T Ren & LH Tan, Estimation of average ejection velocity generated by rib burst under compression load, *International Journal of Rock Mechanics and Mining Sciences*, 2020, 128, 104277.
9. XH Yang, T Ren & XQ He, Experimental study of coal burst risk prediction using fractal dimension analysis of AE spatial distribution, *Journal of Applied Geophysics*, 2020, 177, 104025.
10. XH Yang, T Ren & LH Tan, Size distribution measurement of coal fragments using digital imaging processing, *Measurement*, 2020, 10786.
11. LH Tan, T Ren, XH Yang & XQ He. Numerical study on the fracture characteristics and failure mode of hard coal under coupled static and dynamic loads, *VIII International Scientific Conference "Problems of Complex Development of Geo-resources"*, September 2020, Khabarovsk, Russia.

## **CONTRIBUTION OF OTHERS**

The research works presented in this thesis were primarily carried out by the PhD candidate, which mainly include but not limited to reviewing the literature, conducting experimental works, interpreting experimental results, developing analytical models, and writing manuscripts. All journal and conference papers were written by the PhD candidate with his supervisors. Contributions of others are described below.

Mr Lihai Tan (PhD candidate) contributed to carrying out the experimental work for the co-authored articles.

In addition, Professor Xueqiu He helped in reviewing and editing the co-authored articles.

## **ABSTRACT**

Coal burst, which refers to the brittle failure of coal, has been a serious hazard for underground coal mining, particularly at greater depth. Massive energy accumulated in coal could be dissipated almost instantaneously in the form of kinetic energy when the loading stress exceeding the ultimate strength of coal. This thesis qualitatively and quantitatively examines the energy accumulation and dissipation process associated with coal burst through a comprehensive research program of literature review, theoretical analysis and experimental studies.

The energy accumulation sources, dissipation forms and its influencing factors of coal burst are reviewed based on the energy conservation law and the static-dynamic loads superposition theory. The burst energy is provided by static loads including gravitational and abutment stress, and dynamic loads including fault slipping and roof weighting. Studies indicated that the main driving energy source of coal burst occurred in Australian coal mines resulted from elastic energy storage that has been accumulated during the loading process of coal.

A new coal burst propensity index methodology, which can reflect elastic energy storage and rapid release ability of coal, has been developed for the burst risk evaluation based on uniaxial compression experiments of 45 coal specimens sourced from Australian coal mines. Experimental results indicate that the burst propensity of coal seams can be classified as high when the elastic strain energy index (symbol?) is over 5 and the ultimate strength is greater than 15 MPa.

Additionally, to better understand the energy dissipation in the form of coal fragmentation, a digital image analysis methodology is developed to translate the image of the coal fragments into the size distribution curve of coal fragments. The size distribution of coal

fragments demonstrates that the shape of coal fragments can be simplified into ellipsoid with intermediate/minor axis ratio of 1. Furthermore, the ejection energy is quantitatively calculated based on the fragment size distribution and the energy dissipation analysis of the coal failure process. The calculation finds that the ejection energy only accounts for less than 1% of the stored elastic energy but can cause serious damage. The result indicates that, even without dynamic loads applied by a seismic event, the ejection velocity of coal fragments can easily reach up to 20 m/s, which has been observed in field conditions.

During the uniaxial loading process of coal specimens, an 8-channel acoustic emission (AE) monitoring system is adopted to record the frequency, amplitude and location of acoustic events. Fractal dimension decrease of spatial distribution of acoustic events was clearly observed for all tested specimens. High amplitude AE events are always observed before the failure point of coal specimens, which indicates high level energy dissipation rate in the form of fracture propagation before failure.

To advance the fundamental science of water infusion in coal, the effects of water saturation on mechanical properties and burst propensity of coal are investigated by conducting uniaxial compression tests of 4 groups of coal specimens that are subjected to water immersion for 5 days, 10 days, 15 days and as received respectively. The average moisture content of coal specimens is increased from 2.01 to 3.04 % after 15 days water infusion. Correspondingly, the compressive strength is reduced from 9 to 7 MPa, and elastic strain energy index from 3.42 to 1.14 after 15 days water saturation. The results indicate that the potential of elastic energy storage can be decreased with water infusion.

The superimposition of dynamic load can trigger the failure of coal more violently as a significant amount of energy has to be dissipated instantaneously. To study the energy

dissipation of coal under a dynamic load, 6 coal specimens are tested using drop hammer technique. The peak stress of coal subjected to a dynamic impact load is above 40 MPa, which is almost twice that of coal specimens in a static load. The ejection energy accounts for more than 99 % of the impact energy input while fragmentation energy only accounts for less than 1 %, which means the failure of coal is more violent under impact load.

The study of accumulation and dissipation associated with coal burst advances the understanding of coal burst process and its influencing factors from a view of energy transfer. Most of the tests are conducted under static uniaxial compression load but the significant effect of dynamic load on energy accumulation and dissipation process has been highlighted. The energy accumulation and dissipation of coal under complex and superposition loads can be further studied with the application of a Split Hopkinson Pressure Bar (SHPB) test system combined with distinct-element modelling (DEM) to better explain the mechanism of coal burst in complex geo-stress conditions.

## TABLE OF CONTENTS

<b>THESIS DECLARATION .....</b>	<b>i</b>
<b>ACKNOWLEDGEMENTS.....</b>	<b>ii</b>
<b>PUBLICATIONS .....</b>	<b>iv</b>
<b>CONTRIBUTION OF OTHERS.....</b>	<b>v</b>
<b>ABSTRACT .....</b>	<b>vi</b>
<b>TABLE OF CONTENTS.....</b>	<b>ix</b>
<b>LIST OF FIGURES .....</b>	<b>xiv</b>
<b>LIST OF TABLES .....</b>	<b>xvii</b>
<b>LIST OF SYMBOLS AND ABBREVIATIONS .....</b>	<b>xviii</b>
<b>CHAPTER 1 GENERAL INTRODUCTION .....</b>	<b>1</b>
1.1 Background .....	1
1.2 Problem Statement .....	3
1.3 Research Objectives .....	5
1.4 Research Framework.....	6
1.5 Thesis Outline.....	7
<b>CHAPTER 2 LITERATURE REVIEW .....</b>	<b>10</b>
2.1 Coal Burst in Overseas and Australian Coal Mines .....	10
2.1.1 Coal Burst in Europe.....	10
2.1.2 Coal Burst in the U.S. ....	11
2.1.3 Coal Burst in China.....	12
2.1.4 Coal Burst in Australia.....	14
2.2 Coal Burst Characteristics, Mechanisms, and Classification .....	15
2.2.1 Coal Burst Characteristics.....	15
2.2.2 Coal Burst Mechanism.....	16
2.2.3 Coal Burst Classification .....	20
2.3 Coal Burst Risk Evaluation and Early-warning .....	21
2.3.1 Coal Burst Risk Evaluation.....	21
2.3.2 Coal Burst Risk Early-warning.....	25
2.4 Coal Burst Mitigation.....	27
<b>CHAPTER 3 ANALYSIS OF ENERGY ACCUMULATION AND DISSIPATION OF COAL BURST .....</b>	<b>30</b>
Summary .....	30
Citation .....	30

Abstract .....	31
Keywords.....	31
3.1 Introduction .....	32
3.2 Energy Forms and the Energy Conservation Equation .....	34
3.3 Energy Accumulation.....	37
3.3.1 Mining Depth.....	37
3.3.2 Stiffness.....	38
3.3.3 Seismicity.....	40
3.3.4 Elasticity .....	41
3. 4 Energy Dissipation .....	42
3.4.1 Bulking.....	42
3.4.2 Acoustic Events .....	43
3.5 Energy Sources of Coal Burst in Australia.....	44
3.5.1 Static Load .....	44
3.5.2 Dynamic Load.....	47
3.6 Conclusions .....	48
<b>CHAPTER 4 DEVELOPING COAL BURST PROPENSITY INDEX METHOD FOR AUSTRALIAN COAL MINES .....</b>	<b>50</b>
Summary .....	50
Citation .....	50
Abstract .....	51
Keywords.....	51
4.1 Introduction .....	52
4.2 Relevant Indices .....	53
4.2.1 Elastic Strain Energy Index.....	54
4.2.2 Bursting Energy Index .....	54
4.2.3 Dynamic Failure Time .....	55
4.2.4 Uniaxial Compression Strength .....	56
4.3 Process of Laboratory Test.....	57
4.3.1 Specimen Preparation .....	57
4.3.2 Test Equipment and Procedure .....	58
4.4 Data Processing and Risk Classification .....	59
4.4.1 Data Processing.....	59
4.4.2 Risk Classification of Coal/Rock Burst Propensity .....	71
4.5 Improvement of $W_{ET}$ Test.....	74

4.5.1 Volumetric Strain Indicator for Failure Prediction .....	74
4.5.2 Theoretical calculation of $W_{ET}$ .....	77
4.6 Conclusions .....	78
<b>CHAPTER 5 SIZE DISTRIBUTION MEASUREMENT OF COAL FRAGMENTS USING DIGITAL IMAGING PROCESSING.....</b>	<b>80</b>
Summary .....	80
Citation .....	80
Abstract .....	81
Keywords.....	81
5.1 Introduction .....	82
5.2 Image Acquisition and Image Analysis.....	84
5.2.1 Image acquisition .....	84
5.2.2 Image Analysis.....	85
5.2.3 Morphological Models.....	88
5.3 Results and Discussions .....	90
5.4 Conclusions .....	93
<b>CHAPTER 6 ESTIMATION OF AVERAGE EJECTION VELOCITY GENERATED BY RIB BURST UNDER COMPRESSIVE LOAD .....</b>	<b>95</b>
Summary .....	95
Citation .....	95
Abstract .....	96
Keywords.....	96
6.1 Introduction .....	97
6.2 Theoretical Analysis of Coal Ejection.....	98
6.3 Fragment Energy Calculation.....	100
6.3.1 Energy-size Relationship .....	101
6.3.2 Fragment Size Distribution .....	102
6.3.3 Fragment Energy Calculation .....	103
6.4 Ejection Velocity and Impact Load.....	104
6.4 Coal Ejection Test .....	106
6.5 Experimental Results.....	108
6.6 Case Study.....	110
6.7 Conclusions .....	113

**CHAPTER 7 EXPERIMENTAL STUDY OF COAL BURST RISK PREDICTION USING FRACTAL DIMENSION ANALYSIS OF AE SPATIAL DISTRIBUTION**

**115**

Summary .....	115
Citation .....	115
Abstract .....	116
Keywords.....	116
7.1 Introduction .....	117
7.2 Theoretical Background of Fractal and AE.....	119
7.2.1 Fractal Dimension.....	119
7.2.2 Acoustic Emission .....	122
7.3 Dimension Calculation Based on MATLAB Coding.....	123
7.4 Fractal Behavior of Coal Specimens under Uniaxial Compression Load.....	125
7.4.1 Experimental Setup.....	125
7.4.2 Results and Discussions.....	128
7.5 Conclusions .....	131

**CHAPTER 8 EFFECTS OF WATER SATURATION TIME ON ENERGY DISSIPATION AND BURST PROPENSITY OF COAL SPECIMENS .....**

**133**

Summary .....	133
Abstract .....	134
Keywords.....	134
8.1 Introduction .....	135
8.2 Material and Methodology .....	137
8.2.1 Specimen Preparation .....	137
8.2.2 Test Apparatus and Procedure .....	138
8.2.3 AE Monitoring.....	139
8.2.4 Fragment Analysis .....	140
8.2.5 Burst Propensity.....	141
8.3 Results and Discussions .....	142
8.3.1 Stress-strain Curves .....	142
8.3.2 AE Features.....	143
8.3.3 Fragmentation Characteristics.....	145
8.3.4 Burst Propensity.....	147
8.3.5 Surface Roughness.....	148
8.4 Conclusions .....	158

<b>CHAPTER 9 FRAGMENTATION CHARACTERISTIC AND ENERGY DISSIPATION OF COAL UNDER IMPACT LOAD.....</b>	<b>160</b>
Summary .....	160
Citation .....	160
Abstract .....	161
Keywords.....	161
9.1 Introduction .....	162
9.2 Material and Methods.....	164
9.2.1 Experimental Setup.....	164
9.2.2 Fragment Size Distribution .....	165
9.2.3 Energy Dissipation.....	166
9.3 Results and Discussions .....	168
9.4 Conclusions .....	173
<b>CHAPTER 10 CONCLUSIONS AND RECOMMENDATIONS .....</b>	<b>175</b>
10.1 Energy Accumulation and Dissipation of Coal Burst .....	175
10.2 Evaluation and Prediction of Coal Burst.....	176
10.3 Fragmentation Characteristic and Energy Dissipation of Specimens Failure ...	177
10.4 Influence of Water Saturation and Impact Load .....	179
10.5 Recommendations for Future Studies .....	180
<b>APPENDIX A IMAGE PROCESSING CODE.....</b>	<b>183</b>
<b>APPENDIX B AE DIMENSION ANALYSIS CODE .....</b>	<b>186</b>
<b>REFERENCE .....</b>	<b>188</b>

## LIST OF FIGURES

Figure 1. 1 Documented coal burst accidents in Australia .....	2
Figure 1. 2 Research framework and timeline .....	6
Figure 2. 1 Coal burst propensity index classification.....	21
Figure 3. 1 Schematic diagram of the elastic and plastic energies of coal subjected to uniaxial compression load.....	34
Figure 3. 2 Acoustic emission signal of the tensile failure in coal .....	37
Figure 3. 3 Effect of stiffness of the loading system on the behaviour of coal failure ...	40
Figure 3. 4 Influence of a dynamic load caused by seismicity on a coal burst .....	41
Figure 3. 5 Strain–Stress curves of coal specimens subjected to cyclic loading.....	42
Figure 3. 6 Schematic diagram of coal bulking caused by a concentration of stress ....	43
Figure 3. 7 Stress concentration caused by geological structures.....	45
Figure 3. 8 Generalized stratigraphic column for the geological Sydney Basin .....	47
Figure 4. 1 Schematic diagram of coal burst propensity index.....	54
Figure 4. 2 Correlation between $W$ and $R_C$ .....	57
Figure 4. 3 Universal rock testing system .....	59
Figure 4. 4 Schematic diagram of loading system .....	59
Figure 4. 5 Typical stress-strain curves .....	60
Figure 4. 6 Stress-strain curve of specimen No1 .....	60
Figure 4. 7 Differentia of stress-strain curve of specimen No1 .....	61
Figure 4. 8 $W_{ET}$ test result of Group 1 .....	62
Figure 4. 9 UCS test result of Group 1.....	64
Figure 4. 10 $W_{ET}$ test result of of Group 2.....	66
Figure 4. 11 UCS test result of of Group 2 .....	67
Figure 4. 12 $W_{ET}$ test result of Group 3 .....	69
Figure 4. 13 UCS test result of Group 3.....	70
Figure 4. 14 Failed coal specimens.....	72
Figure 4. 15 Correlation analyses between indices .....	73
Figure 4. 16 Different stages of the deformation process of coal during a uniaxial compression test.....	75
Figure 4. 17 Volumetric strain of uniaxial compression test .....	76
Figure 4. 18 Loading and fitting curve of uniaxial loading test .....	78
Figure 5. 1 Manual sieving with different mesh size .....	84
Figure 5. 2 Schematic diagram of image acquisition setup .....	85
Figure 5. 3 Flow chart of image analysis process.....	86
Figure 5. 4 Image pre-processing.....	87
Figure 5. 5 Size measurement of a fragment.....	87
Figure 5. 6 Size distribution curve of different morphological models .....	90
Figure 5. 7 Original and processed image of specimen A1 .....	91
Figure 5. 8 Original and processed image of specimen A2 .....	91
Figure 5. 9 Original and processed image of specimen A3 .....	91
Figure 5. 10 Original and processed image of specimen A4 .....	92
Figure 5. 11 RMS of image processing and fractal model.....	93

Figure 5. 11 Cumulative size distribution of specimens .....	93
Figure 6. 1 Energy accumulation of rib burst and coal ejection test .....	99
Figure 6. 2 Determination of Lamé's constant through drop coal test .....	105
Figure 6. 3 Coal ejection test with application of uniaxial compression loading system .....	106
Figure 6. 4 Indirect measurement of average ejection velocity .....	107
Figure 6. 5 Stress versus strain curve of coal specimens .....	108
Figure 6. 6 Different size of coal fragments after coal ejection test .....	109
Figure 6. 7 Sketch of cross-sectional diagram of roadways in Greta Seam .....	110
Figure 6. 8 Sketch of cross-sectional diagram of roadways in Xingan Coal Mine.....	111
Figure 6. 9 Fragment energy with different maximum block size .....	112
Figure 7. 1 Fractal measurement method for a distribution of AE event locations .....	122
Figure 7. 2 Process of fractal dimension calculation .....	123
Figure 7. 3 Flow chart for a typical $Nr(R < r)$ calculation .....	125
Figure 7. 4 Uniaxial compression loading test apparatus and AE setup.....	127
Figure 7. 5 Coal specimen and all AE sensors .....	128
Figure 7. 6 Stress vs strain curves of coal specimens subject to uniaxial compression loading.....	128
Figure 7. 7 Two-dimensional location of all AE events of coal specimens .....	129
Figure 7. 8 Stress vs time curves of coal specimens subject to uniaxial compression loading.....	129
Figure 7. 9 Fractal dimension of AE spatial distribution of coal specimens .....	130
Figure 8. 1 Apparatus set-up.....	138
Figure 8. 2 Water saturation of coal specimens .....	139
Figure 8. 3 AE monitoring system .....	140
Figure 8. 4 Fragment size distribution analysis process .....	141
Figure 8. 5 Stress-strain curves of Group D .....	143
Figure 8. 6 AE counts and stress of specimens .....	144
Figure 8. 8 Fractal size distribution of coal specimens .....	146
Figure 8. 7 FSD of specimens .....	146
Figure 8. 9 Burst propensity of coal specimens .....	147
Figure 8. 10 Laser scanning of specimen 1 with 5 days water saturation .....	150
Figure 8. 11 Laser scanning of specimen 2 with 5 days water saturation .....	151
Figure 8. 12 Laser scanning of specimen 1 with 10 days water saturation .....	153
Figure 8. 13 Laser scanning of specimen 2 with 10 days water saturation .....	154
Figure 8. 14 Laser scanning of specimen 1 with 15 days water saturation .....	156
Figure 8. 15 Laser scanning of specimen 2 with 15 days water saturation .....	157
Figure 8. 16 Surface roughness of scanned coal specimens.....	158
Figure 9. 1 Coal specimen preparation .....	164
Figure 9. 2 Drop test system .....	165
Figure 9. 3 Image processing technique .....	166
Figure 9. 4 Energy dissipation of coal specimens under impact and static load .....	168
Figure 9. 5 Impact load of coal specimens.....	169

Figure 9. 6 Average peak stress of coal specimens under quasi-static and impact loads .....	170
Figure 9. 7 FSD of specimen A1.....	171
Figure 9. 8 Comparison of cumulative FSD of coal specimens subject to impact and quasi-static load .....	172
Figure 9. 14 Burst and fragmentation energy of coal specimens under impact load ..	173

## LIST OF TABLES

Table 1. 1 Coal burst occurrence and fatalities by country / region.....	1
Table 2. 1 Geological factors of comprehensive evaluation method .....	23
Table 2. 2 Technical factors of comprehensive evaluation method.....	23
Table 2. 3 Burst risk evaluation form of comprehensive evaluation method .....	24
Table 4. 1 Failure time test results of coal specimens from China and Poland .....	56
Table 4. 2 Test result of Group 1.....	71
Table 4. 3 Test result of Group 2.....	71
Table 4. 4 Test result of Group 3.....	71
Table 4. 5 Coal burst propensity classification proposed by Qi et al .....	71
Table 4. 6 Coal burst propensity classification adopted by Zhang et al .....	71
Table 4. 7 Rock burst propensity classification adopted by Cai.....	72
Table 4. 8 Preliminary risk classification method for Australian coal seam .....	73
Table 4. 9 Determination of coal burst propensity.....	74
Table 5. 1 Morphological models of coal particle.....	89
Table 5. 2 RMSE of different morphological models .....	90
Table 6. 1 Estimated and measured average ejection velocity .....	110
Table 6. 2 Value of main parameters for fragmentation energy estimation.....	112
Table 6. 3 Estimation of ejection velocity and impact load of case study.....	113
Table 8. 1 Coal burst propensity index and risk classification of Australian coal .....	142
Table 8. 2 Surface roughness point and value .....	148

## LIST OF SYMBOLS AND ABBREVIATIONS

### *Symbols*

$a$	Major axis	mm
$A$	Matrix	
$b$	Intermediate axis	mm
$B$	Matrix	
$c$	Minor axis	mm
$C$	Matrix	
$C(r)$	Correlation integrals	
$d$	Diameter	mm
$d_{max}$	Maximum size of coal fragments	mm
$D$	Equivalent size	mm
$D_{max}$	Damage factor at failure point	
$DT$	Duration of dynamic fracture	s
$E$	Young's modulus	MPa
$E_0$	Unloading elasticity modulus	MPa
$E_a$	Energy consumed after the peak	J
$E_{acoustic}$	Acoustic emission energy	J
$E_b$	Energy storage before the peak	J
$E_{burst}$	Kinetic energy carried by burst coal	J
$E_{concentrated}$	Energy caused by concentrated stress	J
$E_{coal}$	Energy from the roof to the coal	J
$E_{dynamic}$	Energy caused by dynamic events	J
$E_{ejection}$	Ejection energy	J
$E_{elastic}$	Elastic energy	J
$E_{em}$	Electromagnetic-emission energy	J
$E_{fracture}$	Energy consumed by fracture propagation	J
$E_{geophysical}$	Geophysical energy	J
$E_{gravity}$	Energy caused by gravitational stress	J
$E_{impact}$	Energy input resulting from impact load	J
$E_{other}$	Other form energy	J
$E_{plastic}$	Plastic energy	J
$E_{residual}$	Residual energy	J
$E_{roof}$	Energy from roof to coal	J
$E_{seismic}$	Micro seismic energy	J
$E_{tectonic}$	Energy caused by tectonic stress	J
$E_{thermal}$	Thermal-radiation energy	J
$F$	Compression load	N
$F_{coal}$	Reaction force given by coal	N

$F(d)$	FSD function	
$F_{\text{roof}}$	Force applied by roof on coal	N
$F_U$	Unloading force	N
$g$	Gravitational acceleration	m/s <sup>-2</sup>
$G$	Gravitational weight	kN
$h$	Height	m
$H$	Dropping Height	m
$i$	Material constant	
$j$	Material constant	
$k$	$\sigma_{cd}/\sigma_{ucs}$ ratio	
$K$	Stiffness of the material	N/m
$K_{\text{coal}}$	Stiffness of the coal	N/m
$K_E$	Bursting energy index	
$K_{\text{roof}}$	Stiffness of the roof	N/m
$K_R$	Ritingers's constant	J/m <sup>2</sup>
$L$	Displacement	m
$L_{\text{coal}}$	Displacement caused by $F_{\text{roof}}$	m
$L_{\text{roof}}$	Displacement caused by $F_{\text{coal}}$	m
$m$	Weight	gram
$M$	Mass	gram
$n$	Fractal dimension	
$N$	AE events number	
$P_{\text{max}}$	Impact Load	kN
$r$	Radius	m
$R$	Distance between any two AE events	m
$R_C$	Uniaxial compression strength	MPa
$p_i$	Selected AE events	
$p_j$	Selected AE events	
$s$	Shape factor	
$S$	Surface area	m <sup>2</sup>
$T_1$	Time corresponding to failure	s
$T_2$	Time corresponding to complete damage	s
$v$	Velocity	m/s
$V$	Volume	m <sup>3</sup>
$W$	Energy input	J
$W_{ET}$	Elastic strain energy index	
<b>Greek letters</b>		
$\rho$	density	kg/m <sup>3</sup>
$\varphi$	Energy efficiency	
$\sigma$	Stress	MPa

$\sigma_{cd}$	Crack damage stress	MPa
$\sigma_{ucs}$	Uniaxial compression stress	MPa
$\sigma_v$	Volumetric strain reversal stress	MPa
$\sigma_{WET}$	Estimated failure stress value	MPa
$\varepsilon_1$	Axial strain	
$\varepsilon_2$	Radial strain	
$\varepsilon_v$	Volumetric strain	
$\varepsilon_e$	Elastic axial strain	
$\varepsilon_{max}$	Total axial strain	
$\varepsilon_p$	plastic axial strain	
$\lambda$	Lame's constant	

### ***Abbreviations***

AE	Acoustic Emission
FSD	Fragment Size Distribution
NFV	North Fork Valley
NSW	New South Wales
RMS	Root Mean Square
RMSE	Root Mean Square Error
SEM	Scanning Electron Microscope
SHPB	Split Hopkinson Pressure Bar
UCS	Uniaxial Compression Strength

# CHAPTER 1 GENERAL INTRODUCTION

## 1.1 Background

Coal burst, which refers to the violent and catastrophic failure of coal, is a serious safety hazard for underground coalmines, and it has attracted intensive research interest from mining and geological scholars (Zhang, Canbulat et al. 2017). In 1738, the first recorded coal burst took place in England (Pan 1999, Wang, Pan et al. 2000). Since then, both the frequency and severity of coal burst have increased with mining depth (Zhou and Xian 1998, Pan 1999, Braeuner 2017). As shown in Table 1.1, coal burst has been a serious security issue that many countries have faced for decades (Calleja and Nemcik 2016). Poland commenced the research of coal burst along with Czechs in 1912 and were the first to propose a coal burst propensity measurement method for coal burst risk evaluation (Shen and Luo 2016). Coal burst caused 401 fatalities from 1949 to 1982 in Poland (Dou and He 2001). Coal burst has had a long history in the U.S. as well. From 1936 to 1993, 172 coal burst accidents caused 83 fatalities and 163 injuries in the U.S. (Christopher 2017). In China, research into coal burst was initially carried out in the early 1960's and more than 147 coal mines experienced coal burst at the end of 2014 (Shen and Luo 2016). After decades of research and the engineering practice of controlling coal burst, these main coal mining counties had a good understanding of coal burst phenomenon and made great advances in forecasting methods and mitigation techniques of coal burst.

**Table 1. 1 Coal burst occurrence and fatalities by country / region**

Country/Region	Time Period	Number of Coal Bursts	Number of Fatalities
Czech Republic/Poland	1983-2003	190	122
Ruhr, Germany	1973-1992	50	27
USA	1943-2003	———	78
USA	1983-2013	337	20
Mainland China	1933-1996	4000	400
Mainland China	2006-2013	>35	>300

As shown in Figure 1.1, coal burst is a new challenge for Australian mining researchers and engineers as the first coal burst accident occurred in 2014. However, considering the increasing coal burst risk with mining depth and intensity going forward, the controlling and mitigation measures of coal burst in Australia need more research. Coal burst has been recognized as a serious safety risk for Australian underground coal mines following a fatal coal burst accident at a NSW underground coal mine in 2014 (Calleja and Nemcik 2016, Hebblewhite and Galvin 2017). Due to the lack of coal burst experience, it is difficult to find mature theories and technologies in Australian to explain, predict, monitor, or control coal burst. There is an need to develop a coal burst risk assessment methodology and prevention technology for Australian coal mines.

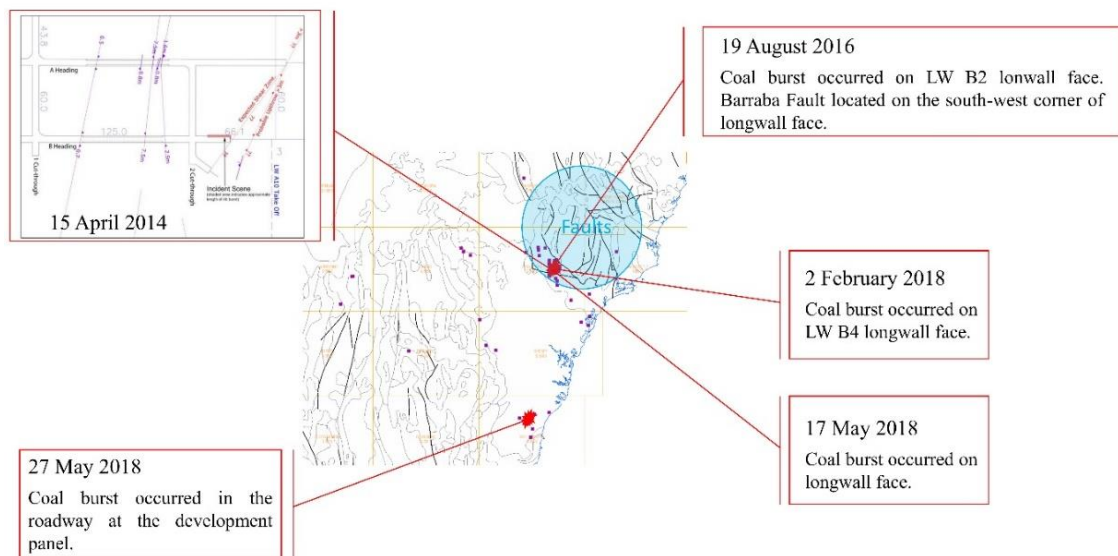


**Figure 1. 1 Documented coal burst accidents in Australia (Ahn, Zhang et al. 2017)**

Extensive study has been conducted to understand the mechanism, prediction and prevention of coal burst (Zhou and Xian 1998) by scholars around the world. Some necessary conditions for coal burst, including stiffness, dynamic load and mechanical properties, have been identified in the past decades of research and engineering practice. In terms of energy, the coal burst process is the energy accumulation and release process of a coal body. Coal burst early-warning method, such as acoustic emission,

electromagnetic radiation, microseismic, infrared and other methods, is the monitoring of different energy forms released during coal burst (Obert and Duvall 1942, Zakupin, Bogomolov et al. 2012). The cause of coal ejection and roadway destruction is the elastic energy stored in the coal (Tan, Sun et al. 1991). Therefore, it is significant to understand the energy accumulation and the dissipation mode in the coal burst process, especially the magnitude of the ejection energy.

## **1.2 Problem Statement**

Coal burst is a particular type of coal failure, which is more violent than other failure modes such as yielding, and is often accompanied by loud noise, coal ejection and seismic events. Coal burst causes damage to the underground structures and threatens the health and safety of the mining workers. Scholars have determined different kinds of classification methods for coal burst according to different standards (He, Xia et al. 2012, Jiang, Pan et al. 2014). From the point of view of material instability, Pan divided coal burst into three types: compression, tensile and shear (Pan 1999). According to Pan's classification method, roof failure and fault slip are tensile and shear types, respectively. Rib burst, pillar bump and floor heave are compression types. Rib burst of roadways accounted for a large number of total coal burst accidents that occurred in underground coalmines. In Colorado in the U.S., nearly half of the coal bursts occurred during roadway development or in the roadways (Christopher 2016). Statistical data shows that 87% of coal burst accidents in China occurred in roadways (Dou, Mu et al. 2014). Coal burst in this thesis refers to the compressive type burst only such as those associated with the rib failure of gateroads.

During the burst process, the blocks of ejected coal from the rib can carry a large amount of kinetic energy because they have mass and velocity (McGarr 1997). The study

conducted by Bieniawski et al. (Bieniawski, Denkhaus et al. 1969) found that the kinetic energy released by coal burst is from the stored elastic energy of coal before its peak stress. Kidybiński found that coal's ability to store and rapidly release elastic strain energy seems to be a fundamental condition of coal burst (Kidybiński 1981). Based on the analysis of the stress-strain curve of coal specimens under uniaxial compression stress, several specific indices that are relevant to elastic energy have been proposed by different researchers to evaluate coal burst propensity. It was proved by Russian, Polish, and Chinese experiences that these indices are good indicators that define the burst risk of coal seams. How these indices can be adopted to evaluate coal burst risk in Australia is of interest to Australian underground mining research.

Many researchers have reported using laboratory observations of particle ejection under triaxial or uniaxial compression load to understand the fragmentation behaviour in the post-failure process of coal specimens and to assess the coal burst properties of coal in fields (He, Jia et al. 2012, Qiu, Feng et al. 2014, Jiang, Su et al. 2015). Because the ejection process is very transient, the coal particles are highly pulverized and the ejection velocity of particles is high during the post-failure of coal, the ejection and travel of all particles is difficult to observe and film by laboratory observations. Hence, the accurate measurement or estimation of ejection velocity will be important for understanding the potential risk and damage of coal burst. The coal burst or brittle failure of coal can be divided into two main steps: the fragmentation from intact coal to blocks/particles and ejection from the coal body to free space. Hence, the kinetic energy can be indirectly calculated based on the difference between elastic energy storage and fragmentation energy as other energy forms are negligible. Hence, the fragmentation energy calculation model based on the energy-size relationship and fragment size distribution (FSD) need to be discussed (Tu, Cheng et al. 2019).

Water infusion has long been taken as an effective way to eliminate coal burst risk as water infusion can loosen and soften coal properties. This method has been applied in the Ruhr Coalfield (Germany) since the 1960's and achieved great success in coal burst mitigation. Water infusion is recommended as a coal burst mitigation method in the coal burst prevention rules published by the Chinese mining authority in 2018 (National Coal Mine Safety Administration 2018). Besides coal outburst, water infusion has been successfully used in preventing gas outburst as well (Aguado and Nicieza 2007). However, not all industrial trials of water infusion for coal burst prevention have been necessarily effective in all situations as the effectiveness of this method can be affected by the water infusion time, coal properties and other parameters of water injection. Hence, some fundamental work including the effects of water infusion time on burst propensity and energy evolution need to be further discussed.

Previous research has shown that coal tends to have more violent and instantaneous failure under impact or dynamic loads as the strength of coal is positively related to loading rate (Okubo, Fukui et al. 2006, Zhao, Wang et al. 2014). For the coal ejection caused by super-critical quasi-static load, ejection energy is transformed from elastic energy stored in the coal body during loading process. For coal failure caused by impact load, the energy source is from energy input caused by the high velocity impact, which will affect the energy dissipation behaviour of coal. The study of the failure behaviour and energy dissipation of coal subject to impact load will contribute to the understanding of coal burst caused by complex load types.

### **1.3 Research Objectives**

The main objectives of this thesis include:

- ❖ To understand the energy conservation laws, energy accumulation sources and dissipation forms during coal burst in underground coal mines.
- ❖ The development of a coal burst risk evaluation methodology based on the qualitative study of elastic energy storage and releasing properties of coal.
- ❖ The provision of an ejection energy and velocity estimation method through the analysis of energy dissipation and fragment size distribution.
- ❖ To study the effect of water infusion and impact load on the burst behaviour of coal from an energy perspective.

## 1.4 Research Framework

Bases on the research problem and objectives, a comprehensive research activities have been carried out in this thesis. The detailed research objectives, tasks, corresponding chapters, and timeline are shown in Figure 1.2.

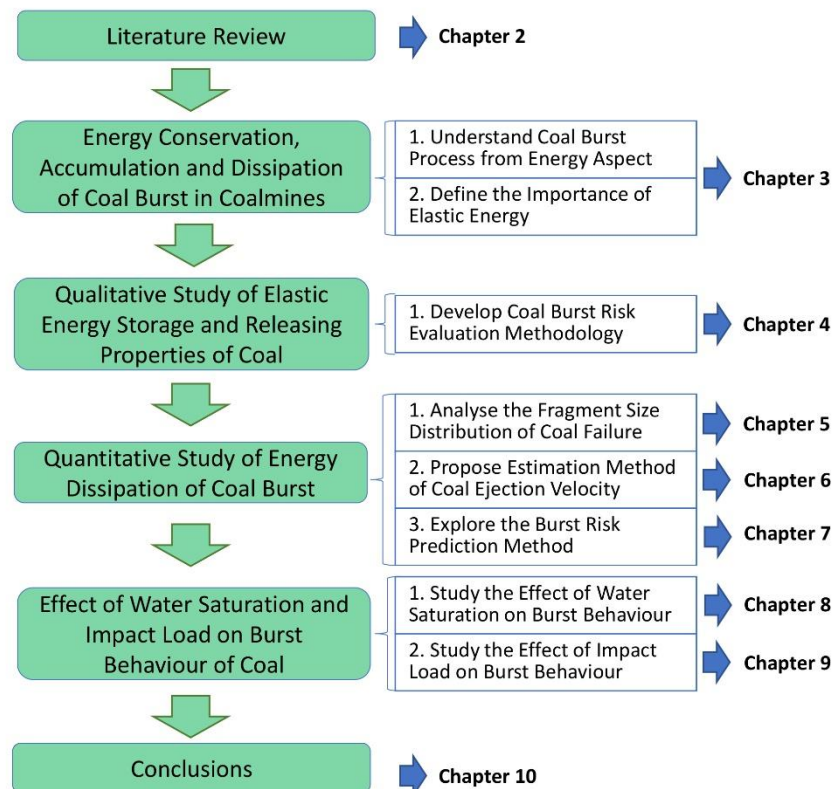


Figure 1. 2 Research framework and timeline

## 1.5 Thesis Outline

The thesis is presented in 10 Chapters. Figure 1.2 shows the main structure of the thesis.

Chapter 1 is a general introduction in which brief background knowledge, the problem statement, research objectives, research framework, and outline of the thesis are provided.

Chapter 2 provides a literature review including coal burst research and experiences in both Australia and other countries. In section 1 of Chapter 2, coal burst situations in Australia and other countries are reviewed, which are related to the analysis of coal burst energy sources in Chapter 3. Besides, the coal burst propensity index, acoustic emission monitoring and the water infusion method introduced in Chapter 2 are all related to the following chapters.

Chapter 3 is based on the paper entitled *Analysis of energy accumulation and dissipation of coal bursts* published on *Energies*. The energy conservation law, accumulation sources and dissipation forms of coal burst in underground coalmines are analyzed in this chapter, which provides the theoretical knowledge and basis for the further energy study of coal specimens. The importance of elastic energy is highlighted in this chapter and will be further studied in Chapter 4.

Chapter 4 is based on the paper entitled *Developing coal burst propensity index method for Australian coal mines* published in the *International Journal of Mining Science and Technology*. This chapter focuses on the coal burst risk evaluation through laboratory measurement of coal burst indices related to the elastic energy storage and fast releasing properties of coal. These indices, named the coal burst propensity index in this thesis, has been widely used in China, Poland, and Russia. The measurement procedure, data analysis method, risk classification standard and improvements are proposed in Chapter

4 based on the theoretical and experimental study of coal specimens taken from the Australian coal seams.

Chapter 5 is based on the paper entitled *Size distribution measurement of coal fragments using digital imaging processing* published in *Measurement*. As mentioned in Section 1.2, the fragmentation energy, which is an important parameter for the estimation of the ejection energy, can be calculated based on the fragment size distribution generated by coal failure. Chapter 5 developed an accurate and fast measurement method of fragment size distribution based on image processing technics. The fractal distribution function for coal fragments generated by uniaxial loading can be established based on image processed data, which provides the foundation of fragmentation characteristic and energy dissipation analysis of coal specimens in the following chapter.

Chapter 6 is based on the paper entitled *Estimation of average ejection velocity generated by rib burst under compression load* published in the *International Journal of Rock Mechanics and Mining Sciences*. Chapter 6 proposed the theoretical estimation equation of ejection velocity generated by coal burst based on fractal fragment size distribution function and energy conservation equation. The feasibility of this method for ejection velocity estimation was verified through innovatively designed “coal ejection test” and case analysis.

Chapter 7 is based on the paper entitled *Experimental study of coal burst risk prediction using fractal dimension analysis of AE spatial distribution* published in the *Journal of Applied Geophysics*. Energy can be dissipated in the form of acoustic emission (AE) during the loading process, which can be used to the early-warning of failure in coal. Chapter 7 experimentally studied the spatial distribution of acoustic emissions released during the loading process of the coal specimen and explored the feasibility of coal burst

prediction according to fractal dimension change of the AE spatial distribution. The analytical solution method of fractal dimension for AE spatial distribution is proposed based on MATLAB coding in this chapter.

Chapter 8 is based on the paper entitled *Effects of water saturation time on energy dissipation and burst propensity of coal specimens*. To understand the water saturation effect on the mechanical properties of coal and demonstrate the possibility of coal burst mitigation by water infusion, Chapter 8 comprehensively studied the effect of water saturation on coal burst propensity, fragmentation characteristics, energy dissipation and acoustic emission of coal through experimental study. The analysis method of burst propensity, fragmentation characteristics, energy dissipation and acoustic emission in this chapter is conducted according to the testing and analysis methods proposed in Chapter 4, 5, 6, 7, respectively.

Chapter 9 is based on the paper entitled *Fragmentation characteristics and energy dissipation of coal under impact load*. This thesis mainly focuses on the brittle failure of coal subject to uniaxial compression load, however, to understand the influence of load types on the burst behavior of coal, experimental studies of the fragmentation characteristics and energy dissipation of coal subject to an impact load was conducted by drop weight testing of coal specimens. The analysis method of fragmentation characteristics, and the energy dissipation in this chapter is conducted according to the testing and analysis methods proposed in Chapter 5 and 6, respectively.

Chapter 10 provides conclusions and recommendations for future work based on results of studies achieved in the thesis.

## **CHAPTER 2 LITERATURE REVIEW**

### **2.1 Coal Burst in Overseas and Australian Coal Mines**

#### **2.1.1 Coal Burst in Europe**

Coal burst is a serious dynamic hazard for underground coalmines in Europe as the mining depth of most coalmines is beyond the critical value (Konicek, Ptacek et al. 2019). Based on European experience, coal burst tends to be violent and catastrophic when the mining depth is beyond 600 m (Patynska and Kabiesz 2009). Many coal mines in Europe including the U.K. (Fedotoval, Kuznetcov et al. 2019), Germany (Casten and Fajklewicz 1993), Poland (Bukowska 2012) and Czech Republic (Číž and Růžek 1997) have experienced personnel casualties and economic losses as a result of coal burst incidents. However, with the enforcement of emission-reduction policies in Europe, many countries such as the U.K. and Germany have closed their deep coalmines and coal burst is no longer a safety issue for these countries (Krzemień, Sánchez et al. 2016).

After decades of research European researchers have achieved a lot with respect to coal burst. German researchers developed de-stress drilling for coal burst control and a drilling-cutting method for stress indirect measurement (Dou and He 2001). Mining researchers in Czech Republic and Poland remain active in coal burst research as there are still many operating coalmines in these two countries (Gombert, Sracek et al. 2019). Coal burst research has more than a 90 year history in these two countries as the first recorded coal burst was in 1912 (Dvorsky and Konicek 2005). The burst propensity index method was firstly proposed and developed by mining researchers in Poland to evaluate the burst proneness of coal seams (Bukowska 2012, Mirosława 2015). In addition, the comprehensive evaluation method of coal burst risk was developed by researchers in these two countries (Dou and He 2001). This method is more reliable as more parameters

and variables are included with the improvement of geological and geophysical exploration methods. It should be noted that the dynamic failure of rock and coal are all termed “rock burst” by Polish and Czech mining researchers as they concluded the burst energy of rock or coal is originally caused by high elastic energy storage resulting from thick overburden or high dynamic load leading to rock failure (Bukowska 2012). Coal burst in Poland and Czech Republic is generally related to large scale seismic events caused by thick sandstone roof breakage, fault slipping or rock mass instability (Konicek and Holecko 2006, Patynska and Kabiesz 2009). Hence, they believe that monitoring of rock mass movement and breakage through micro seismicity or acoustic emission monitoring can early-warn coal burst occurrences in coalmines. Much research into sensor arrangements and early-warning parameters of micro seismicity monitoring have been conducted by researchers in these two countries. Based on the wide application of micro seismicity monitoring, de-stress drilling and risk pre-evaluation, the coal burst accident numbers in Poland has been decreased from over 5000 in 1949 to no more than 5 in 2009 (Patynska and Kabiesz 2009).

### **2.1.2 Coal Burst in the U.S.**

Coal burst has been a major safety hazard for U.S. mining operators for more than one century (Iannacchione and Tadolini 2008). According to a statistical investigation carried out by Iannacchione and Zelanko, 172 coal burst events have resulted in a total of 87 fatalities and 163 injuries from 1936 to 1993 (Iannacchione and Tadolini 2016) (Christopher 2017). However, different with other countries, 61% of the 172 events occurred during pillar recovery as room-and-pillar mining or yield pillar were widely used in U.S. coalmines (Iannacchione and Tadolini 2008). From 1983 to 2017, 283 burst cases were reported to the Mine Safety and Health Administration (MSHA) of U.S. (Christopher 2017). Statistical data has shown that 42% of the 283 burst events occurred

on the longwall face (Christopher 2017) as longwall mining is widely used in many coalmines.

Coal burst in the U.S. is mainly located in Utah, Colorado and Kentucky, which accounted for 52, 33 and 13 percent of reported coal burst cases in the U.S. from 1994 to 2013 (Christopher 2016). In Utah, coal burst is generally linked with a typical mining depth of 450-900m, numerous thick and strong sandstone and siltstone layers and extremely mountainous topography (Christopher and Gauna 2016). Peperakis found that severe bumps at Sunnyside Mine in Utah were attributed to geological faults (Peperakis 1958). Avoiding “critical” pillars which are too large to yield non-violently yet too small to support large abutment stress is also very important for burst mitigation (Christopher 2016). Micro seismicity monitoring was also used in Utah to monitor the regional seismic events caused by coal burst. In recent years, North Fork Valley (NFV) in Colorado, which is an area of extremely mountainous topography, has faced coal burst issues as well. The immediate roof of the most common mining horizons is of weak to moderate strength in this area (Whyatt 2008), which means coal burst in NFV has no obvious link with a hard and thick roof. Besides, coal burst, which often had a greater effect on the floor than ribs, had no direct link with coal-cutting activities and often occurred in the areas of low stress such as maingates or development sections (Christopher 2016). Coal burst in NFV appeared to be driven by large seismic energy releases occurring at some distance from the coal seam, apparently from massive sandstone floors or known geological structure (Rice 1935).

### **2.1.3 Coal Burst in China**

The first documented coal burst accident in China was in 1933, which is later than other countries (Dou and He 2001). Coal burst cases are more diverse in China as coal burst

can happen in coal seams at a wide range of mining depths (200 to over 1000 m) and in different coal seam conditions (gentle to inclined), which is caused by the complicated and diverse geological conditions of coal seams in different areas of China. Coal burst accidents occurred in Shandong, Henan and Anhui Province and generally can be linked to complicated geological structures (faults and folds), deep mining over 1000 m and strong seismic events (Dou, Lu et al. 2006). In area of north-western China such as Shanxi, Shaanxi and Xinjiang Province, the hard and thick sandstone roof generally is a major energy source of coal burst (Yu, Liu et al. 2013). With the increase of mining depth and intensity, both the severity and frequency of coal burst are increasing in China. Coal burst occurred in 32 coal mines in 1985 while more than 147 coal mines were experiencing coal burst in 2014 (Shen and Luo 2016). Chinese mining researchers conducted extensive research into coal burst driving forces, monitoring technics, and controlling measures, which will be introduced in the following part of the literature review.

Coal burst has caused a variety of damage including roof squaring, longwall burst, pillar burst, roadway closure and floor heave in China (Dou, Mu et al. 2014). Literature has shown that floor heave caused by high horizontal stress is a major burst risk for many coal mines (Xu, Dou et al. 2010), which is different from coal burst situations in other countries. The gob-side entry retaining and small size barrier pillar were successfully used in many coal mines to reduce the burst risk of roadways or headings as Chinese researchers believe that stress can be transferred to deep areas with small or no pillar roadways system (Dou and He 2001), which is obviously different with respect to the pillar design principles in Australia. Micro seismicity monitoring is widely adopted to monitor and predict coal burst events in Chinese coalmines (Cai, Dou et al. 2018). Although the burst events are intensive, data shows that the damage of coal burst has been

effectively controlled in China with sufficient risk evaluation, prediction, mitigation, and controlling measures.

#### **2.1.4 Coal Burst in Australia**

Coal burst is a relatively new challenge for Australian underground mining as the first documented accident occurred at Austar Coal Mine in 2014 (Mine Safety Investigation Unit 2016, Hebblewhite and Galvin 2017). More burst accidents occurred at the Appin and Austar Coal Mine from 2014 to 2018 (Mine Safety 2016, NSW Resources Regulator 2018). According to the accident investigation report and literature, all these coal burst cases occurred in the coal mines with over 500 m depth (Zhang, Canbulat et al. 2017), which is not as deep as coal mines in other countries mentioned above. It has been pointed out by many researchers that coal burst intensity and severity will increase with mining depth in Australia (Zhang, Canbulat et al. 2017, Frith, Reed et al. 2020). According to the accident review made by Bruce, gas was not regarded as the obvious factor leading to the burst as limited gas was detected at burst site (Hebblewhite and Galvin 2017). Frith also discussed the effect of horizontal stress on the coal burst (Frith, Reed et al. 2020). ACARP (Australian Coal Industry's Research Program) has funded many research projects and practices including an international coal burst literatures review, experimental and numerical studies of the coal burst mechanism, burst mitigation by pillar design and burst early-warning by seismicity monitoring since 2014 (Shen and Luo 2016). However, the driving forces and controlling measures burst still needs more comprehensive scientific research and extensive engineering practice as the coal burst database in Australia is not as large as for the other countries mentioned above.

Understanding energy accumulation and dissipation of coal burst, which is the topic of this thesis, is important for understanding the driving forces and potential solving

technologies of coal burst in Australia. For example, micro seismicity monitoring was used for coal burst risk early-warning by some coal mines in Poland and China as coal burst cases in these coal mines were linked to seismic energy releasing. However, based on the analysis of seismic and geological data, it was believed by researchers that coal burst in Australia was more likely caused by high static stress (Ahn, Zhang et al. 2017, Frith, Reed et al. 2020). Hence, the elimination of elastic strain energy by coal property weakening and softening might be helpful for coal burst controlling (Dou, Mu et al. 2014). The energy sources of coal burst in Australia will be further discussed in Chapter 3 of this thesis.

## **2.2 Coal Burst Characteristics, Mechanisms, and Classification**

### **2.2.1 Coal Burst Characteristics**

The following characteristics of coal burst have been identified by mining research and practice:

1. Coal burst is always associated with sudden and intensive energy releasing phenomenon such as audible sound, coal ejection, roof weighting, floor heave, or seismic events, which can cause roadway failure, equipment damage and personnel injury (Shen and Luo 2016).
2. It is hard to get a uniformed mechanism for coal burst as coal burst can be caused by many factors including high gravitational stress, high abutment stress, geological structure failure and the superposition of all these factors. Hence, the classification of coal burst and the study of coal burst type by type are fundamental work for coal burst research.
3. The prediction of coal burst, especially burst site, is difficult to achieve as the coal burst mechanism is complex. Coal burst which is linked to seismic events can be early-warned based on the long-term observation and study. However, it is hard

to determine the burst site as coal burst can happen in any place with high stress and energy concentration levels.

4. Typical geological factors such as a hard sandstone channel, deep overburden, folds, faults and thickness change can cause stress and energy concentration in l areas of the coal seam (Rezaei, Hossaini et al. 2015, Wang, Gong et al. 2016), which can increase the risk and scale of coal burst. Hence, clear and detailed geological information is important for the evaluation of coal burst risk.
5. Other dynamic disasters including gas outburst or explosion, wind blast and roof or floor water inrush could be induced by the occurrence of coal burst (Shen and Luo 2016).

### **2.2.2 Coal Burst Mechanism**

**Stress:** Coal is a kind of inhomogeneous sedimentary rock in which natural weaknesses such as voids, bedding planes and cracks widely exists (Xie, Peng et al. 2004). Many researchers have studied the rock failure process induced by crack initiation and propagation (Al-Shayea 2005). Many basic rock strength theories such as the Griffith theory (Brace 1960), Mohr-Coulomb theory (Zhao 2000) and Hoek-Brown theory (Hoek and Brown 1980) were proposed by researchers to determine the failure strength of rock. It has been demonstrated by theoretical, experimental and numerical studies that rock will fail and lose bearing capacity when the applied stress is beyond its strength (Xu, Tang et al. 2003). Coal burst is the brittle and dynamic failure of coal subject to super-critical stress, which is more abrupt than gentle failure such as yield and bulking. In the underground mining environment, stress concentration within the coal body can be induced by many geological and mining-induced factors. Hence, stress theory was developed by Bräuner (Bräuner 2017) to explain the mechanism of coal burst. According to strength theory, the abrupt failure of coal is caused by super-critical stress which is

beyond the strength of the coal body (Dou and He 2001). Stress theory can explain the increasing trend of coal burst cases with mining depth. However, mining research and experience have demonstrated that not all the coal seam will burst when stress is beyond its strength. Critical stress is the necessary condition but not the sufficient condition for coal burst.

**Energy:** It has been recognized that the unstable release of massive energy, mainly in the form of kinetic energy, contributes to the coal burst occurrence (Zhang, Canbulat et al. 2017). The burst event is harmless when the energy release scale is small. For example, the energy release of the yield process is very gentle. Damage and safety hazards from coal burst are caused by the rapid release of massive energy. Researchers believe that coal burst will happen when the energy accumulation rate is much higher than the release rate (Dou and He 2001), which is called the energy hypothesis of coal burst mechanism. That is, coal burst will happen when a large amount of energy cannot be dissipated by a gentle failure process. The energy accumulation can be caused by many reasons, which will be further analyzed in Chapter 3. To understand the general energy accumulation and dissipation process of rock failure, Xie et al. theoretically analyzed the relationship between the energy scale and rock failure based on damage mechanics (Xie, Ju et al. 2005). He et al. conducted the uniaxial, biaxial and triaxial compression test of different rocks to study the failure and energy release process by simulating the burst process in an underground stress environment (He, Miao et al. 2010, He, Jia et al. 2012). These studies demonstrated that coal burst is a violent energy release process. However, the critical energy release rate of coal burst has not been provided by previous research. The reason for the energy release rate increase needs to be analyzed case by case. Hence, more detailed research needs to be conducted around the energy aspect of coal burst.

**Stiffness:** Stiffness is one of the important properties contributing to coal burst when the coal seam is under a high compression load. An experimental study conducted by Cook found that rock specimens tend to violently fail when the stiffness of the loading machine is high (Cook 1965). Bieniawski analyzed the post-failure behavior of rock specimens under different stiffness conditions with respect to the loading machine and found the post-failure curve was steeper when the stiffness was higher (Bieniawski 1967, Bieniawski 1967, Bieniawski 1967, Bieniawski, Denkhaus et al. 1969). Dou et al. and Liu et al. conducted the uniaxial compression test of rock-coal-rock combined specimens to simulate the stiffness conditions of a coal seam in an underground environment and found that coal seams tend to abruptly fail when the stiffness of rock components are high (Dou, Lu et al. 2006, Liu, Wang et al. 2014). All these findings highlighted the contribution of the roof and floor stiffness to the formation of coal burst. The contribution of stiffness to coal burst can also be explained from an energy aspect, which will be introduced in detail in Chapter 3 of this thesis. Energy will flow from high stiffness material to low stiffness material.

**Burst Propensity:** Mining experiences in Poland and Czech Republic indicated that coal burst often happened in hard and brittle coal seams (Karchevsky 2017). Researchers in these countries believe that this phenomenon is caused when the mechanical and physical properties differ between coal seams (Bieniawski, Denkhaus et al. 1969). It has been found by laboratory studies of coal specimens from different coal seams that coal specimens from different coal seams exhibit different failure behavior under the same loading conditions (Kidybiński 1981, Karchevsky 2017). Due to different formation history and conditions, the physical properties of coal seams are different, which will lead to differences with respect to energy storage and energy releasing behavior between coal seams. Coal burst will not happen if a coal seam has a low energy storage ability (Singh

1988). For example, soft coals subject to super-critical stress tend to have gentle deformation. The properties that allow coal seams to store and then rapidly release elastic energy is called the burst propensity of coal. Hence, many scholars proposed parameters qualitatively defining burst propensity to evaluate the burst risk of coal seams (Zhang, Wang et al. 1986, Pan, Geng et al. 2010, Cai, Dou et al. 2016), which will be introduced in remaining part of this chapter.

**Dynamic Load:** It has been well proved by thorough experimental studies that the strength and burst behavior of rock are positively related to loading rate (Okubo, Fukui et al. 2006, Huang and Liu 2013, Li, Zhou et al. 2016). Some researchers conducted the Split Hopkinson Bar (SHPB) tests of rock and found the failure of rock is violent under extremely dynamic load (Li, Zhou et al. 2008, Demirdag, Tufekci et al. 2010, Bailly, Delvare et al. 2011, Fakhimi, Azhdari et al. 2018). During the underground mining process, the dynamic failure of geological structures such as strong layers and faults can be triggered due to stress concentration and re-distribution (Chen 1994, Fan, Li et al. 2018). The stress wave generated by dynamic failure far from the burst site can travel through geo-materials and apply super-critical dynamic load on a coal body, which will then cause the violent failure of the coal. Hence, Dou et al. proposed the dynamic and static load superposition theory to explain the mechanism of coal burst (Dou, Zhao et al. 2006, Dou, He et al. 2015). Dou et al classified coal burst into two types according to the contribution of dynamic load (Dou, He et al. 2012), which will be introduced in the classification of coal burst. For the coal burst dominated by dynamic load, the burst propensity of the coal seam is not the essential condition any more as energy can be remotely transferred from a dynamic failure point to the burst site. In Chapter 3, the burst type and burst energy sources of Australian coal burst cases are analyzed based on literature.

### **2.2.3 Coal Burst Classification**

The classification of coal burst is important as the burst mitigation and controlling measures are different for different types of coal burst. Numerous classifications have been put forward by researchers. Pan divided coal burst into compression type, tensile type and slipping type (Pan 1999) according to the failure types of geo-materials. The energy sources of coal burst are not reflected in this classification. Jiang et al. classified coal burst into strain mode induced by high static load and geological mode resulting from failure of geological structures such as hard roof and fault (Jiang, Wei et al. 2013). For strain mode, the elastic energy is the main energy source of coal burst. The energy source of the geological mode is still not clearly defined in this classification. He et al. classified coal burst into either strain coal burst induced by high static load and impact-induced coal burst caused by remote dynamic impact (He, Xia et al. 2012) according to the location of the energy source. Both static and dynamic load can provide the energy sources required by coal burst in an underground environment. Hence, Dou et al divided coal burst into two types: high static load and strong dynamic load (Dou, Mu et al. 2014). For high static load, most energy released by the coal burst is the elastic strain energy stored in the coal body and the coal burst is triggered by a minor dynamic disturbance. For strong dynamic load, most energy released by the coal burst is transformed from a far-field mine tremor. Chapter 3 concluded that coal burst accidents in Australian coal mines are more likely to be the high static load type. Hence, the study of elastic energy accumulation and dissipation of high static load type coal burst will contribute to the understanding of the burst mechanism and the process of coal burst accidents occurring in Australian coal mines.

## 2.3 Coal Burst Risk Evaluation and Early-warning

### 2.3.1 Coal Burst Risk Evaluation

**Coal Burst Propensity Index:** As introduced in section 2.2.2, the difference in energy storage and release behavior will lead to different burst behavior and propensity in different coal seams. Based on the energy balance analysis of the crack propagation, Bieniawski proposed that elastic energy is associated with the violent failure of rock (Bieniawski 1967). Kidybiński found that coal's ability to store and release rapidly elastic strain energy seems to be a fundamental condition of coal burst (Kidybiński 1981). From the perspective of energy, coal burst is the accumulation and releasing process of elastic energy. The different coal seams' ability to store and release rapidly elastic strain energy differs greatly. Based on the analysis of stress-strain curves for coal specimens under uniaxial compressive stress, many special indices (as shown in Figure 2.1) have been published by different scholars to determine coal burst propensity (Qi, Peng et al. 2011).

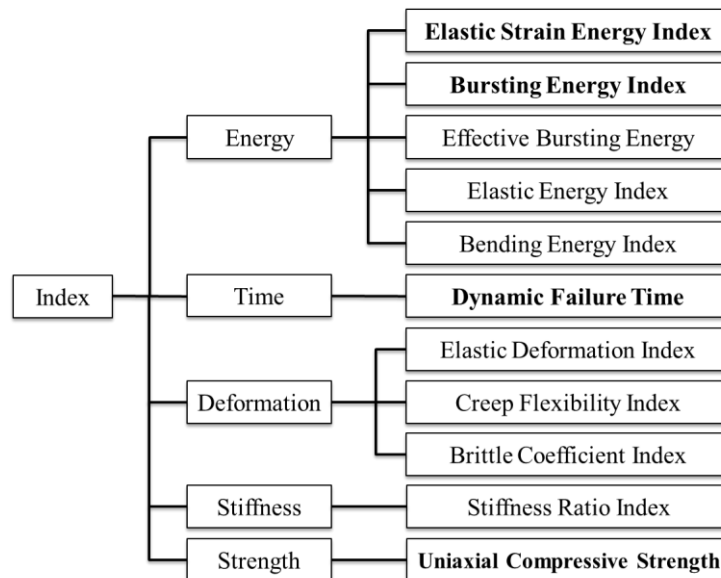


Figure 2. 1 Coal burst propensity index classification

Russian and Polish coal mines adopt an elastic strain energy index ( $W_{ET}$ ) and a bursting energy index to evaluate coal burst liability (Pan 1999, Bräuner 2017). Zhang et al. believes that the duration of the failure process is the comprehensive reflection of energy

accumulation and dissipation characteristics of coal (Zhang, Wang et al. 1986). They propose dynamic failure time to evaluate coal burst propensity. Based on the correlation analysis of mass data, Qi et al. conclude that the uniaxial compressive strength of coal is a good index of coal burst propensity evaluation as well (Qi, Peng et al. 2011). In 2010, China Coal Industry Association summarized these four indices as the bursting liability indices of coal and published the standard test method of these four indices. Some researchers adopted these four indices to evaluate the burst propensity of rock as well. It has been proven by Russian, Poland, and China experience that these four indices are good indicators which define the burst risk of coal seams. Referring to other literature, these four indices are called the coal burst propensity index method in the research. The coal burst propensity index method could be an efficient method to evaluate the coal burst risk of coal seams in the Australian coal mining industry. Nevertheless, the risk classification method and test method of these four indices is diverse in different literature. In chapter 4 of this thesis, the feasibility and effectiveness of this method in Australia was studied.

**Comprehensive Evaluation Method:** For coal burst dominated by dynamic load, the burst propensity index cannot reflect accurately the burst risk of coal seams. Coal burst occurrence is also related to many geological factors and mining technical parameters. In Poland, the coal burst risk can be comprehensively evaluated based on roof conditions, geological structures, burst history, coal seam properties, and mining design (Dou, Mu et al. 2014). Based on the Polish experience, Dou et al. proposed the comprehensive evaluation method according to the Chinese mining and geological conditions (Dou and He 2001). As shown in Table 2.1 and Table 2.2, seven geological factors and twelve technical factors are included.

**Table 2. 1 Geological factors of comprehensive evaluation method (Dou and He 2001)**

Number	Factor	Definition of factors	Conditions	Risk Value
1	R <sub>1</sub>	History of coal burst	No history of coal burst in the coal seam	-2
			Coal burst have occurred in the seam	0
			Several coal burst accidents have occurred in the coal seam or in the coal mine with same mining method	3
2	R <sub>2</sub>	Mining depth	<500m	0
			500m-700m	1
			>700m	2
3	R <sub>3</sub>	Distance from massive strata (UCS≥60MPa) to the coal seam	>100m	0
			100-50m	1
			<50m	3
4	R <sub>4</sub>	Stress concentration	>10% Original	1
			>20% Original	2
			>30% Original	3
5	R <sub>5</sub>	Roof rock layer thickness characteristic	<50	0
			≥50	2
6	R <sub>6</sub>	Compressive strength of coal	UCS≤16MPa	0
			UCS>16MPa	2
7	R <sub>7</sub>	Elastic strain energy index	<2	0
			2-5	2
			≥5	4

\*R<sub>geological factors</sub> = Sum of R<sub>1</sub> to R<sub>7</sub> / Sum of the maximum index value of the factors included

**Table 2. 2 Technical factors of comprehensive evaluation method (Dou, He et al. 2015)**

Number	Factor	Definition of factors	Conditions	Risk Value
1	R <sub>1</sub>	Vertical distance between working face and goaf or stop working line	>60cm	0
			30-60cm	2
			<30cm	3
2	R <sub>2</sub>	Unmined coal seam	Top coal or bottom coal >1m	3
3	R <sub>3</sub>	Full seam mining height (without distressing)	<3m	0
			3m-4m	1
			>4m	3
4	R <sub>4</sub>	Face length	>300m	0
			150-300m	2
			<150m	4
5	R <sub>5</sub>	Development roadways besides goaf	No pillars or <3m	0
			3-10m	2
			10-15m	4
6	R <sub>6</sub>	Distance to goaf less than 50m	Heading face	2
			Longwall face	3
		Distance to pillar less than 50m	Heading face	1
			Longwall face	3

7	R <sub>7</sub>	Distance between new roadway and old roadway less than 50m	Old roadway has been fulfilled	1
			Old roadway has not been fulfilled	2
		Distance between longwall face and old roadway less than 50m	Old roadway has been fulfilled	1
			Old roadway has not been fulfilled	2
		Distance between longwall face and bifurcation less than 50 m	Heading face or lonwall face	3
8	R <sub>8</sub>	Distance between longwall face and fault which fault throw beyond 3m less than 50m	Near hanging wall	1
			Near footwall	2
9	R <sub>9</sub>	Distance between	>15	2
10	R <sub>10</sub>	Longwall face near the	Heading face or longwall face	2
11	R <sub>11</sub>	The pressure relief level of protective seam method	Weak	-2
			Medium	-4
			Strong	-8
12	R <sub>12</sub>	Treatment of mined-out area	Fulfilling method	2
			Caving method	0

\*R<sub>technical factors</sub> = Sum of R<sub>1</sub> to R<sub>12</sub> / Sum of the maximum index value of the factors included

The burst risk (R<sub>b</sub>) can be evaluated according to Table 2.3. This method has now been recommended as the risk evaluation method in the *Coal Mine Safety Regulations* of China. This method is based on long-term coal burst controlling experience and thorough analysis of massive coal burst cases in China. However, it is hard to conclude a similar comprehensive evaluation method for Australian coal mines as the burst database has not been well established in Australia.

**Table 2. 3 Burst risk evaluation form of comprehensive evaluation method**

Value of Risk	Risk Level	Remark
R <sub>b</sub> < 0.3	Extremely Low	Mining can be carried out according to the rules of operation.
R <sub>b</sub> = 0.3-0.5	Low	Careful mining work can be carried out according to the rules of operation.
R <sub>b</sub> = 0.5-0.75	Moderate	Burst control and forecasting measures need to be taken during mining.
R <sub>b</sub> =0.75-0.95	High	Mining operations should be stopped, and unnecessary personnel should be evacuated from dangerous locations. Burst control and forecasting measures need to be taken during mining.
R <sub>b</sub> >0.95	Extremely high	External advice should be sought from experts on the use of coal burst prevention methods. Comprehensive measures and methods should be adopted. Mining operations should be stopped, and unnecessary personnel should be evacuated from dangerous locations.

\*W is the maximum value of W<sub>geological factors</sub> and W<sub>technical factors</sub>

### 2.3.2 Coal Burst Risk Early-warning

**Electromagnetic Emission Monitoring:** It has been found in geosciences that rich electromagnetic emissions can be observed before the occurrence of geo-hazards (Yamada, Masuda et al. 1989). Research has demonstrated that electromagnetic emission induced by rock fracture is positively correlated to the crack intensity inside the rock/coal body (Frid and Vozoff 2005, Borisov 2018), which means rich electromagnetic emission can be observed prior to the rock/coal failure. Hence, the monitoring of electromagnetic emission can give early-warning of potential rock/coal dynamic failures. Many researchers have explored the application of this method in the early-warning of coal burst risks (Frid 2001, Dou and He 2004, Xiao, He et al. 2006, Li, Wang et al. 2016). However, this method has the following two limitations: (a) The monitoring area is limited as the sensor can only detect the electromagnetic signals within 20 m due to the shielding effect of the rock/coal body and rapid attenuation of the electromagnetic signal. (b) The early-warning accuracy cannot be guaranteed as background noise caused by mining equipment is strong in underground environments.

**Acoustic Emission Monitoring:** It has long been noticed by mining researchers that the dynamic failure of rock/coal is always associated with audible noises (Obert and Duvall 1942). Experimental studies conducted by many researchers have found that rich sub-audible acoustic signals, also named acoustic emission, can be detected during the cracking progress of rock/coal (Obert and Duvall 1942, Ohnaka and Mogi 1982, Guarino, Garcimartin et al. 1998, Shadrin and Klishin 2018), which is similar to electromagnetic emission. It is widely believed that the acoustic emission is caused by the friction and expansion of crack surfaces at a micro scale (Sikorski 2012). Compared with electromagnetic emission, the background noise caused by humans and instruments is very low as the frequency of acoustic emission detected for coal failure early-warning is

very high. With a reasonable design of the sensor array, the location of acoustic emission sources can be acquired according to an algorithm (Hirata, Satoh et al. 1987, Xie and Pariseau 1993), which enables the highlighting of intensive crack areas and an understanding of the failure process. Acoustic emission monitoring has been a widely-used method to understand energy release (Zhao, Jiang et al. 2007) and the crack propagation (Kong, Wang et al. 2016) process, and to provide for the early-warning of the failure (Dou and He 2004, He, Dou et al. 2011) of coal in the laboratory. However, the monitoring area of this method is still limited as acoustic signals will attenuate rapidly within a short travelling distance. In this thesis, the theoretical and experimental study of coal brittle failure early-warning by acoustic emission monitoring is introduced to find a suitable precursor of coal burst.

**Micro Seismicity Monitoring:** It has been demonstrated by decades of research and in-field applications that micro seismicity monitoring technology has a promising ability to locate potentially violent rock fracture. Micro seismicity monitoring is a passive observation of very small-scale earthquakes which occur in the underground environment as a result of human activities or geophysical processes such as mining (Potvin and Hudyma 2001, Trifu and Shumila 2010), hydraulic fracturing (Urbancic, Shumila et al. 1999), magmatic processes (Chouet 1996, Shelly and Hill 2011) and underground gas migration (Verdon, Kendall et al. 2011, Oye, Aker et al. 2013). Micro seismicity monitoring provides an important window into the evolving structure and dynamic processes occurring within active rock fracture zones and is a critical component of geodynamic hazards monitoring efforts (Hansen and Schmandt 2015). The micro seismicity monitoring technology also has been successfully adopted in the monitoring and warning of geodynamic hazards posed by coal burst (Lu, Liu et al. 2015). The phenomenon that stressed rock can release micro-level signals was discovered by two

researchers of the U.S. Bureau of Mines Obert and Duvall in 1938 (Ge 2005, Ge 2010). In the early 1960s, South African researchers developed a 16 channel micro seismicity system with positioning functionality for rock burst monitoring in gold mines (Ge 2010). In 1970, under the sponsorship of the U.S. Bureau of Mines, The Pennsylvania State Rock Mechanics Laboratory conducted a research project to investigate the application of micro seismicity techniques in coal mine safety (Hardy and Mowrey 1976). Based on the study of the micro seismicity phenomenon associated with mining activities, the micro seismicity monitoring system has been a useful monitoring tool for burst early-warning in coalmines. It provides a continuous and real-time 4D (3-dimension location and time) record of seismicity associated with rock/coal failure in a more than ten square kilometres region. The early warning of coal burst through micro seismicity monitoring needs to be based on the following conditions: (a) The link between seismicity events and coal burst needs to be identified through long-term on-site observation and analysis. Due to the complex mechanism of coal burst, not all the types of coal burst can be early warned by this method. (b) Suitable indicators or precursors need to be adopted to demonstrate the risk level. Sometimes, a comprehensive and fuzzy analysis of multi-parameters is needed for this method. Hence, the fundamental knowledge of micro seismicity and coal burst still needs to be further explored to build a more reliable early-warning method.

## **2.4 Coal Burst Mitigation**

**Pressure Relief Drilling:** Pressure relief drilling is a mitigation measure to eliminate the stress concentration in coal seams and surrounding rock (Gu, Xiao et al. 2014). The coal around the pressure relief boreholes drilled in a highly stressed zone will fracture and fail, which can lead to the formation of a crushed zone with a much lower stress than that of the stress concentration zone and have a much larger diameter than that of a single borehole (Zhang, Li et al. 2019). The high stress concentration zone will be replaced by

a pressure relief zone and transferred deeper into the coal seam with the implementation and interconnection of multiple pressure relief boreholes (Xiong and He 2006). Pressure relief drilling with a specific boreholes size and layout proposed based on geological and technical conditions has been widely adopted in many coal mines (Varley and Whyatt 2008, Yang 2012, Soucek, Konicek et al. 2013). The pressure relief drilling method can be combined with other burst mitigation methods such as blasting, hydraulic fracturing and water injection to get a better de-stress effect. It should be noted that stress can be re-concentrated within a pressure released zone during the mining process and further de-stressing measures may need to be applied (Li, Zhou et al. 2009).

**Destress Blasting:** Destress blasting can be adopted to reduce the stress concentration within a rock/coal body by further fracturing and crushing intact rock/coal when pressure relief drilling cannot provide a sufficient mitigating effect. It has been verified by numerical and practical studies that destress blasting with reasonable blasting parameter design can reduce the degree of stress concentration and transfer the stress peak to deeper areas (Saharan and Mitri 2011, Liu, Cao et al. 2017). Numerical model (Li, Kang et al. 2009, Wei, Wang et al. 2011), theoretical analysis (Konicek, Soucek et al. 2013) and seismicity monitoring (Konicek, Soucek et al. 2013) were proposed by scholars to evaluate the effectiveness of this method for burst mitigation. However, it needs to be noted that the operations of destress bursting need to be carefully evaluated as coal burst can be artificially induced by blasting as well (Liu, Cao et al. 2017).

**Water Infusion:** Water infusion has long been taken as an effective way to eliminate coal burst risk as water infusion can loosen and soften coal. Theoretically, water infusion can change coal properties in two ways. Firstly, water infusion can reduce the burst risk or scale by weakening the elastic behaviour before and after failure (Xiong, Zhao et al. 2011,

Guo, Tan et al. 2017). Water infusion can decrease the critical stress reached within coal body by increasing the pore pressure (Perera, Ranjith et al. 2011). However, some fundamental research around water saturation time on the burst mitigation effect still needs to be progressed (GuhaRoy, Singh et al. 2017, Liu, Xu et al. 2017). In this thesis, the effect of water saturation on the energy dissipation and burst propensity of coal specimens is studied in Chapter 8.

**Hydraulic Fracturing:** Hydraulic fracturing, which was first proposed in 1947 for oil and gas stimulation, has been successfully applied in coal mines to cut hard rooves (Fan, Dou et al. 2012), to fracture hard coal (Ouyang 2012) and to reduce and redistribute stress (Zhu, Feng et al. 2017). Hydraulic fracturing by high pressure water injection can achieve the fracturing and softening of the coal body at the same time. Hydraulic fracturing can reduce the outburst risk as the permeability can be enhanced by crack propagation (Lama and Saghafi 2002). Compared with distress blasting, hydraulic fracturing is the preferred way to deal with hard roof and stress concentration with less dynamic disturbance to underground structures and there is a lower risk of associated outburst in gassy coal seams (Lin, Deng et al. 2016). The further developed directional hydraulic fracturing technic can achieve improved efficiency and security with respect to burst prevention (He, Dou et al. 2012, Xia, Zhang et al. 2018).

## **CHAPTER 3 ANALYSIS OF ENERGY ACCUMULATION AND DISSIPATION OF COAL BURST**

### **Summary**

This chapter focuses on the analysis of the energy accumulation and dissipation process associated with coal burst, especially the coal burst cases in Australia. As introduced in Chapter 2, coal burst can be divided into several types based on the energy sources and burst behavior. This chapter reviewed the possible leading factors of burst energy accumulation overseas and in Australia. Based on the analysis in this chapter, it is concluded that the energy of coal burst in Australia is mainly from elastic strain energy stored in the coal body. Therefore, the burst propensity indexes related to elastic energy of coal will be developed as a coal burst risk evaluation method in the next chapter.

### **Citation**

This chapter is based on the paper published in *Energies* with the following citation:

Yang XH, Ren T, Remennikov AM, He XQ & Tan LH, Analysis of energy accumulation and dissipation of coal bursts. *Energies*, 2018, 11(7), 1816-1827. doi: 10.3390/en11071816

## **Abstract**

Coal bursts are a serious dynamic hazard for underground coalmines, and they attract extensive interest from mining and geotechnical researchers worldwide. More recently, coal-burst incidents were reported in some Australian coalmines as a result of inadequate geological assessment of coal-burst hazards. The coal-burst process is closely associated with the accumulation of elastic energy and the rapid dissipation of kinetic energy. This chapter introduces the essential geological conditions for energy accumulation, and the likely precursors for rapid energy dissipation leading to coal burst, which can be used by Australian coalmines to determine their coal-burst risk accordingly. Different energy forms and their transformations during the coal-burst process are introduced in detail in this chapter. The dominant geological factors resulting in the accumulation of massive energy are analyzed, and the likely precursors associated with the instant release of elastic energy are discussed.

## **Keywords**

Coal burst; Energy; Mine hazards; Underground mining

### **3.1 Introduction**

The violent and catastrophic failure of coal, called “coal burst” in underground mining, can release a large amount of energy in the forms of acoustic emission, mine seismicity, and coal ejection. The long history of coal bursts in Poland, Russian, the United States, and China is well–documented (Whyatt, Blake et al. 1900, Christopher 2017). It is illustrated by mining experience of these countries where both the frequency and the severity of coal bursts increase with mining depth. There are no recorded coal burst accidents in Australia before 2014, as Australian coalmines are generally characterized by shallow mining depths, simple geological conditions, advanced mining technology, and reasonable geotechnical design. However, following four coal-burst accidents, happening in 2014 (Hebblewhite and Galvin 2017), 2016 (Mine Safety 2016), 2018 (Department of Planning and Environment 2018), and 2018 (Department of Planning and Environment 2018), it is believed by researchers and engineers that Australian coalmines will face significant safety hazards caused by coal burst going forward.

Thorough research was conducted over decades into the potential driving mechanism of coal burst, and technologies aimed at solving associated problems were investigated. There are many hypothesized mechanisms for coal burst discussed by researchers, arising from various aspects including stress (Whyatt 2008), stiffness (Bieniawski 1967), energy (Zhang, Canbulat et al. 2017), and coal properties (Kidybiński 1981). Advanced techniques, such as hydraulic fracturing (Huang, Li et al. 2014), destress blasting (He, Dou et al. 2012), and water infusion (Frid 2000, Liu, Xu et al. 2017), are adopted in coalmines to mitigate the risk of coal burst. These theories and technologies may be able to explain the formation of coal burst or may be able to diminish the damage of potential coal burst accidents following the first recognized case of a coal burst accident at a coalmine. However, the risk of coal burst is generally hard to recognize for coalmines

with no history of coal burst. Particularly in Australian coalmines, coal burst hazards are hard to recognize, as there is no pre-assessment process or real-time monitoring apparatus for coal burst risk.

Energy concepts associated with coal burst are of great interest in the field of coal burst research. Based on the mechanical behavior of coal subject to uniaxial compression stress, Bieniawski et al. found that coal burst only happened when a large amount of elastic energy is stored in the coal body (Bieniawski, Denkhaus et al. 1969). Many researchers have carried out detailed research into the forms of energy dissipation associated with coal burst, and proposed various coal burst monitoring and early-warning methodologies, such as electromagnetic radiation (Song, Wang et al. 2012), acoustic emission (Yamada, Masuda et al. 1989), and micro seismic techniques (Trifu and Shumila 2010, Li, Wang et al. 2016, Li, He et al. 2018). Dou et al. believes that the key to mitigating coal burst is decreasing the elastic energy stored in the coal or surrounding rock of the area being mined (Zhang, Canbulat et al. 2017). In other words, coal burst only happens when massive elastic energy stored in the coal is instantaneously released. This chapter aims to introduce the essential geological conditions for energy accumulation, and the likely precursors for rapid energy dissipation in coalmines, which can assist Australian coalmines in determining their coal burst risk accordingly. To achieve this aim, various energy forms and energy balances featured during coal burst are introduced in detail. Then, the dominant geological factors resulting in the accumulation of massive energy are analyzed. Furthermore, the likely precursors associated with the instant release of elastic energy are discussed.

### 3.2 Energy Forms and the Energy Conservation Equation

Coal burst is described as an energy phenomenon accompanying coal deformation and fracture, in the form of brittle and violent failure induced by mining disturbances (Singh 1988). The energy consumed by coal exists in various forms, and only a part of the total energy can lead to personal casualties or equipment damage. In the context of material science, coal is classified as an elastic/plastic material. Hence, as shown in Figure 3.1,

Kidybiński divided the energy consumed by coal before peak strength into two parts: elastic energy ( $E_{\text{elastic}}$ ) and plastic energy ( $E_{\text{plastic}}$ ). He also believed that elastic energy is related to coal burst following the irreversible consumption of plastic energy during the unrecoverable deformation and fracture of coal.

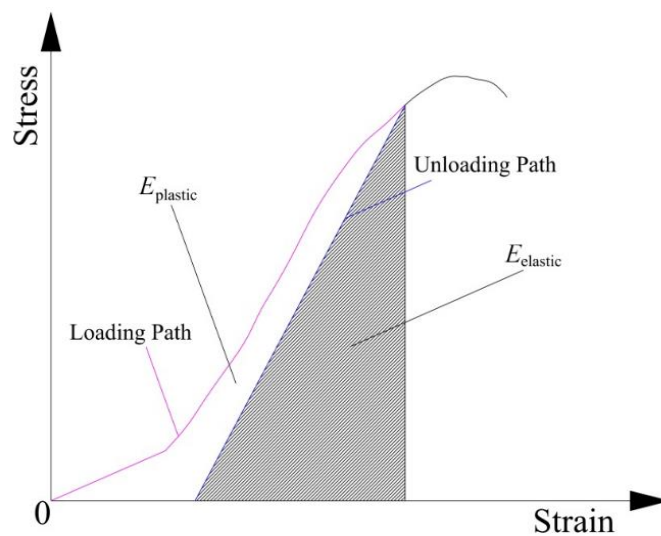


**Figure 3. 1 Schematic diagram of the elastic and plastic energies of coal subjected to uniaxial compression load**

Most researchers accept this deduction, as it was proven via laboratory tests (Guo, Tan et al. 2017) and through mining experience (Zhang, Canbulat et al. 2017) that coal burst only happens in coal seams with a high elastic energy storage. The  $E_{\text{elastic}}/E_{\text{plastic}}$  ratio consequently became a widely adopted indicator for the evaluation of coal burst risks (Sirait, Wattimena et al. 2013, Cai, Dou et al. 2016), which will be further discussed in the next chapter. Elastic energy, transformed into kinetic energy, can manifest itself in

ejected coal, leading to fatal accidents (NSW Mine Safety Investigation Unit 2015, Zhang, Canbulat et al. 2017). However, it was found in experimental research on granite specimens that the kinetic energy carried by ejected rock particles only accounts for less than 1% of the elastic energy stored before peak strength (Su, Jiang et al. 2016). That is, a large amount of elastic energy is dissipated in other forms during the gentle failure of rock.

It was found by researchers that rich acoustic signals were detected at the failure points of concrete and rock materials (Landis and Lucie 2002, Sikorski 2012, Shadrin and Klishin 2018). A similar phenomenon also happened during the failure process of coal (Ranjith, Jasinge et al. 2010). Many scholars conducted detailed studies on the mechanism underlying the acoustic emission of geo-materials (Kurita and Fujii 1979, Lockner, Byerlee et al. 1991, Sikorski 2012, Shadrin and Klishin 2018). It was found by researchers that the acoustic emission of geo-materials is positively related to the material's fracture and deformation. A reasonably good correlation between fracture energy ( $E_{\text{fracture}}$ ) and acoustic emission (AE) energy ( $E_{\text{acoustic}}$ ) was found by Landis on mortar specimens (Landis and Lucie 2002). Shkuratnik et al. found that acoustic emission is positively related to the compression stress applied to a coal specimen (Shkuratnik, Filimonov et al. 2004, Shkuratnik, Filimonov et al. 2005). The uniaxial compression tests of Australian coal specimens, conducted by Ranjith et al., also led to the same conclusions as that of Shkuratnik (Ranjith, Jasinge et al. 2010). Figure 3.2 describes the acoustic emission signals detected in our laboratory during the loading process of tension failure applied to a coal specimen. As shown in Figure 3.2, rich acoustic emission signals were received by the acoustic emission monitoring system. Hence, coal and other geo-materials release a large amount of fracture energy at the failure point. This energy is consumed by the growth of the micro-fracture (Yamada, Masuda et al. 1989). It was pointed out by

some researchers that geo-materials receive no energy input from outside at the failure point (Xie, Ju et al. 2005). Therefore, the fracture energy dissipated at the failure point is from the internal elastic energy stored in coal, which also explains why kinetic energy accounts for less than 1% of the total elastic energy. Furthermore, other energy dissipation forms, including electromagnetic-emission energy ( $E_{em}$ ), microseismic energy ( $E_{seismic}$ ), and thermal-radiation energy ( $E_{thermal}$ ), are also positively related to fracture energy (Yamada, Masuda et al. 1989, Zhao, Jiang et al. 2007, Amitrano, Arattano et al. 2010, Verdon, Kendall et al. 2011, Song, Wang et al. 2012, Li, Wang et al. 2016). It is worthy of note that all of these forms of energy correspond to the energy dissipation at, and just after, the failure point of coal.

During coal bursts, the movement of ejected coal consumes elastic energy, termed coal ejection energy ( $E_{ejection}$ ). Some of the elastic energy may remain stored in the coal even after the coal burst, which is herein referred to as residual energy ( $E_{residual}$ ). Hence, the conservation of elastic energy during coal burst can be represented by the following equation:

$$E_{elastic} = E_{ejection} + E_{fracture} + E_{acoustic} + E_{em} + E_{seismic} + E_{thermal} + E_{residual} \quad (3.1)$$

Generally, the accumulation of elastic energy results from gravitational stress ( $E_{gravity}$ ), tectonic stress ( $E_{tectonic}$ ), concentrated stress ( $E_{concentrated}$ ), and dynamic stress ( $E_{dynamic}$ ) (Zhang, Canbulat et al. 2017, Skrzypkowski 2018). Hence, the complete balanced equation for energy in an underground coal body can be written as follows (Skrzypkowski 2018):

$$E_{gravity} + E_{tectonic} + E_{concentrated} + E_{dynamic} = E_{elastic} + E_{plastic} \quad (3.2)$$

During the gentle failure of coal, most of the elastic energy dissipates into other forms of energy, excluding that of coal ejection. Coal can be ejected from the surrounding areas of the underground space, forming burst hazards when its energy is high enough.

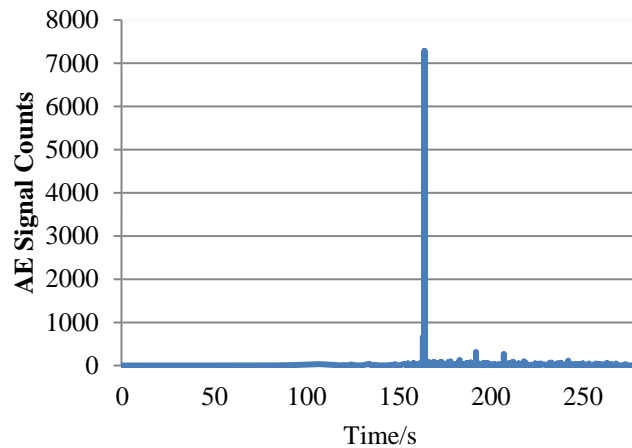


Figure 3. 2 Acoustic emission signal of the tensile failure in coal

### 3.3 Energy Accumulation

The energy accumulation of coal burst is dominated by specific geological conditions such as mining depth, roof and floor stiffness, seismicity events, and coal properties. It was found by Kelly that many coal-mining projects in Australia have inadequate or incorrect geological assessments (Whyatt 2008). An explanation of the contribution of these factors to the accumulation of elastic energy can be helpful for Australian coalmines to evaluate the risk of coal burst occurrence, according to their geological conditions.

#### 3.3.1 Mining Depth

The increase in the severity and frequency of coal burst with mining depth was found by researchers worldwide (Whyatt 2008, Iannacchione and Tadolini 2016, Christopher 2017, Vardar, Tahmasebinia et al. 2017). Mining depth can directly contribute to the increase in risk of coal burst from two aspects. Firstly, coal is under high gravitational stress, and becomes more prone to failure as gravitational stress increases with mining depth. Additionally, the high gravitational stress results in more energy being introduced into

the coal body. The mechanical properties of coal resources found deeper underground are more brittle and more prone to burst. The geological features associated with deep mining are more complicated, and are also often related to hard sandstone roofs (Whyatt 2008), which can further result in a large accumulation of energy in the geological structure. According to an investigation based on documented cases of coal burst in Poland, Russian, and China, the risk of coal burst increases sharply when the mining depth extends beyond 500 m (Dou, Zhao et al. 2006). The mining depths of the Appin coalmine and the Austar coalmine (the sites of two incidents of coal burst in Australia) are both around 550 m (Hebblewhite and Galvin 2017). However, it should be noted that coal burst can also occur at shallow depths if the stored energy in the coal seam is high enough, which is often related to complicated geological structures such as faults and folds.

### **3.3.2 Stiffness**

Stiffness of the roof and floor is one of the main factors giving rise to coal burst (Vardar, Tahmasebinia et al. 2017). Experimental study also proved that the surrounding rock stiffness had an obvious influence on the failure mode of the coal specimen (Huang and Liu 2013). The influence of the surrounding rock stiffness on coal burst was deduced based on mining experience and laboratory studies. Generally, coal tends to fail violently when the stiffness of the roof and floor is high. A theoretical explanation of the influence of stiffness can be easily derived from the aspect of energy. The definition of stiffness is given as:

$$K = F/L \quad (3.3)$$

where  $K$  is stiffness of the material,  $F$  is the compression force applied to the material, and  $L$  is the displacement caused by the applied force.

According to Newton's third law, the force between the roof and the floor has the following relationship:

$$F_{\text{roof}} = F_{\text{coal}} \quad (3.4)$$

where  $F_{\text{roof}}$  is the force applied to the coal seam by the roof, and  $F_{\text{coal}}$  is the reaction force applied to the roof by the coal.

In terms of the roof, the energy input from the coal can be described as:

$$E_{\text{roof}} = F_{\text{coal}} \times L_{\text{roof}} \quad (3.5)$$

where  $E_{\text{roof}}$  is the energy flowing from the coal to the roof, and  $L_{\text{roof}}$  is the displacement caused by  $F_{\text{coal}}$ .

In terms of the coal seam, the energy input from the roof can be described as:

$$E_{\text{coal}} = F_{\text{roof}} \times L_{\text{coal}} \quad (3.6)$$

where  $E_{\text{coal}}$  is the energy flowing from the roof to the coal, and  $L_{\text{coal}}$  is the displacement caused by  $F_{\text{roof}}$ .

In most cases, the stiffness of the roof is higher than that of the coal:

$$K_{\text{roof}} > K_{\text{coal}} \quad (3.7)$$

where  $K_{\text{roof}}$  is the stiffness of the roof, and  $K_{\text{coal}}$  is the stiffness of the coal.

Consequently, the displacement of the coal is larger than that of the roof:

$$L_{\text{coal}} > L_{\text{roof}} \quad (3.8)$$

Hence, the final flow of energy flow goes from the roof to the coal:

$$E_{\text{coal}} > E_{\text{roof}} \quad (3.9)$$

Based on the above analysis, the direction of energy flow between the coal and the roof is controlled by their difference in stiffness. As the difference in stiffness between the coal and the roof increases, more energy will flow into the coal seam. This also explains why a hard roof presents a complicated problem for coalmines, as more energy will be transferred from the roof to the coal seam under these conditions. Similarly, the stiffness of the floor also has the same influence on coal. As shown in Figure 3.3, a high stiffness

of the surrounding rock can lead to sudden and violent uncontrolled post-failure behaviour (Vardar, Tahmasebinia et al. 2017).

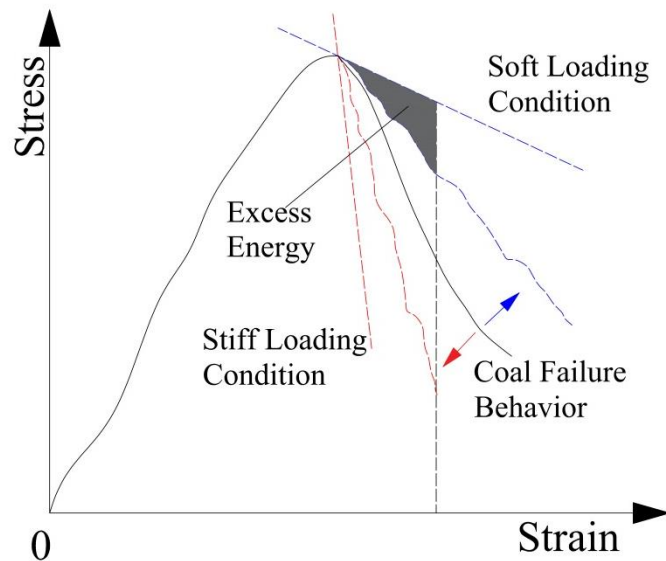


**Figure 3. 3 Effect of stiffness of the loading system on the behaviour of coal failure**

### 3.3.3 Seismicity

Seismicity is a common phenomenon associated with mining and tunneling activities. As shown in Figure 3.4, seismic waves, which are released by artificially triggered or naturally induced seismicity, can introduce a surprisingly high level of stress on the coal in a very short time. Hence, massive seismic energy is transferred to the coal. Furthermore, it is clear that the stress-bearing ability and the energy-storage capacity of coal are both positively correlated to the loading rate (Okubo, Fukui et al. 2006, Li, Zhou et al. 2016). Therefore, coal burst resulting from seismicity events are more dangerous and destructive. A detailed explanation of coal burst under superposition of seismicity (dynamic load) and geo-stress (static load) was given by Dou (Li, Dou et al. 2015). An observation of the seismic events in areas featuring occurrences of coal burst revealed that Australian mines experience a significantly lower frequency of seismic activity compared to that of coalmines worldwide (Ahn, Zhang et al. 2017), which may explain why coal bursts appear less devastating in Australia.

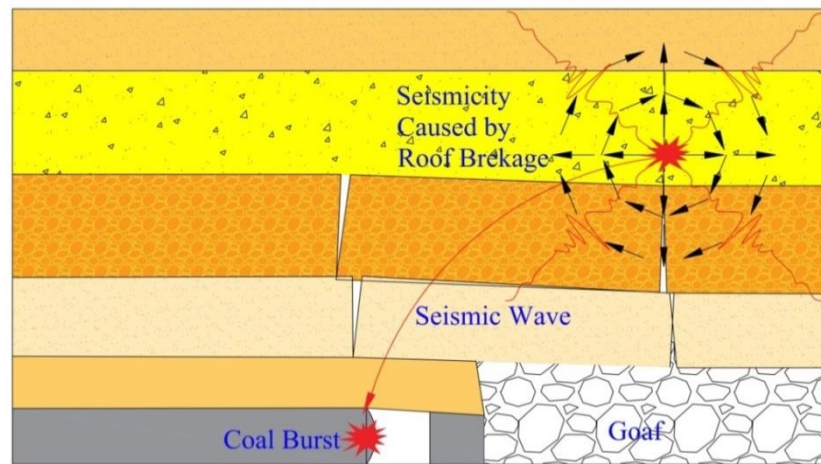


**Figure 3. 4 Influence of a dynamic load caused by seismicity on a coal burst (Li, Dou et al. 2015)**

### **3.3.4 Elasticity**

Coal seams demonstrate different mechanical behavior in response to the same loading path, due to differences in physical and chemical properties. As discussed above, it was found that coal burst often occurs in coal seams with high elastic energy. Hence, the elasticity of coal contributes to the formation of coal bursts. Laboratory tests introduced in Chapter 4 also found that coal seams which have a history of coal bursts show good elastic behavior. Some coal specimens were collected from New South Wales and Central Queensland in Australia. Specimen 1 and specimen 2 were from the Bulli seam in New South Wales, which is at a depth of 550 m. The coal burst at the Appin coalmine occurred in the Bulli seam. Specimen 3 and specimen 4 were from a coal seam with a depth of 250 m. All specimens were cut and ground into pieces with a 50 mm diameter and a 100 mm length, before being subjected to a cyclic loading path with a control loading rate featuring a displacement of 0.1 mm/min. As shown in Figure 3.5, the elastic energy accounted for a larger percentage during the loading processes of specimen 1 and specimen 2. Furthermore, the post-failure behaviors of specimen 1 and specimen 2 were gentler and less brittle. To evaluate the elastic behavior of coal seams, various indices and methods were put forward by scholars. The coal burst propensity index, which includes four

indices proposed by Russian, Polish, and Chinese scholars, is a widely adopted method of evaluating the elasticity of coal (Kidybiński 1981, Guo, Tan et al. 2017). It is recommended by many researchers worldwide that the elasticity of coal seams should be evaluated.

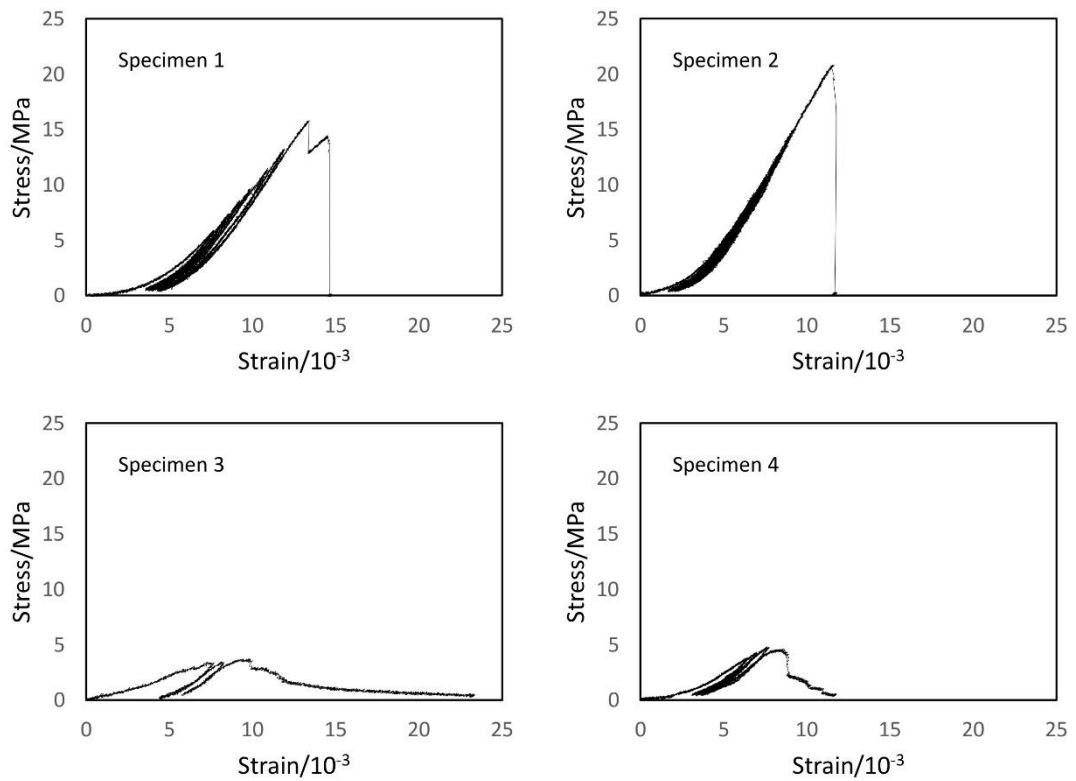


**Figure 3. 5 Strain–Stress curves of coal specimens subjected to cyclic loading**

### **3. 4 Energy Dissipation**

Some phenomena may be likely precursors of the catastrophic failure of coal prior to the occurrence of coal burst, which can potentially serve to mitigate the associated hazards.

#### **3.4.1 Bulking**

Massive ejected bodies of coal with high kinetic energies can lead to equipment damage and personal injury. The double fatalities which happened at the Austar coalmine in Australia were caused by ejected coal (Hebblewhite and Galvin 2017). Coal ejections due to coal burst generally last for a very short time, during which massive kinetic energy is

released. However, as a heterogeneous and nonlinear geo-material, coal may feature a concentration of stress in natural occurring areas of structural weakness. As shown in Figure 3.6, solid coal with areas of weakness bulk due to the concentration of stress. Small-scale coal splits can even occur in these areas if the stored energy is large enough. Generally, before the dynamic failure of coal, bulking begins to appear, or an abnormal increase in area is observed.

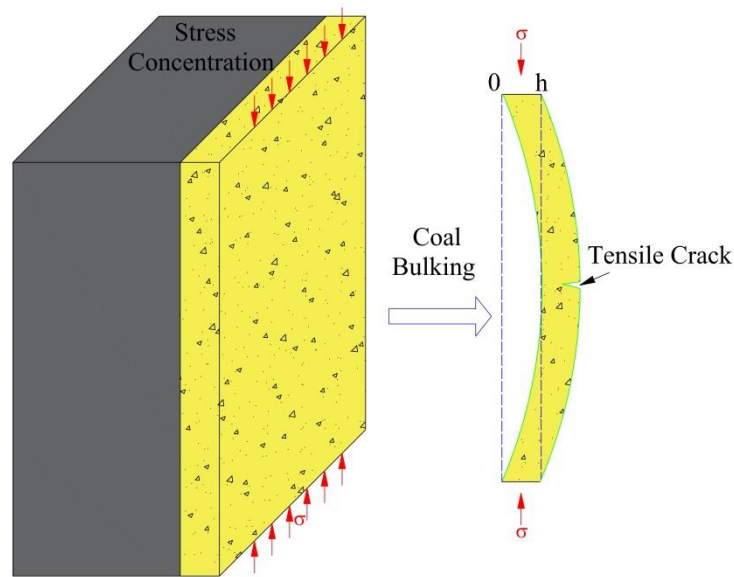


**Figure 3. 6 Schematic diagram of coal bulking caused by a concentration of stress**

### 3.4.2 Acoustic Events

It was found by scholars that acoustic, electromagnetic, and micro seismic events are positively associated with cracks in solid materials (Yamada, Masuda et al. 1989, Trifu and Shumila 2010, Song, Wang et al. 2012). In particular, prior to the dynamic and disastrous failure of coal, the frequency and magnitude of these events increase sharply. Most of these phenomena can only be observed and detected using specific and advanced monitoring equipment. Many coalmines identified as having a high risk of coal burst in Poland, China, and the US utilise various types of equipment to monitor coal fractures. However, the installation and maintenance costs of this monitoring equipment are considerably high. The training process around the use of a forecasting model is also time-

consuming. Hence, in Chapter 7 of this thesis, the coal burst prediction method is proposed based on the fractal dimension analysis of AE spatial distribution. Most coalmines in Australia have no available equipment for the monitoring of coal fractures at this moment. Although most acoustic signals are inaudible without the use of specific sensors, the acoustic events associated with large-scale solid coal fractures can sometimes be heard by the human auditory system. Many mining engineers and workers mention that the dreary sound of coal cracking can be heard in coalmines with concentrations of high stress and energy.

### **3.5 Energy Sources of Coal Burst in Australia**

#### **3.5.1 Static Load**

Mining depth has been identified as an important factor for the formation of coal burst. According to the analysis of coal burst cases in Poland and China, Dou, et al., (Dou, Zhao et al. 2006) found that the first coal burst accidents in coalmines generally happened when mining depth approached 350m and the frequency and severity of coal bursts sharply increased with the mining depth changing from 350 to 600m. Some scholars found that nearly all coal burst accidents in the main coalfields of the U.S. occurred at depths greater than 300m, and most were in excess of 400m (Christopher 2016). The contribution of mining depth to coal bursts mainly result from the increasing gravitational stress. More strain energy will be stored in coal under the high gravitational stress conditions (Dou and He 2001). The mining depth of two coalmines with coal burst accidents in Australia are around 500m (Mine Safety 2016). Hence, the strain energy accumulation lead by high gravitational stress plays an important role in the formation of coal burst accidents in Australia as the mining depth of the coalmines is already beyond the mining depth of the majority of burst accidents revealed by international research. More seriously, almost all coalmines in Australia have plans for deeper mining, which means the stress

environments will be more complicated and more energy will be stored in coal seams (Zhang, Canbulat et al. 2017).

It has been shown by numerous studies that the complicated geological structures caused by folds, faults and coal seam thickness variation have a noticeable influence on the coal burst occurrence (Iannacchione and Tadolini 2016). Dou and He, et al., (Dou and He 2001) found that 72% of coal burst accidents in the Longfeng Colliery were related to faults. The numerical study conducted by Chen, et al., (Chen, Li et al. 2012) found that stress will concentrate near the coal face when the coal face approaches a fault. Christopher (Christopher 2017) found that coal burst accidents in the U.S have a close relationship with faults. Folds, which are created by compressional tectonic stress, may have high residual tectonic stress in the geological structures. Through stress regression analysis at Huanghuiyan Colliery, Jiang, et al., (Jiang, Song et al. 2018) found that stress concentration tends to exist in the area near the syncline axis. The influence of geological structures on stress distribution is shown in Figure 3.7.

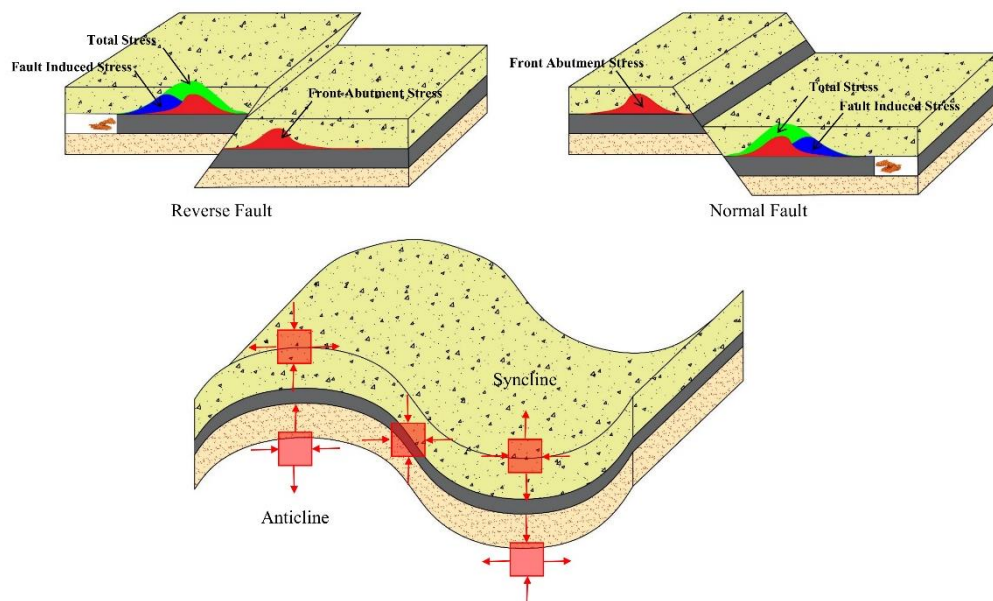


**Figure 3. 7 Stress concentration caused by geological structures (Jiang, Song et al. 2018)**

Compared with the geological conditions of the other main coal mining countries such as China, the U.S. and Canada, most of the coalmines in Australia are in coal seams with simple geological conditions and covered by gentle and ordered sedimentary basins. However, evidence shows that complicated geological structures are involved in the coal burst occurrences in Australia as well. According to the investigative reports published by the NSW Department of Industry, two coal burst accidents that happened in 2014 and 2016 are both in fault zones (Mine Safety 2016, Hebblewhite and Galvin 2017). As well, as shown in Fig.3, these two coal burst accidents also happened in an area with many large faults. The coal burst accidents that happened on 2 February 2018 and 17 May 2018 are also relevant to the geological problems caused by faults. The latest coal burst accidents occurred in the Bulli seam. In general, faults are not intense in the Bulli seam but this seam is often associated with folds and the regional geological structure of this seam is a broad syncline (Hutton 2009). The Bulli seam in the area where coal bursts have occurred is under bad roof conditions caused by orthogonal joints (Brook 2016).

As mentioned above, stiffness of the surrounding rocks is one of the main factors giving rise to coal burst. As shown in Figure 3.8, the Branxton Formation, which generally consists of more than 400 meter thick sandstone and conglomerate units, is described as a strong and massive roof above the Greta seam (Mine Safety 2016). The existence of a high stiffness roof is a potential factor that can cause massive elastic energy accumulation in the Greta seam. However, the Bulli seam in the Illawarra Measures, which is the coal seam mined in the Southern coalfields, is under a weak and highly jointed roof. Hence, there may be no roof above Bulli seam as thick and hard as the Branxton Formation.

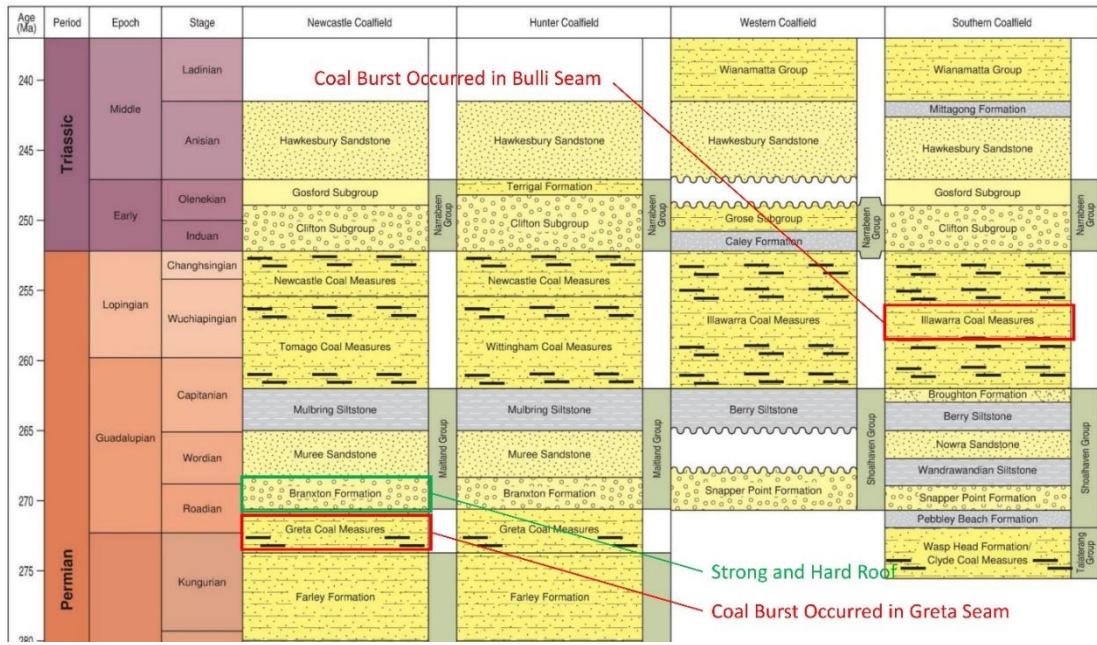


Figure 3.8 Generalized stratigraphic column for the geological Sydney Basin (Herron et al, 2018)

### 3.5.2 Dynamic Load

After the first coal burst accidents occurred in 2014, Ahn et al. (2017) analysed the seismic events that occurred within the New South Wales mining regions from June 2006 to June 2016 and found no clear correlation between coal bursts and the past-recorded seismic events. Geoscience Australia, a preeminent geoscience organization supported by the Australian government, operates a high-quality seismograph network that provides ongoing coverage for locating and recording earthquakes that occur within Australia. Using the earthquake monitoring data published by Geoscience Australia, the seismic events that occurred near coal burst spots from March 2014 to June 2018 are drawn in Figure 6. It is clearly illustrated by the seismic data that there were no monitored seismic events near coal burst spots before and after the coal burst accidents. Hence, there was no large-scale mining induced earthquake in the mining areas when coal bursts were happening. In 2013, the CSIRO established a micro seismic monitoring system at the 2014 coal burst site to monitor the longwall weighting. The field monitoring results clearly demonstrated the effectiveness of micro seismic monitoring to early-warning

longwall caving and weighting events (Shen, Luo et al. 2013). However, most of the micro seismic events recorded by geophones were weak.

### **3.6 Conclusions**

Coal bursts are the catastrophic failures of underground coal, which are closely associated with violent and instant releases of energy. This chapter tried to explain the necessary formation conditions and likely precursors of coal burst in the context of energy, which will provide the basic background of the following chapters. The accumulation and dissipation of energy during coal bursts were analyzed. Based on the analysis, the following conclusions can be drawn:

- (1) Generally, destruction and safety hazards are caused by ejection energy, as a result of the transformation of elastic energy. The accumulation of elastic energy in coal is dominated by geological conditions, such as mining depth, surrounding rock stiffness, seismicity events, and its mechanical properties. Mining depth and seismicity events are sources of energy caused by static loads and dynamic loads, respectively. The influence of these factors on the accumulation of elastic energy was established through energy analysis.
- (2) According to the analysis of stiffness, energy flows from the surrounding rock (high stiffness) to the coal (low stiffness). Hence, for coalmines with stiff roofs and floors, the elastic energy tends to concentrate in the coal seam.
- (3) The elasticity of coal is determined by its capacity and ability to store elastic energy. It is recommended from our laboratory tests that the ability of coal seams to store elastic energy should be evaluated using the coal-burst propensity index prior to commencing the extraction of long-wall faces or roadways. Australian

coalmines can determine their potential risk of coal bursts according to the results of the coal-burst propensity evaluation and other geological conditions.

- (4) Some audible or visible phenomena, such as bulking and acoustic events, may appear prior to the occurrence of coal bursts. These phenomena indicate a concentration of high energy in the body of the coal, suggesting the possibility of imminent coal burst.
- (5) Deep mining and complicated geological structures are the common characteristics of coalmines with coal burst history in Australia. According to international experience, these factors can result in stress and strain energy concentration in coal.
- (6) There is heavy and massive strata above the Greta seam while the roof of the Bulli seam is weak and poor. A high stiffness roof is one of the potential factors which can cause elastic energy accumulation of the Greta seam. But the strong roof may not be a source of strong dynamic load as there is no reported seismic events related to roof weighting.

## **CHAPTER 4 DEVELOPING COAL BURST PROPENSITY INDEX METHOD FOR AUSTRALIAN COAL MINES**

### **Summary**

Chapter four develops the coal burst propensity index method for coal burst risk evaluation in Australian coal mines. The coal burst propensity index method, which is a widely used coal burst risk evaluation method in many countries, includes four indexes related to elastic energy storage and its ability to be rapidly released. The experimental testing of Australian coal specimens is introduced in this chapter. The test procedure, modified risk classification form and improved data analysis method are proposed based on theoretical and experimental study.

### **Citation**

This chapter is based on the paper published in *International Journal of Mining Science and Technology* with the following citation:

Yang XH, Ren T, Tan LH, Remennikov AM & He, XQ, Developing coal burst propensity index method for Australian coal mines. *International Journal of Mining Science and Technology*, 2018, 28(5), 783-790. doi: 10.1016/j.ijmst.2018.08.008

## **Abstract**

Coal burst is the violent failure of overstressed coal, and it is often accompanied by sound, coal ejection and seismic events. It is subsequently recognized as a serious safety risk in Australia after double fatalities due to coal burst occurred at the Austar coal mine. Considering the increasing trend of coal burst severity and frequency with mining depth, there is an urgent need to develop coal burst risk assessment methods for Australian underground coal mines. The coal burst propensity index method is a widely used method of burst risk evaluation of coal as it was developed based on the coal burst research and practice of many countries. This chapter presents the experimental and theoretical research of the coal burst propensity index method for coal burst risk assessment in Australia. The definition of the four indexes including the elastic strain energy index ( $W_{ET}$ ), bursting energy index ( $K_E$ ), dynamic failure time ( $DT$ ) and uniaxial compression strength ( $R_C$ ) is introduced in the first part of this chapter. Then, the standard laboratory test process and test parameters of the coal burst propensity index are presented. The  $DT$  test is conducted with a 0.3 mm/min displacement control loading rate while another test is at 0.5 mm/min. Besides this, the data processing and risk classification method of burst propensity index is improved. Differentiate analysis of the stress-strain curve is adopted in the data processing of the  $DT$  and  $K_E$  index. A four-level risk classification form of burst risk is recommended for Australian underground coal mines. Finally, improvements of the  $W_{ET}$  test, including volumetric strain indicator method and theoretical calculation method, are discussed.

## **Keywords**

Coal Burst; Coal Burst Propensity; Risk Evaluation; Underground Mining

## 4.1 Introduction

Coal burst is recognised as a serious safety risk for Australian coal mines after coal burst fatalities occurred at the Astar Coal Mine (Calleja and Nemcik 2016, 2017). Because of insufficient coal burst experience, it is difficult to find mature theories and technologies in Australian to explain, predict, monitor, or control coal burst. Many researchers believe that the severity and frequency of coal burst increase with increasing mining depth, hence there is an urgent need to develop the coal burst risk assessment and risk mitigation technology for Australian underground coal mines (Dou and He 2001, Braeuner 2017). Coal burst is a serious safety issue that many countries have faced for decades. To avoid casualties caused by coal burst, extensive study has been made in this area by scholars worldwide. Based on analysis of energy balances associated with the crack propagation process, Bieniawski proposed that elastic energy is associated with the violent failure of rock (Bieniawski 1967). Kidybiński found that coal's ability to store and rapidly release elastic strain energy seems to be a fundamental condition of coal burst (Kidybiński 1981). As pointed out in Chapter 3, coal burst is the process of accumulation and dissipation of elastic energy. Different coal seams' ability to store and rapidly release elastic strain energy differs because of the difference in the mechanical properties of the various coal seams. These particular mechanical properties which cause distinct coal burst performance of coal seams is called the coal burst propensity by scholars (Czeczewska and Zuo 1986).

Based on the analysis of stress-strain curves of coal specimens under uniaxial compression stress, several special indices have been published by different researchers to evaluate coal burst propensity. Russian and Poland coal mines adopted the elastic strain energy index and bursting energy index to evaluate coal burst propensity (Pan 1999, Braeuner 2017). Zhang et al. believed that the duration of the failure process is the

comprehensive reflection of energy accumulation and dissipation characteristics of coal (Zhang, Wang et al. 1986). They proposed dynamic failure time to evaluate coal burst propensity. Based on the correlation analysis of mass data, Qi et al. concluded that the uniaxial compression strength of coal is a proper index of coal burst propensity evaluation as well (Qi, Peng et al. 2011). In 2010, the China Coal Industry Association summarized these four indices as bursting liability indices of coal and published the standard test methods of these four indices. Some researchers adopted these four indices to evaluate the burst propensity of rock as well (Cai 2016). It was proved by Russian, Polish, and Chinese experience that these four indices are good indicators to define the burst risk of a coal seam. In this thesis, these four indices are named the coal burst propensity index. How this coal burst propensity index method can be adopted to evaluate coal burst risk in Australia is of interest to Australian underground coal mines. To develop the coal burst propensity index methodology for Australian coal mines, experimental and theoretical research is introduced in this chapter. The definition of every index is introduced in Section 4.2. Then the laboratory test process of the coal burst propensity index is presented. Also, data processing and risk classification of tests are introduced. Finally, solutions for the low success rate of  $W_{ET}$  tests are discussed.

## **4.2 Relevant Indices**

The coal burst propensity index method includes four indices which are the elastic strain energy index ( $W_{ET}$ ), the bursting energy index ( $K_E$ ), the duration of dynamic fracture ( $DT$ ) and the uniaxial compression strength ( $R_C$ ) (National Standards of the People's Republic of China 2010). These four indices are proposed by different scholars and every index represents a particular property related to the elastic energy of coal.

### 4.2.1 Elastic Strain Energy Index

The elastic strain energy index ( $W_{ET}$ ) is an indication of the proportion of elastic energy storage of coal when coal is near critical stress. Descriptions of this index have been given by Kidybiński (Kidybiński 1981, Braeuner 2017). As shown in Figure 4.1a, coal is loaded until the stress reaches 80%-90% of the ultimate strength and then unloaded. The elastic strain energy index is the ratio between elastic energy ( $E_e$ ) and plastic energy ( $E_p$ ) (Kidybiński 1981, Singh 1988, Braeuner 2017). The unloading point is around 80% to 90% of the strength as the elastic energy proportion during this period is similar to that at the failure point. The uniaxial compression strength test needs to be conducted first on the coal specimens from the same coal seam to determine the average strength as the  $W_{ET}$  test needs a realistic estimation of 80% of the coal strength. The coal burst energy source is elastic energy while plastic energy is consumed by the permanent deformation of the coal (Jin and Xian 1993, Mou, Dou et al. 2006). A high elastic energy index means a high elastic energy percentage during the loading process. Therefore, the elastic strain energy index can indicate the coal burst risk from the perspective of the elastic energy proportion before ultimate strength.

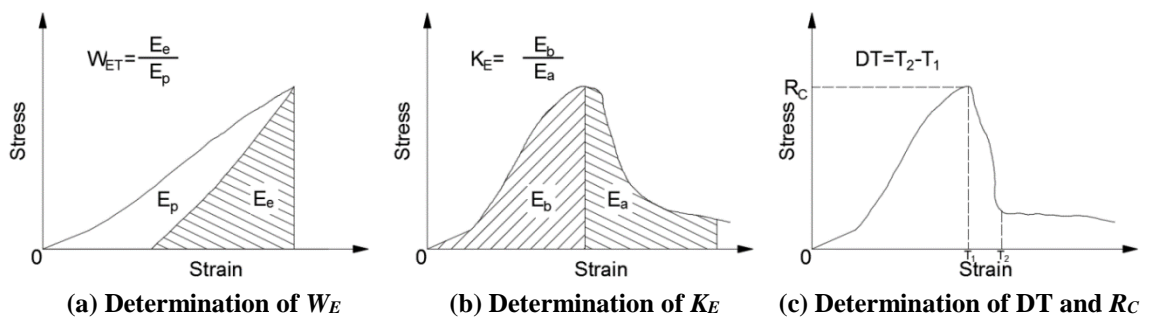


Figure 4. 1 Schematic diagram of coal burst propensity index

### 4.2.2 Bursting Energy Index

The bursting energy index ( $K_E$ ) is called the burst energy coefficient in some papers (Goodman 1989). As shown in Figure 4.1b, a vertical line across the peak value point divides the load-displacement curve of the uniaxial compression test into two parts. The

bursting energy index is the ratio between  $E_b$  and  $E_a$ .  $E_b$  represents the energy storage before peak stress point.  $E_a$  is deformation energy consumed after the peak stress point (National Standards of the People's Republic of China 2010). Different from  $W_{ET}$ ,  $K_E$  is focused on the description of the energy dissipation mode during coal failure. For the coal burst process, the energy equivalence relation can be expressed by the following equation:

$$E_p + E_e = E_{burst} + E_{deformation} + E_{other} \quad (4.1)$$

where  $E_p$  is the plastic energy of coal,  $E_e$  is the elastic energy of coal,  $E_{burst}$  is the coal burst energy,  $E_{deformation}$  is energy consumed by deformation after the peak value and  $E_{other}$  is energy consumed by other energy forms such as acoustic emission, micro seismic and electromagnetic radiation.

According to equation (4.1), coal seams with a low  $K_E$  value will fail gentler as more energy is dissipated by deformation.

### 4.2.3 Dynamic Failure Time

Under uniaxial compression conditions, the duration between ultimate strength to complete damage of the coal specimens is called the dynamic failure time ( $DT$ ) (As shown in Figure 4.1c). The violence of the coal burst is reflected in the instantaneous energy released as well (Zhang, Wang et al. 1986). Therefore, the duration of the destruction time of coal can reflect the severity of energy dissipation during coal failure. Zhang et al. conducted a dynamic failure time test with a 0.5-1.0 MPa/s loading rate on specimens from different coal seams. Based on the test results of 1070 specimens from 11 different coal seams in China and Poland, Zhang et al. concluded 6 typical failure types. The dynamic failure time test results of these 6 types are shown in Table 4.1. According to Table 4.1, dynamic failure time is a simple and efficient index to evaluate coal burst propensity as coal seams with short dynamic failure times are at more of a risk to burst.

**Table 4. 1 Failure time test results of coal specimens from China and Poland**

Type Number	Appearance of Coal Burst in Specific Coal Seams	Failure Time (ms)	Quantity of Specimen
1	Magnitude and frequency both are high (China Coal Seam)	35	34
2	Magnitude and frequency both are high (Poland Coal Seam)	14	23
3	Magnitude and frequency both are high (Poland Coal Seam)	11	35
4	Magnitude is low (China Coal Seam)	254	31
5	Magnitude is low (Poland Coal Seam)	423	39
6	No coal burst appearance (China Coal Seam)	2504	20

#### 4.2.4 Uniaxial Compression Strength

Uniaxial compression strength (As shown in Figure 4.1c) was considered as a coal burst propensity indicator in Polish coal mines (Czeczewska and Zuo 1986, Wan, Liu et al. 1999). Under uniaxial compression conditions, the energy input of coal specimens is equal to the work done by load. The elastic energy input can be expressed as follow (Meng, Han et al. 2015):

$$W = \frac{R_C^2}{2E} \quad (4.2)$$

where  $W$  is the summation of energy input;  $R_C$  the uniaxial compression strength of the coal specimen; and  $E$  is the Young's modulus of the specimen. Based on laboratory testing, the relationship between uniaxial compression strength and young's modulus can be written as follow (Colwell and Frith 2006):

$$R_C = 4.1141E^{0.9176} \quad (4.3)$$

Substituting equation (4.3) into equation (4.2), the relationship between  $W$  and  $R_C$  is drawn in Figure 4.2. It is demonstrated in Figure 4.2 that the elastic energy storage of coal specimens is monotonically increasing with uniaxial compression strength when uniaxial compression strength ranges from 0 to 50. Some scholars found that there is a positive correlation between  $R_C$  and other burst propensity indices(Li 2011, Qi, Peng et al. 2011).

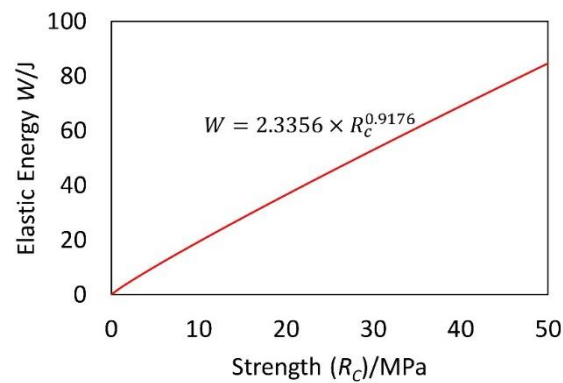


**Figure 4. 2 Correlation between  $W$  and  $R_c$**

### **4.3 Process of Laboratory Test**

#### **4.3.1 Specimen Preparation**

Three groups of cylindrical specimens are prepared with a 55mm diameter and a length of 110mm. Each group of specimens consists of 15 pieces and each group is from the same coal seam. Every group of specimens is subdivided into three equal sets. Coal blocks of Group 1 are soft and gassy coal from central Queensland. Coal blocks of Group 2 and Group 3 are hard coal taken from a coal mine in New South Wales. To maintain the original state of the coal, all coal blocks were wrapped with plastic and aluminum membranes. For ensuring the integrity of the coal specimens, coal blocks are cemented before coring. The coring direction is vertical to the joint of the coal seam. Coal cores are processed into test specimens through the process of cutting and grinding the two ends. All conditions of the specimens, except specimen size, should meet the requirements (parallelism, flatness and verticality) as defined for the uniaxial compression strength method of ISRM (International Society of Rock Mechanics) (Guo, Tan et al. 2017). Strain gauges will be installed on the middle of the specimen along the vertical direction of the specimen. In addition, all specimens should be wrapped with plastic and aluminum membranes and then stored in a room with consistent temperature before testing to eliminate the impacts of humidity, temperature, and other factors. The period of storage should preferably not exceed 30 days.

### 4.3.2 Test Equipment and Procedure

$K_E$  and  $R_C$  can be obtained using the same set of specimens.  $W_{ET}$  and  $DT$  tests each need a separate set of specimens. All the physical information such as diameter, length, color and joints for every specimen shall be recorded before testing. All loading and unloading work is undertaken by the Instron 8033 universal testing machine with displacement control. A picture and the schematic diagram of the loading machine are shown in Figure 4.3 and Figure 4.4. The specific test process for one group is as follows.

$R_C$  and  $K_E$  test: Load one set of specimens at a constant displacement rate of 0.3 mm/min until residual strength. All the data from the loading process should be recorded by the loading system. Then, the average failure force ( $F$ ) of this set will be determined. Finally unloading point  $F_U$  ( $0.8 * F$ ) for the  $W_{ET}$  test will be calculated.

$W_{ET}$  Test: (1) Select the second set of specimens. (2) Load specimen with 0.3 mm/min displacement control loading rate until  $F_U$ . (3) Then unload specimen at the same rate until 1%-5% of  $F$ . (4) Repeat loading and unloading process on this specimen until failure. The maximum load of every round is 5% higher than the previous round. All the data for the loading process should be recorded by the loading system.

$DT$  Test: (1) Select the third set of specimens. (2) Load specimen with a 0.5 mm/min displacement control loading rate until its residual strength.

All the data from the loading process should be recorded by the loading system. The frequency of data collection should be not less than 1 kHz.



**Figure 4. 3 Universal rock testing system**

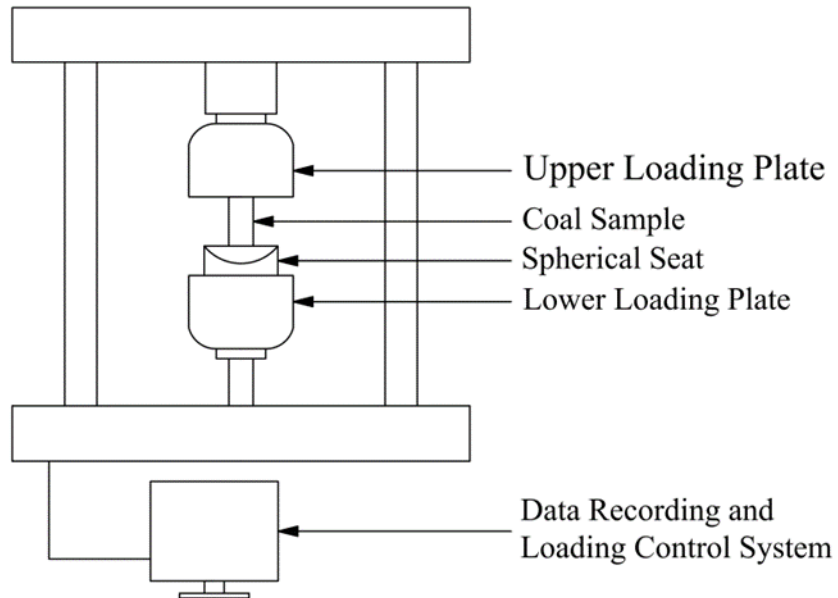


**Figure 4. 4 Schematic diagram of loading system**

## **4.4 Data Processing and Risk Classification**

### **4.4.1 Data Processing**

The process of data analysing involves the adoption of Qtiplot and Microsoft Excel.  $R_c$  and  $W_{ET}$  can be calculated according to the definition of the index introduced in Section

4.1. The determination of the complete damage point is the most important part of the  $K_E$  and  $DT$  calculation. The  $K_E$  calculation method of Type I and Type II is given from the literature (National Standards of the People's Republic of China 2010). However, Figure 4.6, the stress-strain curve of specimen No1 of Group 3, shows another failure type. In this situation, the red arrow point of Figure 4.8 which is the differentiate change-point can be regarded as the complete damage point. This method can be adopted for the  $DT$  calculation as well. All the test results are listed in Table 4.2 to Table 4.4.

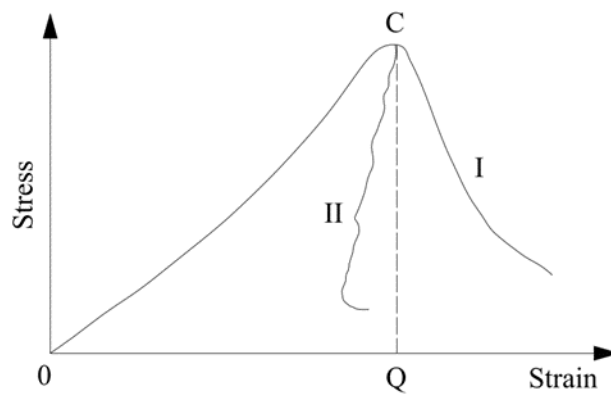


**Figure 4. 5 Typical stress-strain curves**

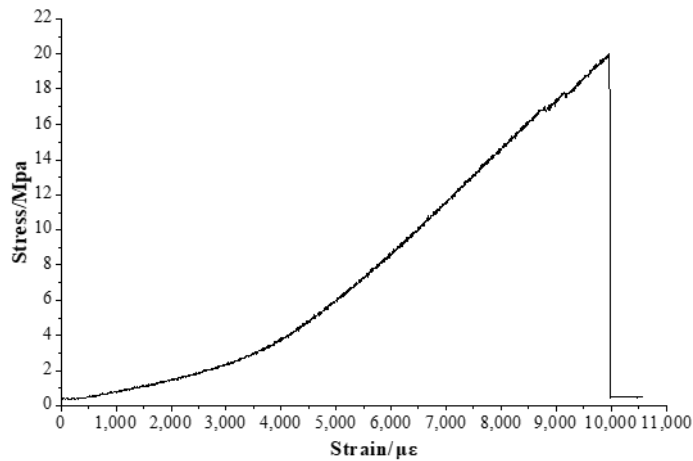


**Figure 4. 6 Stress-strain curve of specimen No1**

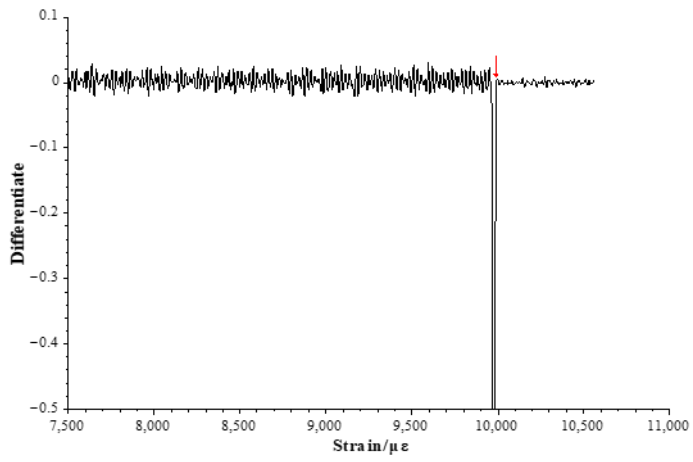
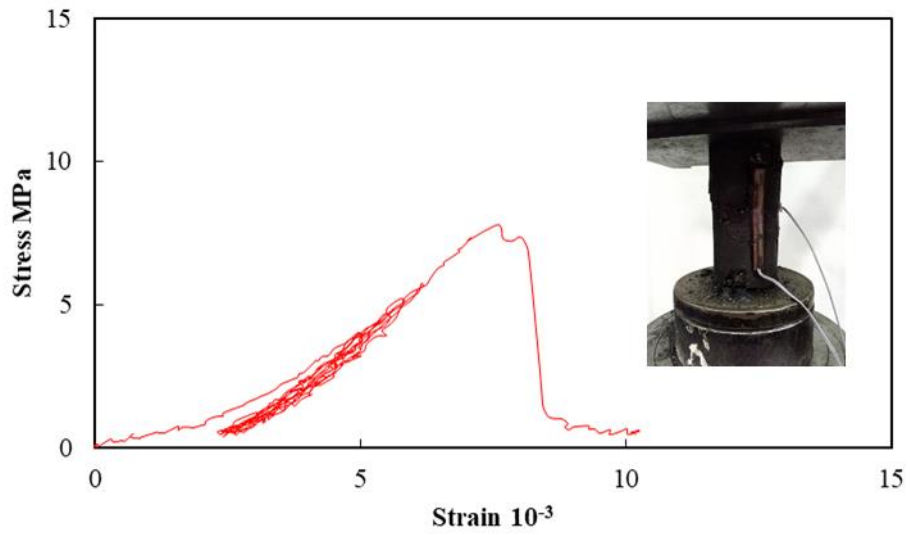
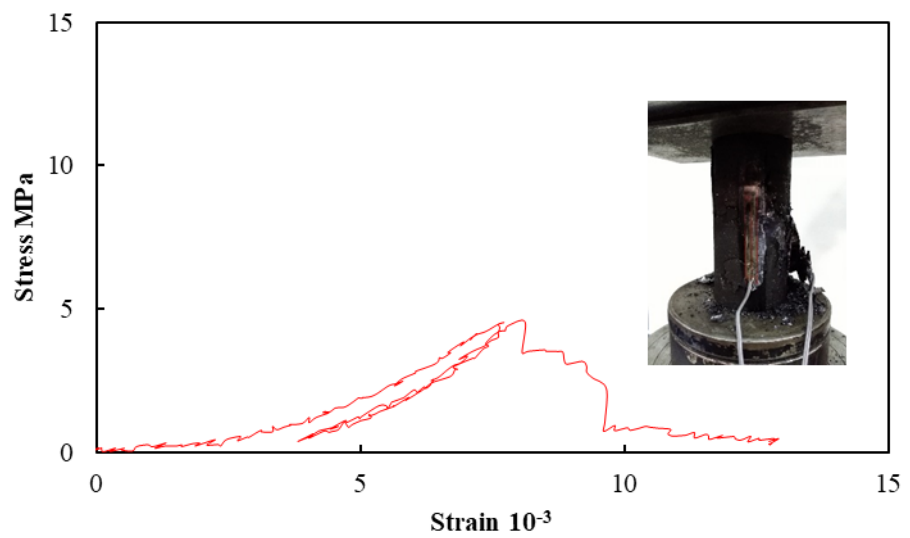


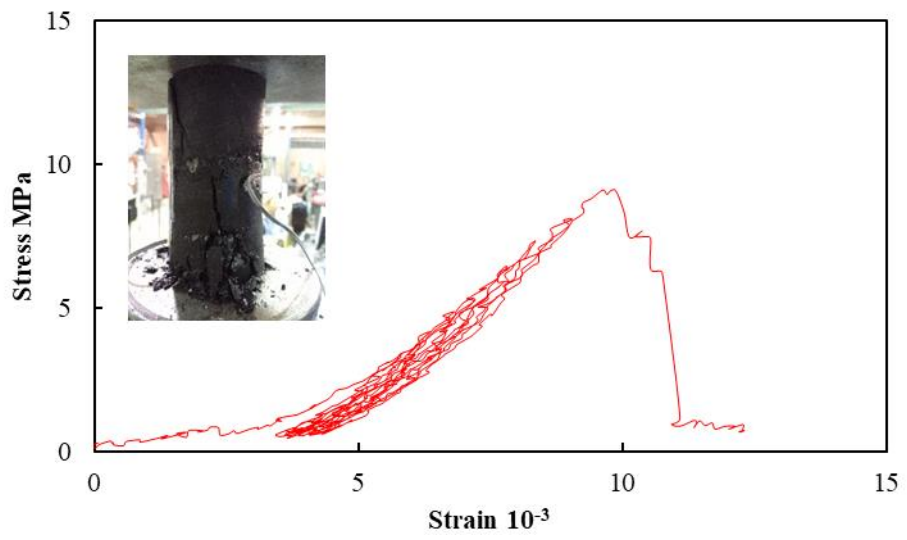
Figure 4. 7 Differentia of stress-strain curve of specimen No1



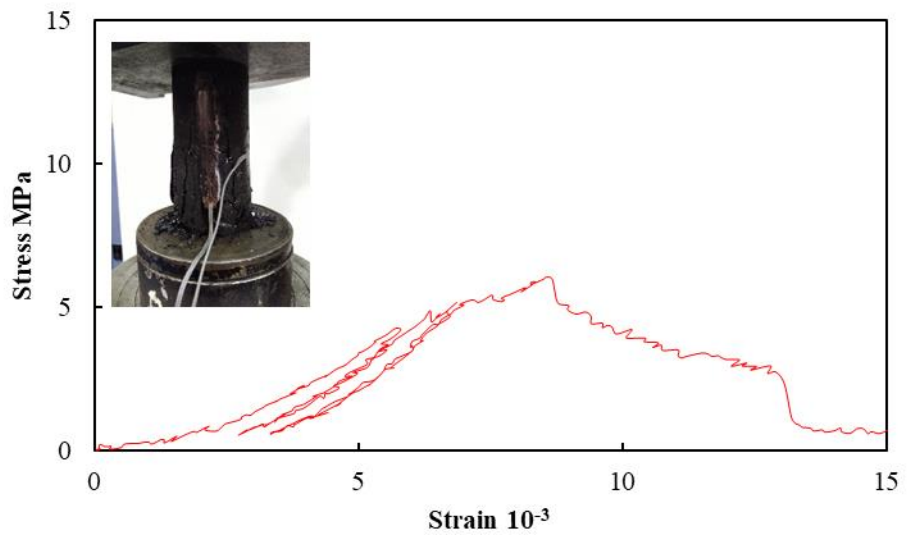
a. W<sub>ET</sub> 1 of Group 1



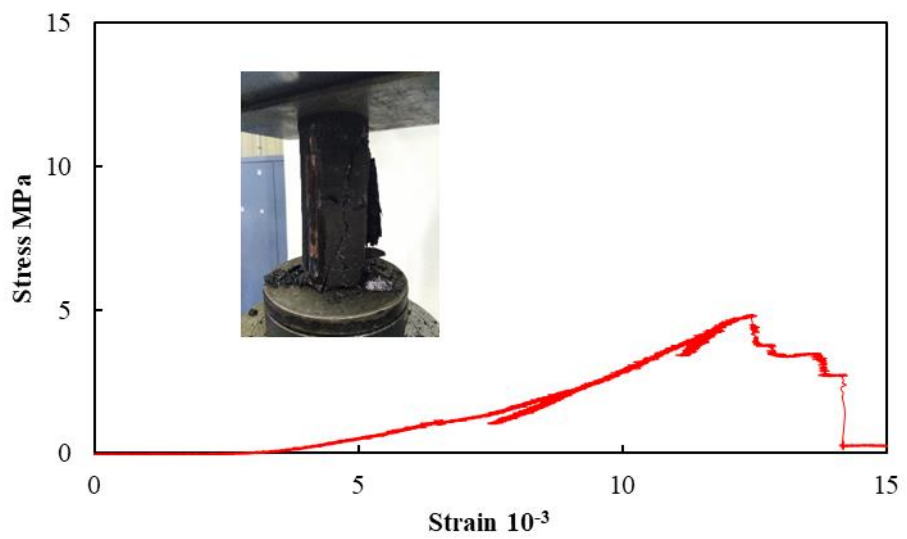
b. W<sub>ET</sub> 2 of Group 1



c. W<sub>ET</sub> 3 of Group 1

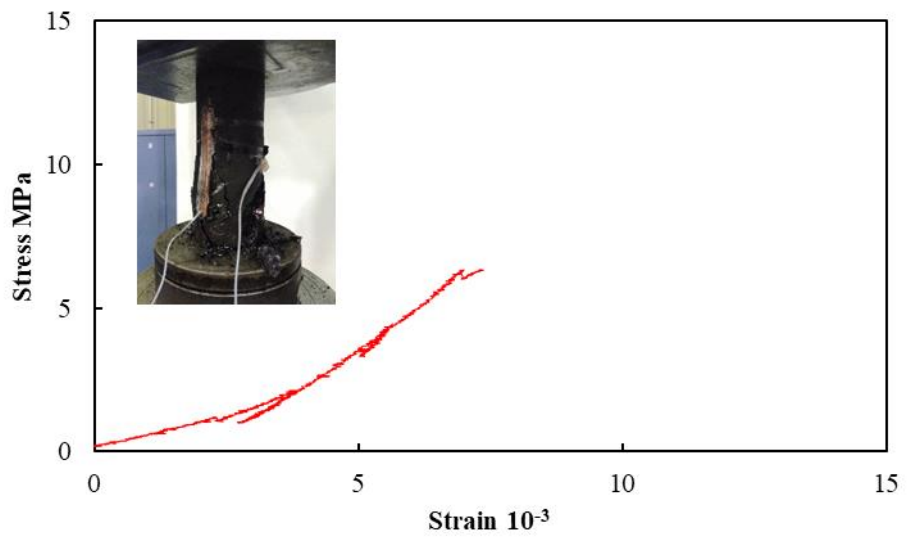


d. W<sub>ET</sub> 4 of Group 1

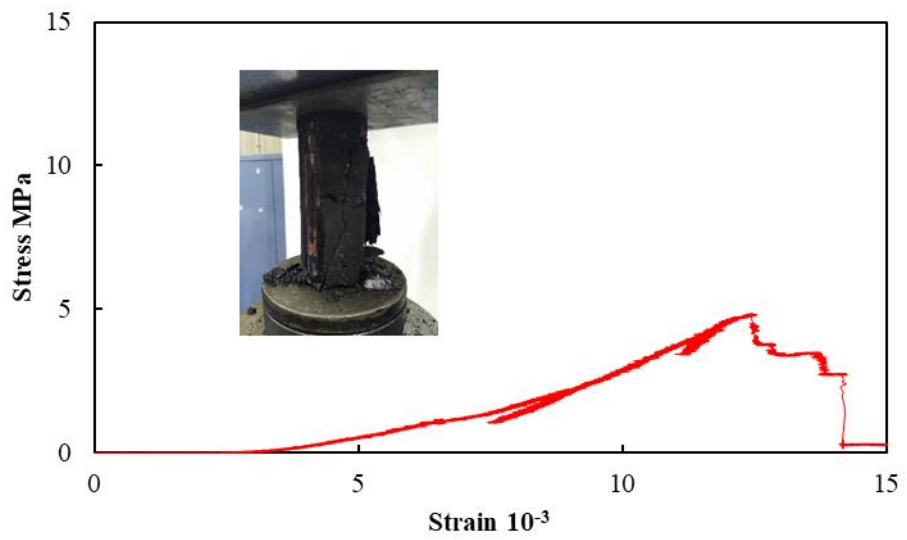


e. W<sub>ET</sub> 5 of Group 1

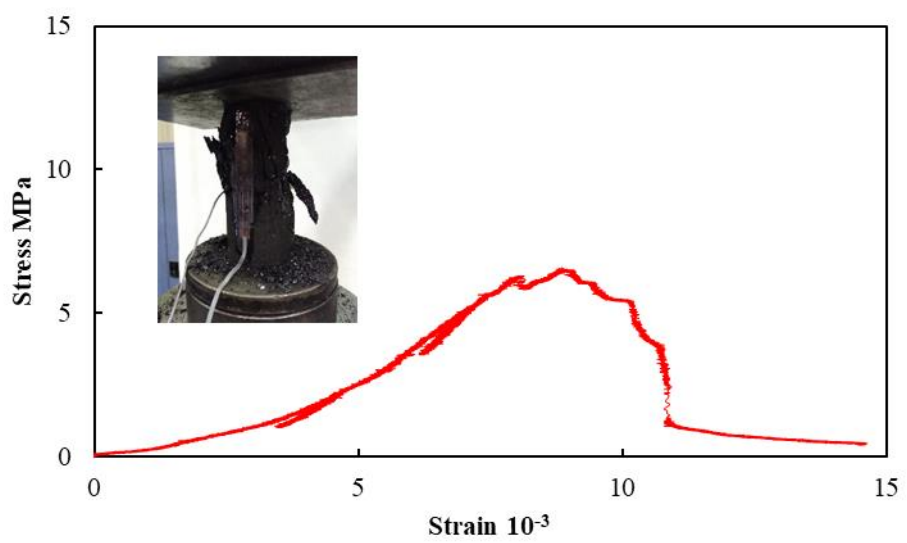
**Figure 4. 8 W<sub>ET</sub> test result of Group 1**



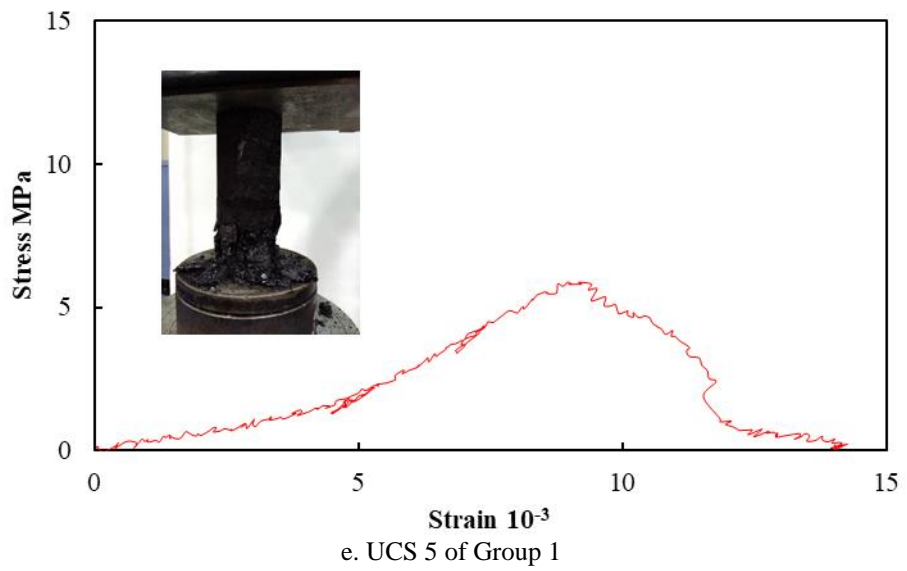
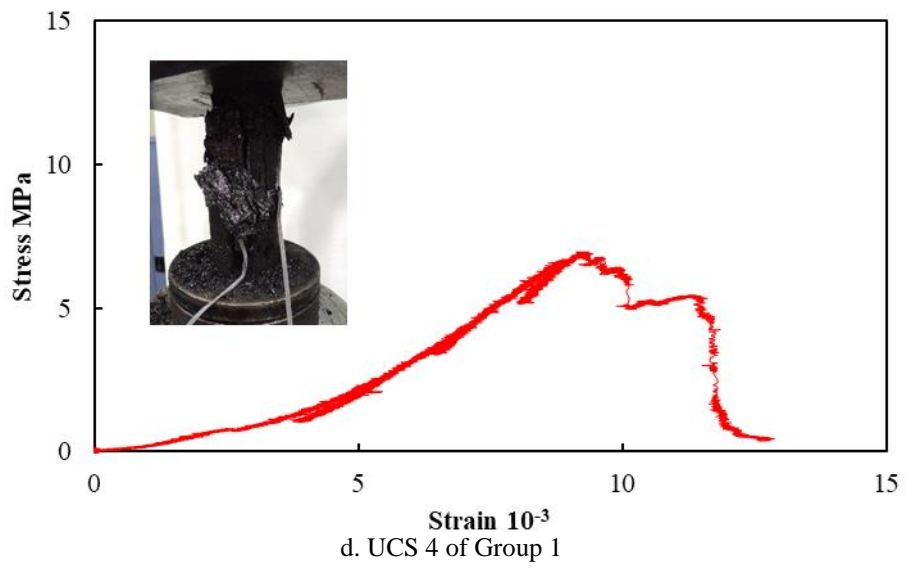
a. UCS 1 of Group 1



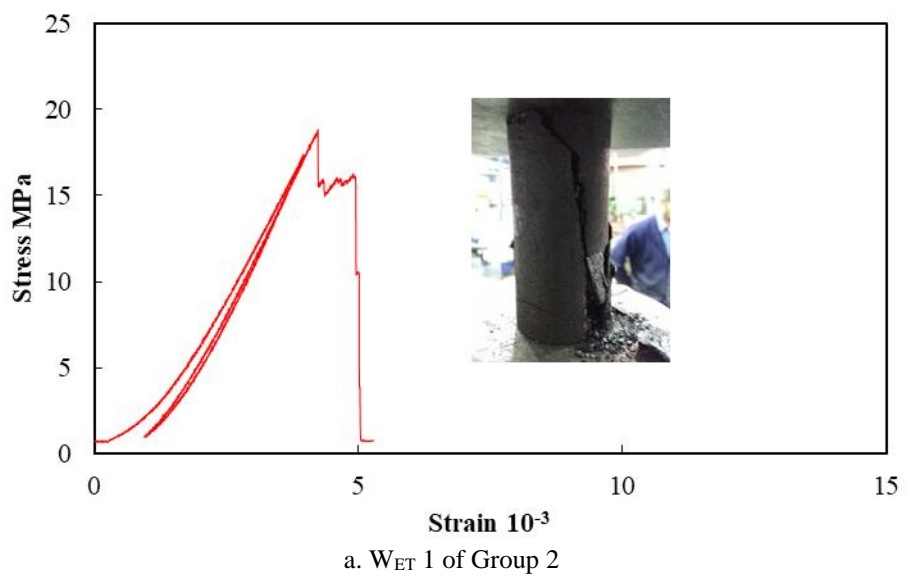
b. UCS 2 of Group 1

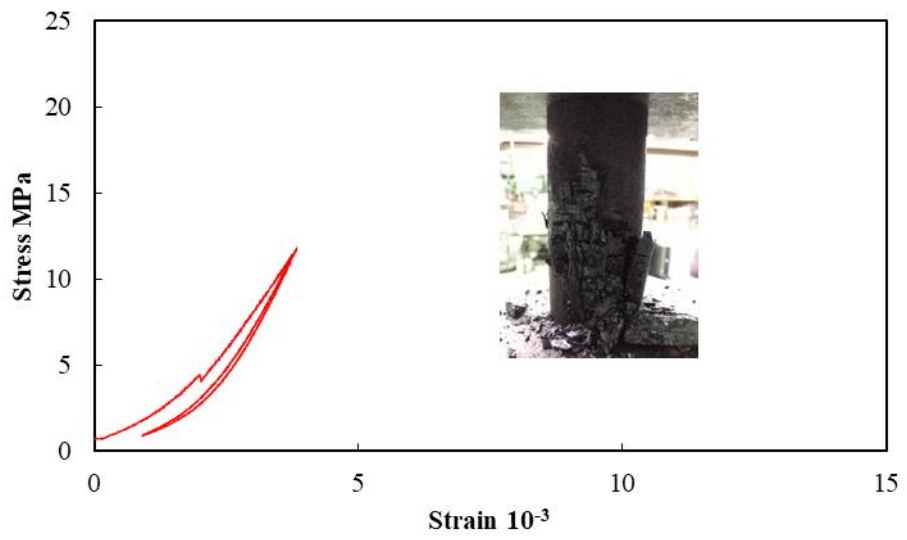


c. UCS 3 of Group 1

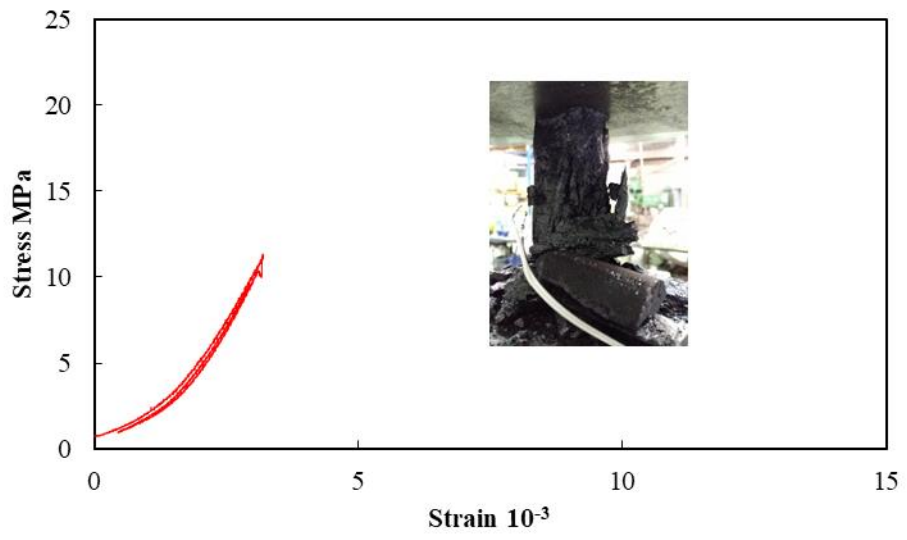


**Figure 4. 9 UCS test result of Group 1**

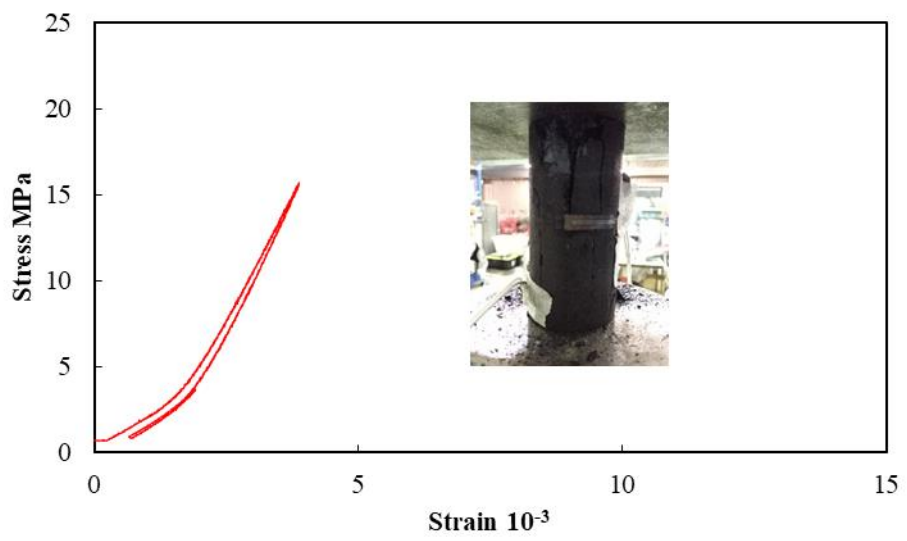




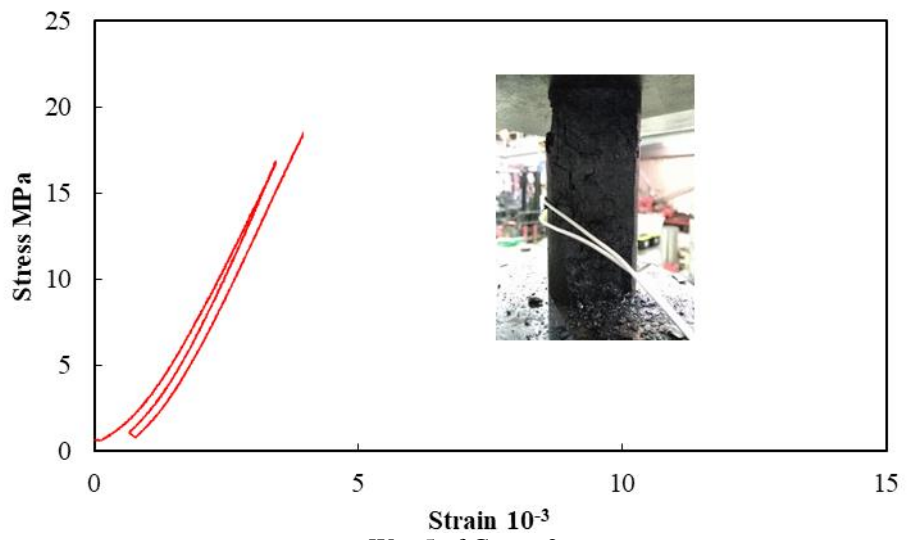
b. W<sub>ET</sub> 2 of Group 2



c. W<sub>ET</sub> 3 of Group 2

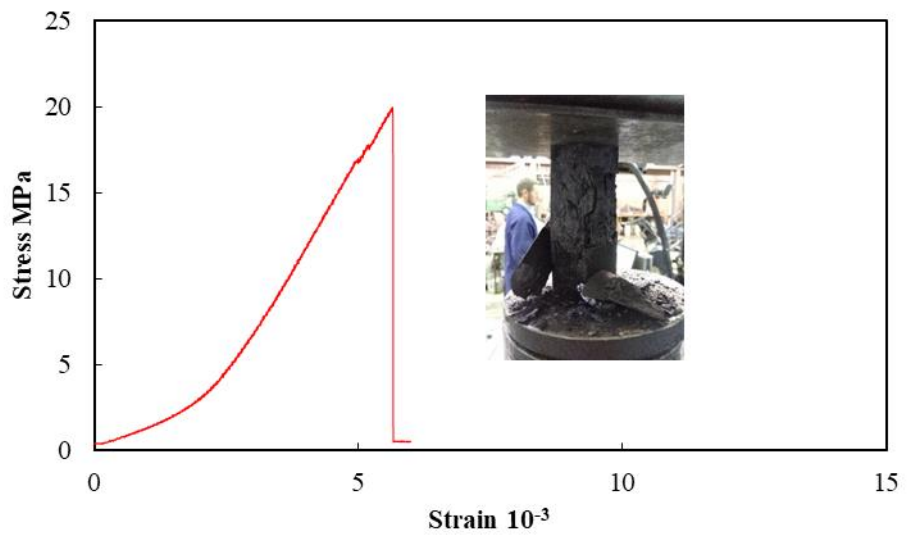


d. W<sub>ET</sub> 4 of Group 2

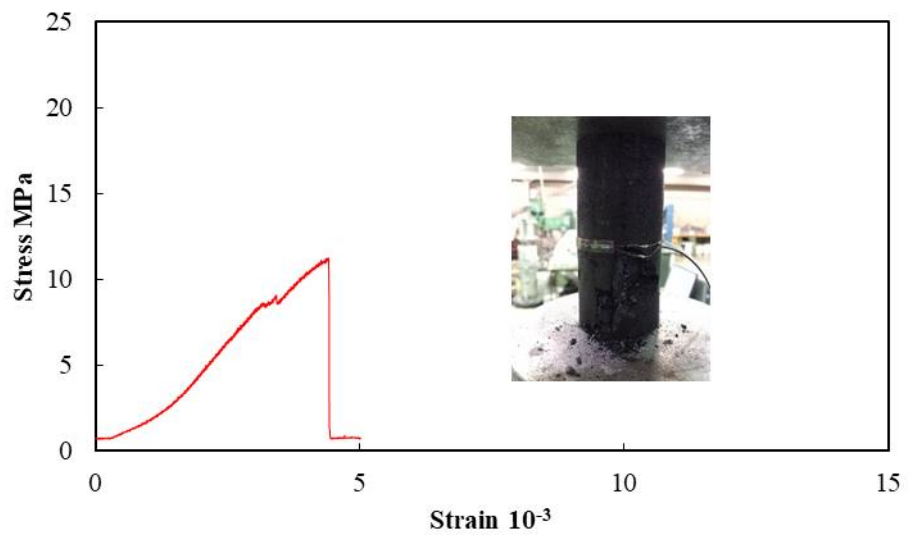


e. W<sub>ET</sub> 5 of Group 2

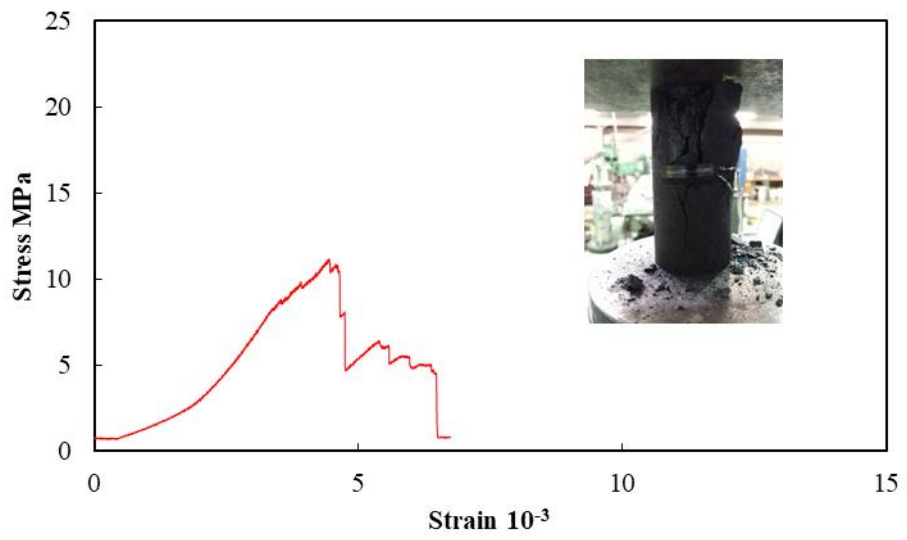
**Figure 4. 10 W<sub>ET</sub> test result of of Group 2**



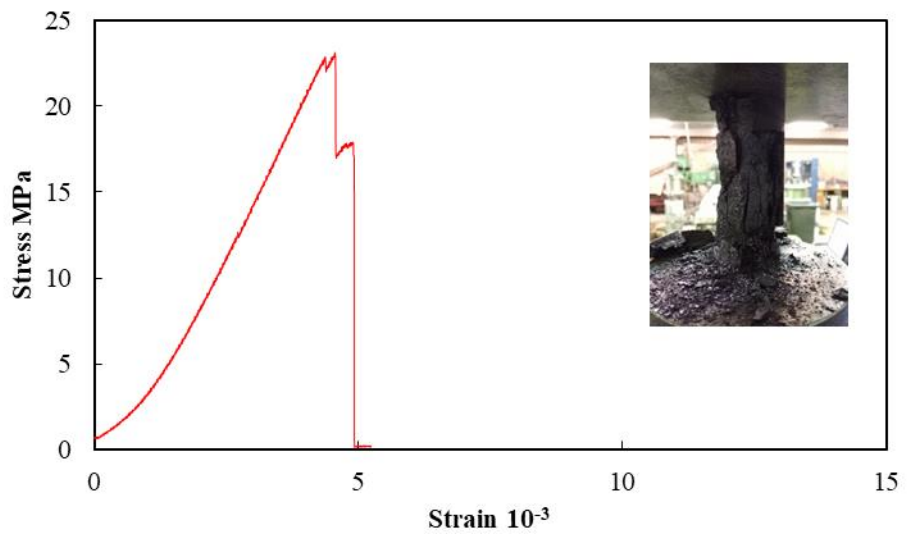
a. UCS 1 of Group 2



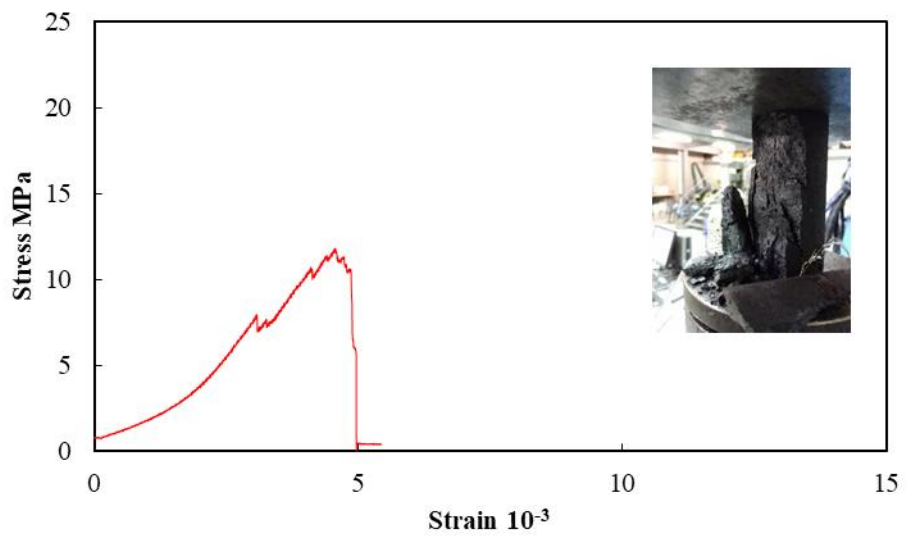
b. UCS 2 of Group 2



c. UCS 3 of Group 2

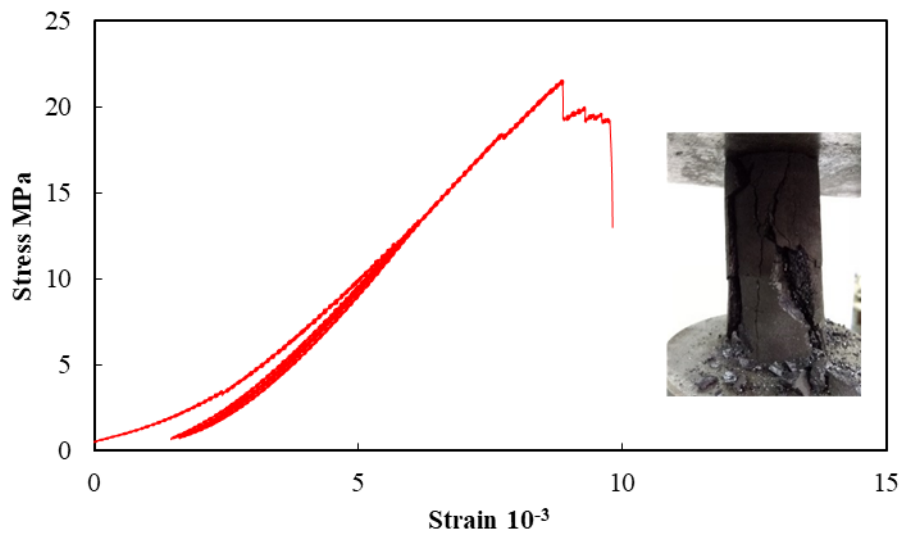


d. UCS 4 of Group 2

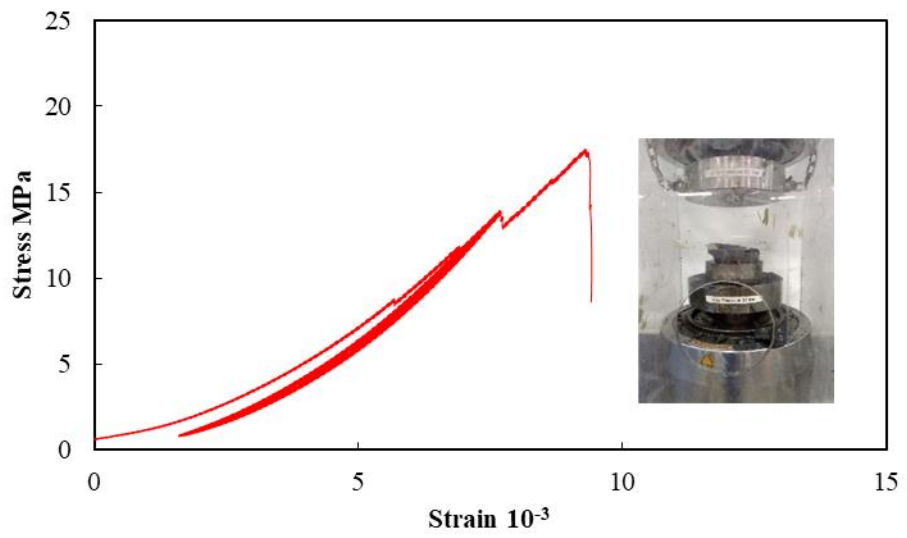


e. UCS 5 of Group 2

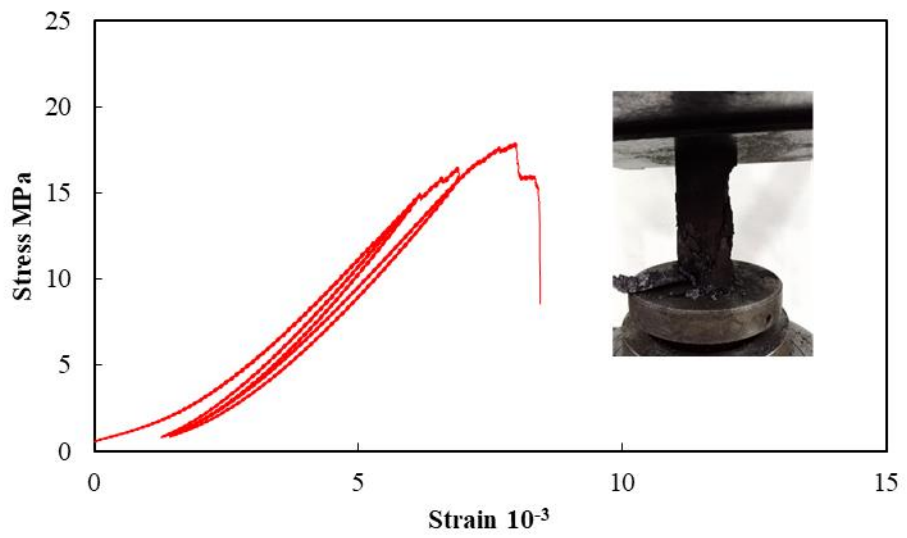
Figure 4. 11 UCS test result of of Group 2



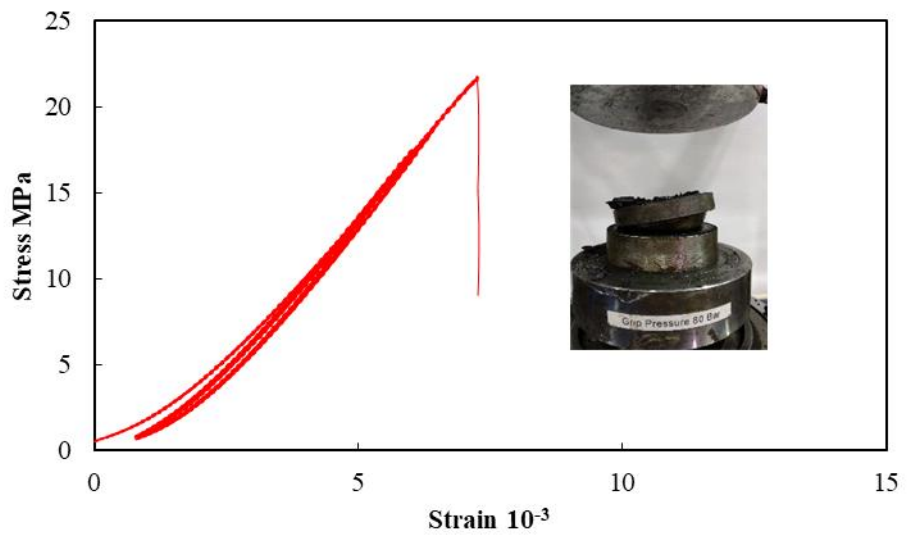
a.  $W_{ET}$  1 of Group 3



b.  $W_{ET}$  2 of Group 3

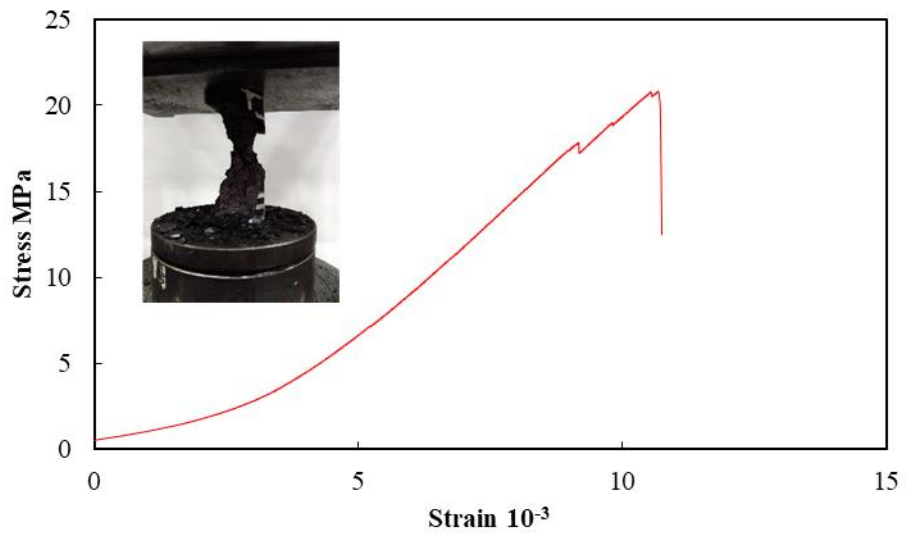


c.  $W_{ET}$  3 of Group 3

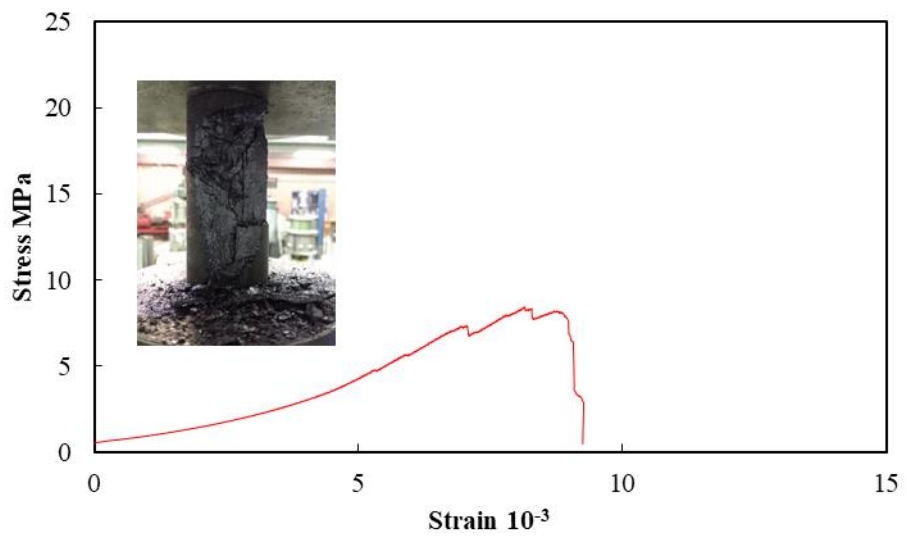


d. W<sub>ET</sub> 4 of Group 3

Figure 4. 12 W<sub>ET</sub> test result of Group 3



a. UCS 1 of Group 3



b. UCS 2 of Group 3

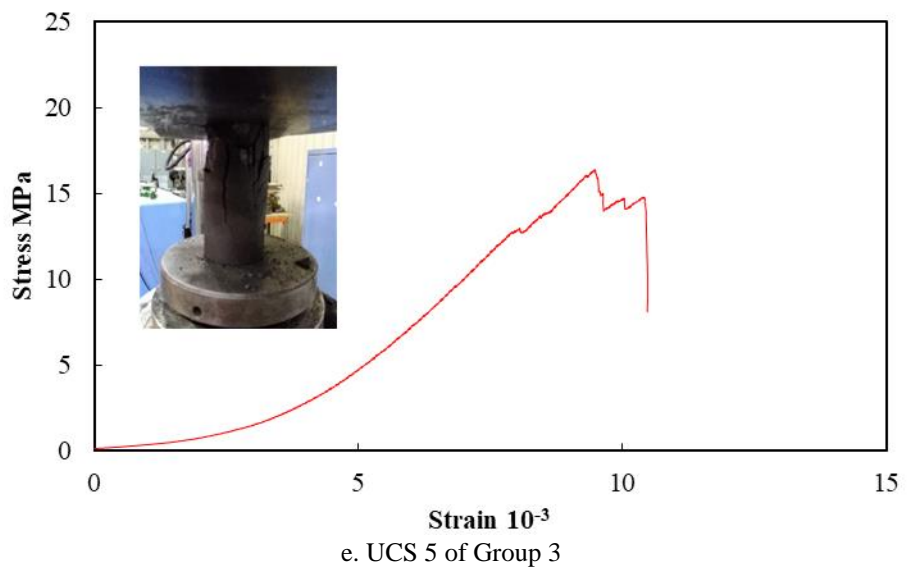
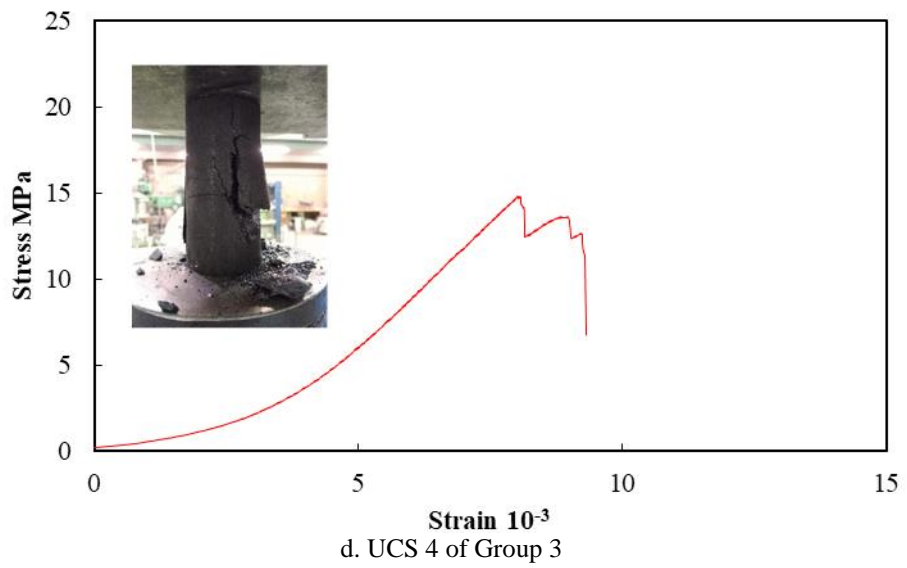
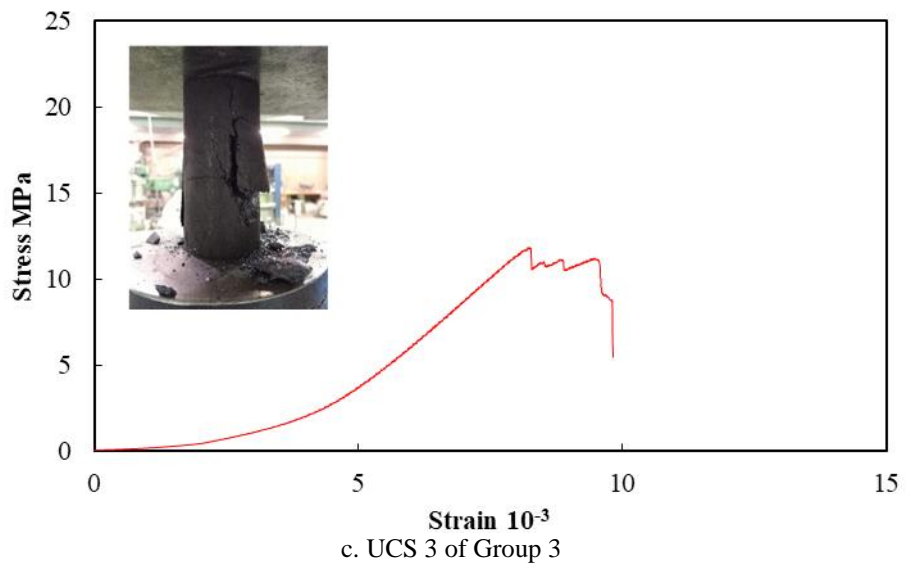


Figure 4. 13 UCS test result of Group 3

**Table 4. 2 Test result of Group 1**

Index	Test Result					Average
$W_{ET}$	2.35	2.33	2.99	2.38	1.46	2.30
$K_E$	2.13	2.99	1.84	1.66	1.54	2.03
$DT/s$	18.99	33.00	33.24	57.60	1.40	28.85
$R_C/MPa$	5.39	4.70	6.38	6.77	7.6	6.17

**Table 4. 3 Test result of Group 2**

Index	Test Result					Average
$W_{ET}$	5.69	2.92	6.34	8.36	8.31	6.32
$K_E$	101.12	2.42	1.66	7.25	5.99	4.33
$DT/s$	2.10	1.00	5.40	12.10	13.40	6.80
$R_C/MPa$	20.01	11.28	11.22	23.20	11.77	15.50

**Table 4. 4 Test result of Group 3**

Index	Test Result					Average
$W_{ET}$	3.21	3.12	3.67	4.65	*	3.66
$K_E$	3.75	68.79	1.77	2.45	3.84	2.95
$DT/s$	0.76	16.16	1.93	8.88	2.67	6.08
$R_C/MPa$	8.48	23.85	11.95	14.84	16.42	15.11

\*Data not logged due to recording system trouble

#### 4.4.2 Risk Classification of Coal/Rock Burst Propensity

These four indices are widely adopted by scholars to determine the burst propensity of coal. Some researchers discuss the application of these indices in the evaluation of rock burst risk as well. However, the risk classification methods vary depending on the literature source. Tables 4.5 to 4.7 are the risk classification methods reported in different literature sources (Zhang, Wang et al. 1986, Mao, Chen et al. 2001, Qi, Peng et al. 2011, Cai 2016).

**Table 4. 5 Coal burst propensity classification proposed by Qi et al**

Burst Propensity	None	Low	High
Index	$W_{ET}$	$W_{ET} < 2$	$2 \leq W_{ET} < 5$
	$K_E$	$K_E < 1.5$	$1.5 \leq K_E < 5$
	$DT/ms$	$DT > 500$	$50 < DT \leq 500$
	$R_C/MPa$	$R_C < 7$	$7 \leq R_C < 14$
			$5 < W_{ET}$
			$5 \leq K_E$
			$DT \leq 50$
			$14 < R_C$

**Table 4. 6 Coal burst propensity classification adopted by Zhang et al**

Burst Propensity	None	Moderate	High
Index	$W_{ET}$	$W_{ET} < 2$	$2 \leq W_{ET} < 5$
	$K_E$	$K_E < 1.5$	$1.5 \leq K_E < 5$
	$DT/ms$	$DT > 500$	$50 < DT \leq 500$
			$5 < W_{ET}$
			$5 \leq K_E$
			$DT \leq 50$

**Table 4. 7 Rock burst propensity classification adopted by Cai**

Burst Propensity		None	Weak	Medium	High
Index	$W_{ET}$	$W_{ET} < 2$	$2 \leq W_{ET} < 3.5$	$3.5 \leq W_{ET} < 5$	$5 \leq W_{ET}$
	$K_E$	$K_E < 2$	$2 \leq K_E < 3.5$	$3.5 \leq K_E < 5$	$5 \leq K_E$

According to Tables 4.5 and 4.6,  $K_E$  and  $W_{ET}$  of Group 1 and Group 3 are at the same level. However, as shown in Figure 4.8, the failure behaviors of specimens from Group 3 are much more violent than that of Group 1. The coal burst propensity level should be consistent with the failure severity of the coal specimens. According to the risk classification in Table 5 and 6, Group 1 and 3 have the same burst propensity. However, it is obvious that the burst behavior of Group 3 is much more severe than Group 2. Hence, Table 4.7 is more suitable for the classifying of burst risk. The adjustments of the risk classification method of  $R_C$  and  $DT$  can be based on the correlation analysis between indices (Li, Liang et al. 2011, Qi, Peng et al. 2011). According to test data from Tables 4.2 to 4.4, correlation of  $K_E$  with  $R_C$  is plotted in Figure 4.14a. Figure 4.14b is the correlation between  $DT$  and the uniaxial compressive strength (UCS) of  $DT$  test specimens.

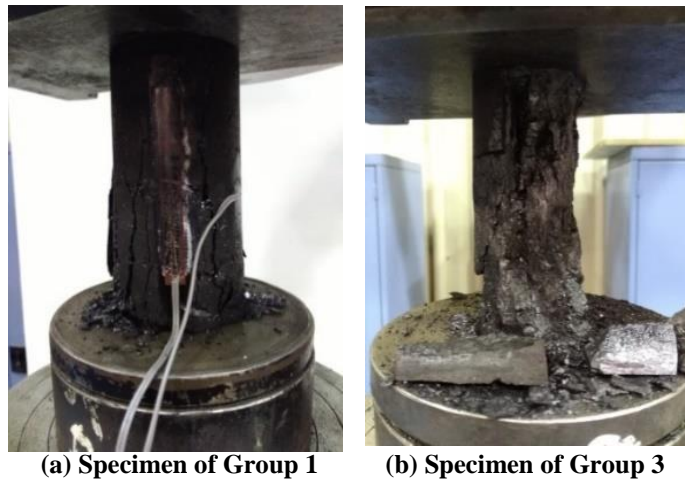


**Figure 4. 14 Failed coal specimens**

Taking the number in Table 4.7 as abscissa, the risk classification method of  $R_C$  can be determined through finding the corresponding ordinate on the slope in Figure 4.15. Uniaxial compressive strength under different loading rates can be expressed as follow:

$$\frac{\sigma_F}{\sigma_S} = \left(\frac{\varepsilon_F}{\varepsilon_S}\right)^{\frac{1}{131}} \quad (4.4)$$

where  $\sigma_F$  is the peak strength at a high strain rate ( $\varepsilon_F$ ); and  $\sigma_S$  is the peak strength at a low strain rate ( $\varepsilon_S$ ).

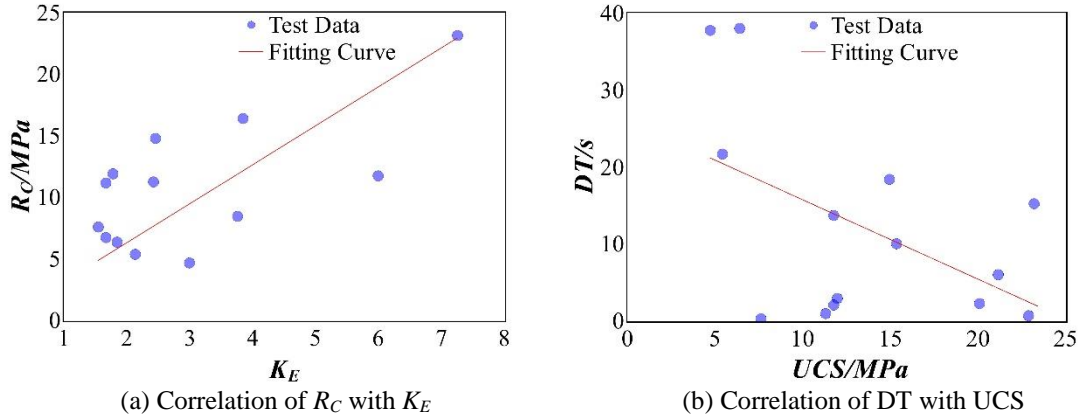


**Figure 4.15** Correlation analyses between indices

It is demonstrated by Equation 4.4 that the difference in strength caused by the loading rate can be ignored in this test. Therefore, the correlation between  $DT$  and  $UCS$  can be regarded as the correlation between  $DT$  and  $R_C$ . Based on the analysis above, a preliminary risk classification method is recommended in Table 4.8 for Australian coal seams. However, a larger specimen base should be tested to justify and improve the risk classification method of Table 4.8. Fuzzy evaluation methods can be adopted if the value of  $W_{ET}$ ,  $K_E$ ,  $R_C$  and  $DT$  are conflicting with each other (Qi, Peng et al. 2011, Cai, Dou et al. 2016). The weighting factors of the four indices are equal.

**Table 4.8** Preliminary risk classification method for Australian coal seam

Burst Propensity		None	Low	Moderate	High
Index	$W_{ET}$	$W_{ET} < 2$	$2 \leq W_{ET} < 3.5$	$3.5 \leq W_{ET} < 5$	$5 \leq W_{ET}$
	$K_E$	$K_E < 2$	$2 \leq K_E < 3.5$	$3.5 \leq K_E < 5$	$5 \leq K_E$
	$DT/s$	$DT > 20$	$15 < DT \leq 20$	$10 < DT \leq 15$	$DT \leq 10$
	$R_C/MPa$	$R_C < 5$	$5 \leq R_C < 10$	$10 \leq R_C < 15$	$R_C \geq 15$

Coal burst propensity determination of Group 1, Group 2 and Group 3 is based on the risk classification method for Australian coal seams in Table 3.8. The coal burst propensity of Group 2 and Group 3 is high while Group 1 is Low. The consistency of coal burst

propensity of the same coal seams and the difference of coal burst propensity of different coal seams are presented by Table 4.9.

**Table 4. 9 Determination of coal burst propensity**

Group No	Source	$W_{ET}$	$K_E$	$R_C/MPa$	$DT/s$	Burst Propensity
Group 1	Queensland	2.30	2.03	6.17	28.85	Low
Group 2	New South	6.32	4.33	15.50	6.80	High
Group 3	New South	3.66	2.95	15.11	6.08	High

#### **4.5 Improvement of $W_{ET}$ Test**

The test for  $W_{ET}$  needs a relatively accurate estimation of the failure strength of the specimen as the unloading operation needs to start from at least 80% of the failure strength. Failure strength of  $W_{ET}$  specimens is defined by the average uniaxial compression strength of coal specimens from the same coal seam. Because of the difference between specimens, the true value of the failure strength can be lower than the estimated value. Some specimens even fail before 80% of the estimated value. This may lead to the wrong  $W_{ET}$  test result or even no result. Two possible solutions for  $W_{ET}$  test improvement are discussed further.

##### **4.5.1 Volumetric Strain Indicator for Failure Prediction**

In general, as shown in Figure 4.16, the pre-peak deformation processes of rock under uniaxial compression can be divided into four stages: (I) crack closure, (II) elastic deformation, (III) crack initiation and stable crack growth, (IV) crack damage and unstable crack growth (Ranjith, Jasinge et al. 2010, Xue, Qin et al. 2014, Lei, Qi et al. 2015). The demarcation point between stage III and stage IV, which is the volumetric strain reversal point, corresponds to the crack damage stress ( $\sigma_{cd}$ ). For a cylindrical specimen under uniaxial compression loading, volumetric strain ( $\varepsilon_v$ ) can be given as follows (Martin and Chandler 1994):

$$\varepsilon_v = \varepsilon_1 + 2\varepsilon_3 \quad (4.5)$$

Where  $\varepsilon_1$  is axial strain that is positive and  $\varepsilon_3$  is radial strain being negative.

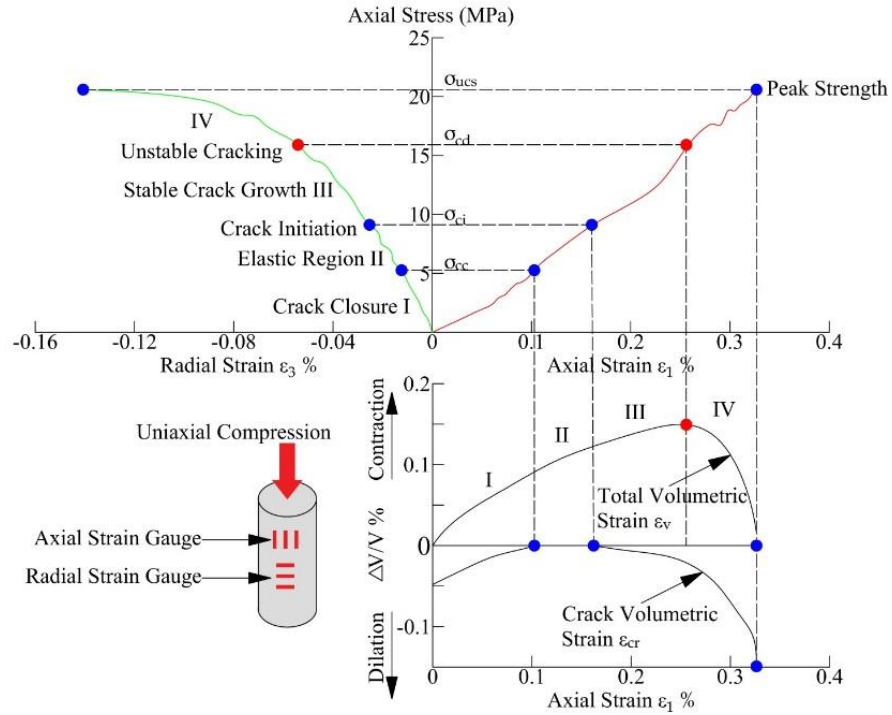


**Figure 4. 16 Different stages of the deformation process of coal during a uniaxial compression test**

It is demonstrated by statistical analysis that the ratio of  $\sigma_{cd}/\sigma_{ucs}$  for low-porosity (<10 %) rocks is a reliable indicator for predicting the damage and failure of rock specimens (Xue, Qin et al. 2014), i.e. the ratio of  $\sigma_{cd}/\sigma_{ucs}$  for a type of rock is near a constant.  $\sigma_{ucs}$  refers to the uniaxial compression strength of rock specimens. To investigate the effectiveness of this indicator for failure prediction of coal, uniaxial compression tests of three coal specimens is conducted in a laboratory. The preparation of specimens is the same as the preparation process of coal burst propensity test specimens introduced in Section 4.2.1. As shown in Figure 4.17, it is illustrated by the test results that the trend of the volumetric strain curve of coal is similar to that of low-porosity rock. Therefore, the failure strength of  $W_{ET}$  specimens can be estimated as follows:

$$\sigma_{WET} = a * \sigma_v \quad (4.6)$$

Where  $\sigma_{WET}$  is the estimated failure stress value of the  $W_{ET}$  test specimen,  $a$  is the average  $\sigma_{cd}/\sigma_{ucs}$  ratio calculated based on the  $R_C$  test result and  $\sigma_v$  is the stress corresponding to the volumetric strain reversal point of the  $W_{ET}$  test specimen.

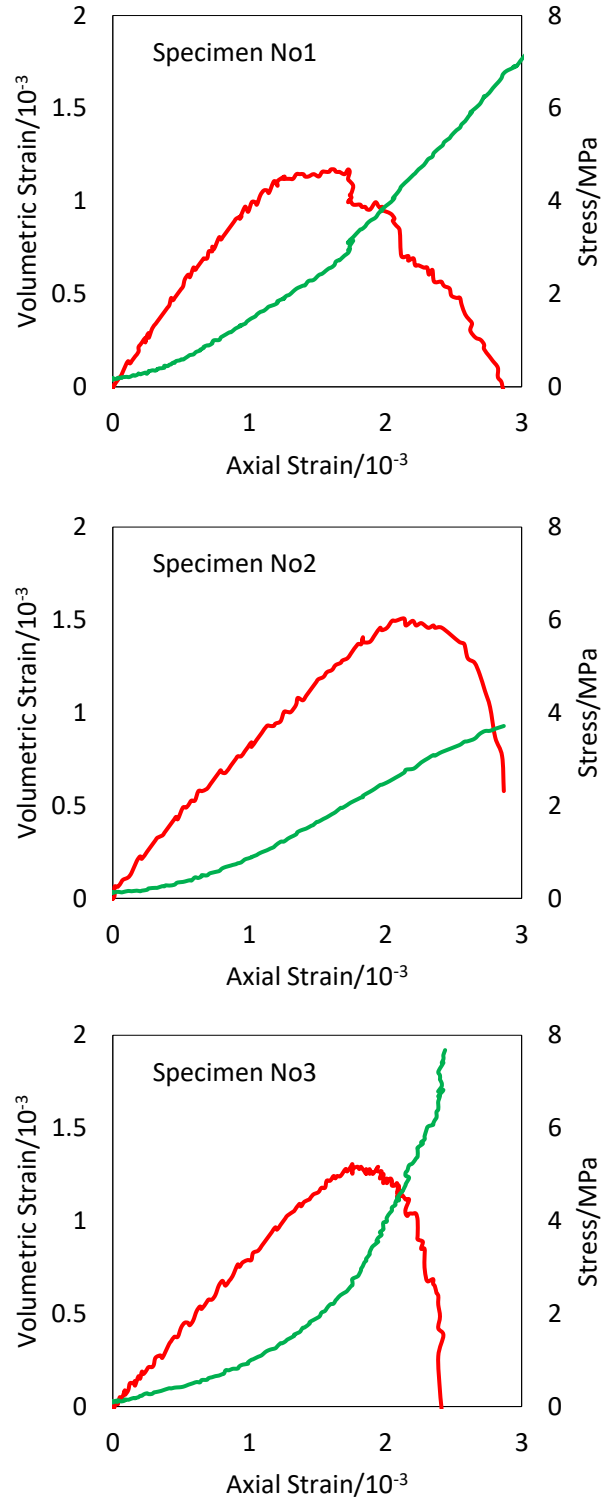


Figure 4. 17 Volumetric strain of uniaxial compression test

#### 4.5.2 Theoretical calculation of $W_{ET}$

The method presented in Section 4.5.1 still requires complex experimental and computational processes. Besides laboratory measurement,  $W_{ET}$  results can be theoretical calculated by the following analysis. According to Figure 4.1,  $W_{ET}$  can be expressed as follows:

$$W_{ET} = \frac{E_e}{E_p} = \frac{E_e}{E_s - E_e} \quad (4.7)$$

Where  $E_s$  is the total energy absorbed from outside when the specimen is failing.

$E_s$  and  $E_e$  can be calculated as follow(Cai, Dou et al. 2011):

$$E_s = \int_0^{\sigma_{ucs}} V \delta d\varepsilon \quad (4.8)$$

Where  $\sigma_{ucs}$  is the failure strength of the specimen,  $V$  is the volume of the specimen,  $\sigma$  is the stress of the specimen and  $\varepsilon_1$  is the axial strain of the specimen:

$$E_p = \frac{1}{2} V \sigma_{ucs} \varepsilon_e \quad (4.9)$$

$\varepsilon_e$  is the elastic axial strain of specimen at failure point.

The relationship between total axial strain and elastic axial strain at the failure point can be written as (Xie 1990, Zheng. and Zhang 1996):

$$\frac{\varepsilon_p}{\varepsilon_{max}} = \frac{\varepsilon_{max} - \varepsilon_e}{\varepsilon_{max}} = D_{max} \quad (4.10)$$

where  $\varepsilon_{max}$  is the total axial strain of the specimen at the failure point,  $\varepsilon_p$  is the plastic axial strain of the specimen at the failure point,  $\varepsilon_e$  is the elastic axial strain of the specimen at the failure point and  $D_{max}$  is the damage factor of the specimen at the failure point. Equation 3.7 also can be expressed as follow(Cai, Dou et al. 2011):

$$\varepsilon_e = \varepsilon_{max}(1 - D_{max}) \quad (4.11)$$

According to the damage evolution equation of rock (Yin, Zhang et al. 2002),  $D_{max}$  can be calculated as follow:

$$D_{max} = \left(\frac{\varepsilon_{max}}{m}\right)^n \quad (4.12)$$

Where  $m$  and  $n$  are material constants.

Substituting equation 3.9, 3.8, 3.6 and 3.5 into equation 3.4, the  $W_{ET}$  value can be calculated as follow:

$$W_{ET} = \frac{\frac{1}{2}\sigma_{ucs}\varepsilon_{max}\{1 - (\frac{\varepsilon_{max}}{m})^n\}}{\int_0^{\sigma_{ucs}} \sigma d\varepsilon - \frac{1}{2}\sigma_{ucs}\varepsilon_{max}\{1 - (\frac{\varepsilon_{max}}{m})^n\}} \quad (4.13)$$

As shown in equation 3.11,  $a$  and  $n$  can be determined by the fitting method of damage constitutive equation of the loading curve before peak.

$$\delta = E\varepsilon[1 - (\frac{\varepsilon}{a})^n] \quad (4.14)$$

The accuracy of the calculated  $W_{ET}$  value is dominated by the accuracy of fitting. The example fitting curve is shown as Figure 4.18.

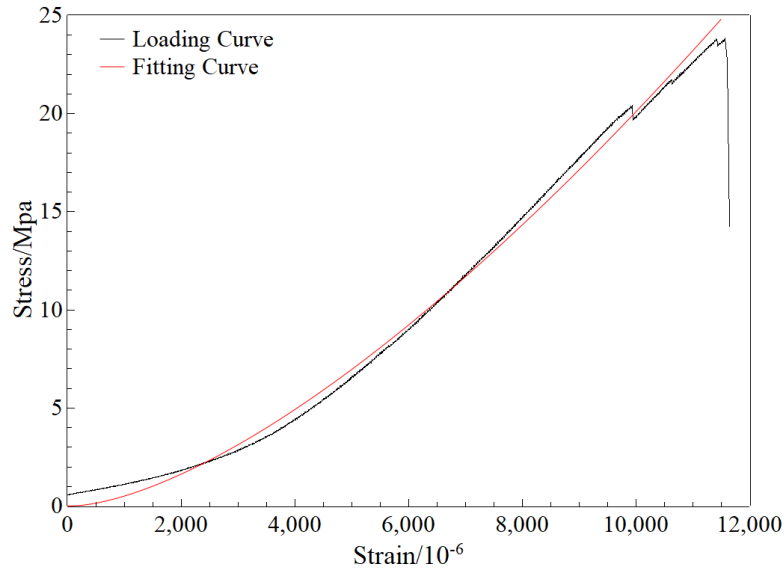


Figure 4. 18 Loading and fitting curve of uniaxial loading test

## 4.6 Conclusions

Violent failure of coal such as coal burst is a potential risk which can lead to casualties and equipment damage. It is demonstrated by extensive research that the failure mode of coal seams is dominated by the mechanical properties of the coal. The property that causes overstressed coal seams to violently burst is called coal burst propensity. The quantitative evaluation method of coal burst propensity was formed after several decades of study of the uniaxial loading behavior of coal. This chapter aims to develop the coal burst

propensity index method for coal burst risk evaluation in Australian coal mines. Not only has this method been widely adopted in Polish, Russian and Chinese coal industries but the feasibility of the application in Australia has also been verified by our testing. Three groups of coal specimens are tested in the laboratory. The differential analysis method of  $K_E$  and  $DT$  data and a preliminary four level coal burst risk classification form are proposed in this chapter. It has been demonstrated by the final test results that the coal burst propensity index method is an effective way to evaluate the burst risk of coal mines. Further tests with different coal seams are required to develop specific coal burst propensity classification methods for Australian coal seams. The improvement method for the  $W_{ET}$  test including the volumetric strain indicator method and theoretical calculation method are discussed. The theoretical calculation result is dominated by the fitting accuracy. The volumetric strain indicator method, although the test process is complex, can provide an accurate estimation of the unloading point of the  $W_{ET}$  test. In future tests, these two methods can be used together to improve the test efficiency. After the  $R_C$  test, the theoretical calculation method can be adopted to get the fitting result. If the fitting result is unsatisfactory, the  $W_{ET}$  test with the application of the volumetric strain indicator method can be arranged.

## **CHAPTER 5 SIZE DISTRIBUTION MEASUREMENT OF COAL FRAGMENTS USING DIGITAL IMAGING PROCESSING**

### **Summary**

This chapter develops the size distribution measurement method for coal fragments using digital image processing. The elastic energy storage within coal specimens will be dissipated mostly in two ways: fragmentation and ejection. In chapter six, the ejection energy, which is a key parameter for the support and protective structure design, will be calculated based on the fragment size distribution and energy-size relationship. This chapter provides a fast and precise measurement method of fragment size distribution for chapter six, eight and nine to study the fragmentation characteristic of coal.

### **Citation**

This chapter is based on the paper published in *Measurement* with the following citation:

Yang XH, Ren T & Tan LH, Size distribution measurement of coal fragments using digital imaging processing, *Measurement*, 2020, 10786. doi: 10.1016/j.measurement.2020.107867

## **Abstract**

This chapter focuses on the size distribution measurement of coal fragments by digital imaging processing. The fast and precise measurement of coal fragments, which is important to understand the crack propagation and the energy dissipation process of coal failure, has not been achieved in previous research. In this paper, an image analysis method using MATLAB is proposed to measure the fragment size distribution of coal fragments. The acquisition setup, analysis step and coding process for fragment size distribution measurement by digital image processing are introduced in detail. The statistical size distribution of coal fragments measured by image processing is compared with the theoretical distribution function and manual sieving results. This chapter provides an innovative and efficient method for size distribution measurement in the study of this coal failure process.

## **Keywords**

Size Distribution; Measurement; Coal Fragments; Digital Image; Processing; MATLAB

## 5.1 Introduction

Coal fragmentation is a common physical and mechanical phenomenon that exists in the brittle failure of coal subject to static, impact and dynamic loads, during which coal fragments of different sizes can be generated. The analysing of fragment size distribution (FSD) will contribute to understanding the energy dissipation characteristics and stress history of coal specimens (Liu, Li et al. 2014, Yang, Ren et al. 2020). Sieving is a traditional and indirect way to measure the statistical fragment distributions of solid fragments. The sieving method, which is cheap and easy, has been the main method for size determination (Bowen 2002). However, it has a limitation on the sampling data due to the discrete diameters of the membrane (Li, Li et al. 2018). Fernlund introduced the Danish Box for the measurement of aggregate size (Fernlund 2005). However, this method is time-consuming as aggregates are measured one by one. Callipers though have this same limitation. The sedimentation method has been adopted to analysis pulverized solid particles (Tafesse, Fernlund et al. 2012). But the analysis process of this sedimentation method is costly as professional instruments need to be used to complete the analysis. Hence, more reliable and efficient ways need to be used for the measurement of fragment size distribution.

In the last few years, measurement processes, especially the fast and accurate image processing method for determining the size and shape of solids, has been well-developed based on the wide application of computer science. With the advancement of digital image acquisition equipment, low cost software packages and mathematical analysis algorithms, different methods were used by some researchers to measure the size distribution of solid particles (Wu and Yu 2012, Peregrina-Barreto, Terol-Villalobos et al. 2013). Tafesse et al. described the procedure of image processing for grain size measurement and compared the image processed data with the results gathered by

mechanical sieving (Tafesse, Fernlund et al. 2012). Tafesse' study didn't demonstrate the efficiency of this method as each image contained no more than 15 particles. Fernlund introduced the determination of aggregate size through image processing (Fernlund 2005). However, the detailed procedure of image processing has not been mentioned in his research. Kumara et al. adopted image processing to measure the size of gravel and generated the gradation curve with ellipse shape assumptions (Kumara, Hayano et al. 2012). The size range of selected gravel in his research was 0-20 mm. Different from gravel, the brittle failure of coal specimens can generate thousands of pieces of debris ranging from several millimetres to tens of millimetres during laboratory uniaxial compression tests, which increases the challenge of accuracy and efficiency of image processing. Influenced by the physical properties of materials, the instrument setup and analysis algorithm for the measurement of coal are not the same as with other geo-materials. Nevertheless, the application of image processing for size distribution measurement of coal fragments has never been touched by previous research.

In this chapter, we aim at demonstrating the feasibility of measurement of coal fragments size distribution by using an image processing technic. The image analysis is achieved by the application of MATLAB. The image acquisition and analysis procedures are described in Section 5.2. In Section 5.3, the statistical size distribution of coal fragments measured by image processing is compared with the fractal distribution function and manual sieving results.

## 5.2 Image Acquisition and Image Analysis

### 5.2.1 Image acquisition

The coal fragments generated by the uniaxial compression test were separated into several regimes through manual sieving (Figure 5.1) for further image processing. The sieve adopted in this study has four mesh sizes including  $d = 2.5, 5, 10$  and  $20$  mm



**Figure 5. 1 Manual sieving with different mesh size**

To get high-quality images for analysis, a high-resolution Nikon single-lens camera was used to capture the image of the coal fragments. As shown in Figure 5.2, the camera was remotely controlled by a mobile phone through a wireless connection to guarantee the consistency of the camera settings and positioning. During the image acquisition, a white canvas with the specimen number and size range was placed under the coal fragments to create a luminous background. Fragments were evenly arranged on the canvas to avoid touching and overlapping each other, which is helpful when generating the distinct boundaries of each fragment, hence reducing unnecessary image processing. Photographing was conducted in a room without light disturbance in order to minimize the error caused by any shading or tilting effects (Tafesse, Fernlund et al. 2012).

Additional light needed to be applied if there were shadows caused by indoor light conditions.

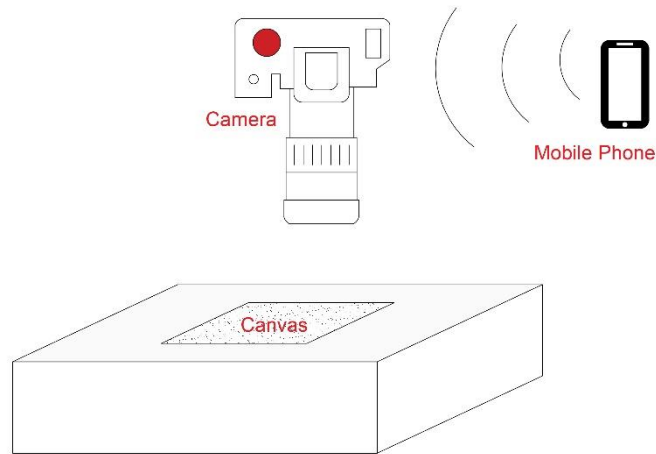


**Figure 5. 2 Schematic diagram of image acquisition setup**

### **5.2.2 Image Analysis**

The image analysis process was done by the image processing toolbar of MATLAB which provides a comprehensive set of algorithms and workflow apps for image processing, analysis, visualization and algorithm development (Krishnan, Priyadharshini et al. 2019). The image analysis procedures adopted in this chapter are shown in Figure 5.3. The image was read in colour by image reading code, and then transferred into a grayscale binary image by image binarization. In this chapter, watershed segmentation, which is a powerful tool used to detect and distinguish touching debris in images (Rabbani and Ayatollahi 2015), was used to detected edges on the binary image so as to separate coal fragments within the image. Watershed segmentation contains three main steps: computing of the segmentation function, marking of segmentation objects and computing foreground and background markers. These image processing operations including image reading, image binarization and watershed segmentation are called image pre-processing. The result of the image after every step is shown in Figure 5.4. Depending on the quality of the pre-processed image based on the separation situation of fragment boundaries, number of

noise elimination, image sharpening, contrast enhancement and edge-preserving filtering would be decided. Then the image pixel was transferred into a real-world physical unit through scale calibration.

As shown in Figure 5.5, the fragment size can be represented by the intermediate axis as the ellipsoid shape is generally used to represent the irregular shape of fragments (Kumara, Hayano et al. 2012, Hamzeloo, Massinaei et al. 2014). The shorter axis, which is the thickness of fragments, cannot be directly measured by 2-D images. The morphological features of the coal fragment will be introduced in the following section.

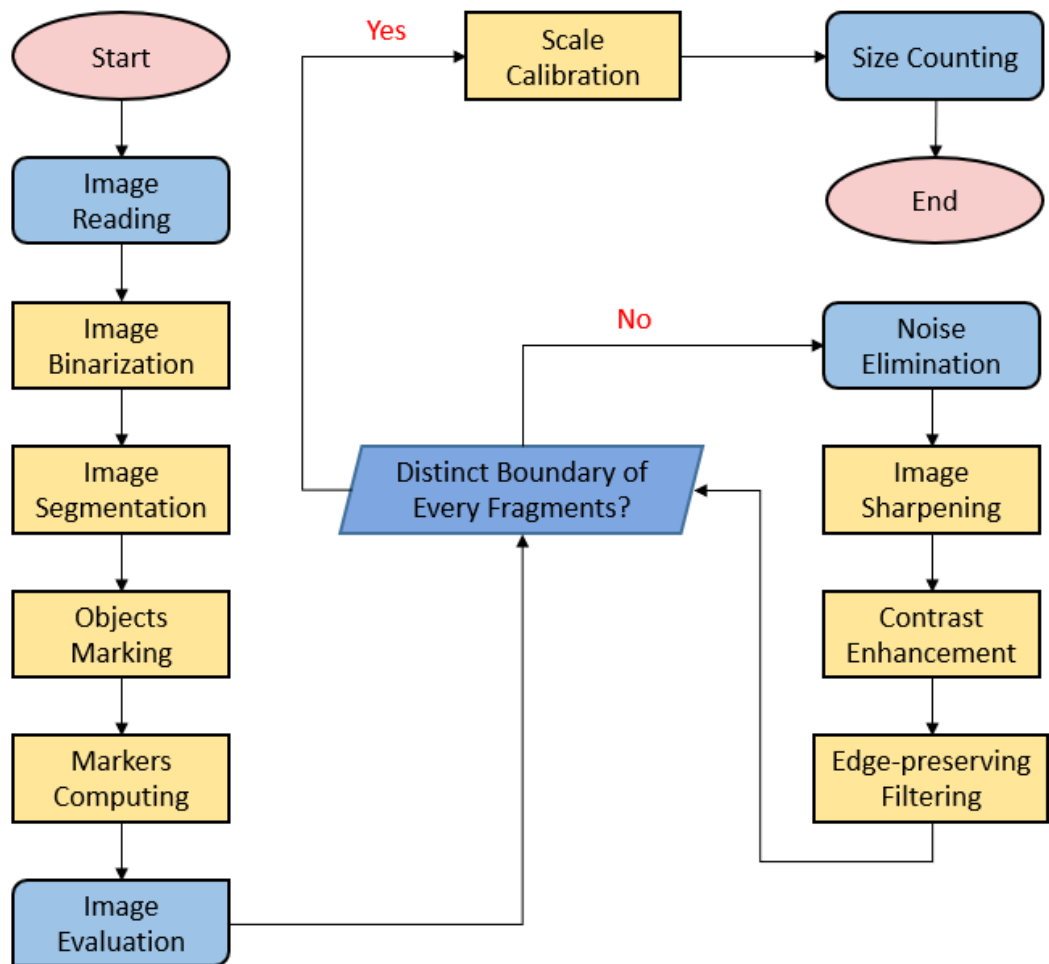
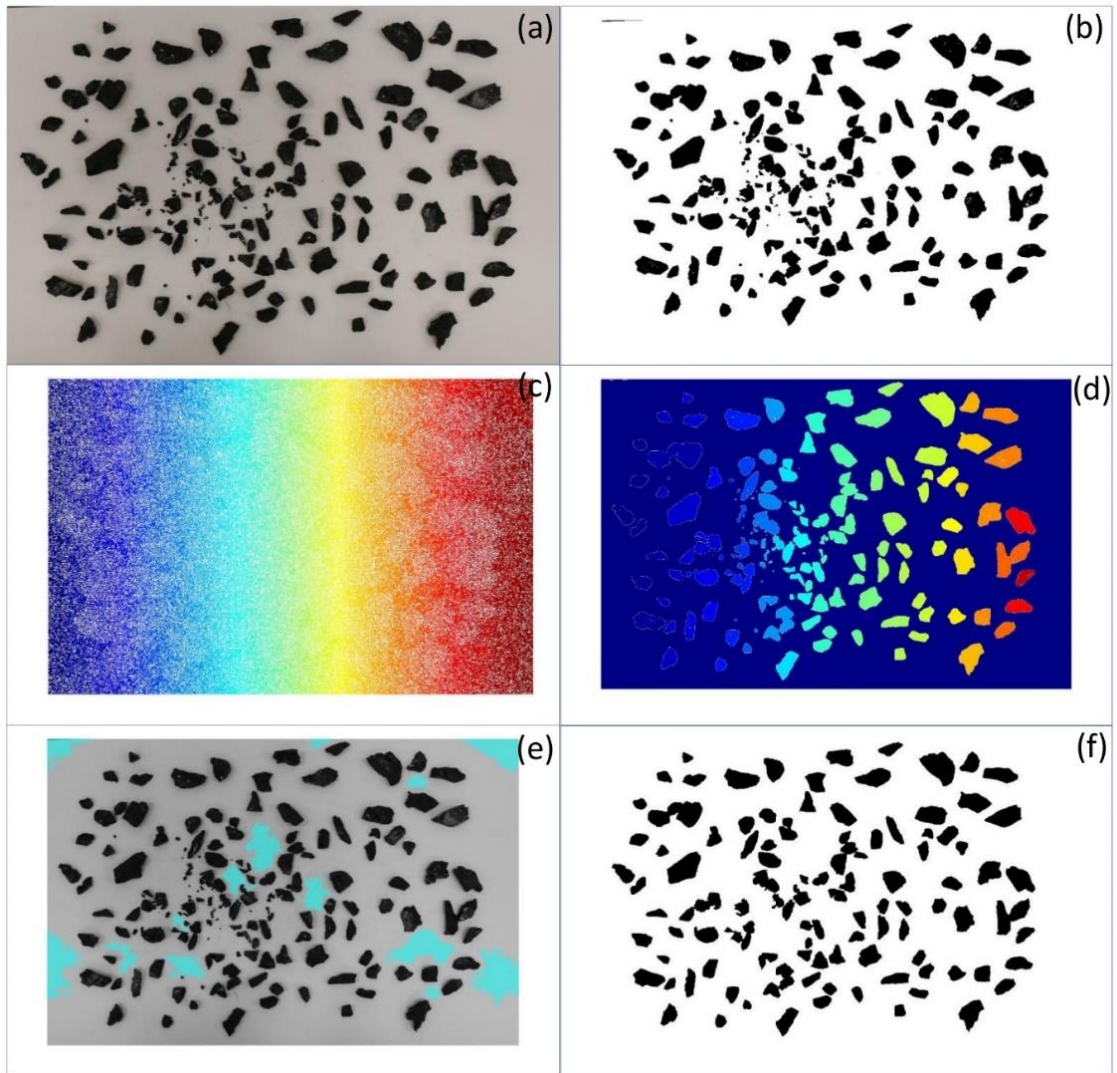
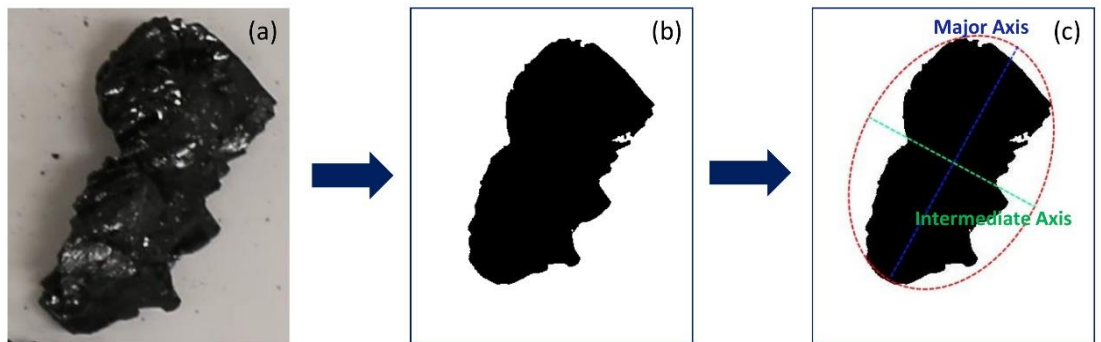


Figure 5. 3 Flow chart of image analysis process



(a) Original image (b) Binary image (c) Watershed segmentation (d) Foreground objects marking (e) Background markers computing (f) Final image.

**Figure 5. 4 Image pre-processing**



(a) Original image

(b) Binary image

(c) Equivalent area ellipse

**Figure 5. 5 Size measurement of a fragment**

### 5.2.3 Morphological Models

Five different morphological models, including hexahedron, octahedron, dodecahedron, sphere and ellipsoid, are compared to characterize the coal fragments. The sphere was the most widely used model in the numerical and theoretical study of the conveyance of crushed coal particles (Wang, Cheng et al. 2019, Chen, Li et al. 2020). Hexahedron has been used by Hilton et al. to simulate the gas-particle flow dynamics of pneumatic conveying systems. More agglomerate polyhedrons, including octahedron and dodecahedron, were used by Zhou et al. to represent the coal and gangue particles crushed by impact loads (Zhou, Liu et al. 2016, Zhou, Liu et al. 2017, Zhou, Liu et al. 2017). More recently, ellipsoid was believed to be a proper model to represent coal particles crushed by compression load (Yang, Ren et al. 2020).

The weight calculation equation for a hexahedron is:

$$W = \rho \times (\sqrt{S})^3 \quad (5.1)$$

where  $W$  is the weight of a particle,  $\rho$  is the density of the particle and  $S$  is the area of the particle measured by the digital image processing.

The weight calculation equation for an octahedron is:

$$W = \frac{\sqrt{2}}{3} \times \rho \times (\sqrt{S})^3 \quad (5.2)$$

The weight calculation equation for a dodecahedron is:

$$W = \frac{15+7\sqrt{5}}{4} \times \rho \times (\sqrt{1.6} \times \cos 18^\circ \times \sqrt{S \times \tan 18^\circ})^3 \quad (5.3)$$

The weight calculation equation for a sphere is:

$$W = \frac{4\pi}{3} \times \rho \times \left(\sqrt{\frac{S}{\pi}}\right)^3 \quad (5.4)$$

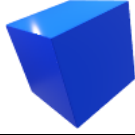
The weight calculation equation for an ellipsoid is:

$$W = \frac{4\pi}{3} \times \rho \times \frac{a}{2} \times \frac{b}{2} \times \frac{b}{2} \quad (5.5)$$

where  $a$  and  $b$  are major and minor axis lengths, respectively.

The morphological model and its calculation equation are summarized in Table 5.1.

**Table 5. 1 Morphological models of coal particle**

Model	Hexahedron	Octahedron	Dodecahedron	Sphere	Ellipsoid
Shape					
Particle Weight	$\rho \times (\sqrt{S})^3$	$\frac{\sqrt{2}}{3} \times \rho \times (\sqrt{S})^3$	$\frac{15 + 7\sqrt{5}}{4} \times \rho \times (\sqrt{1.6} \times \cos 18^\circ \times \sqrt{S \times \tan 18^\circ})^3$	$\frac{4\pi}{3} \times \rho \times \left(\frac{S}{\pi}\right)^3$	$\frac{4\pi}{3} \times \rho \times \frac{a}{2} \times \frac{b}{2} \times \frac{b}{2}$

The size distribution of coal particles can be described by the fractal cumulative functionality named the fractal model (Peng, Ju et al. 2015, Yang, Ren et al. 2020):

$$F(d) = \left(\frac{d}{d_{max}}\right)^{3-n} \quad (5.6)$$

where  $F(d)$  is the cumulative mass fraction of the coal particles smaller than size  $d$ ,  $d_{max}$  is the maximum size of coal particles and  $n$  is the fractal dimension of the Fragment size distribution.

According to equation 5.6, the fractal distribution curve of coal particles sizes, as shown in Figure 3, is plotted based on experimental data. The manual sieved data was used to calibrate the fractal dimension of the distribution curves. The fit of the modelled fractal distribution to the sieve sizes can be evaluated by the root mean square error (RMSE) from the following expressions:

$$RMSE = \sqrt{\frac{1}{n} \sum_{i=1}^n (X_i - Y_i)^2} \quad (5.7)$$

where  $X_i$  is the cumulative mass fraction measured by manual sieving,  $Y_i$  is the cumulative mass fraction estimated by the fractal distribution model and  $n$  is the number of data points.

According to equations listed in Table 5.1, the size distribution curves of different morphological models and fractal distribution curves of test result are shown in Figure

5.7 based on image processed data. It can be seen from Figure 5.7 that the distribution curves of ellipsoid and sphere models have a higher correlation to the fractal distribution curve, which means ellipsoid and sphere models are more suitable to characterize coal particles generated by impact load compared with other models.

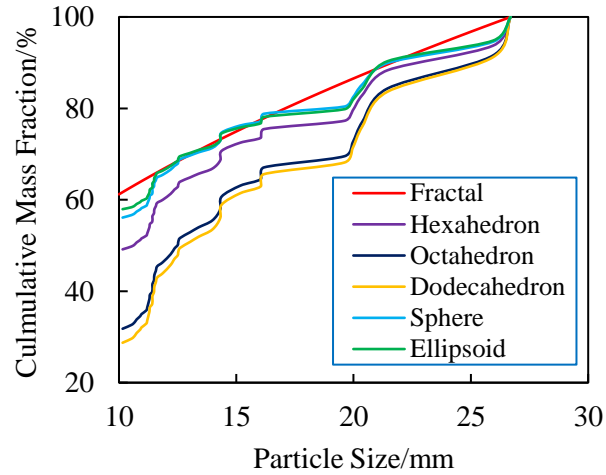


**Figure 5. 6 Size distribution curve of different morphological models**

To evaluate the goodness of fit between morphological model curves and fractal distribution curves, the RMSE of each model, as shown in Table 5.2, is calculated according to equation 5.7. The distribution curve established based on an ellipsoid model has the lowest RMSE, which means the ellipsoid model is more suitable than other models to characterize coal particles crushed by an impact load.

**Table 5. 2 RMSE of different morphological models**

Model	Hexahedron	Octahedron	Dodecahedron	Sphere	Ellipsoid
RMSE	8.41	21.44	23.76	3.53	2.71

### 5.3 Results and Discussions

The uniaxial compression loading tests of four cylindrical coal specimens with a 50 mm diameter and 100 mm length were conducted in the laboratory to get coal fragments after brittle failure. The test procedures had been detailed in previous publications (Yang, Ren et al. 2018). Fragment size distribution (FSD) of shattered coal specimens was firstly manually sieved by mesh, and then analysed by the image processing method introduced above. As shown in Figure 5.7 to 5.10, the binary image was analysed by the MATLAB

image processing toolbar and each fragment was taken as an ellipsoid characterized by a major axis, intermediate axis and minor axis. The length of the major axis and intermediate axis of every fragment could be directly measured by software and the length of the minor axis was the same as the intermediate axis in this chapter. The density of coal specimens measured in the laboratory was  $1.41 \text{ t/m}^3$ . The weight of every fragment could be calculated based on equation 5.5.

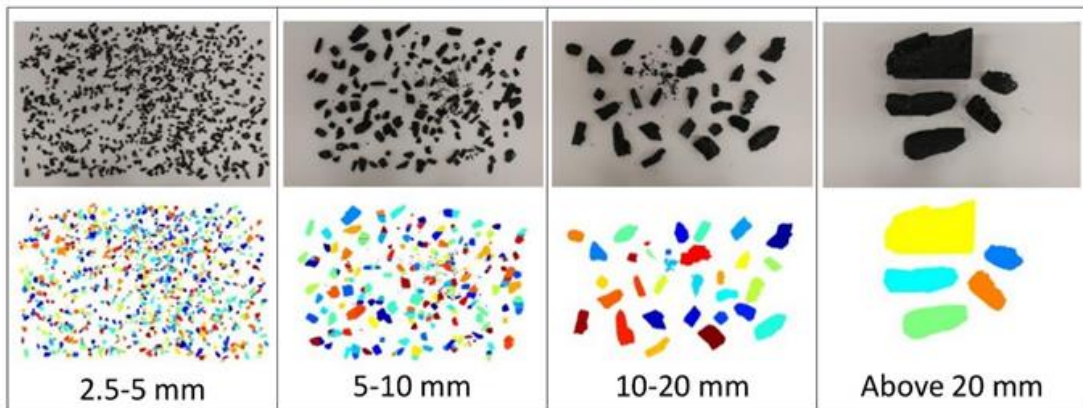


**Figure 5. 7 Original and processed image of specimen A1**

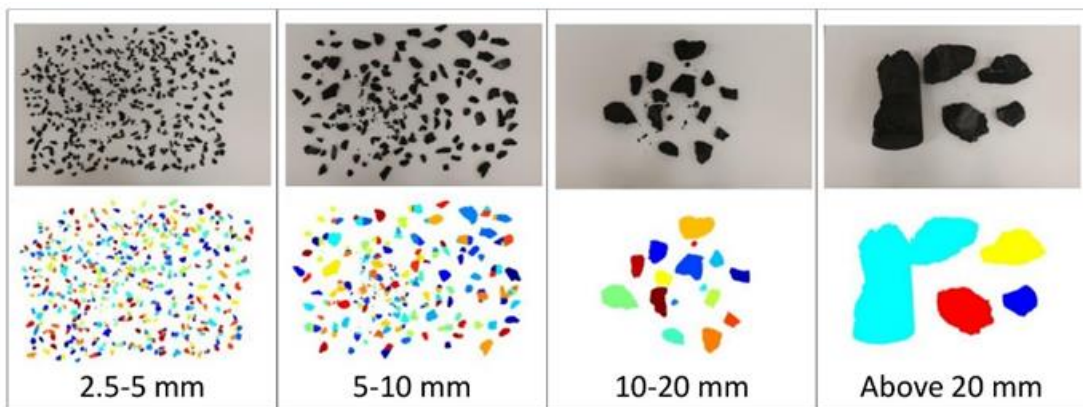


**Figure 5. 8 Original and processed image of specimen A2**

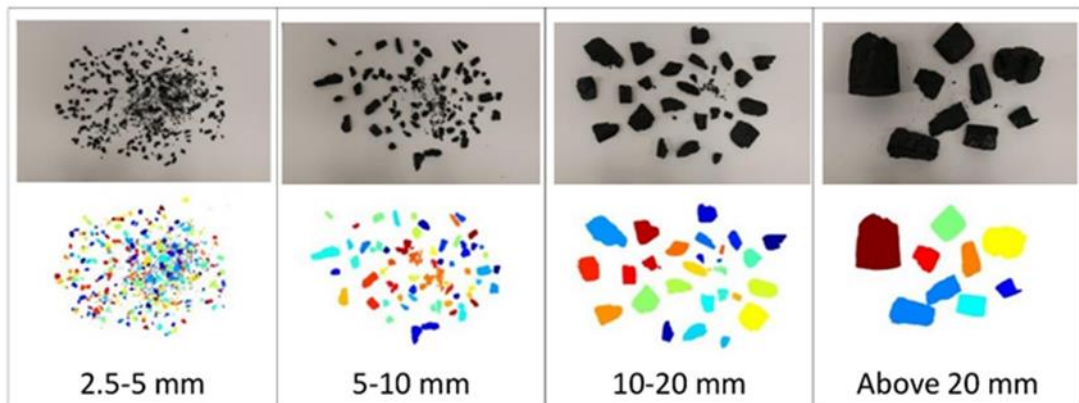


**Figure 5. 9 Original and processed image of specimen A3**

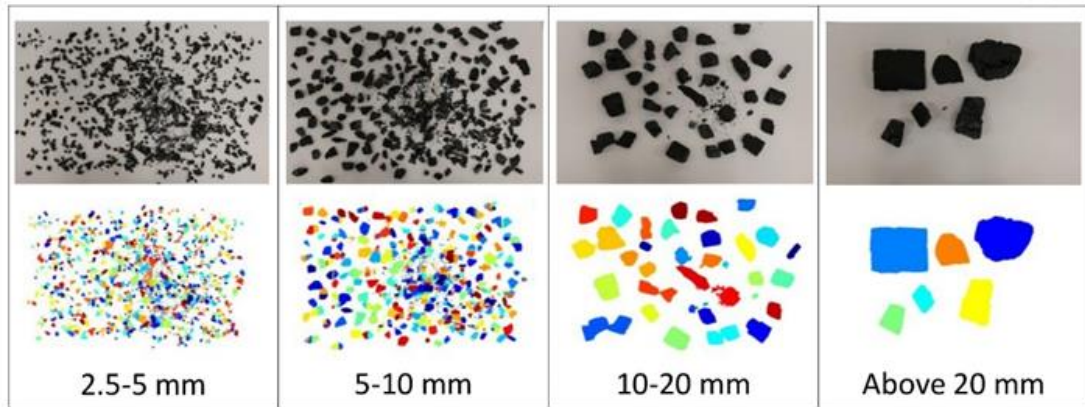


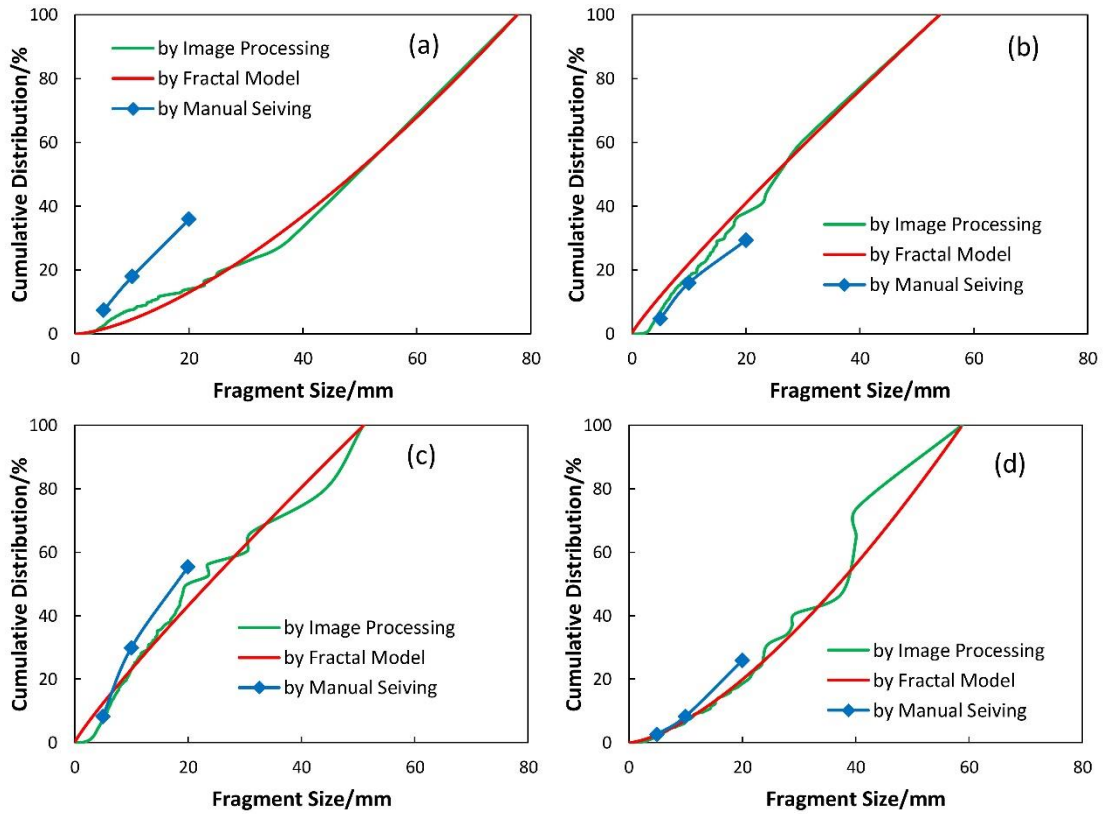
Figure 5. 10 Original and processed image of specimen A4

Fragmentation distributions of coal specimens generated by uniaxial compression loading tests has been described by the exponential function  $F(d)$  that represents the statistical distribution of the fragments number frequency and the cumulative distribution function and is called the fractal model (Peng, Ju et al. 2015, Liu, Zhang et al. 2016):

$$F(d) = \left(\frac{d}{d_{max}}\right)^{(3-n)} \quad (5.3)$$

where  $F(d)$  is the cumulative mass fraction of the fragments smaller than size  $d$ ,  $d_{max}$  is the maximum size of FSD and  $n$  is the fractal dimension of FSD, which is related to the coal properties.

To demonstrate the accuracy of the size distribution measurement of coal fragments using digital image processing, the image-processed, manual sieved and fractal modelled cumulative distribution curves of these four specimens are shown in Figure 5.11. As shown in Figure 5.12, the image-processed results work even better than the fractal model proposed by previous research as the RMS (Root Mean Square) error between manual sieving curve and image processing curve is lower.



(a) A1, (b) A2, (c) A3, (d) A4

**Figure 5. 12 Cumulative size distribution of specimens**

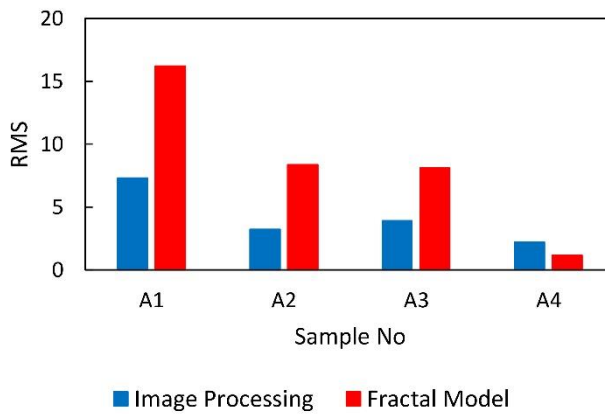


**Figure 5. 11 RMS of image processing and fractal model**

## 5.4 Conclusions

The brittle failure of coal specimens can generate thousands of pieces of debris ranging from several millimetres to tens of millimetres during laboratory uniaxial compression tests. However, the fast and precise measurement of coal fragments, which is important for understanding the crack propagation and energy dissipation process of coal failure,

has not been achieved by previous research. This chapter proposed the application of an image processing technique in measurement of coal fragments generated by uniaxial compression tests.

The image processing method based on the MATLAB image process toolbar is proposed in this chapter. The acquisition setup, analysis step and coding process for image processing are introduced in detail. The watershed method is adopted for fragment segmentation in this chapter. It has been shown by the comparison of images before and after image processing that the image processing method proposed in this chapter is suitable for coal fragment measurement.

In this chapter, the fragment in the image is taken as ellipsoid characterized by major axis, intermediate axis, and minor axis. The image processed cumulative distribution of coal specimens is generated based on image analysis results, the ellipsoid volume equation and the intermediate–minor axis value relationship. The comparisons between image-processed, manual sieved and fractal modelled cumulative distribution curves are shown in Figure 4.7 demonstrating that digital image processing is an efficient and accurate tool to measure the size distribution of coal fragments.

The operational speed of image processing was low as coal fragments were separated into several regimes through manual sieving prior to image processing. Manual sieving is not essential any more as this research has demonstrate the feasibility of coal FSD measurement through image processing. In the future applications, only one picture needs to be taken and processed, which can save more time. The image analysis was based on MATLAB coding and the data will be stored automatically. It is highly possible to make all these operations more intelligent by the application of programming, AI, and learning.

## **CHAPTER 6 ESTIMATION OF AVERAGE EJECTION VELOCITY GENERATED BY RIB BURST UNDER COMPRESSIVE LOAD**

### **Summary**

This chapter proposes a novel method to estimate the ejection energy and velocity of coal burst based on energy and fragmentation analysis introduced in the previous chapters. Coal ejection, which is a common phenomenon associating with coal burst, can cause severe equipment damage and casualties. The ejection energy and velocity are important parameters for the design of roadway supports and protective structures. In this chapter, a new ejection energy calculation function is proposed based on Rittingers's theory and the fractal FSD model, which provides a novel mathematical model for the quantitative study of the energy dissipation process of coal fragmentation in both this chapter and chapter 9.

### **Citation**

This chapter is based on the paper published in *International Journal of Rock Mechanics and Mining Sciences* with the following citation:

Yang XH, Ren T & Tan LH, Estimation of average ejection velocity generated by rib burst under compression load, *International Journal of Rock Mechanics and Mining Sciences*, 2020, 128, 104277. doi: 10.1016/j.ijrmms.2020.104277

## **Abstract**

The ejection velocity associated with coal burst is an important parameter for support and protective structures designed for protection against coal ejection where the support or protection design rationale is to dissipate or absorb the kinetic energy carried by ejected coal. This paper provides a novel method to estimate the average particle ejection velocity of rib burst based on the energy dissipation and coal fragmentation of coal brittle failure. This research shows that the scale of kinetic energy released by coal burst in underground roadways can reach over  $10^7$  J, which can result in ejected coal having an initial velocity of over 26 m/s causing serious or even fatal injury to miners without sufficient protection.

## **Keywords**

Coal Burst; Fragmentation; Ejection Velocity; Underground Mining

## 6.1 Introduction

As mentioned in Chapter 3, coal burst is always accompanied by a sudden release of accumulated elastic energy, micro seismic events, and ejection of a large amount of coal into the roadway or longwall face, which can lead to personnel casualties, equipment damage and even significant economic losses. Rib burst of roadways accounted for a large number of total coal burst accidents occurring in underground coalmines. In Colorado in the U.S., nearly half of the coal bursts occurred during roadway development or in the roadways (Christopher 2016). The statistical data shows that 87% of coal burst accidents in China occurred in roadways (Dou, Mu et al. 2014). The blocks of ejected coal from ribs can carry a large amount of kinetic energy because they have both mass and velocity (McGarr 1997). The velocity of ejected rock is an important parameter for the evaluation of coal burst reliability, design of roadway supports and the selection of protective measures (special protective structures around working space or personal protection equipment) (Kaiser, MacCreath et al. 1996).

Many researchers have reported using laboratory observations of particle ejection under triaxial or uniaxial compression load to understand the fragmentation behaviour in the post-failure process of coal specimens and to assess the burst properties of coal in on-site underground mining engineering (He, Jia et al. 2012, Qiu, Feng et al. 2014, Jiang, Su et al. 2015). Because the ejection process is very transient, the coal particles are highly pulverized and the ejection velocity of particles is high during post-failure of coal, the ejection and travel of all particles is difficult observe and film in laboratory observations.

In this chapter, we present a novel method for ejection velocity estimation based on energy and fragmentation analysis. A new fragment energy calculation function is proposed based on Rittingers's theory and the fractal model, which provides a novel

mathematical model for the quantitative study of the energy dissipation process of coal/rock fragmentation. Based on the energy analysis and fragmentation study, we present a method to estimate the average ejection velocity of coal ejections. A laboratory test is designed to verify the feasibility of this method for the estimation of ejection velocity of coal specimens with a high burst propensity. Also discussed in this chapter is a case study to demonstrate the feasibility of this method for the ejection velocity estimation of rib burst in underground roadways. The method introduced in this chapter could further advance our skill in reliably estimating rib burst intensity and enable a better understanding of the brittle failure of coal, which can help the mining industry to understand the energy scale of coal burst hazards and hence improve underground mining safety by addressing sufficient protection and controlling measures.

## 6.2 Theoretical Analysis of Coal Ejection

As shown in Figure 6.1a, after the excavation of roadways, ribs will deform elastically and plastically and accumulate a certain amount of elastic energy under the compression load provided by vertical compression stress. The study conducted by Bieniawski et al. (Bieniawski, Denkhaus et al. 1969) has found that the kinetic energy released by coal burst is from the stored elastic energy of coal before peak strength. Xie et al. gives the calculation equation of elastic energy stored by coal under a compression load (Xie, Ju et al. 2005):

$$E_{elastic} = \frac{V}{2E_0} \sigma^2 \quad (6.1)$$

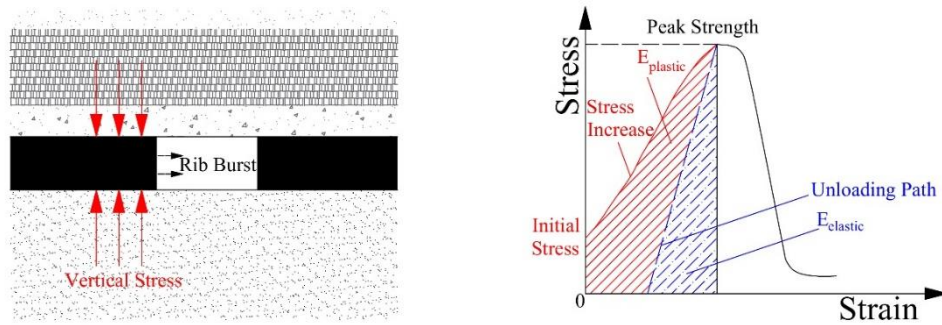
where  $E_0$  is the unloading elasticity modulus,  $V$  is the volume of the specimen and  $\sigma$  is the compression stress.

Hence, according to equation 6.1, the elastic energy stored in the coal body before a coal burst can be calculated based on its stressed condition and coal properties. The

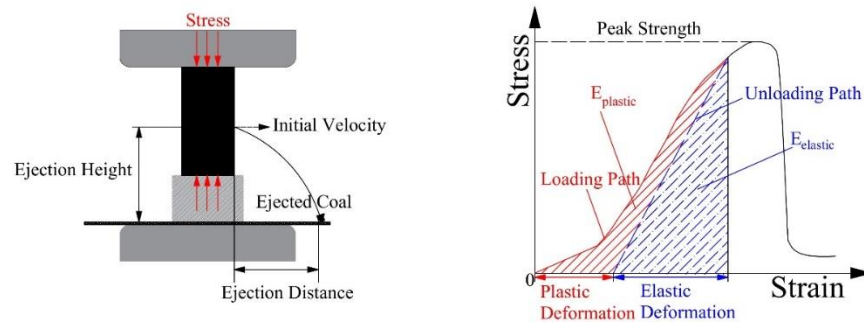
conservation of elastic energy during a rib burst or coal ejection can be represented by the following equation (Tu, Cheng et al. 2019):

$$E_{elastic} = E_{fragment} + E_{kinetic} + E_{geophysical} + E_{residual} \quad (6.2)$$

where  $E_{fragment}$  is the energy dissipated by coal fragmentation,  $E_{kinetic}$  is the kinetic energy carried by the ejected coal,  $E_{geophysical}$  is the energy released in the form of geophysical signals and  $E_{residual}$  is the remaining energy of the coal body after failure.



(a) Sketch of energy accumulation of rib burst



(b) Sketch of energy accumulation of coal ejection test

Figure 6. 1 Energy accumulation of rib burst and coal ejection test

Most of the elastic energy dissipates in the form of work during the coal burst process, resulting in the fragmentation and ejection of coal particles. The geophysical energy, which accounts for a limited portion of the total elastic energy, is dissipated as acoustic or seismic energy (Tu, Cheng et al. 2019). The experiments conducted by Zhao et al. have shown that the strength of the burst-prone coal will suddenly drop to around zero after peak strength (Zhao and Jiang 2010), i.e. the residual energy of the burst-prone coal is negligible. Therefore, the kinetic energy can be calculated by the following equation

based on equation 6.2 as geophysical energy and residual energy only account for a limited part of the total elastic energy:

$$E_{kinetic} = E_{elastic} - E_{fragment} \quad (6.3)$$

### 6.3 Fragment Energy Calculation

Coal fragmentation is a common physical and mechanical phenomenon that exists in a variety of situations from the cutting of coal (Liu, Liu et al. 2015), comminution (crushing and grinding) of coal (Li, Li et al. 2018), up to coal combustion (Saha, Dally et al. 2017). In underground mining operations, the cutting of coal is the main step in the mining process, which consumes 80%-90% of the power of the entire shearer and road-header (Liu, Liu et al. 2015). Comminution is an important operation in coal processing where the coal block coming from coalmines is crushed into fragments with a reduced size and accounts for 80% of the electricity consumption of mineral processing circuits (Numbi and Xia 2015, Numbi and Xia 2016). Hence, thorough research has been made by international researchers around the energy consumption of mineral fragmentation as fragmentation during mineral mining and processing is an energy-consuming operation.

Fragmentation energy is an essential parameter for improving the efficiency of the shearer, road-header, and crusher. The relationship between the fragmentation energy and the particle size for single size particles has been extensively researched over the last century. Energy-size equations based on theoretical and experimental studies have been put forward by Rittinger, Kick and Bond (Morrell 2008), known as the three theories of comminution. Hukki (Hukki 1961) and Voller (Voller 1983) suggested the general form of the energy-size relationship based on these three theories. Charles (Liu, Zhang et al. 2016) and Stamboliadis (Stamboliadis 2007) developed the energy calculation model by considering the complex size distribution of fragmentation in their study. Research on the

fragment size distribution (FSD) of brittle materials including rock, ore and concrete with the means of a theoretical study (Hou, Xu et al. 2015) and statistical analysis (Hogan, Farbaniec et al. 2017) continues to be an active research field. The mathematical equations widely used to describe the FSD are the Rosin-Ramler (R-R) model and the Gates-Gaudin-Schuhmann (G-G-S) model (Stamboliadis 2007). However, this experimental data and these theoretical equations mentioned in the literature are mostly limited to rock or other ores, or pulverized coal (Liu, Zhang et al. 2016). Hence, it is necessary to develop calculation models for coal fragmentation with a coarse and wide size distribution as the fragments from mechanical failure have a wide size range. In this section, the energy-size relationships and FSD models of coal fragmentation are combined together to give the calculation models of coal fragmentation energy for complex fragment size distributions.

### 6.3.1 Energy-size Relationship

The relationships between fragmentation size and specific energy consumption have been thoroughly studied by many researchers. Rittinger believed that the energy consumed by mineral fragmentation is proportional to the new surface area generated as all the energy is dissipated by overcoming the molecular cohesion among new fragment surfaces (Jankovic, Dundar et al. 2010). Taking the coal fragment as a platonic solid or sphere, the volume of a fragment is directly proportional to the cube of fragment size while the surface area is directly proportional to the square of the size. The surface area change of coal after fragmentation can be expressed as:

$$S = a * V * \left( \frac{1}{d} - \frac{1}{D} \right) \quad (6.4)$$

Where  $S$  is the surface area change of coal,  $V$  is the total volume of fragments,  $d$  is the fragment size after failure,  $D$  is the equivalent size of total fragments before failure and  $a$  is the shape factor which is constant related to fragment shape.

Hence, Rittinger's theory can be written in the following equation:

$$E_{fragment} = K_R * a * V * \left(\frac{1}{d} - \frac{1}{D}\right) \quad (6.5)$$

Where  $K_R$  is fragmentation energy consumed by the formation of per unit surface area, also called Rittinger constant, which is only related to the mineral properties.

Kick proposed that the energy required for mineral fragmentation with a given size is proportional to the volume of the resulting fragments (Locat, Couture et al. 2003). Tavares et al. believe that Kick's theory is suitable for the fragmentation energy calculation of relatively large particles based on experimental data (Tavares and King 1998). Kick's theory can be expressed as:

$$E_{fragment} = K_K * a * V * (\log D - \log d) \quad (6.6)$$

Where  $K_K$  is the energy index in Kick's theory, which depends on mineral properties.

Bond's theory suggests that deformation happens initially inside the intact rock or ore under applied forces until a threshold is reached at which time the crack emerges (Liu, Zhang et al. 2016). Hence, the fragmentation energy is proportional to the total length of the new cracks generated during coal fragmentation. The resulting equation based on Bond's theory is:

$$E_{fragment} = K_B * a * V * \left(\frac{1}{\sqrt{d}} - \frac{1}{\sqrt{D}}\right) \quad (6.7)$$

Where  $K_B$  is a constant named Bond's index, which is related to the mineral properties.

### 6.3.2 Fragment Size Distribution

For real coal fragmentation and crushing processes, the coal fragments satisfy specific size distribution laws rather than having a uniform size. Hence, the fragment size distribution (FSD) needs to be taken into consideration for the calculation of fragmentation energy. The most widely used mathematical equations mainly used to

describe FSD are the Rosin-Ramler (R-R), the Gate-Gaudin-Schuhmann (G-G-S) and the fractal distribution.

The GGS model can be given by the following expression (Macias-Garcia, Cuerda-Correa et al. 2004):

$$F(d) = \left(\frac{d}{d_{max}}\right)^m \quad (6.8)$$

Where  $F(d)$  is the cumulative mass fraction of the fragments smaller than size  $d$ ,  $d_{max}$  is the maximum size of FSD and  $m$  is the adjustable parameter dependant on rock properties.

The RR model is defined by (Rosin and Rammler 1933):

$$F(d) = 1 - \exp\left[-\left(\frac{d}{d_0}\right)^m\right] \quad (6.9)$$

Where  $d_0$  is the characteristic fragment size in mm usually corresponding to 63.2% of the total volume of distribution  $F(d)$ .

The Fractal model can be written as (Liu, Zhang et al. 2016):

$$F(d) = \left(\frac{d}{d_{max}}\right)^{(3-n)} \quad (6.10)$$

Where  $n$  is the fractal dimension of FSD, which is related to rock properties.

### 6.3.3 Fragment Energy Calculation

According to the volume formula, the equivalent size of total fragments before failure is (Stamboliadis 2007):

$$D = \sqrt[3]{\frac{6V}{\pi}} = \sqrt[3]{\frac{6 \times W \times F(d)}{\pi \rho}} = \sqrt[3]{\frac{6W}{\pi \rho} \times \left(\frac{d}{d_{max}}\right)^{3-n}} \quad (6.11)$$

where  $W$  is the total weight of all coal particles and  $\rho$  is the density of coal.

Experimental research has shown that Rittinger's theory is suitable for the calculation of fragment energy (Tu, Cheng et al. 2019). The Fractal model was appropriately adopted by some researchers to describe the fragment size distribution of cylindrical coal specimens subject to uniaxial cyclic loading conditions (Li, Zhang et al. 2018). Hence, substituting equations (6.10) and (6.11) into equation (6.5), the fragment energy can be calculated based on the fragment size distribution and Rittingers's theory:

$$E_{fragment} = \int_0^{d_{max}} K_R \times a \times \frac{W}{\rho} \times \left(\frac{d}{d_{max}}\right)^{3-n} \times \left[ \frac{1}{d} - \frac{1}{\sqrt[3]{\frac{6W}{\pi\rho} \times \left(\frac{d}{d_{max}}\right)^{3-n}}} \right] \quad (6.12)$$

The value of  $K_R$  and  $a$  for coal has been proposed in other literature studies, which will be introduced further of this thesis. The value of  $W$ ,  $d_{max}$  and  $n$  can be determined based on the analysis of coal fragmentation after coal burst. The fragmentation energy can be calculated based on coal fragmentation characteristic after coal burst.

#### 6.4 Ejection Velocity and Impact Load

The calculation equations of kinetic energy and ejected coal mass (volume) have been given in section 6.2 and 6.3, respectively. Hence, the average ejection velocity ( $v$ ) of coal blocks can be derived according to the work-energy theorem:

$$v = \sqrt{\frac{2(E_{elastic} - E_{fragment})}{m}} \quad (6.13)$$

where  $m$  is the weight of total ejected particles.

The impact load caused by falling rock can be calculated according to the following equation (Labieuse, Descoedres et al. 1996):

$$P_{max} = 1.765 \times G^{3/5} \times \lambda^{2/5} \times R^{1/5} \times H^{3/5} \quad (6.14)$$

where  $P_{max}$  is the impact load,  $G$  is the gravitational weight,  $R$  is the equivalent radius of dropped coal,  $\lambda$  is Lamé's constant which is related to the materials properties and  $H$  is the drop height.

The equivalent radius of ejected coal blocks can be calculated based on the sphere assumption of coal blocks by (Yan, Zhang et al. 2018):

$$R = \left(\frac{3G}{4\pi g\rho}\right)^{1/3} \quad (6.15)$$

where  $g$  is gravitational acceleration.

Hence, the impact load caused by coal ejection with an initial velocity can be estimated by the following equation:

$$P_{max} = 1.765 \times G^{3/5} \times \lambda^{2/5} \times R^{1/5} \times \left(\frac{v^2}{2g}\right)^{3/5} \quad (6.16)$$

To determine Lamé's constant for coal blocks, an innovatively designed drop coal test system was established in the laboratory. As shown in Figure 6.2, coal blocks were dropped from the top of a pipe with a maximum 6 m height. The pipe, which is right above the steel plate, was used for guiding the travel path of coal blocks. A load sensor was placed under the steel plate to record the load generated by the dropped coal. A protective box was placed above the steel plate to stop the splashing of crushed coal particles, hence, to protect the experiment operators and apparatus. The high-speed camera, which can take 4000 pictures per second, is placed in front of the drop coal system to film the drop process of the coal blocks. An additional light is applied to provide better light conditions by offsetting the shadows caused by the indoor light conditions. The measured Lamé's constant of coal is 19302.22 kN/m<sup>2</sup>.

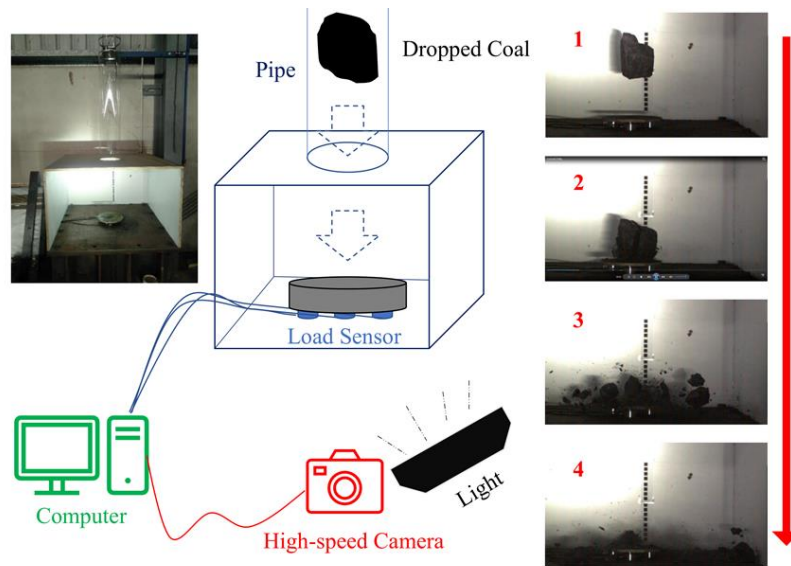


**Figure 6. 2 Determination of Lamé's constant through drop coal test**

## 6.4 Coal Ejection Test

As shown in Figure 6.1b, a coal specimen with high burst propensity will have a similar failure process comparable to rib burst and the ejection velocity of coal particles can be calculated by the method proposed above. As shown in Figure 6.3, a laboratory test is designed to verify the feasibility of this method for the estimation of ejection velocity. The experiment conducted in this thesis is called a “coal ejection test”, modified based on the uniaxial compression test. In the tests, a grey plastic platform was placed under the bottom of coal specimens to receive all the ejected particles and record the location of particles, hence to calculate the measured value of ejection velocity based on projectile motion equations. As shown in Figure 6.4, the platform is divided into several different areas and the measured velocity is the weighted average of the initial velocity of coal particles in these areas. All particles distributed in the same area are weighted together as pulverized coal particles cannot be measured by a balance separately. After the test, the post-failure specimen includes ejected particles and the remaining part was sieved to analysis the fragment size distribution of coal brittle failure.

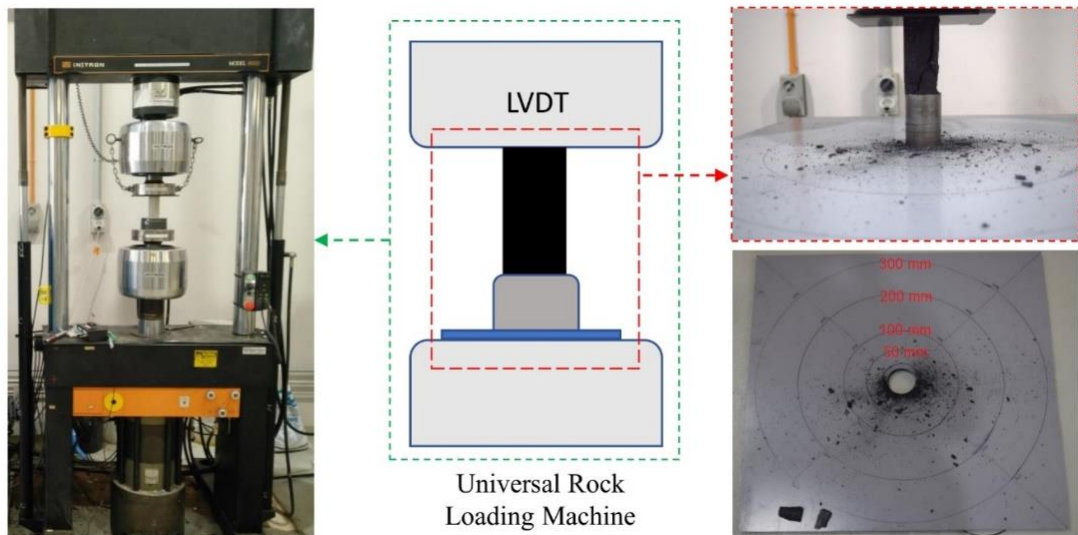


**Figure 6. 3 Coal ejection test with application of uniaxial compression loading system**

A total of 4 specimens taken from an Australian local coal mine were tested under uniaxial compression load displacement control. All the coal specimens were prepared by a 54

mm diameter coring machine in the laboratory. The drilling direction was oriented perpendicular to the joint direction. To maintain the original physical state of the coal, all blocks taken from the site were fully wrapped with aluminium and plastic membranes. Coal cores were processed into 108 mm high coal specimens through the process of cutting and polishing both ends, similar to the test requirements mentioned in Chapter 3. All other conditions (parallelism, flatness and verticality) of the coal specimens should meet the requirements for the application of the uniaxial compression strength method published by ISRM (International Society of Rock Mechanics) guidelines (Yang, Ren et al. 2018).

A 500-tonne digital hydro-powered Instron universal testing machine was used in the testing. The vertical displacement of the coal specimens was continuously logged by a linear variable differential transformer (LVDT) fixed on the upper loading platen of the machine and then recorded by the controlling system. The loading rate is 0.5 mm/min displacement. A spherical seat was placed under the coal specimens to provide a uniform axial stress distribution on the end of coal specimen.

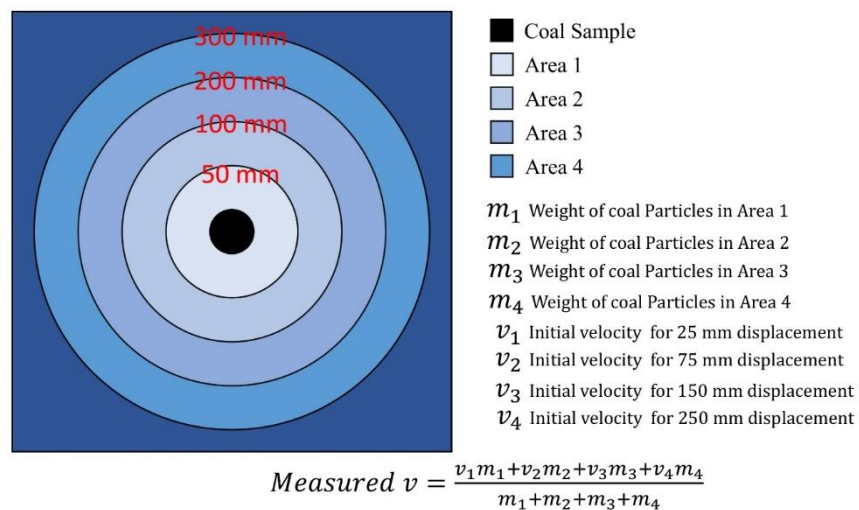


**Figure 6. 4 Indirect measurement of average ejection velocity**

## 6.5 Experimental Results

The stress-strain curves of these four specimens are shown in Figure 6.5. As shown in Table 6.1, the peak strengths of these four coal specimens are 14.85, 21.06, 14.8, and 16.83 MPa, respectively. Referring to the risk classification form for Australian coal seams proposed in Chapter 4, the coal seam from which these four specimens were taken is classified as high burst propensity coal as the average uniaxial compression strength of the coal specimens is above 15 MPa (Qi, Peng et al. 2011). The stored elastic energy of the coal specimens can be determined based on the relationship equation between uniaxial compression strength and young's modulus (Colwell and Frith 2006) and equation 6.1.

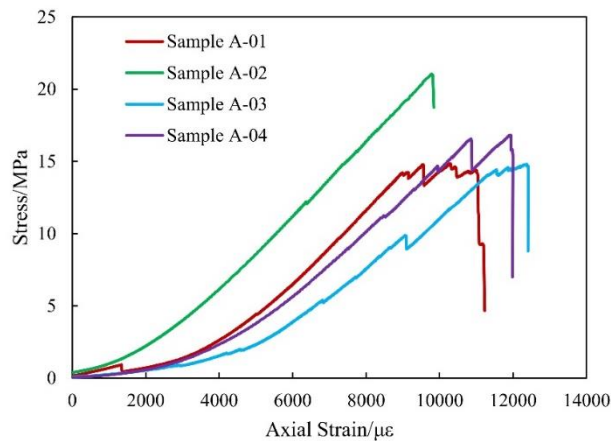


**Figure 6. 5 Stress versus strain curve of coal specimens**

In the experiment, the failure of coal under uniaxial compression load is brittle and rapid, leading to the production of numerous fragments owing to the sudden release of elastic energy (Peng, Ju et al. 2015). The weight of the total ejected particles of every specimen is recorded in Table 6.1. As shown in Figure 6.6, the size distribution of coal fragments was determined by using a series of sieves with different mesh sizes. Based on the image processing method introduced in Chapter 5, the statistical relationship of fragment size distribution of such coal can be determined based on the experimental data and equation (6.7). In the test conducted by Tu et al., the values of the Rittinger constant ( $K_R$ ) and shape factor ( $a$ ) for intact coal are 969.18 J/m<sup>2</sup> and 1.5 respectively (Tu, Cheng et al. 2019).

Other parameters including density, dimension of size distribution, unloading elasticity modules and total weight of coal fragments were determined by this test. The average weight ( $W$ ) of the coal specimen is 338 grams. The density ( $\rho$ ) of the coal specimens is  $1.37 \text{ g/cm}^3$ . The fractal dimension of size distribution ( $n$ ) is 1.09 for uniaxial compression test of coal (Peng, Ju et al. 2015). Hence, the value of fragment energy of every coal specimen can be calculated according to equation 6.12. And, the estimated ejection velocity can be calculated according to equation 6.13. The indirectly measured ejection velocity of every specimen is calculated according to Figure 6.4.

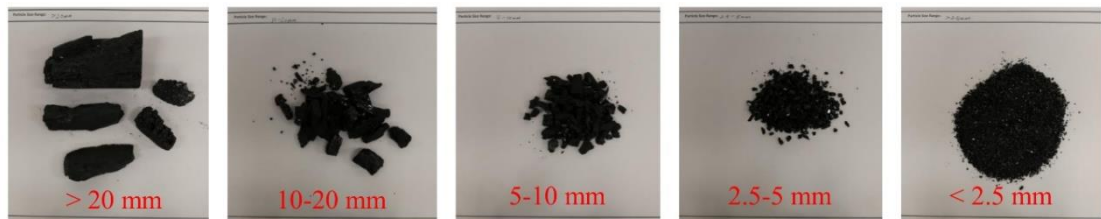


**Figure 6. 6 Different size of coal fragments after coal ejection test**

As shown in Table 6.1, more than 90 percent of the stored elastic energy is consumed by fragmentation of coal while kinetic energy only accounts for no more than 10 percent, which is complementary with the test result conducted by Chen et al (Chen, Su et al. 2019). The theoretically estimated ejection velocity based on energy dissipation and Fragment size distribution of coal brittle failure is higher than the measured ejection velocity based on the weight and location of ejected particles. At the same time, it should be noted that some unavoidable factors including the rotation of irregular particles, the initial ejection angle, the dragging effect of air and the randomness of ejection position can make the measured velocity lower than the true value (Jiang, Su et al. 2015). Hence, the estimated velocity can indicate the ejection feature of coal specimens as the estimated velocity has a positive correlation with measured velocity and the difference between these two values could be caused by the factors listed above.

**Table 6. 1 Estimated and measured average ejection velocity**

Specimen No	$E_{elastic}$ (J)	$E_{fragment}$ (J)	$E_{kinetic}$ (J)	$m$ (g)	Estimated $v$ (m/s)	Measured $v$ (m/s)
A-01	6.72	6.46	0.26	152.81	1.85	1.23
A-02	9.23	9.01	0.16	9.27	5.79	4.60
A-03	6.70	6.59	0.11	6.37	5.99	5.49
A-04	7.53	7.33	0.20	46.50	2.93	1.86

## 6.6 Case Study

It is not clear whether size effect will influence the accuracy of this estimation method as the scale of rib burst is thousands of times that of the coal specimens. As shown in Figure 6.7 and Figure 6.8, two rib burst cases were selected for case study analysis in this chapter.

**Case 1:** On 15 April 2014, a pressure burst occurred in the left hand sidewall at an Australian underground coalmine in the Greta Seam with a mining depth of 480 to 560 m (Hebblewhite and Galvin 2017). According to the investigation report of the burst accident, approximately 38 m<sup>3</sup> (52.06 t coal with 1.37 g/cm<sup>3</sup> density) of coal was ejected from the sidewall of the roadway at a depth of 555 m (Hebblewhite and Galvin 2017).

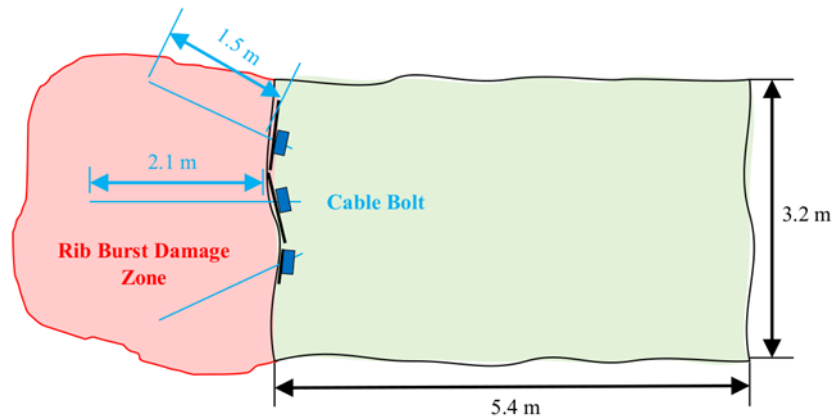


**Figure 6. 7 Sketch of cross-sectional diagram of roadways in Greta Seam**

Considering the 2.5 t/m<sup>3</sup> density of rock strata (Baghel 2009) and the 2.87 times stress concentration over the roadway induced by mining and extraction work (Rezaei, Hossaini et al. 2015), the sidewall bore approximately 39.82 MPa vertical stress. Previous research has indicated the low possibility of considerable dynamic energy involvement in this burst

case (Yang, Ren et al. 2019). Hence, the elastic energy stored in this coal can be calculated using the same method used in laboratory studies. The value of elastic energy ( $E_{elastic}$ ) is 25.39 MJ.

**Case 2** is the “6.26” rib burst accident that occurred in the Xingan Coal Mine of China. The mined coal seam in this coal mine is under 680 m of overburden with a 6.8 m average thickness (Wang et al., 2016). This rib burst accident, which was occurred on 26 March 2012 in the No.1 longwall panel, caused a 45 m long damaged zone in the tailgate side and released  $9.07 \times 10^5$  J energy (Wang et al., 2016). Hydraulic props used for supporting the roof in the tailgate were completely damaged during the burst occurrence.

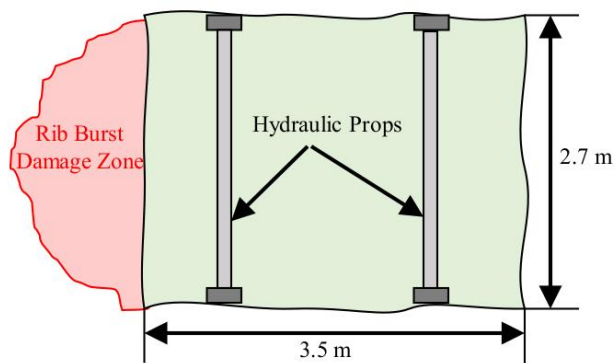


**Figure 6. 8 Sketch of cross-sectional diagram of roadways in Xingan Coal Mine**

Table 6.2 shows the key parameters extracted from experimental result and burst site data for ejection velocity estimation. Assuming the mechanical properties of the coal in the burst site are the same as the coal specimens used in this test, the theoretical value of fragmentation energy can be calculated according to equation 6.11. However, the maximum size of ejected blocks ( $d_{max}$ ) for this rib burst event is unknown as this data has not been mentioned in the previous research. The picture of the burst cavity on page 21 of the accident report (Mine Safety Investigation Unit 2016) (the picture cannot be copied due to copyright issues) has shown that the size of the ejected coal blocks are between 1/3 and 1 times that of the cable bolt length. It can be seen from Figure 6.6 that

the change of block size has a limited influence on the final value of fragment energy. Rittingers's theory assumes that fragmentation energy is proportional to the newly generated surface of coal particles during the failure process. The best explanation of Figure 6.9 is that the new surface area of pulverized coal particles and medium size coal blocks account in most part for most of the total newly generated surface. According to Figure 6.9, the value of the fragment energy ( $E_{fragment}$ ) for case 1 is 6.93 to 7.03 MJ. Fragmentation energy during the rib burst only accounts for around 27% of the total elastic energy stored while this number is more than 90% in the test results. The percentage of fragmentation energy might be negatively correlated to burst scale as the volume of coal is negatively correlated to its specific surface area, which needs to be further studied in future research.

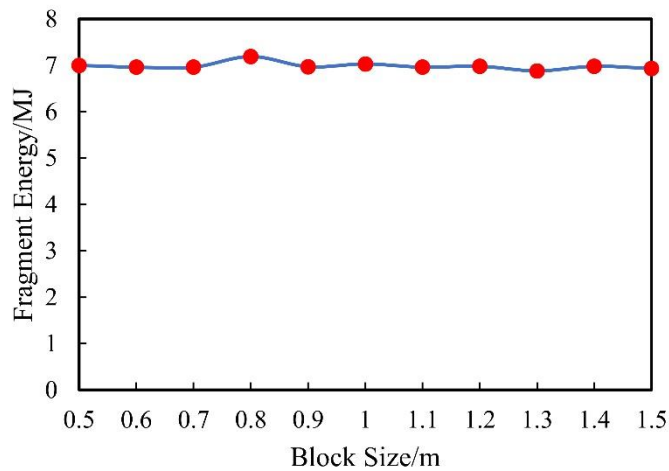


Figure 6. 9 Fragment energy with different maximum block size

Table 6. 2 Value of main parameters for fragmentation energy estimation

Mining Depth (m)	Stress Concentration Factor	Vertical Stress (MPa)	Shape Factor	Density (g/cm <sup>2</sup> )	Volume of Ejected Coal (m <sup>3</sup> )	Weight of All Fragments (t)	$K_R$ (J/m <sup>2</sup> )
555	2.87	39.82	1.5	1.37	38	52.06	969.18

Based on the analysis above and Equation 6.12, the average initial speed of ejected coal particles in case 1 ranges from 26.55 to 26.62 m/s. The destructive potential of 38 m<sup>3</sup> of coal moving at over 26.55 m/s (95.58 km/h) has been introduced in literature (Qiu, Feng et al. 2014), which explains the fatalities associated with this burst accident. Russell et al.

analysed this accident as well and the moving velocity in their paper is 22 m/s (Frith, Reed et al. 2019), which is identical with the estimated value in this chapter. Similarly, with test results, estimated value in this chapter is higher than the value in other references. But the gap is acceptable as this case study analyse is based on limited data extracted from literature. The result also indicates that, even without dynamic loads applied by a seismic event, the ejected velocity can easily reach up to 26 m/s or even larger. The analysis of case study 2 follows the same process as that for case study 1. The case study results are shown in Table 6.3.

**Table 6. 3 Estimation of ejection velocity and impact load of case study**

Case No	Elastic Energy /MJ	Fragmentation Energy/MJ	Kinetic Energy/ MJ	Slab Bulking Thickness/m	Volume of Ejected Coal/m <sup>3</sup>	Ejection Velocity/ m·s <sup>-1</sup>	Impact Load/ kN
Case 1	25.58	7.15	18.43	3	38.40	26.47	2.42×10 <sup>6</sup>
Case 2	121.52	22.68	98.84	3	121.5	34.46	7.17×10 <sup>6</sup>

## 6.7 Conclusions

The burst in the ribs of underground roadways is an important coal burst type, which can result in very high ejection velocities of coal blocks or particles. The ejection velocity is a vital parameter for not only support and protective structural design but also burst scale estimation in burst-prone coal mines.

In this chapter, a novel method to estimate the ejection velocity of coal based on the energy dissipation and fragment size distribution of coal brittle failure was presented. Based on energy dissipation analyses, equation 5.8 was obtained to calculate the ejection velocity of coal. The fragmentation theory and fractal size distribution are combined to get the theoretical calculation model of fragment energy. The developed “coal ejection test” indicate the positive correlation between estimated velocity and measured velocity, which means the estimated velocity can indicate the ejection feature of coal specimens in

the laboratory. Subsequently, the proposed method is applied to a rib burst case in an underground roadway, and the estimated ejection velocity is highly comparable with the observations of rib burst damage and other research outcomes.

The method for assessing coal ejection velocity developed in this study can be used as a basis for further research regarding the proper roadway support and protective structure design for use in burst-prone coal mines.

## **CHAPTER 7 EXPERIMENTAL STUDY OF COAL BURST RISK PREDICTION USING FRACTAL DIMENSION ANALYSIS OF AE SPATIAL DISTRIBUTION**

### **Summary**

This chapter experimentally investigates the fractal characteristic of AE spatial distribution during the uniaxial compression loading process of coal. As introduced in chapter 2, AE is a widely used method to study the loading and failure process of geo-materials in the laboratory. This chapter aims to find the possible precursor of coals abrupt failure based on AE monitoring, which may assist with understanding the early-warning signs associated with coal burst through micro seismicity monitoring as the locating principal of these two methods are the same. AE monitoring will also be adopted in the next chapter for reflecting the crack propagation intensity inside coal specimens during the loading process.

### **Citation**

This chapter is based on the paper published in the *Journal of Applied Geophysics* with the following citation:

Yang, XH, Ren T & He XQ, Experimental study of coal burst risk prediction using fractal dimension analysis of AE spatial distribution, *Journal of Applied Geophysics*, 2020, 177, 104025. doi: 10.1016/j.jappgeo.2020.104025

## **Abstract**

The sustainable and clean mining of coal is essential for Australia and the world as coal is a key energy source. However, with the increase of mining depth, many coalmines are facing potential coal burst hazards as deep mining is always associated with high gravitational stress and complicated geology. More recently, the coal burst risk has been highlighted by accidents occurring at Austar and Appin coalmines in Australia. Assumedly, due to a long-time mining history at relatively shallow mining depths, coalmines in Australia have no coal burst history and no corresponding risk control plans, techniques and equipment. This paper proposes a novel method for coal burst risk prediction based on fractal dimension analysis of AE spatial distribution. Also, this paper introduces the mathematical analysis method of fractal dimension based on a dimension calculation formula and MATLAB coding. Finally, obvious fractal dimension decrease of AE spatial distribution is observed in experimental studies of coal specimens with high burst propensity, promising the feasibility of coal bursts prediction through AE monitoring.

## **Keywords**

Coal Burst; Underground Mining; Risk Prediction; AE Monitoring; Fractal Dimension

## 7.1 Introduction

Coal is a vital energy resource for the world as it accounted for 30 percent of world primary energy consumption and 40 percent of world total electricity generation in 2015. As the fourth largest producer and the second largest exporter of coal resources (Geoscience Australia and ABARE 2010), Australia manages a big underground mining industry which consist of many underground coalmines and employees thousands of mine workers. The sustainable and clean mining of coal is essential for Australia and the world. With the application of advanced mining equipment such as hydraulic-powered supports and continuous miners, mining, and extraction jobs in Australian coalmines with less than 500 meters depth is considerably safe and productive. However, with the increase in mining depth, many coalmines are facing potential coal burst hazards as deep mining is always associated with high gravitational stress and complicated geology. To achieve sustainable development of coal mining, mitigating the safety hazards posed by coal burst is an important task for future mining. Coal burst refers to the instantaneous instability of coal, which is always associated with noise, coal ejection and seismic events. As mentioned in Chapter 3, several coal burst accidents occurred in Australian coalmines from 2014 to now, which lead to double fatalities of mine workers (Yang, Ren et al. 2020). Hence, the Australian government and industry have spent millions of dollars to fund research on the driving force and technologies to solve coal burst in recent years. In 2018, 22 miners were trapped in the Longyun coalmine in China when both ends of the roadway were accidentally blocked by coal burst events and finally only one miner survived. These reportable incidents associated with coal ‘bursts’ or ‘bumps’ have highlighted the need for the research of coal burst. Mining and geotechnical researchers in Poland, Russia, China, and the U.S. have completed decades of research relating to coal burst. However,

there is no evidence that the coal burst hazards have been well controlled in deep coalmines (Christopher 2017).

Similar to the instantaneous failure of other brittle material such as rock, concrete and metal, the coal burst process is always associated with the releasing of rich geophysical signals including acoustic emission (AE) (Kong, Wang et al. 2016), micro seismic (Ge 2005) and electromagnetic radiation (Song, Wang et al. 2012). The AE monitoring technique and apparatus have been well developed by researchers and technicians for the reflection of stress conditions and the crack propagation process of solid material. AE can provide a continuous and real-time 4D (3-dimension location and time) record of crack events associated with coal failure inside the coal body. The generation mechanism of AE signals and locating principal of AE sources have been comprehensively explained in many papers (Sikorski 2012). Some researchers believe that AE monitoring could be an essential tool for coal burst risk monitoring and prediction (Zhao and Jiang 2010). The accuracy and efficiency of coal burst risk prediction based on AE monitoring is largely dependent on the selection and analysis of risk parameters.

It was found in previous research that the frequency-magnitude relationship of the rock cracking process is in accordance with the Gutenberg-Richter relationship, i.e. has the self-similarity characteristic (Scholz 1968, Lockner 1993, Hainzl 2003). Hence, many researchers applied fractal theory to the study of rock dynamic failure as self-similarity is the specific feature of fractal phenomenon. The fracture position of rock failure demonstrates the fractal feature as the fragments size and shape generated during compression tests of rock specimens display fractal characteristics (Hou, Xu et al. 2015, Li, Li et al. 2018, Li, Zhang et al. 2018). Hence, the locations of geophysical signal sources are also fractal as the geophysical phenomenon is associated with rock fracture.

Previous research proved that the decrease in the spatial fractal dimension of micro seismicity could be potentially used to predict coal failure, and the larger its value, the more stable the coal specimen (Lu, Mai et al. 2005). The study of the fractal dimensions of AE could be a promising way of determining the early warning of coal failure as the generation mechanism and locating principal of AE are similar to that of micro seismicity.

Fractal dimension, a dimensionless index for describing fractal patterns in fractal geometry, may have different forms and calculation equations depending on the area of application. In the previous chapter, to simplify the calculation process, AE phenomenon was not included. This chapter aims to clarify the definition and calculation formula of the fractal dimension for AE spatial distribution and to study the feasibility of coal burst risk prediction using the fractal dimension analysis of AE spatial distribution, thus enhancing the mine safety by the AE monitoring technique. The chapter is structured as follows. Section 7.2 briefly reviews the theoretical background related to fractal dimension and acoustic emission. Then section 7.3 introduces the mathematical analysis methodology of fractal dimension of AE Spatial Distribution. Finally, an experimental study is conducted to verify the feasibility of coal burst prediction using fractal dimension analysis of AE spatial distribution.

## **7.2 Theoretical Background of Fractal and AE**

### **7.2.1 Fractal Dimension**

The history of fractal goes back to the 17th century when mathematician and philosopher Gottfried Leibniz studied recursive self-similarity (Zmeskal, Dzik et al. 2013). More than two centuries later in the 1970s, mathematician Mandelbrot, who is generally recognized as the father of fractal geometry, coined the word fractal from the Latin adjective fractus and began to give a general, comprehensive and systematic introduction to fractal

geometry in his books and essays (Mandelbrot 1983). The concept of fractal is difficult to define formally because of the complexity of mathematical meanings. Initially, fractal was a geometric terminology that refers to the morphological features of filling space in the non-integer dimension form. Geometrically, fractals refer to the complex patterns created by repeating a simple self-similar shape at different scales. In geoscience, fractals are a natural consequence of self-similarity resulting from scale-independent processes (Shen 2011). However, the application scope of fractal theory already far exceeds the geometric area. Fractal theory is currently widely adopted in the study of solid mechanics such as soil mechanics (Tyler and Wheatcraft 1992), fracture mechanics (Cherepanov, Balankin et al. 1995) and especially rock mechanics (Thompson 1991). The application of fractal theory in rock mechanics research includes two primary directions: the physical fractal feature of rock and the mechanical fractal behaviour of rock. In research with regard to the physical features of rock, the fractal distribution of pore structures and rock particle size has been discussed (Thompson 1991). It has also been found that rock fragments from rock/coal burst tests under high loading rates also exhibit fractal features (Xie 1990, Tian, Liu et al. 2016). This reveals the geometrical fractal character of rock. However, the most important application of fractal theory is in the research of the non-geometric and abstract features in rock mechanics. Xie combined fractal theory and damage mechanics to study the fractal features of coal stress-strain (Xie 1990), spatial distribution of coal micro-fracturing (Xie and Pariseau 1993) and coal burst (Xie 1996). The fractal features of many energy forms such as micro seismic (Feng, Yu et al. 2016), acoustic emission (Lu, Mai et al. 2005) and electromagnetic radiation (Frid and Vozoff 2005) associated with coal failure have been found as well. Fractal is becoming an important research tool for the study of coal failure.

The concept of fractal dimension plays a vital role in fractal theory (Mandelbrot 1983). It is revealed by many researchers that dimension is an important factor which can reflect the violent coal failure behaviour (Lu, Mai et al. 2005). The dimensional measurement of spatial distribution of acoustic emission events associated with the coal fracture process showed that the lowest fractal dimension is generally produced near the occurrence of strong failure of coal (Hirata, Satoh et al. 1987). That is, the fractal dimension of AE spatial distribution has a sudden decrease before coal burst. Dimension, a dimensionless index for describing fractal patterns, may have different types and calculation equations depending on the area of application (Zmeskal, Dzik et al. 2013). The correlation integrals  $C(r)$  for the AE events distribution  $(p_1, p_2, \dots, p_N)$  can be given by (Hirata, Satoh et al. 1987):

$$C(r) = \frac{2}{N(N-1)} N_r(R < r) \quad (7.1)$$

where  $N_r(R < r)$  is the number of pairs  $(p_i, p_j)$  with a distance smaller than  $r$ ,  $N$  is the number of total AE events in the coal specimen,  $r$  is the radius of the selected region and  $R$  is the distance between any two AE event locations in the selected region. Then, the fractal dimension  $D$  for AE spatial distribution is (Xie and Pariseau 1993)

$$D = \frac{\ln[C(r_1)] - \ln[C(r_2)]}{\ln(r_1) - \ln(r_2)} \quad (7.2)$$

As shown in Figure 7.1, AE events are represented by red dots.  $r_1$  and  $r_2$  are the radii of the selected concentric circles. The detailed mathematical analysis methodology of fractal dimension for AE spatial distribution will be introduced in the following section.

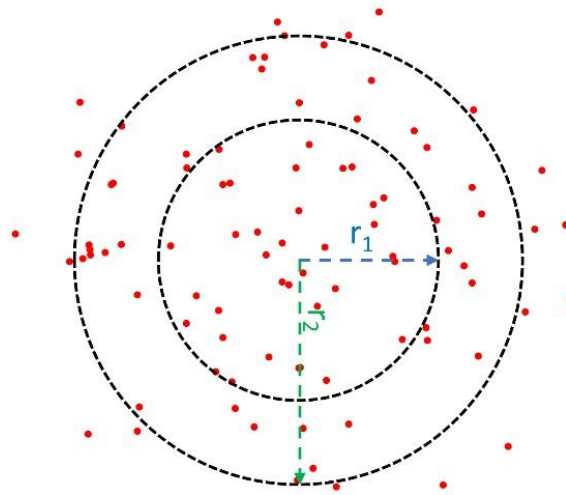


**Figure 7. 1 Fractal measurement method for a distribution of AE event locations**

### **7.2.2 Acoustic Emission**

Acoustic emission is defined as the transient elastic energy that is spontaneously released when coal undergoes deformation, fracture, or both (Sikorski 2012). Generally, AE signals refer to the elastic wave with a 1 kHz to 1 MHz frequency. As one of the most important non-destructive evaluation (NDE) methods, AE has been widely adopted to study the damage mechanics of coal caused by crack initiation and propagation under an applied stress (Ranjith, Jasinge et al. 2010). From the 1950s onward, recording and analysis of AE parameters have been used to predict the dynamic hazards of coal at both mine sites (He, Dou et al. 2011) and in the laboratory (Shkuratnik, Filimonov et al. 2004). The AE information generated from coal cracking can be measured by an array of sensors attached to the surface of coal and processed using seismic analysis techniques. Information generated by AE recording of coal includes (1) calculative event number (counts of total AE events received by sensor), (2) source locations, (3) amplitude distributions, (4) and frequency characteristics of emission events (Ohnaka and Mogi 1982). The acoustic emission will be defined as an AE event if the signal can be detected by more than 4 sensors. The determination of sources location is based on the theoretical principal of the AE locating algorithm (Li, He et al. 2019) while the other information

can be directly obtained from AE signals recorded by sensors. Study of amplitude distributions and frequency characteristics of AE has laid the foundation for AE signal monitoring through geophysical instruments. It has been proven by previous research that the rises, falls minima and maxima of AE rates correspond to the definite stage of the stress-strain curve for coal (Shkuratnik, Filimonov et al. 2004). Research regarding source location of AE events has found that the spatial distribution of AE events released by rock has fractal behaviour, which holds promise for an application to coal dynamic hazards, such as coal burst and slope slipping, through fractal analysis (Song, Wang et al. 2012).

### 7.3 Dimension Calculation Based on MATLAB Coding

Figure 7.2 shows the calculation process of fractal dimension. As shown in Figure 7.2, step 2 and 3 are based on equation 7.1 and 7.2 respectively while step 1 has not been clearly defined by previous research. According to the definition of  $N_r(R < r)$ , Figure 7.3 shows the flow chart for a typical process of  $N_r(R < r)$  calculation. Symbol  $a$  is the counting of eligible pairs and symbol  $b$  is the counting of calculation steps. The input value of these two symbols is zero. However, this process is time-consuming as dozens of AE events can be recorded by the AE monitoring apparatus.

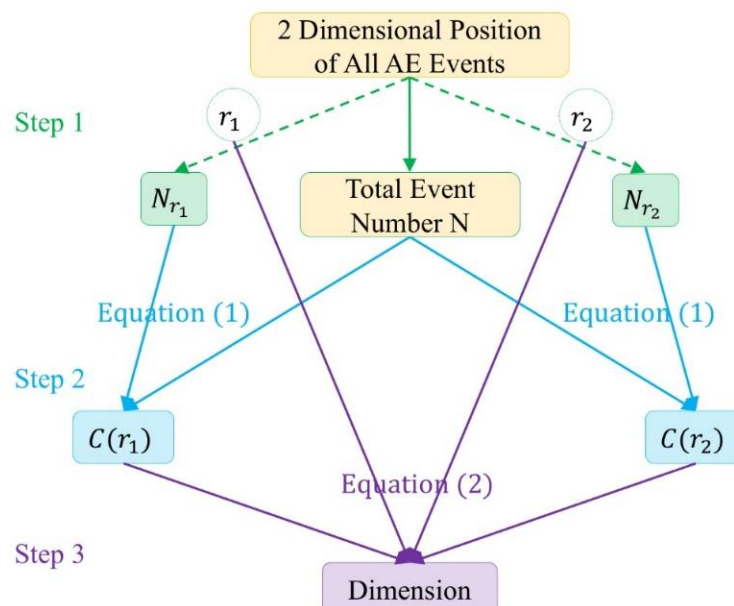


Figure 7. 2 Process of fractal dimension calculation

In this thesis, the mathematical analysis of step 1 will be conducted with the multi-paradigm numerical computing program MATLAB R2018a, which makes the analysis process more efficient and precise.

The two-dimensional position of all AE events will be defined in matrix  $A$  as follows:

$$A = \begin{bmatrix} x_1 & y_1 \\ \vdots & \vdots \\ x_N & y_N \end{bmatrix} \quad (7.3)$$

Then, the distance matrix  $B$  of all AE events will be defined by the MATLAB code below:

```
>> dismat = pdist(A)
>> B = squareform(dismat)
```

The elements below the diagonal line of Matrix  $B$  is the distance of all pairs  $(p_i, p_j)$ .

$$B = \begin{bmatrix} d_{11} & d_{12} & \dots & d_{1N} \\ d_{21} & d_{22} & \dots & d_{2N} \\ \vdots & \vdots & \vdots & \vdots \\ d_{N1} & d_{N2} & \dots & d_{NN} \end{bmatrix} \quad (7.4)$$

The elements below the diagonal line can be extracted by typing:

```
>> C = tril(B, -1)
```

The mathematical expression of Matrix  $C$  is:

$$C = \begin{bmatrix} 0 & 0 & \dots & 0 \\ d_{21} & 0 & \ddots & \vdots \\ \vdots & \vdots & \ddots & \vdots \\ d_{N1} & d_{N2} & \dots & 0 \end{bmatrix} \quad (7.5)$$

Finally, the  $N_r(R < r)$  will be computed by the following code:

```
>> N_r(R < r) = sum(C(:) > 0 & C(:) < r)
```

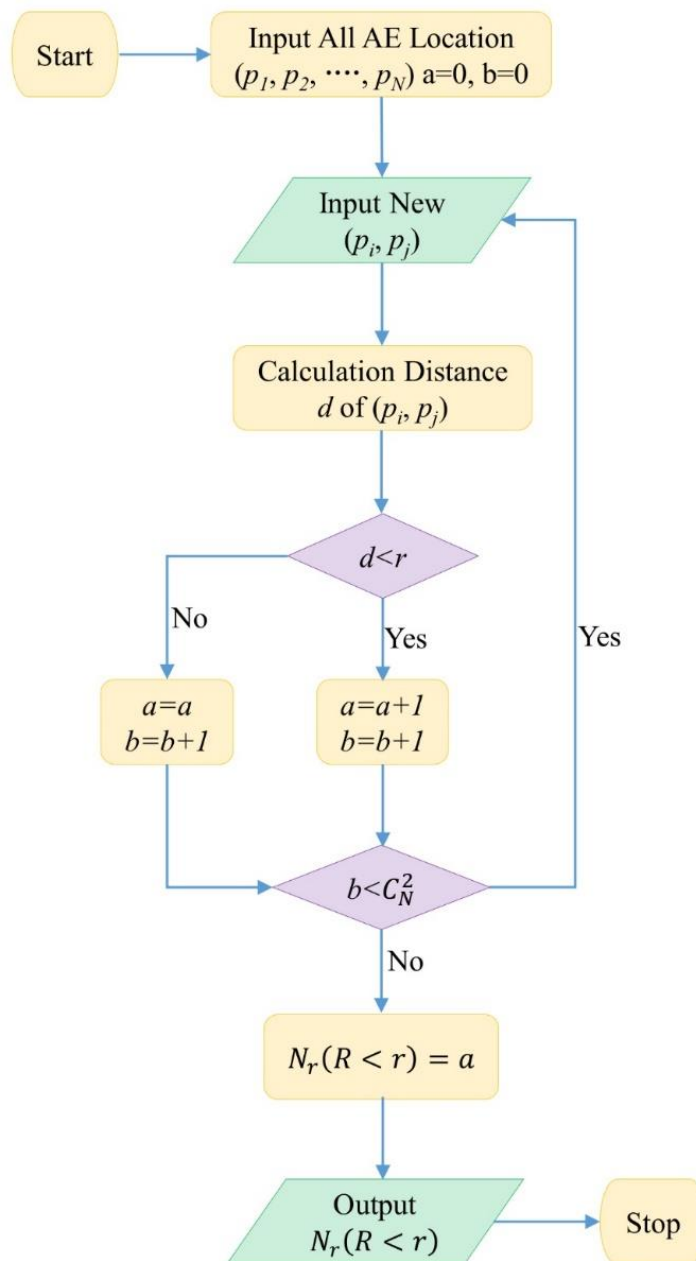


Figure 7. 3 Flow chart for a typical  $N_r(R < r)$  calculation

## 7.4 Fractal Behavior of Coal Specimens under Uniaxial Compression Load

### 7.4.1 Experimental Setup

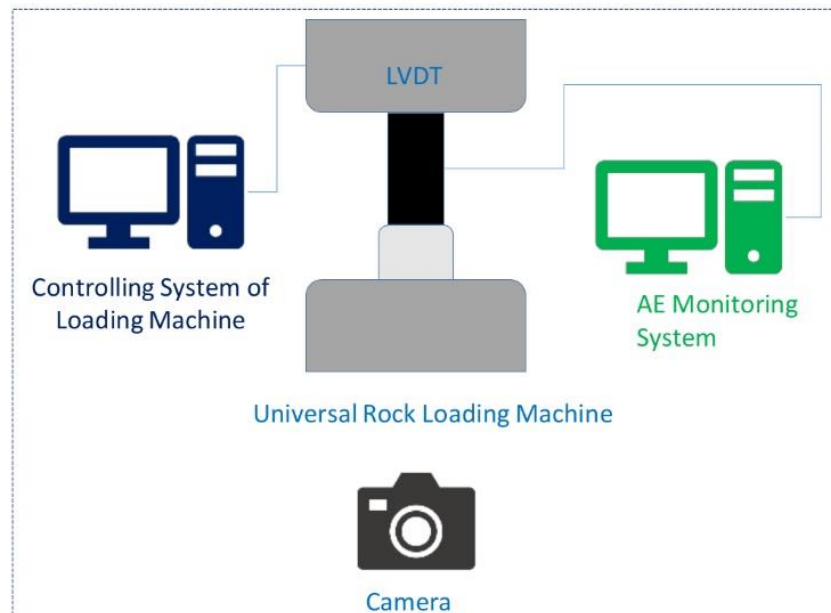
To verify the feasibility of coal failure early-warning using fractal dimension analysis for AE spatial distribution, the uniaxial compression loading tests for coal specimens taken from Australian coal seams with burst history were carried out in the laboratory. These coal specimens are classified as having a high level of burst proneness according to the

burst propensity index tests in Chapter 4 and Chapter 6. A total of 4 specimens were tested under uniaxial compression load displacement control. Two specimens (A set) were tested under a 0.1 mm/min loading rate and another two specimens (B set) under a 0.5 mm/min loading rate as the failure pattern of coal specimens under the higher loading rate is more violent and more similar to coal burst. All the coal specimens were drilled from coal blocks in the laboratory. The coring direction was oriented perpendicular to the joint direction. To maintain the original state of the coal, all blocks taken from the site were fully wrapped with aluminium and plastic membranes. Coal cores were processed into test specimens through the process of cutting and grinding the two ends. The specimens were cylindrical and had a diameter of 54 mm and a length twice the diameter. All conditions of the specimen except specimen size meet the requirements (parallelism, flatness, and verticality) for application of the uniaxial compression strength method according to International Society of Rock Mechanics guidelines.

The loading machine used for this test was a 500 kN electrohydraulic servo universal testing machine (Instron 8033) guided by a controlling computer, which can achieve displacement loading and record the displacement, load, and time during the loading process. The axial displacement and applied load of coal was measured by LVDT and then recorded by the control system of the loading machine. The Express-8 multichannel AE system made by Physical Acoustics was used to acquire the AE data. To film the visual data of coal expansion and failure, a Nikon D5300 SLR camera was placed in front of the loading machine. The test apparatus and arrangement are shown in Figure 7.4.



(a) Test apparatus



(b) Schematic diagram

**Figure 7. 4 Uniaxial compression loading test apparatus and AE setup**

As shown in Figure 7.5, eight AE sensors were attached to the outside surface of the specimens according to the 3D position pre-designed. The AE data was detected by sensors and then directly transferred to the AE processing software installed on the computer. The software simultaneously analysed and recorded all the information for the AE events.

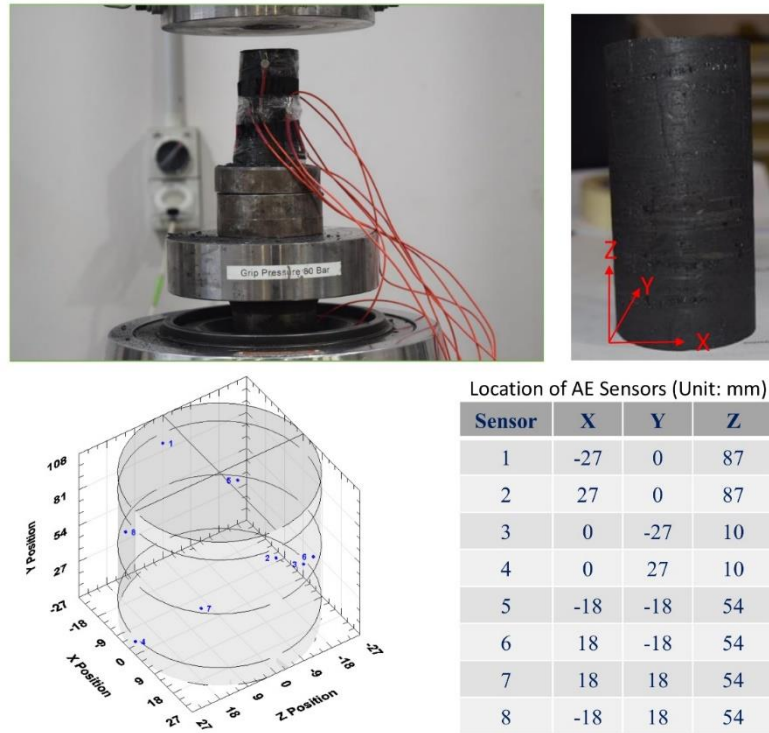


Figure 7.5 Coal specimen and all AE sensors

## 7.4.2 Results and Discussions

As shown in Figure 7.6 and Figure 7.7, loading results indicate that the coal specimens tend to have a high strength and abrupt failure under a high loading rate.

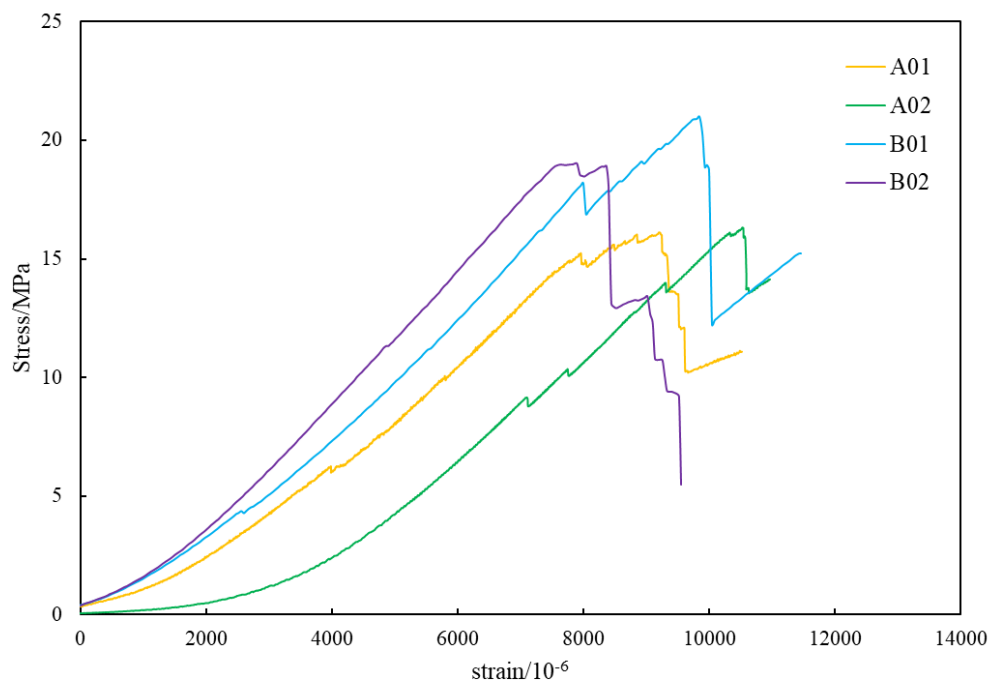
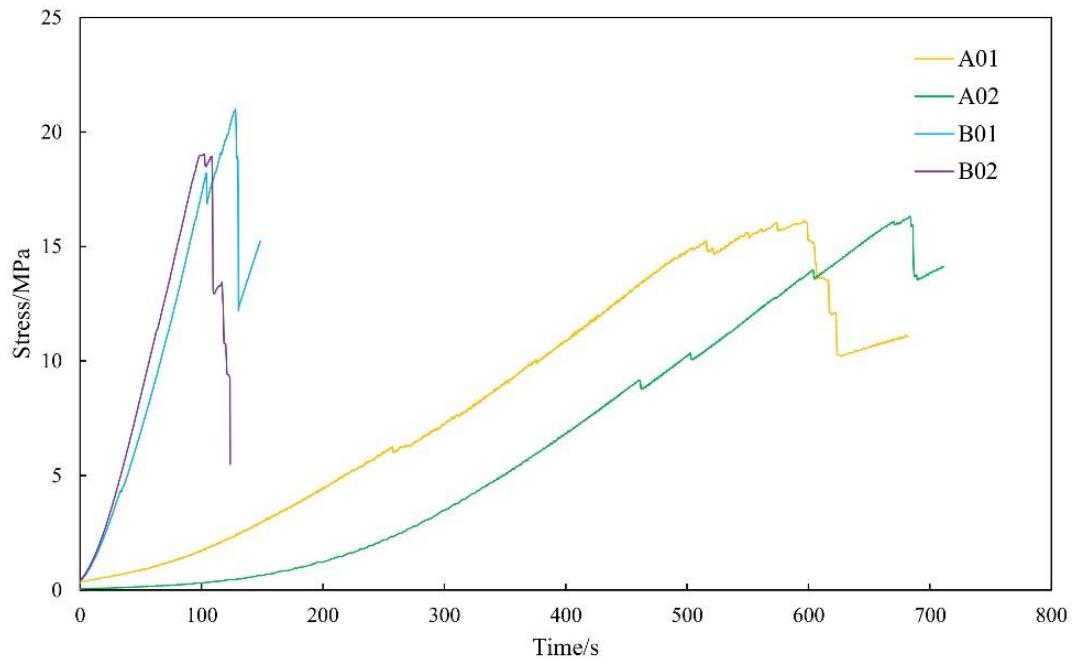
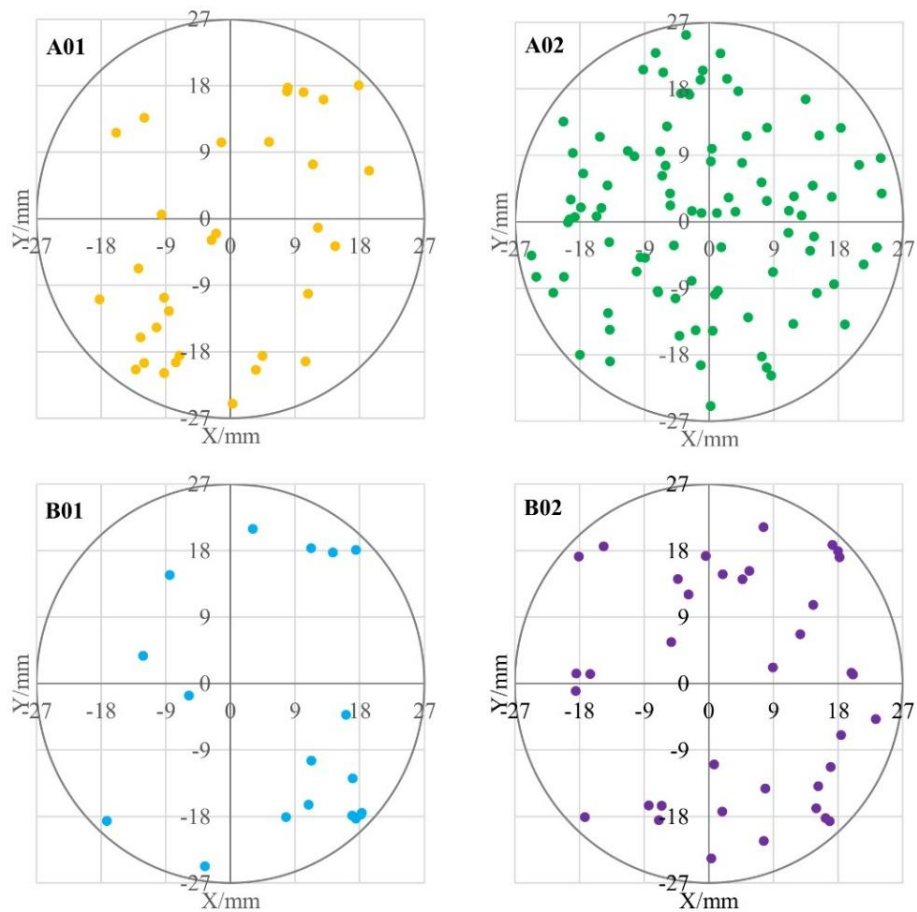


Figure 7.6 Stress vs strain curves of coal specimens subject to uniaxial compression loading



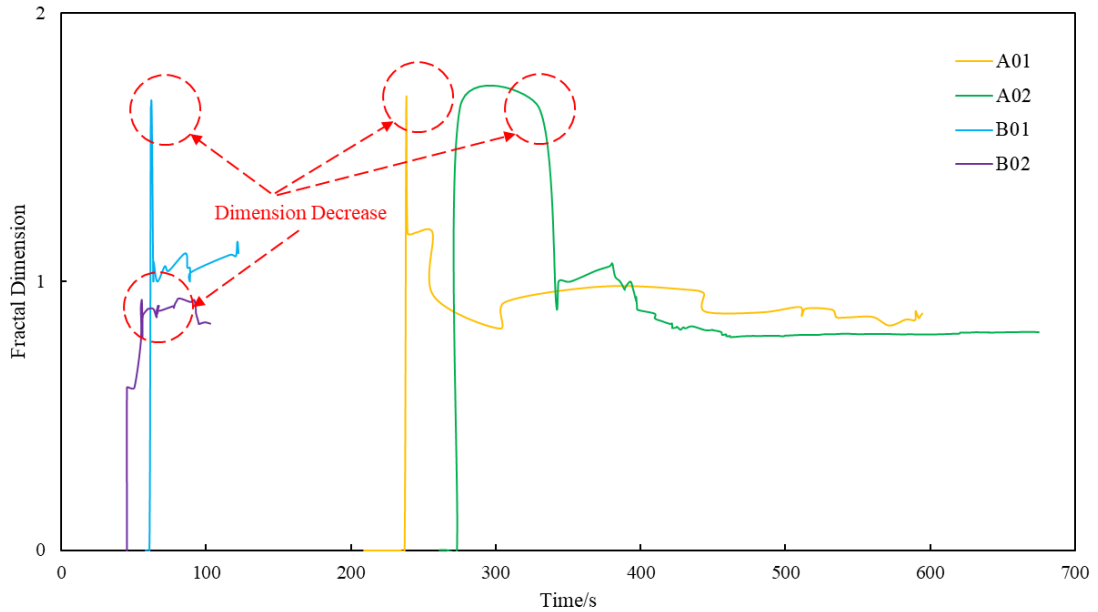
**Figure 7. 8 Stress vs time curves of coal specimens subject to uniaxial compression loading**

Figure 7.8 shows the two-dimensional location of all AE events of four coal specimens subject to uniaxial compression loading.



**Figure 7. 7 Two-dimensional location of all AE events of coal specimens**

According to the mathematical analysis process of fractal dimension introduced in section 7.3, the fractal dimension vs time curve of all coal specimens is shown in Figure 7.9.



**Figure 7.9 Fractal dimension of AE spatial distribution of coal specimens**

In Figure 7.9, the fractal dimension of specimen A01, A02 and B01 have a sharp decrease before failure while that of specimen B02 has a small decline. That is, the fractal dimension of AE spatial dimension of all specimens has a visible decrease before coal failure. It is worth noting that the time duration between the failure point of the coal specimen and the sudden drop of fractal dimensions is very different for Group A and Group B. For Group A, coal specimens loaded with 0.1 mm/min displacement control, the sudden drop point is around 5 minutes before coal failure. For Group B, coal specimens loaded with 0.5 mm/min displacement control, the sudden drop point is around 50 seconds before coal failure. It has been mentioned in previous research that coal tends to have a more violent failure under a higher loading rate (Yang, Ren et al. 2020). According to Figure 7.9, the early warning time for violent failure is shorter than for gentle failure. The time duration between the failure point and sudden drop is very important for on-site applications of this method. There will be no time to take any mitigation measures if the time duration is too short. The early warning process will

interfere with mining operations if the time duration is too long. The experimental results have shown that the analysis of fractal dimensions is a promising way to predict coal burst as an obvious drop of fractal dimensions has been observed. However, real site trials need to be conducted to verify the feasibility of this method as it is not clear whether the time duration between real coal burst and the sudden drop is correct for early warning.

## **7.5 Conclusions**

This chapter aims to enhance the mining safety and sustainability by mitigating the safety hazards caused by coal burst. Based on the analysis above, the main contributions of this thesis are:

- (1) This chapter provides a brief review of the application of fractal theory and AE techniques in mining science. Equation 6.1 and equation 6.2 give the mathematical formula for fractal dimension calculation of AE spatial distribution.
- (2) The mathematical analysis process for fractal dimension of AE events is introduced in detail within section 6.3. This chapter proposes the mathematical analysis method of fractal dimension based on dimension calculation formula and MATLAB coding, which lays the basis for real-time monitoring and automatic warning of coal burst risk by analysis of the AE data.
- (3) The loading rate has an obvious influence on the strength and failure behaviour of coal. Coal specimens tend to have high strength and brittle failure under higher loading rates, which corresponds with the results of other researchers.
- (4) As shown in Figure 6.8, obvious fractal dimension decrease of spatial distribution of AE is observed, which promises the possibility of coal bursts prediction through AE monitoring.

(5) More coal specimens from different coalmines and onsite tests should be carried out in future research to explore the potential application for coal burst prediction based on fractal dimension analysis of AE or other geophysical data.

## **CHAPTER 8 EFFECTS OF WATER SATURATION TIME ON ENERGY DISSIPATION AND BURST PROPENSITY OF COAL SPECIMENS**

### **Summary**

This chapter experimentally studies the effect of water saturation time on burst propensity, fragmentation characteristics and acoustic emission of coal specimens. Water infusion has long been understood to be an effective way to eliminate coal burst risk as water infusion can loosen and soften coal properties. Based on the coal burst energy analysis methods or indexes adopted in chapter four to seven, this chapter comprehensively evaluates the effect of water saturation time on the coal burst behaviour of coal, demonstrating and exploring the possibility of coal burst control by water infusion.

## **Abstract**

Water infusion has long been taken as an effective way to eliminate coal burst risk as water infusion can loosen and soften coal properties. However, not all industrial trials of water infusion for coal burst prevention has been necessarily effective in all situations as the effectiveness of this method can be impacted by the water infusion time, coal properties and the parameters of water injection. Hence, some fundamental work including the effects of water infusion time on burst propensity and energy evolution need to be further discussed. In this thesis, four groups of coal specimens with 5 days, 10 days, and 15 days water saturation times or as received are tested under uniaxial compression load with the application of AE monitoring. To comprehensively compare the burst behaviour of coal specimens under different water saturation times, stress-strain curves, AE counts, fragmentation characteristics and burst propensity of these groups are analysed. It was found with this research that sufficient water saturation can mitigate the coal burst behaviour of coal specimens while insufficient water infusion might not reach the burst mitigation aims.

## **Keywords**

Coal Burst; Water Saturation; Burst Propensity; Acoustic Emission; Coal Fragmentation

## 8.1 Introduction

With an increase of mining depth, the coal body is generally impacted by more complicated geological conditions and supercritical stress, which may lead to catastrophic failure of coal causing personal casualties and economic losses. The catastrophic failure of coal, also called coal burst, can release large amount of stored energy in the forms of loud sounds, coal ejection and even seismic events (Yang, Ren et al. 2018). Coal burst now has become one of the major safety concerns faced by future mining operations as it has been mentioned in literature that both the coal burst frequency and severity increase with mining depth (Zhang, Canbulat et al. 2017). Poland started the research of coal burst along with Czechs in 1912 and was the first to propose the coal burst propensity measurement method for coal burst risk evaluation (Shen and Luo 2016). Coal burst caused 401 fatalities from 1949 to 1982 in Poland (Dou and He 2001). Coal burst has a long history in the U.S. as well. From 1936 to 1993, 172 burst accidents caused 83 fatalities and 163 injuries in the U.S. (Christopher 2017). In China, research into coal burst was initially carried out in the early 1960's and more than 147 coal mines experienced coal burst to the end of 2014 (Shen and Luo 2016). After decades of research and engineering practice of coal burst control, these chief coal mining countries had a good understanding of the coal burst phenomenon and have made great progress with forecasting methods and solving techniques for coal burst. In Australia, coal burst is a new challenge for mining researchers and technicians as the first coal burst accident occurred in 2014. However, considering the increasing coal burst risk with mining depth and intensity going forward, the control and mitigation measures of coal burst in Australia need more research.

The water infusion method was primarily developed and applied in European coal mines, mainly for dust control (Ren, Plush et al. 2011). This method typically involves the pre-

mining injection of water into the coal seam to increase its moisture content and therefore reduce dust generation during mining. Water infusion has long been taken as an effective way to eliminate coal burst risk as water infusion can loosen and soften coal properties. This method has been applied in the Ruhr Coalfield (Germany) since the 1960's and achieved great success in coal burst mitigation. As reported by Bräuner, the uniaxial compression strength and elastic modulus of Ruhr coal was reduced by 60-70 % and 40-70 % respectively by increasing the moisture content from 1 to 5 % (Brauner 1994), which means the elastic energy scale stored in coal can be reduced by water infusion. In Colorado, the pillar infusion used at the Elk Creek Mine demonstrated that infusion increased the yielding of the pillar, reducing the occurrence of damaging bumps (Varley and Whyatt 2008). Water infusion is recommended as a coal burst mitigation method in the coal burst prevention rules published by the Chinese mining authority in 2018 (National Coal Mine Safety Administration 2018). as water infusion has been successfully used for preventing coal and gas outburst (Aguado and Nicieza 2007). Theoretically, water infusion can decrease the strength of coal by increasing pore pressure (Frid 2000). The increasing moisture content can soften coal and mitigate coal burst risk by consuming more energy plastically. However, not all industrial trials of water infusion for coal burst prevention has been necessarily effective in all situations as the effectiveness of this method can be affected by the water infusion time, coal properties and the parameters of water injection. Hence, some fundamental work including the effects of water infusion time on burst propensity and energy evolution needs to be further discussed.

The burst propensity index method and fragmentation analysis method has been introduced in Chapter 3 and Chapter 4, respectively. The aim of this chapter is to investigate the influence of water saturation time on energy dissipation and burst

propensity of coal specimens through experimental study, hence providing a better understanding of the influence of water on the mechanical behaviour and burst characteristics of the coal body during the underground infusion process. Four groups of coal specimens with 0 day, 5 days, 10 days and 15 days water saturation time are tested under a uniaxial compression load with the application of AE monitoring. However, considering the confining effect caused by the layout of the sensors, only two sensors are used to record the AE counts during the loading process. Stress-strain curves for all coal specimens are introduced to demonstrate the average strength change of the coal specimens after different water infusion times. AE is analysed to demonstrate the influence of water infusion on the plastic energy dissipation in the form of crack and fracture propagation. Fragmentation characteristics of coal specimens, which is seldom touched on by previous research, is analysed based on image processing techniques to demonstrate energy dissipation during brittle failure of coal specimens. The burst propensity of every group is also calculated in this chapter.

## **8.2 Material and Methodology**

### **8.2.1 Specimen Preparation**

Coal blocks taken from local coal mines were cored and processed into 54 mm diameter and 108 mm long cylindrical coal specimens before testing. The drilling direction of all coal specimens was oriented perpendicular to the joint direction of the coal blocks. To maintain the original moisture content of the coal and to avoid damage during delivery, all blocks taken from the underground were fully wrapped with aluminium and plastic membranes. All other conditions (parallelism, flatness, and verticality) of the coal specimens should meet the standards for the application of the uniaxial compression strength method published in the International Society of Rock Mechanics guidelines. All

coal specimens were well wrapped before the test with plastic membranes and stored in the laboratory at a relatively constant temperature and humidity.

### 8.2.2 Test Apparatus and Procedure

As shown in Figure 8.1, the tests were all conducted on a 500 kN hydro-servo Instron-8033 universal rock testing machine. The axial displacement and applied load for the coal specimens were recorded by the data acquisition system. All specimens were loaded with a displacement control loading rate of 0.5 mm/min, which is the loading rate for the coal burst propensity test. To obtain the effect of saturation time on energy dissipation and burst propensity of the coal specimens, four test schemes were designed based on saturation time. The saturation time of coal specimens was designed for 5 days, 10 days, and 15 days or as received. As shown in Figure 8.2, coal specimens were saturated for the designed time in the container before the tests.



Figure 8. 1 Apparatus set-up

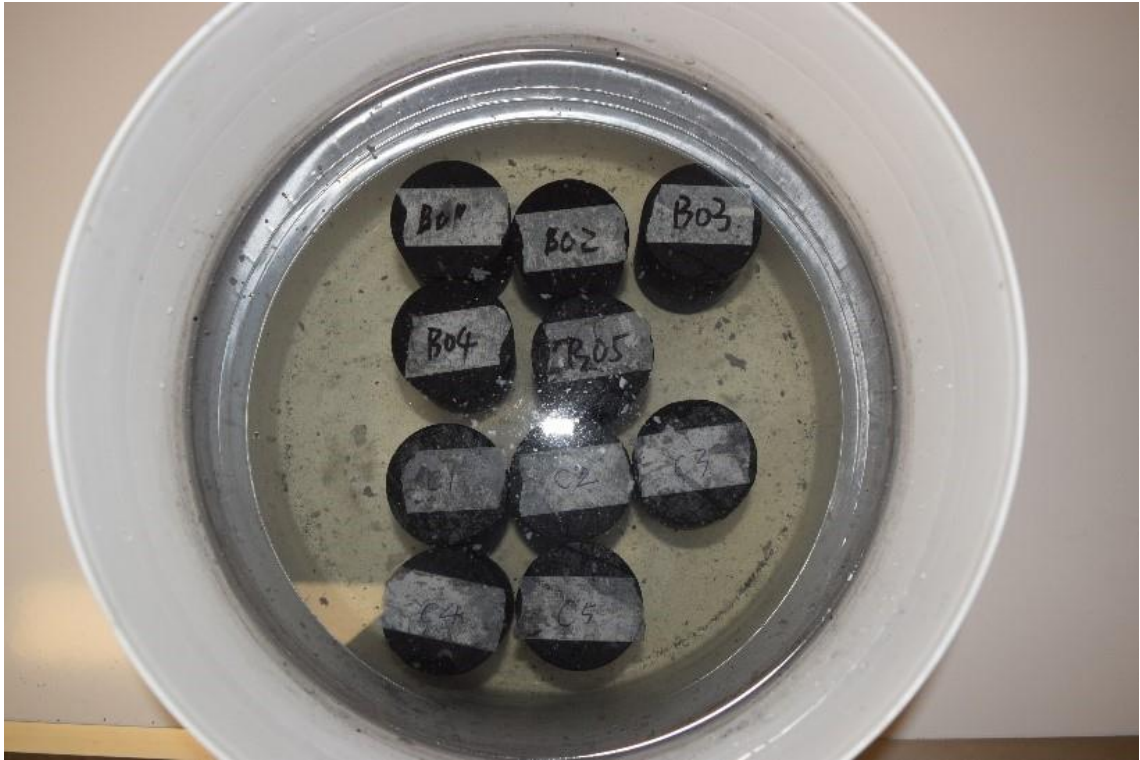


**Figure 8. 2 Water saturation of coal specimens**

### **8.2.3 AE Monitoring**

As an important non-destructive evaluation and monitoring methods, AE monitoring has been widely adopted to study the damage mechanics of coal caused by crack initiation and propagation under applied stress (Ranjith, Jasinge et al. 2010). It has been proven by previous research that the AE event counts can reflect the stress change and fracture intensity inside the coal body (Lou, Song et al. 2019). During the test, AE sensors were attached to the surface of the coal specimens to continuously record AE data generated inside the coal specimens. As shown in Figure 8.3, the AE system adopted in this test was an Express-8 AE system, which can achieve a 10 kSPS sampling rate with 1 kHz to 1.2 MHz bandwidth. AE monitoring was started at the same time as uniaxial compression loading. All the data including event counts, amplitude distributions and frequency characteristics was automatically recorded in the computer for analysis.



**Figure 8. 3 AE monitoring system**

#### **8.2.4 Fragment Analysis**

Fragmentation is a common mechanical phenomenon that exists in the brittle failure of coal subjected to static, impact, and dynamic loads, during which coal fragments with difference sizes can be generated. The analysis of the fragment size distribution (FSD) of coal, which has rarely been studied in previous research, is important for the understanding of energy dissipation characteristics and fracture activities within coal specimens (Yang, Ren et al. 2020). As introduced in Chapter 5, FSD analysis of fragmented coal specimens was conducted using a combination of the manual sieving method and image processing techniques. Coal fragments generated by the uniaxial compression test were sieved into several regimes and then digitally analysed through image processing utilising MATLAB software. The sieve adopted in this study has four sieve sizes including  $d = 2.5, 5, 10$  and  $20$  mm . The image processing operations including image acquisition, image reading, image binarization, watershed segmentation

and statistical measurements. Every step of the fragment analysis and its result are shown in Figure 8.4.

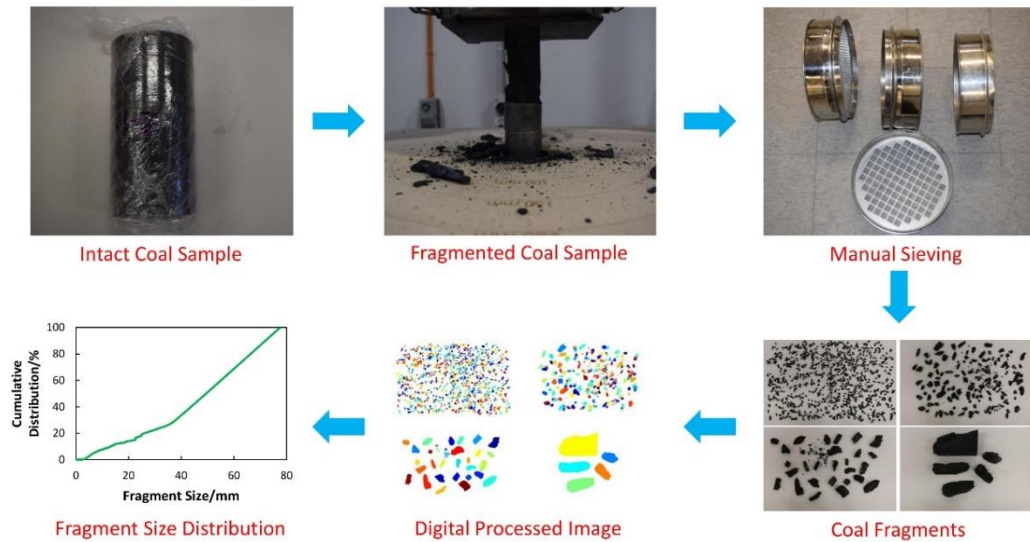


**Figure 8. 4** Fragment size distribution analysis process

### 8.2.5 Burst Propensity

The Coal burst propensity index method, which includes the uniaxial compressive strength ( $R_C$ ), elastic strain energy index ( $W_{ET}$ ), bursting energy index ( $K_E$ ) and dynamic failure time ( $DT$ ), is a widely used method for coal burst risk evaluation (Guo, Tan et al. 2017). Russian and Polish coal mines adopted  $W_{ET}$  and  $K_E$  to evaluate the burst risk of coal (Kidybiński 1981). Zhang et al. and Qi et al. proposed  $DT$  and  $R_C$ , respectively for coal burst propensity evaluation (Yang, Ren et al. 2018). In 2010, the China Coal Industry Association summarized these four indices as the burst propensity index method and published the measurement standard of these four indices. Based on previous research and the Chinese standard, as shown in Table 8.1, chapter 4 proposed the burst propensity measurement method and risk classification form for Australian coal. The burst propensity of coal specimens with different water saturation times were all determined based on the calculation of these four indices.

**Table 8. 1 Coal burst propensity index and risk classification of Australian coal**

Index	$R_C$ /MPa	$DT$ /s	$K_E$	$W_{ET}$
Test Method	Uniaxial Loading			Uniaxial Loading-Unloading
Schematic Diagram				
High	$RC \geq 15$	$DT \leq 10$	$KE \geq 5$	$WET \geq 5$
Moderate	$10 \leq RC < 15$	$10 < DT \leq 15$	$3.5 \leq KE < 5$	$3.5 \leq WET < 5$
Low	$5 \leq RC < 10$	$15 < DT \leq 20$	$2 \leq KE < 3.5$	$2 \leq WET < 3.5$
None	$RC < 5$	$DT \geq 20$	$KE < 2$	$WET < 2$

### 8.3 Results and Discussions

#### 8.3.1 Stress-strain Curves

Elastic and mechanical weakening from water saturation are widely known to occur in sedimentary rocks including sandstone, limestone and coal (Pimienta 2014). Figures 8.5 demonstrate how water saturation affects the strength and elastic behaviour of coal specimens. As shown in Figures 8.5, both strength and elastic modulus of Group D are obviously lower than Group A, B and C, which means the strength of coal specimens has been weakened with long term water saturation. The explanation of strength reduction after water saturation can be given by existing research as water molecules react easily with clay and mineral contents in coal and consequently soften its bond structure (Perera, Ranjith et al. 2011). However, the strength of B2 and C1, specimens with 5- and 10- days water saturation, respectively, are unreasonably high. Considering the natural weakness and inhomogeneous properties of the coal specimens, it is possible that the strength of the coal specimens is in a very wide range during the laboratory uniaxial compression tests.

The increase of pore pressure contributes to the reduction of strength as well. The elastic behaviour of the coal specimens has been obviously weakened by water infusion as the slope of stress-strain curves are lower with longer water infusion time, which means the stiffness of the specimens has been reduced.

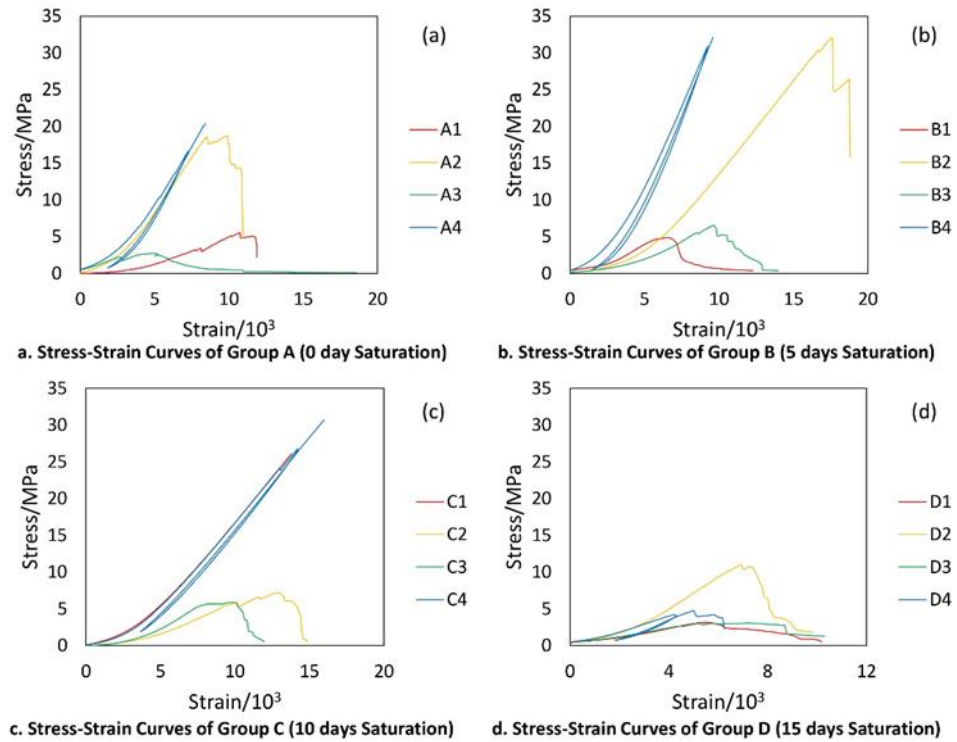
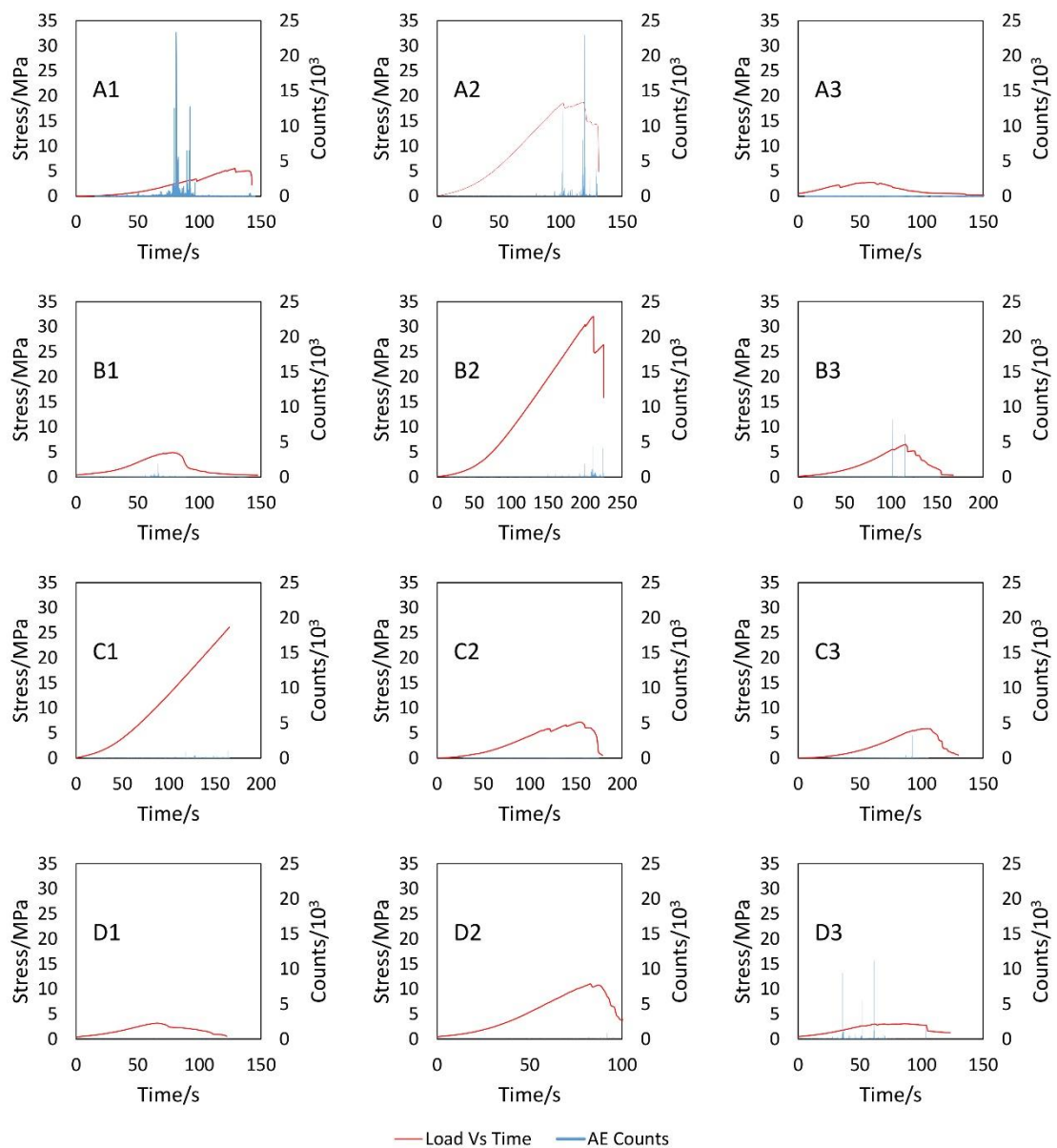


Figure 8. 5 Stress-strain curves of Group D

### 8.3.2 AE Features

AE data generated by the AE system for each uniaxial loaded specimen was examined, and the results are shown in Figure 8.6. It has been widely accepted by researchers that the counts of AE can be used to identify the fracture propagation inside coal (Perera, Ranjith et al. 2011). According to Ranjith et al. (Ranjith, Jasinge et al. 2010), the pre-failure stress curve of coal specimens can be divided into three crack propagation periods: crack closure period with very few AE counts, stable crack propagation period with a linear increment of AE counts and unstable crack propagation period with an exponential increment of AE counts. It can be seen from Figure 8.6 that the magnitude of AE counts has been significantly decreased by water infusion, which indicates the low intensity of

crack activities inside water saturated coal specimens during the uniaxial loading process. The observed effects of water saturation on AE counts is consistent with previous research done by Perera et al. (Perera, Ranjith et al. 2011). The SEM observation of coal microstructures has demonstrated that the surface area and total volume of the internal micro structures of coal specimens can be greatly increased by saturation (Liu, Xu et al. 2017). That is, the fracture tips of the coal microstructure have been weakened, which explains the reduction of AE counts after water saturation.



**Figure 8. 6 AE counts and stress of specimens**

### 8.3.3 Fragmentation Characteristics

The fragmentation characteristics, which have not been discussed in any detail by previous research, are important in order to understand the energy dissipation characteristics and the burst mechanism of coal specimens (Liu, Li et al. 2014). It has been found in previous research that the ejection velocity associated with coal burst can be estimated based on energy dissipation and coal fragmentation (Yang, Ren et al. 2020). To provide a comprehensive understanding of the water saturation effect on the failure behaviour of coal specimens, the FSD of selected coal specimens is analysed using a combination of manual sieving and image processing techniques as introduced in Chapter 5. It has been well-documented by previous research that the FSD of coal can be statistically described by the fractal model (Peng, Ju et al. 2015). The fractal dimension of the model is adjusted based on the image processed curve.

Figure 8.7 shows the cumulative size distribution of selected coal specimens obtained by manual sieving, imaging processing and fractal modelling. It can be seen from Figure 8.7 that the similarity of the curves generated by different methods is very high, that is, fractal modelling and image processed curves are both suitable to characterise the FSD of coal specimens. The fractal size distributions of coal specimens are compared in Figure 8.8 to demonstrate the water saturation influence on the fragmentation characteristics of coal. Generally, sufficient water saturation can make the fragmentation mode more stable as the curves of D1 and D2 in Figure 8.30 are similar. However, coal specimens with insufficient water saturation (specimen B1 and C1) may have more random fragmentation patterns than those without water saturation. This phenomenon might result from the uneven water distribution inside the coal specimens (Zhou, Cai et al. 2016).

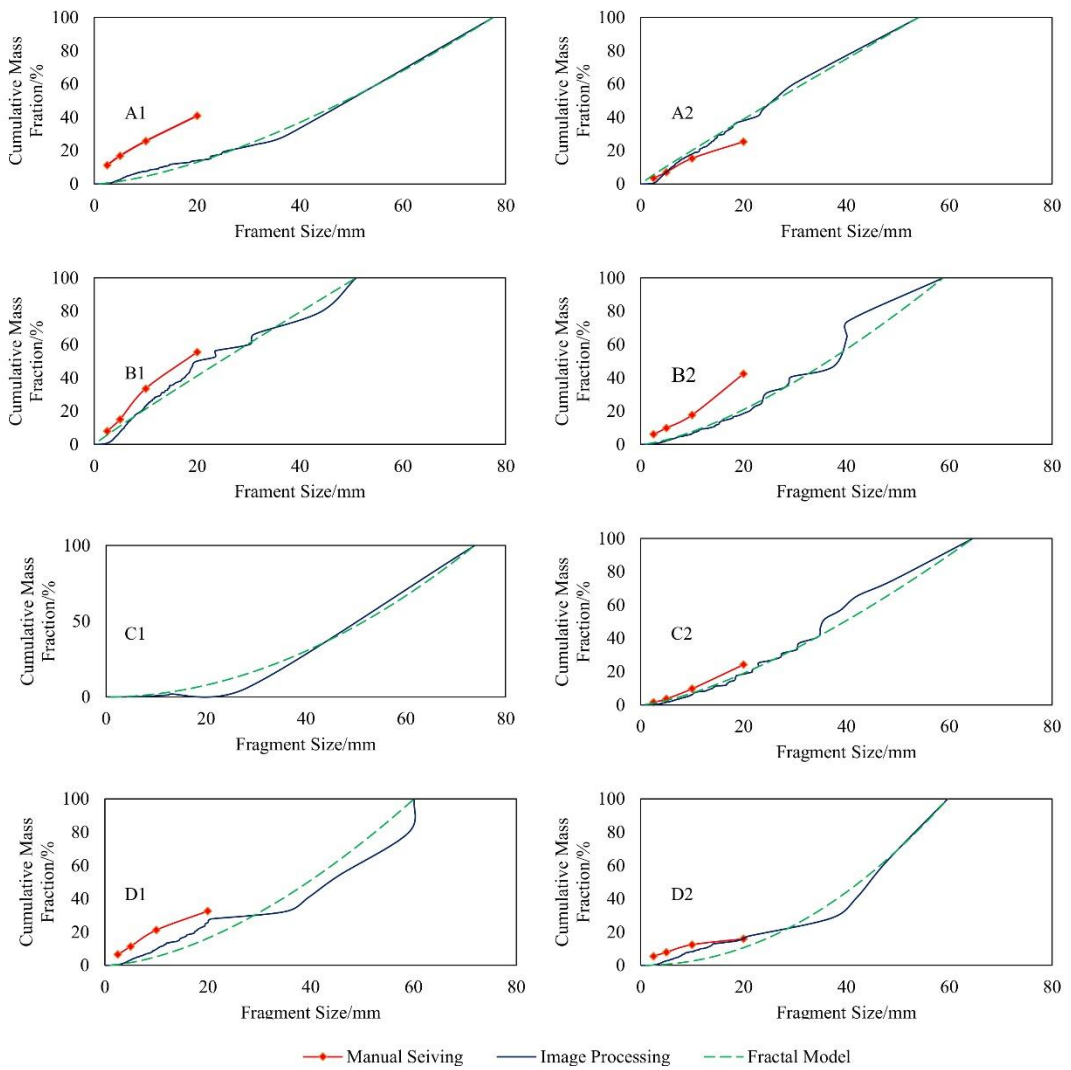


**Figure 8. 7 FSD of specimens**

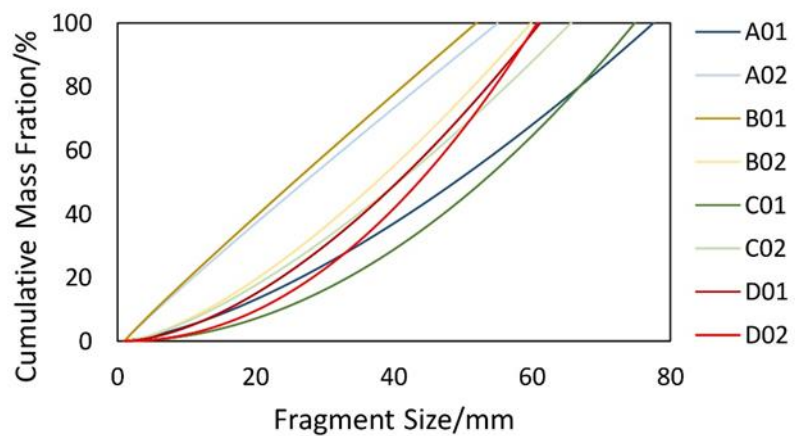


**Figure 8. 8 Fractal size distribution of coal specimens**

### 8.3.4 Burst Propensity

It has been mentioned in literature that the strength and burst propensity of rock and coal decrease with moisture content (Meng, Pan et al. 2009). The burst propensity index method has been widely used to evaluate the burst risk of coal seams in many countries (Yang, Ren et al. 2018). The burst propensity indexes of these four groups of coal specimens are calculated based on Figure 8.5 and Table 8.1 and the results are shown in Figure 8.9. According to Figure 8.9, the burst propensity of group D is the lowest as the coal specimens of group D have been saturated with the longest time. The burst propensity of group B and C are even higher than group A, although group B and C have been saturated for 5 and 10 days, respectively. It has not been indicated by previous research that in-sufficient water saturation may increase the burst propensity of coal. Both experimental and numerical studies suggested that the burst propensity should decrease with the water saturation time (Guo, Tan et al. 2017, Liu, Xu et al. 2017).

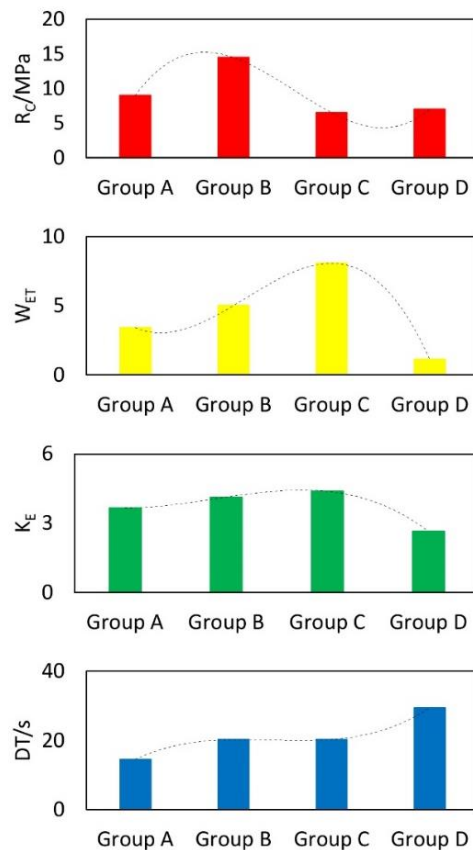


Figure 8. 9 Burst propensity of coal specimens

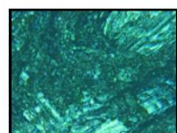
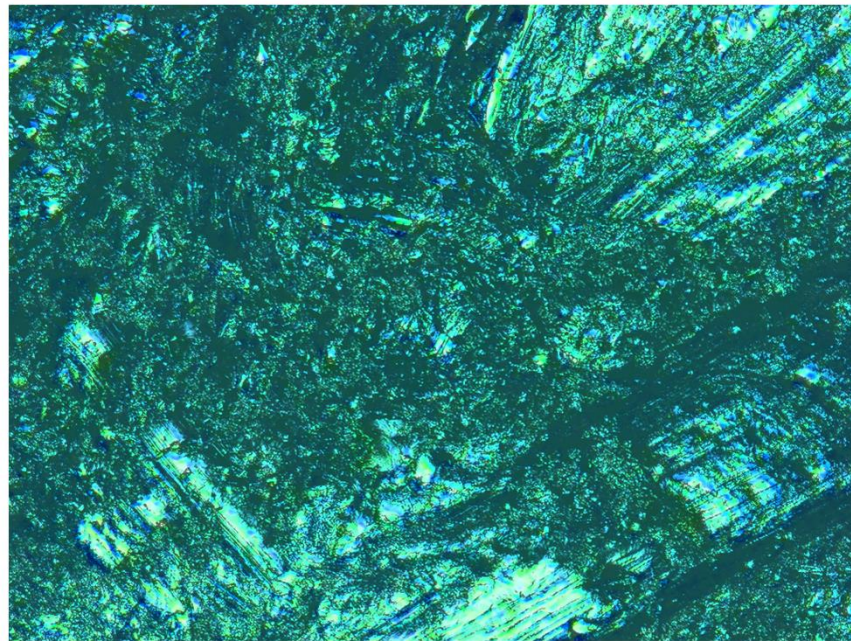
It is unclear whether this phenomenon is caused by the difference between coal specimens. A different correlation between saturation time and burst propensity may occur if more specimens were tested.

### 8.3.5 Surface Roughness

To demonstrate the water saturation effect on the microstructure of coal, a KEYENCE VK-X100 3D laser scanning microscope was used to scan the micro surface and measure the roughness of coal specimens with different saturation times. The KEYENCE VK-X100 3D laser scanning microscope is one of the leading microscopes for obtaining a high-resolution surface image and to measure the surface characteristics of different materials (Shehata, Mohamed et al. 2018). Two disk specimens with a 50 mm diameter and 25 mm thickness from the same coal seam as the water infusion specimens were processed in the laboratory for scanning observation. Three points were marked on one surface of each specimens. The measured roughness and corresponding figure number of each point are listed in Table 8.2. The scanned pictures are shown in Figure 8.10 to 8.15.

**Table 8. 2 Surface roughness point and value**

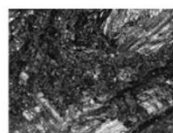
Specimen	Point No	Saturation Time/Days	Roughness/ $\mu\text{m}$	Figure No
1	1	5	136.55	8.10a
1	2	5	76.69	8.10b
1	3	5	155.94	8.10c
2	1	5	84.01	8.11a
2	2	5	97.32	8.11b
2	3	5	87.09	8.11c
1	1	10	48.16	8.12a
1	2	10	41.47	8.12b
1	3	10	74.05	8.12c
2	1	10	48.16	8.13a
2	2	10	50.33	8.13b
2	3	10	113.79	8.13c
1	1	15	30.72	8.14a
1	2	15	70.22	8.14b
1	3	15	116.73	8.14c
2	1	15	50.82	8.15a
2	2	15	47.85	8.15b
2	3	15	67.50	8.15c



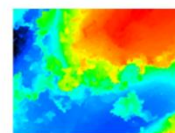
Laser+Optical



Optical

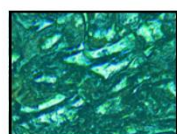
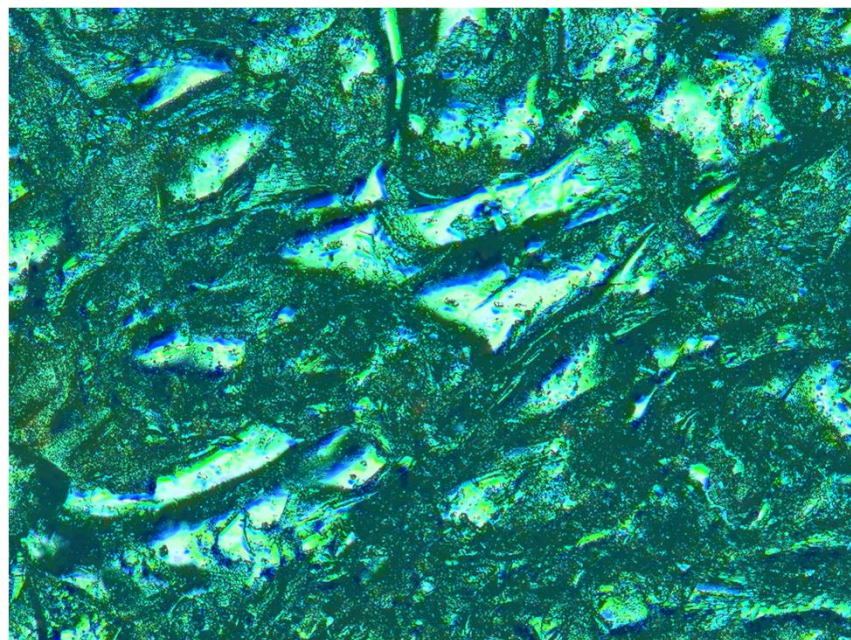


Laser intensity

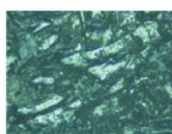


Height

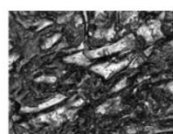
a. Specimen 1 point 1



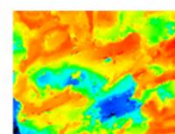
Laser+Optical



Optical

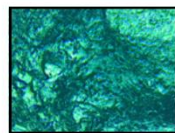
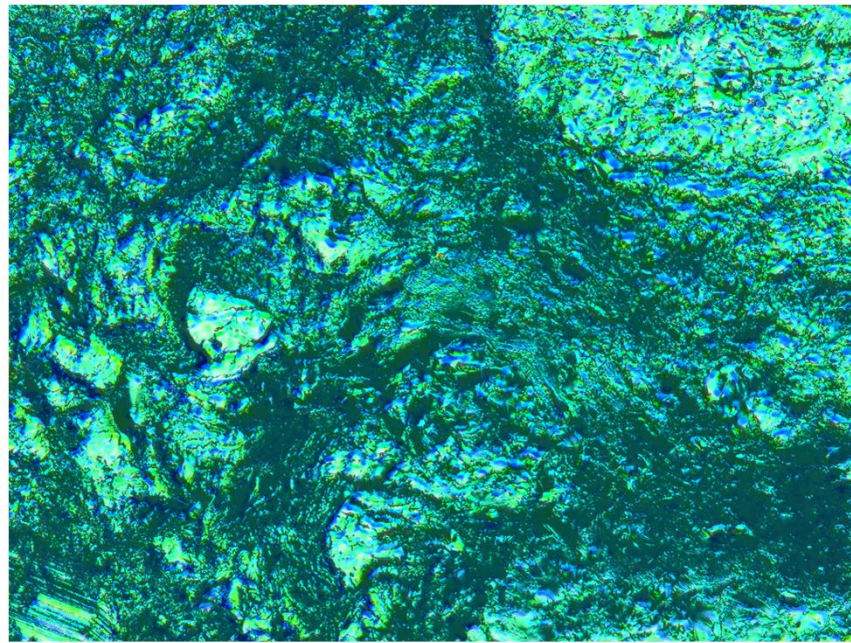


Laser intensity

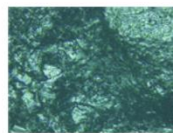


Height

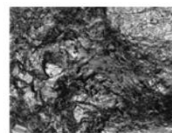
b. Specimen 1 point 2



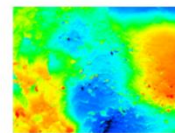
Laser+Optical



Optical



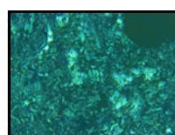
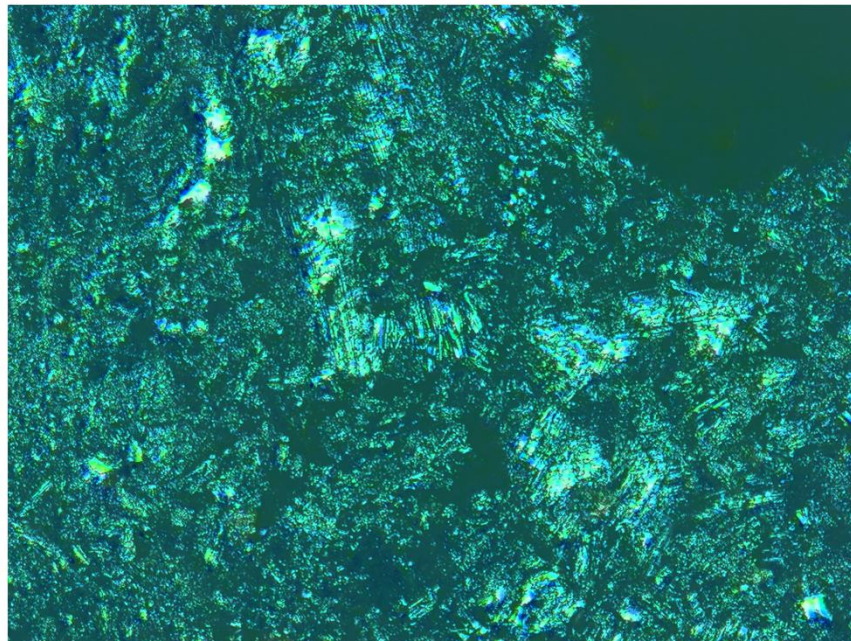
Laser intensity



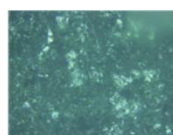
Height

c. Specimen 1 point 3

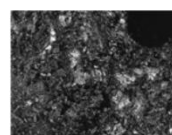
Figure 8. 10 Laser scanning of specimen 1 with 5 days water saturation



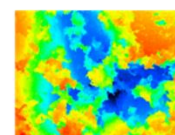
Laser+Optical



Optical

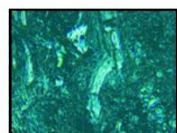
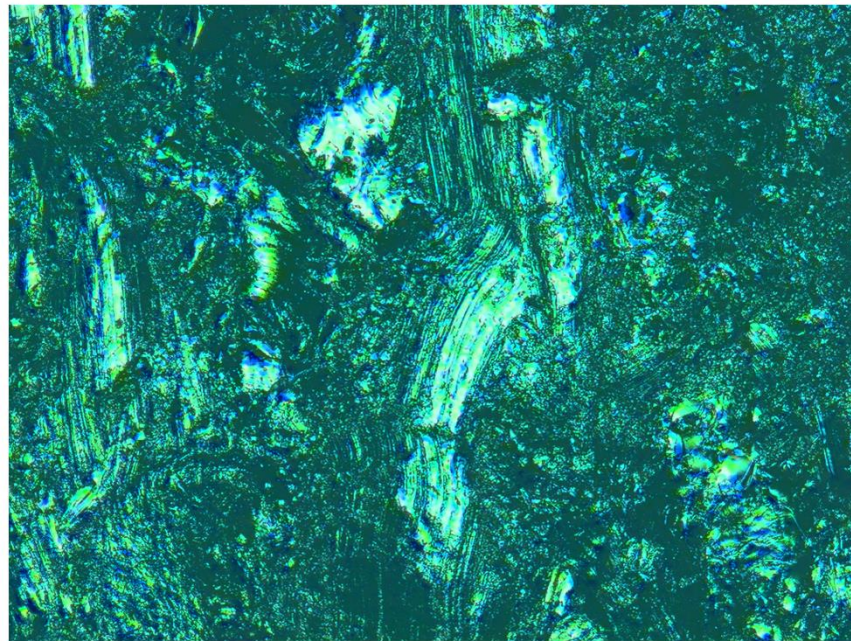


Laser intensity

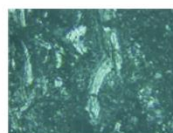


Height

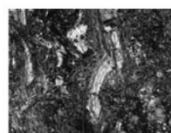
a. Specimen 2 Point 1



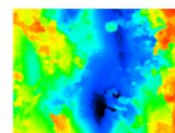
Laser+Optical



Optical

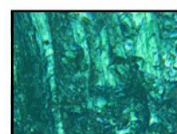
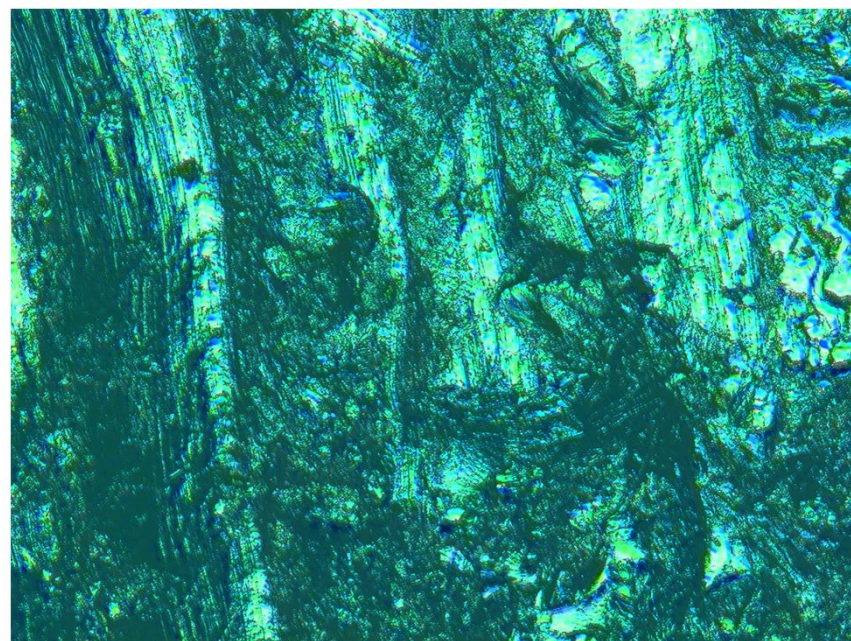


Laser intensity



Height

b. Specimen 2 Point 2



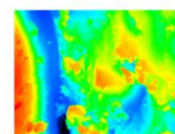
Laser+Optical



Optical



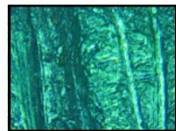
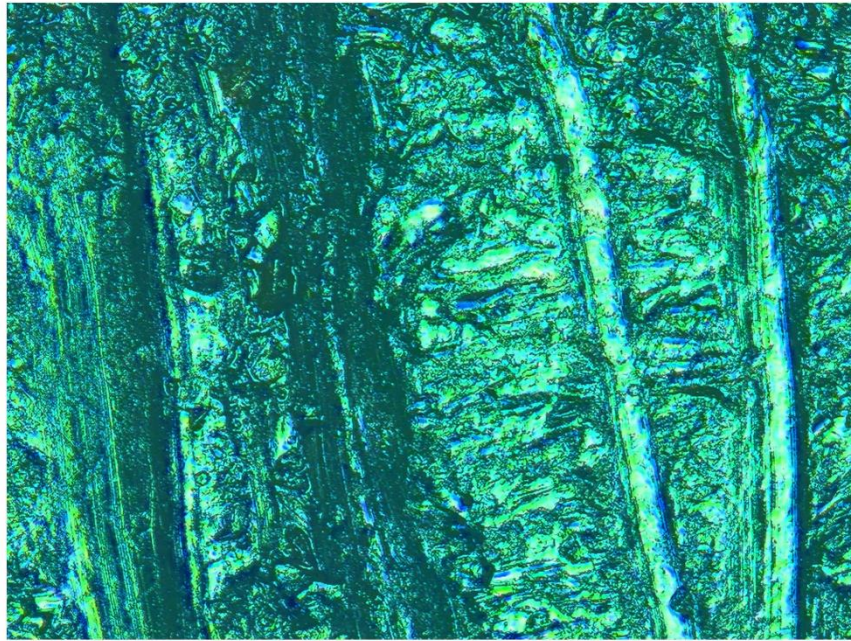
Laser intensity



Height

c. Specimen 2 Point 3

Figure 8. 11 Laser scanning of specimen 2 with 5 days water saturation



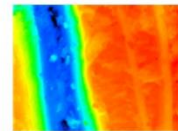
Laser+Optical



Optical

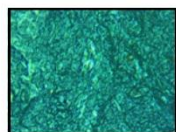
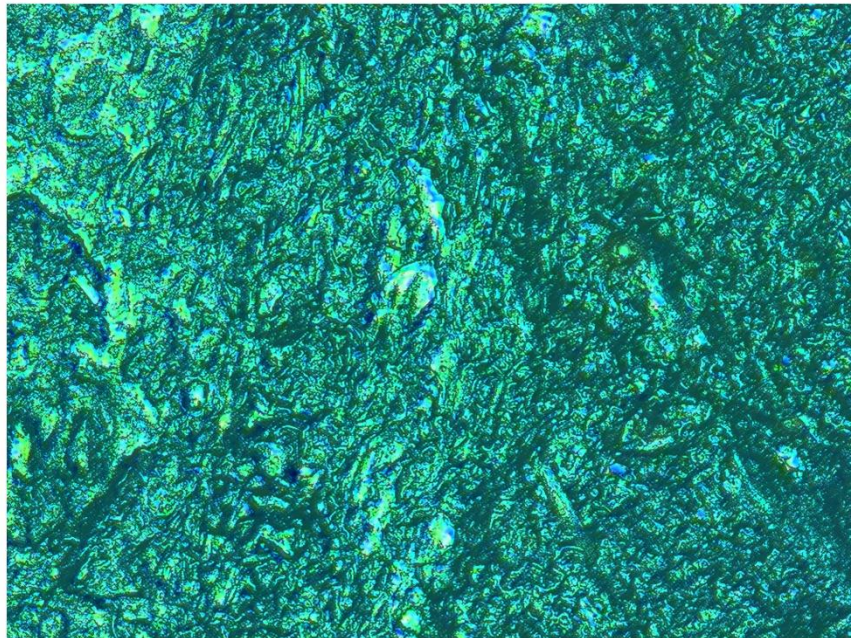


Laser intensity

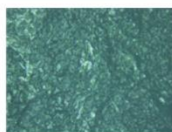


Height

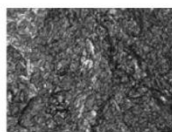
a. Specimen 1 point 1



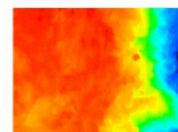
Laser+Optical



Optical

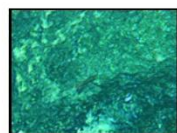
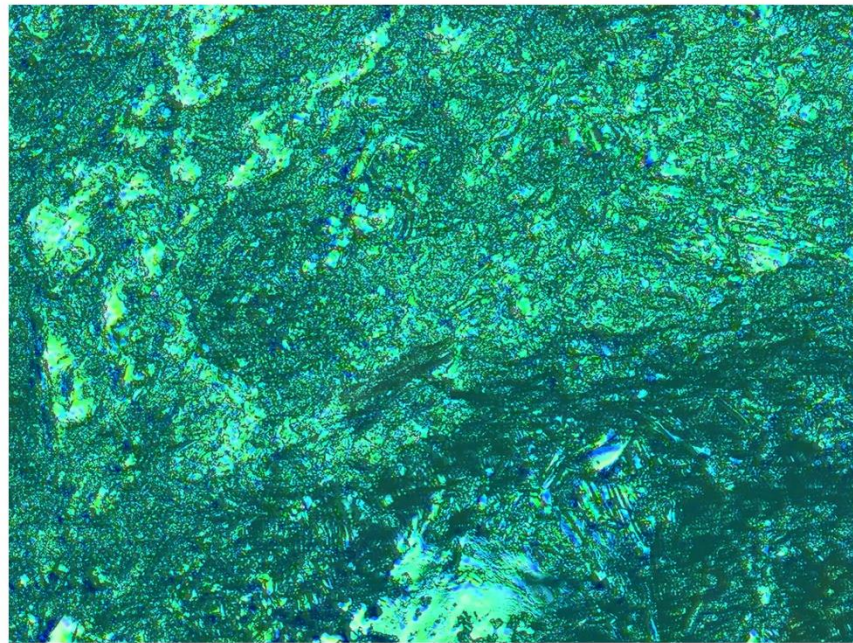


Laser intensity

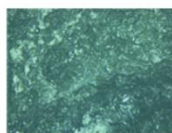


Height

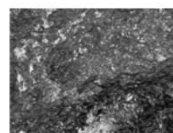
b. Specimen 1 point 2



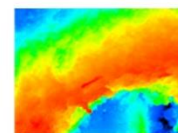
Laser+Optical



Optical



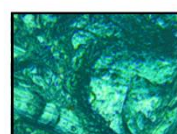
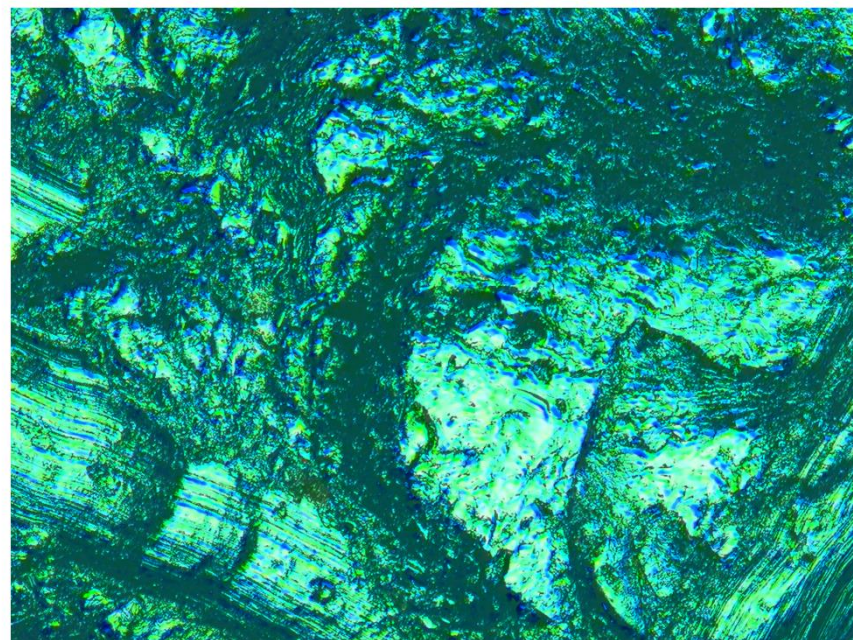
Laser intensity



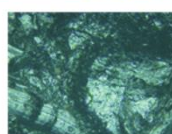
Height

c. Specimen 1 pint 3

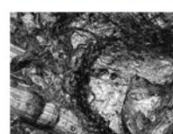
Figure 8. 12 Laser scanning of specimen 1 with 10 days water saturation



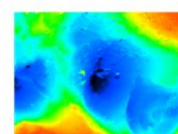
Laser+Optical



Optical

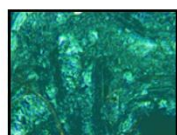
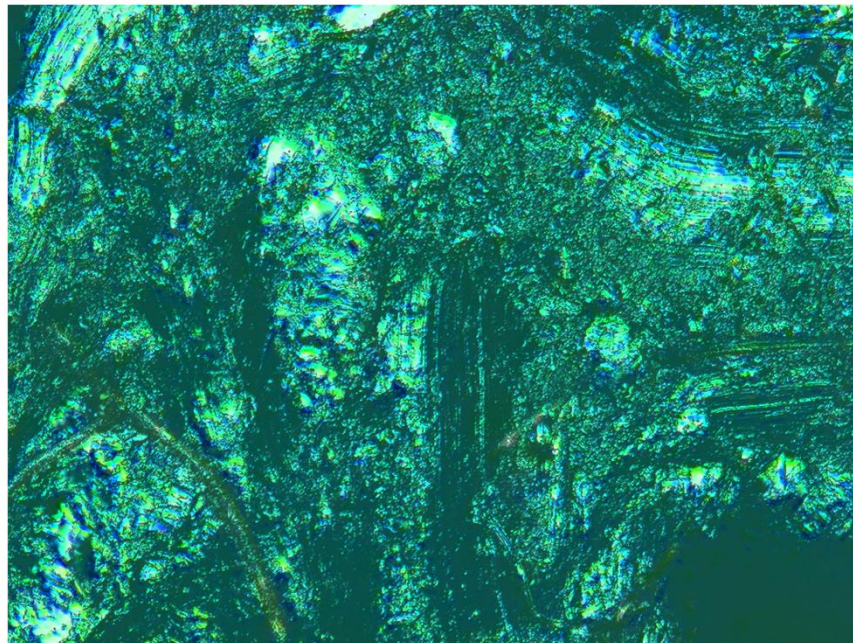


Laser intensity



Height

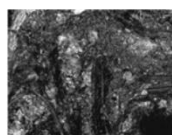
a. Specimen 2 point 1



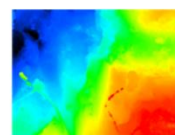
Laser+Optical



Optical

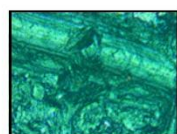
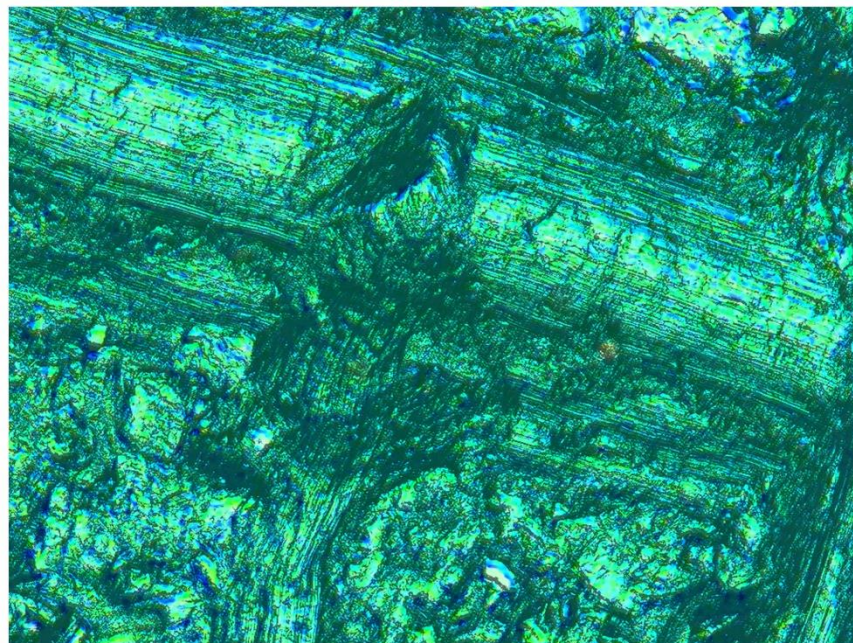


Laser intensity

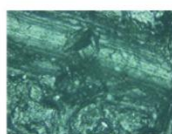


Height

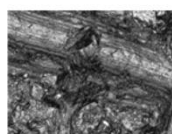
b. Specimen 2 point 2



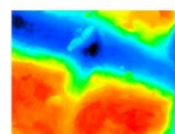
Laser+Optical



Optical



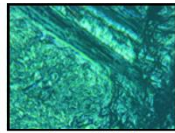
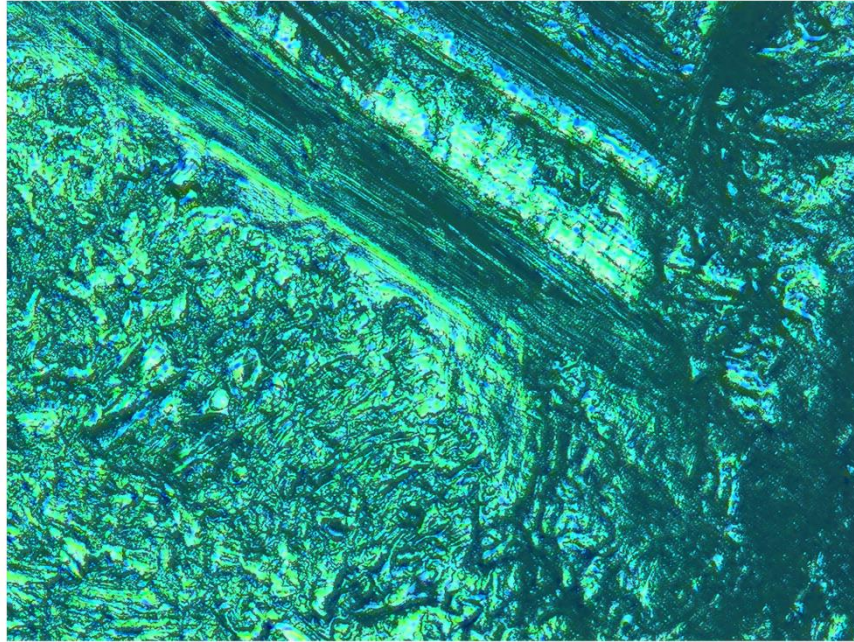
Laser intensity



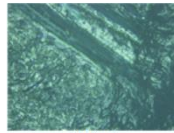
Height

c. Specimen 2 point 3

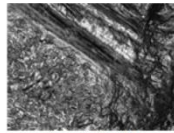
Figure 8. 13 Laser scanning of specimen 2 with 10 days water saturation



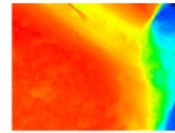
Laser+Optical



Optical

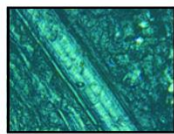
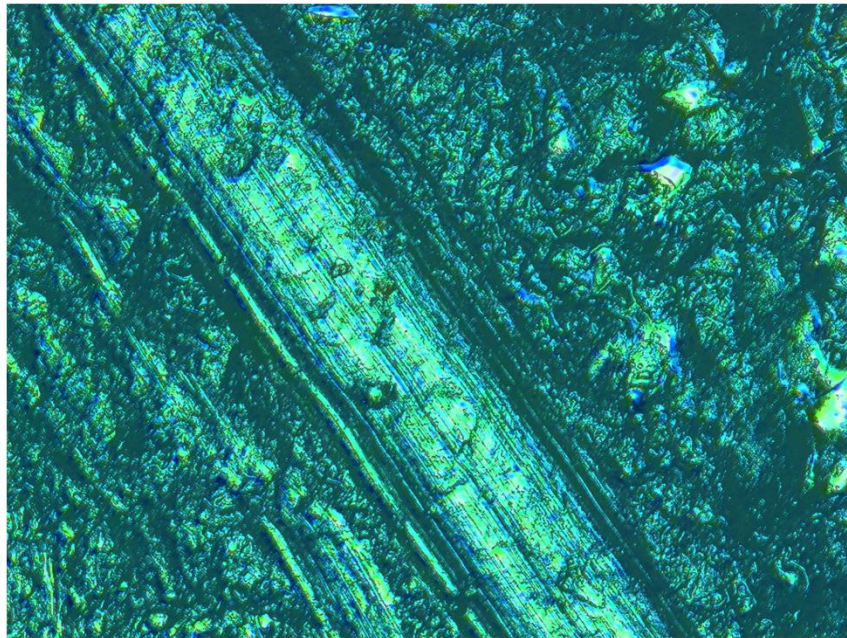


Laser intensity

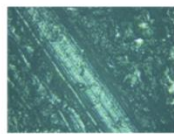


Height

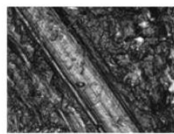
a. Specimen 1 point 1



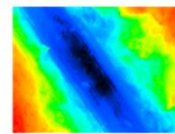
Laser+Optical



Optical

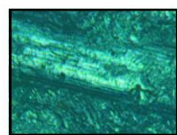
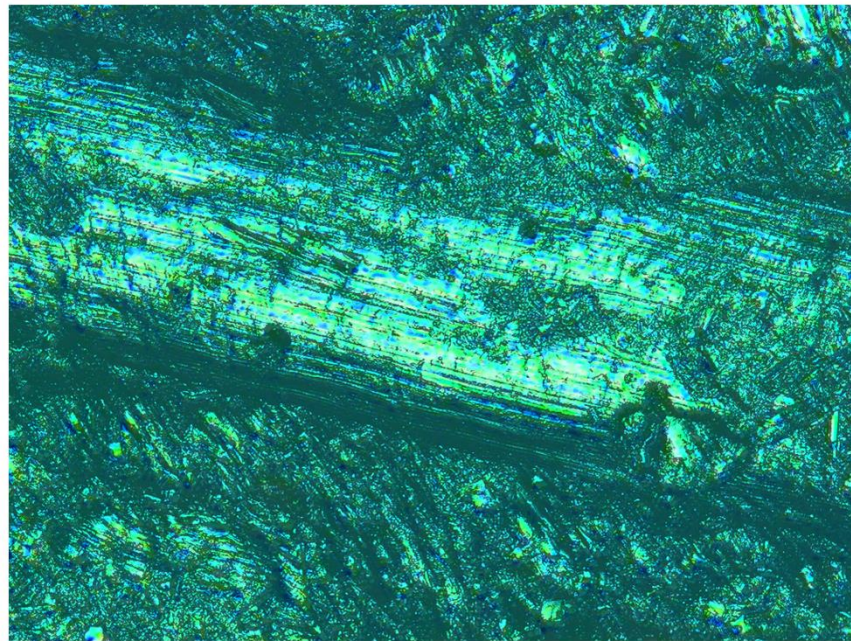


Laser intensity

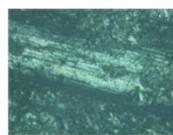


Height

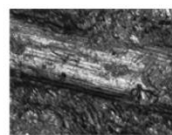
b. Specimen 1 point 2



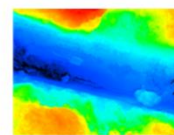
Laser+Optical



Optical



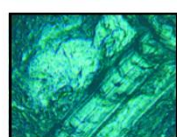
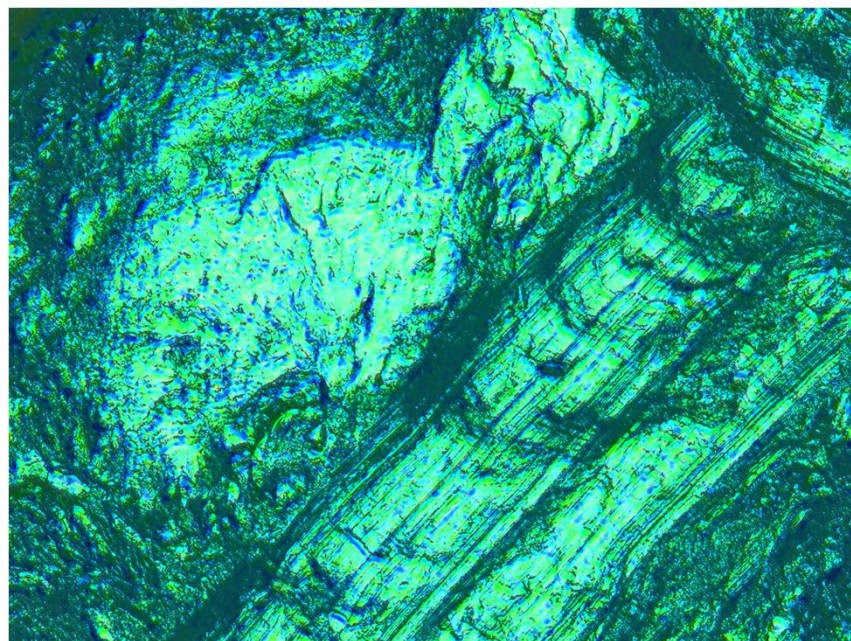
Laser intensity



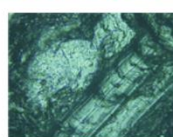
Height

c. Specimen 1 point 3

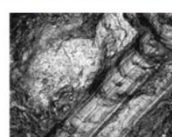
Figure 8. 14 Laser scanning of specimen 1 with 15 days water saturation



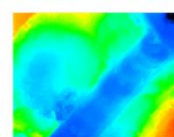
Laser+Optical



Optical

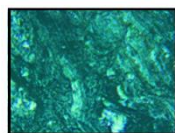
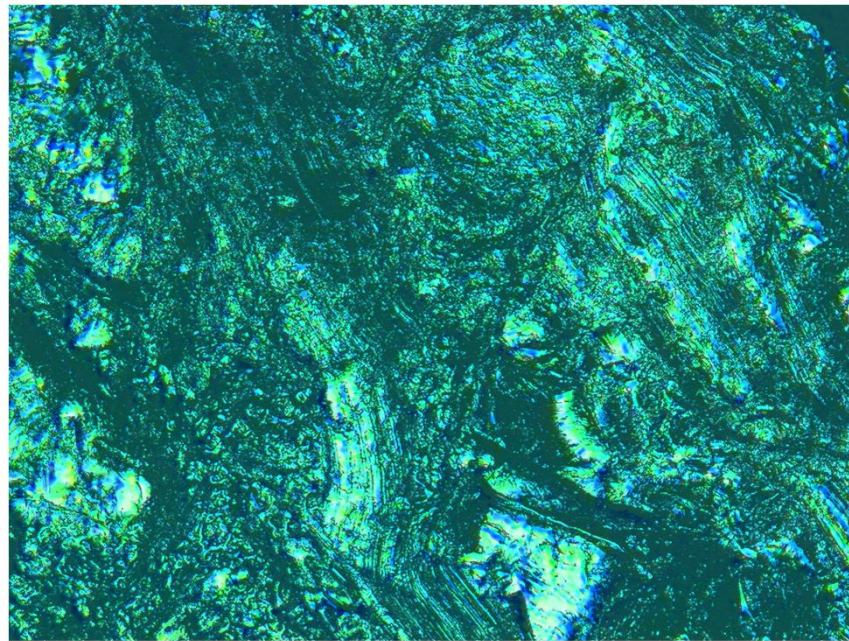


Laser intensity

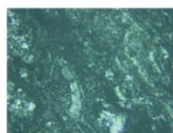


Height

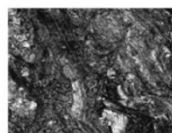
a. Specimen 2 point 1



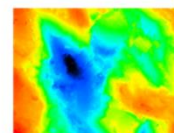
Laser+Optical



Optical

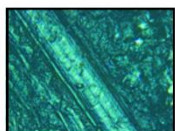
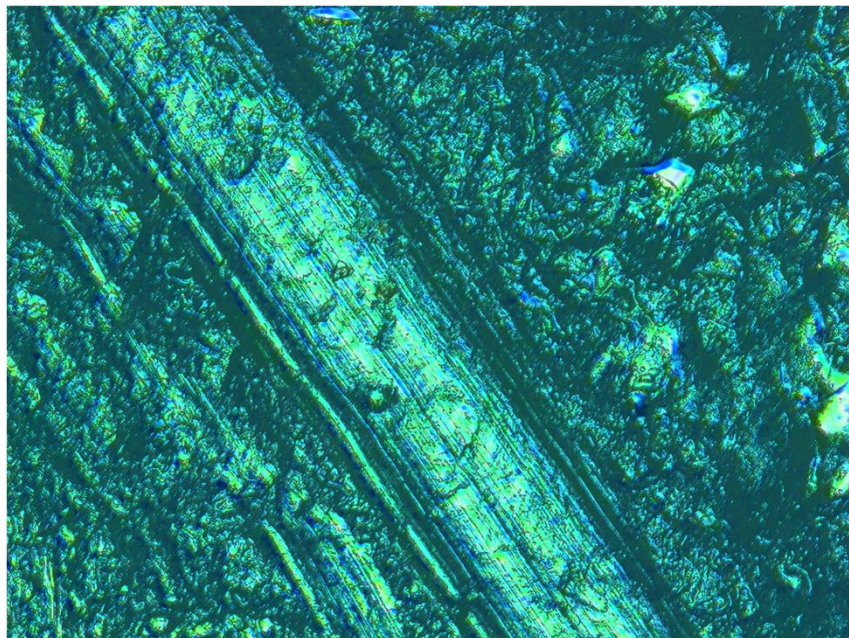


Laser intensity

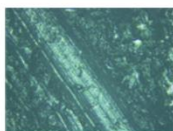


Height

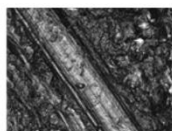
b. Specimen 2 point 2



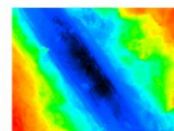
Laser+Optical



Optical



Laser intensity



Height

c. Specimen 2 point 3

Figure 8. 15 Laser scanning of specimen 2 with 15 days water saturation

Figure 8.16 shows the average surface roughness of coal specimens with different water saturation times. It can be seen from Figure 8.10 to 8.16 that the surface structure is smoother after water infusion. The surface roughness of coal specimens with 10 days saturation is similar to those with 15 days saturation, which also demonstrates that the water absorption and penetration activity is very slow after 10 to 15 days saturation. Hence, coal specimens are not sufficiently saturated with a saturation time of less than 10 days.

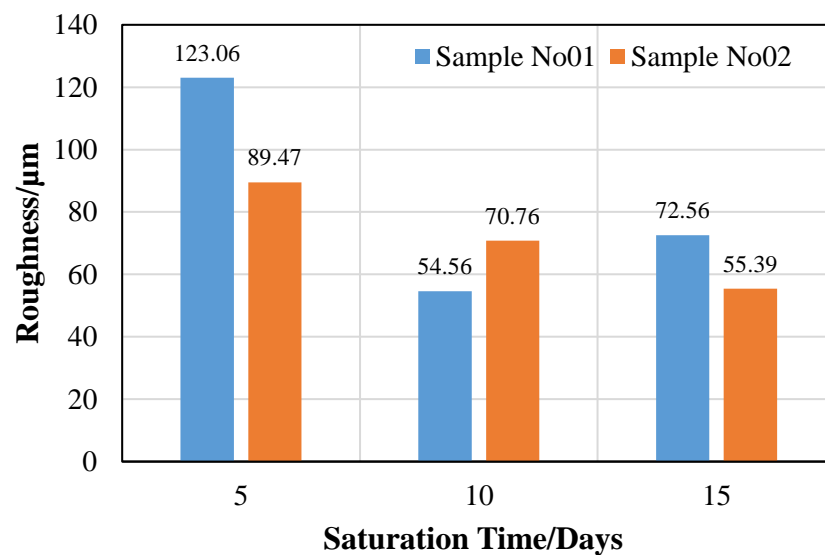


**Figure 8. 16 Surface roughness of scanned coal specimens**

#### **8.4 Conclusions**

Water infusion was taken as an effective way to mitigate coal burst risk by many researchers. However, the effect of the water saturation time on burst propensity and energy dissipation of coal needs more scientific research to provide a better understanding of the influence of water on the mechanical behaviour and burst characteristics of coal bodies during the underground infusion process. In this Chapter, coal specimens taken from local coal mines were tested under natural and different saturation times. To comprehensively compare the burst behaviour of coal specimens with different water saturation times, stress-strain curves, AE counts, fragmentation characteristics and burst

propensity of these groups are analysed. The following conclusions can be drawn based on the test results:

- (1) Sufficient water infusion can decrease the strength of coal specimens. However, the natural weaknesses and inhomogeneous properties of coal specimens can make the strength of some saturated specimens higher than un-saturated coal specimens.
- (2) The magnitude of AE counts has been significantly decreased by water infusion, which indicates the low intensity of crack activities inside water saturated coal specimens during the uniaxial loading process.
- (3) Sufficient water saturation can make the fragmentation mode more stable while in-sufficient water saturation can make fragmentation patterns more random. This phenomenon might result from the uneven water distribution inside the coal specimens when coal specimens are in-sufficiently saturated.
- (4) Different from previous research, the burst propensity has not been mitigated by water saturation when the saturation time is 5 or 10 days. It is unclear whether this phenomenon is caused by the difference between coal specimens. The burst propensity of group D is much lower than other groups as it is saturated for the longest time.

## **CHAPTER 9 FRAGMENTATION CHARACTERISTIC AND ENERGY DISSIPATION OF COAL UNDER IMPACT LOAD**

### **Summary**

Chapter 9 presents the fragmentation characteristics and energy dissipation of coal specimens under impact load. It has been mentioned in Chapter 3 that this thesis focuses on the research of coal burst resulting from super-critical compressive load. Chapters 4 to 8 focus on the study of coal burst under static load as coal burst cases in Australia are mainly caused by static loads. However, dynamic and impact loads such as roof weighting, fault slipping, and hard roof breakage may affect the coal burst behavior of coal. Based on fragmentation and the energy analysis method adopted in the previous chapters, this chapter finds that most of energy will be dissipated in the form of ejection.

### **Citation**

This chapter is based on the paper accepted by the *International Journal of Geomechanics* with the following citation:

Yang, XH, Ren T, Tan LH & Remennikov AM, Fragmentation Characteristic and Energy Dissipation of Coal under Impact Load, *International Journal of Geomechanics*, doi: 10.1061/(ASCE)GM.1943-5622.0002007.

## **Abstract**

With the increase in mining depth, the catastrophic failure of coal under super-critical stresses, complicated geological conditions and mining-induced disturbances is becoming one of the major safety risks associated with underground mining. Research around the failure patterns of coal under an impact load is helpful to understand coal burst behaviour hence allowing mitigation of the associated safety hazards by providing sufficient control measures and protective equipment. To investigate the fragmentation characteristics and coal burst behaviour of coal under impact load, drop weight testing of coal Specimens was undertaken in the laboratory. It was found in this chapter that coal Specimens subject to impact loads have a high peak stress, pulverized fragmentation, and intensive burst energy. The fragments produced by the impact load have a relatively consistent distribution mode, which can be characterised by the fractal model. For coal Specimens subjected to an impact load, the coal burst energy accounts for more than 99 % of the impact energy input while fragmentation energy only accounts for no more than 1 %.

## **Keywords**

Fragmentation Characteristics; Coal Burst; Impact Load; Drop Weight; Energy Dissipation

## 9.1 Introduction

As the fourth largest producer and second largest exporter of coal resources, Australia has a big underground mining industry which consists of many underground coalmines and thousands of mining workers (Geoscience Australia and ABARE 2010). It has been well-documented that the catastrophic failure of coal can cause severe damage to mine workers and equipment (Zhang, Canbulat et al. 2017). However, the failure of brittle materials including coal is not adequately understood at this stage (Grady 2008). Previous research has shown that coal tends to have more violent and instantaneous failure under impact or dynamic load as the strength of coal is positively related to the loading rate (Okubo, Fukui et al. 2006, Zhao, Wang et al. 2014). Research of the failure pattern of coal under an impact load is helpful in understanding its burst behaviour and hence mitigating the associated safety hazards by addressing sufficient mitigation measures and utilizing protective equipment.

Fragmentation is a common physical and mechanical phenomenon that exists for the failure process of geo-materials under static, impact and dynamic loads (Li, Li et al. 2018, Li, Zhang et al. 2018). It has been pointed out by many researchers that the study of the fragment size distribution (FSD) is important for the understanding of energy dissipation and the failure mechanisms of geo-materials. Grady analysed the experimental and theoretical size distribution of solid materials resulting from dynamic fragmentation based on the power-law character (Grady 2008). Liu et al. compared the FSD of sandstone specimens subject to impact load and static load and found the crushing degree of fragments generated by impact load is higher, accompanied with blocky characteristics (Liu, Li et al. 2014). Deng et al. conducted dynamic uniaxial compression tests of rock specimens with the application of the SHPB system and proposed the energy consumption model of rock fragmentation based on fractal rock mechanics and fracture mechanics

theory (Deng, Chen et al. 2016). Chen et al. found that the energy dissipation of fragments declines linearly with an increase in the loading rate from 0.5 to 4.0 MPa/s (Chen, Su et al. 2019). It has been proven by this research that the fragmentation characteristics of rock subject to an impact load is obviously different from being subjected to a quasi-static load. Based on previous research of rock fragmentation, Yang et al. proposed the energy calculation model of coal fragmentation subject to quasi-static load based on Rittingers's theory and the fractal model (Yang, Ren et al. 2020). The experimental study conducted in Chapter 5 demonstrated that this model can be used to study the fragmentation characteristics and energy dissipation during the catastrophic failure of coal. However, the research of coal fragmentation subject to an impact load has not been well-developed.

The drop weight system has been adopted by many researchers to study the dynamic fragmentation features of different materials including concrete (Rahmani, Kiani et al. 2012), rock (Whittles, Kingman et al. 2006), glass (Sam, Joren et al. 2014) and other materials (Rajput, Burman et al. 2018). Through the drop weight testing of granite, Hogan et al. offered insight into the catastrophic dynamic fragmentation of rock under low-energy impact and provided useful data for the numerical modelling of rock fragmentation (Hogan, Rogers et al. 2012). The drop weight tests done by Reddish et al. indicated that the degree of fragmentation formed a non-linear relationship with impact energy (Reddish, Stace et al. 2005). Remennikov and Kaewunruen investigated the impact energy absorption capacity of concrete through drop weight tests (Remennikov and Kaewunruen 2007). Hence, drop weight testing is a widely used method to apply impact load onto materials and to investigate the corresponding dynamic fragmentation characteristics. In a drop weight testing system, a hammer with known height and weight will be given an impact velocity and energy by a gravitational acceleration to impact the specimens placed underneath. The impact energy can be calculated based on measuring

the dropped weight and calculating the resultant velocity. The FSD generated by drop weight tests can be determined by manual sieving and the image processing technique. Then the energy dissipation can be analysed based on the impact energy input and fragmentation energy consumption (Yang, Ren et al. 2020).

To investigate the fragmentation characteristics and energy dissipation of coal under an impact load, the drop weight testing of coal specimens was conducted in the laboratory. 6 coal specimens taken from local coal seams were tested by a 0.72 kN drop weight with an 0.5 m height. Experimental results are compared with the fragmentation characteristics and energy dissipation of coal specimens subject to quasi-static load.

## 9.2 Material and Methods

### 9.2.1 Experimental Setup

Coal blocks were taken from a local coal seam and delivered to the laboratory at the University of Wollongong. To maintain the original state of the coal, all blocks were fully wrapped with aluminium and polymer membranes during delivery. As shown in Figure 9.1, coal blocks were processed into 50 mm \* 50 mm \* 100 mm prismatic specimens through the process of cutting and grinding.



**Figure 9. 1 Coal specimen preparation**

In this study, a steel incident plate was used to distribute impact load to the coal specimen through the transmission bar. The impact load was achieved by a free-fall drop weight that can be dropped from a maximum height of 2.5 m, equivalent to the maximum drop velocity of 7 m/s. The impact load was monitored by a load cell and then recorded by the

connected computer. A transmission bar was placed above the specimen to transfer the impact load. The coal specimen was placed between the transmission bar and the base. To guide the descent of the transmission bar and maintain the direction of the impacting load, bolts were installed between the transmission bar and base.

The drop height was determined based on a series of pre-test experiments to cause complete fragmentation of the coal specimen. The drop weight adopted has a weight of 73.35 kg, which is equivalent to 0.72 kN. It was found that due to the friction of the guiding runner that the incident plate's experimental velocity average reduces to 98 % of the theoretical value (Remennikov and Kaewunruen 2007). Therefore, the test system efficiency needs to be considered during the impact energy calculation process based on the energy conservation theory.

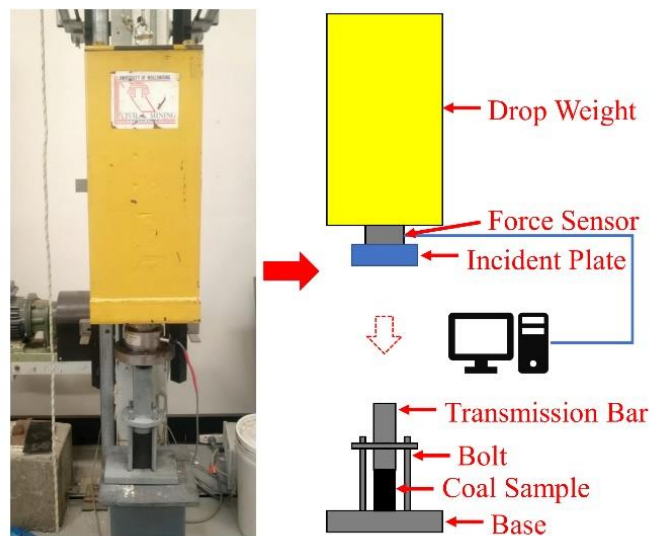


Figure 9. 2 Drop test system

### 9.2.2 Fragment Size Distribution

FSD is important for the understanding of the failure process and fragmentation characteristic of the material. As mentioned in the introduction, it has been found by many researchers that the FSD of rock generated by super-critical quasi-static, impact or dynamic loads can be characterised by typical functions. Experiments done by Li et al. found that the fractal model is appropriate for the FSD of coal specimens resulting from

uniaxial compression loading. Uniaxial compression testing of coal specimens completed as part of our previous research has verified that the fractal model can be used to describe the FSD of coal specimens under quasi-static load (Yang, Ren et al. 2020). However, the statistical and exponential FSD of coal subject to an impact load has not been well understood.

In this chapter, FSD analysis was carried out by a combination of the manual sieving method and the image processing technique introduced in Chapter 5. Coal fragments generated by impact load testing were sieved into several regimes and then digitally analysed through image processing within MATLAB software. The selected meshes have different sizes including  $d = 2.5, 5$  and  $10$  mm. The sieving and image analyse process is shown in Figure 9.3. The cumulative mass distribution curve of each specimen could be plotted based on the sieved and image processed data.

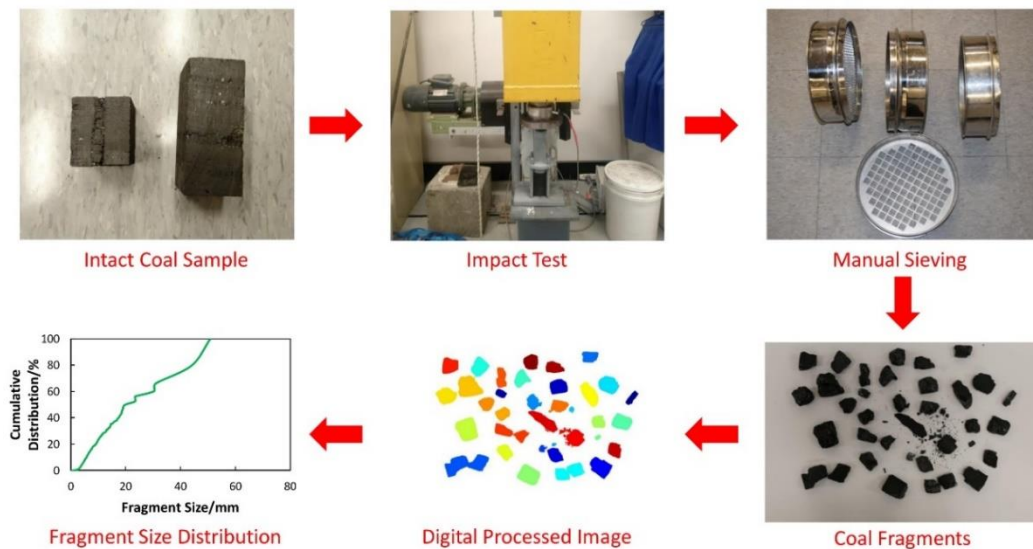


**Figure 9. 3 Image processing technique**

### 9.2.3 Energy Dissipation

During the brittle failure of coal specimens subject to quasi-static load, most of the energy will be dissipated in the form of fragmentation energy. According to Equation 6.3, the energy conservation for this process can be written as (Yang, Ren et al. 2020):

$$E_{dissipation} = E_{burst} + E_{fragmentation} \quad (9.1)$$

where  $E_{dissipation}$  is the energy stored in the coal specimens during the loading process,  $E_{fragmentation}$  is energy consumed by coal fragmentation and  $E_{burst}$  is the kinetic energy carried by the burst coal.

During the impact load test, energy was input by the impact load and then dissipated in the forms of fragmentation and burst. Refer to equation (1), conservation of energy for this process can be written as:

$$E_{impact} = E_{burst} + E_{fragmentation} \quad (9.2)$$

where  $E_{impact}$  is the energy input resulting from the impact load.

According to the equation for gravitational potential energy, the impact energy can be acquired as follow:

$$E_{impact} = m \times g \times h \times \varphi \quad (9.3)$$

where  $m$  is the weight of the dropped hammer,  $g$  is gravitational acceleration,  $h$  is the drop height and  $\varphi$  is the energy efficiency of the test system (As mentioned above,  $\varphi = 0.98$ ).

The fragmentation energy can be calculated based on the FSD function and Rittinger's theory (Yang, Ren et al. 2020). Burst energy is the difference between impact energy and fragmentation energy. Generally, burst energy only accounts for no more than 1 % of the total energy dissipation during the brittle failure of the coal specimens subject to quasi-static load (Su, Jiang et al. 2016). Based on the test results, the energy dissipation of coal specimens subject to impact load can be analysed.

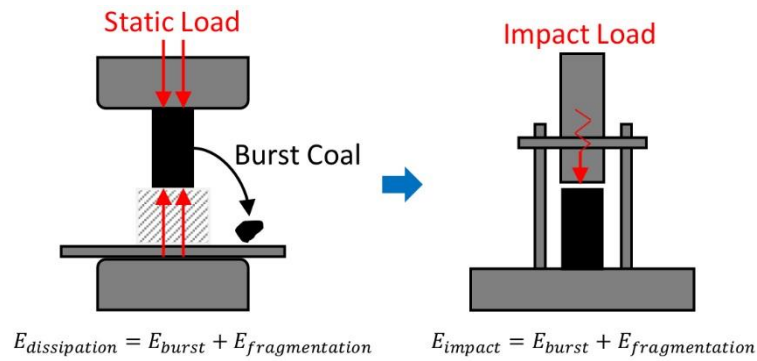


**Figure 9. 4 Energy dissipation of coal specimens under impact and static load**

### 9.3 Results and Discussions

As shown in Figure 9.2, a load cell mounted onto the incident plate was adapted to record the impact load during the testing process. The recorded impact load histories for each specimen is shown in Figure 9.5. The arrival time for the impact load pulse for each specimen was different as data sampling and the weight drop were triggered by the recording button of the software and release button of the testing apparatus, respectively. The peak impact load for each specimen is marked by the red arrow in Figure 9.5. It can be seen that 2-3 main impact load pulses were captured by the force sensor for each specimen. The lower impact pulses appeared 0.2 s after test initiation and are caused by the impact between the drop weight and the transmission bar as the coal specimens have been completely destroyed by the high impact load pulse. The peak load is contained by the first impact load pulse. Although the drop height is the same, the peak impact load for each specimen is different as coal is inhomogeneous. As shown in Figure 9.6, the average peak stress of the coal specimens subject to impact load is 39.88 MPa according to the peak impact load data in Figure 9.5. The coal tested by the impact load test is from the same site as the coal specimens adopted in Chapter 6. According to our previous research introduced in Chapter 6, the average peak stress of coal specimens subject to a quasi-

static load is 16.82 MPa. It is obvious that impact load increases the peak stress of the coal specimens.

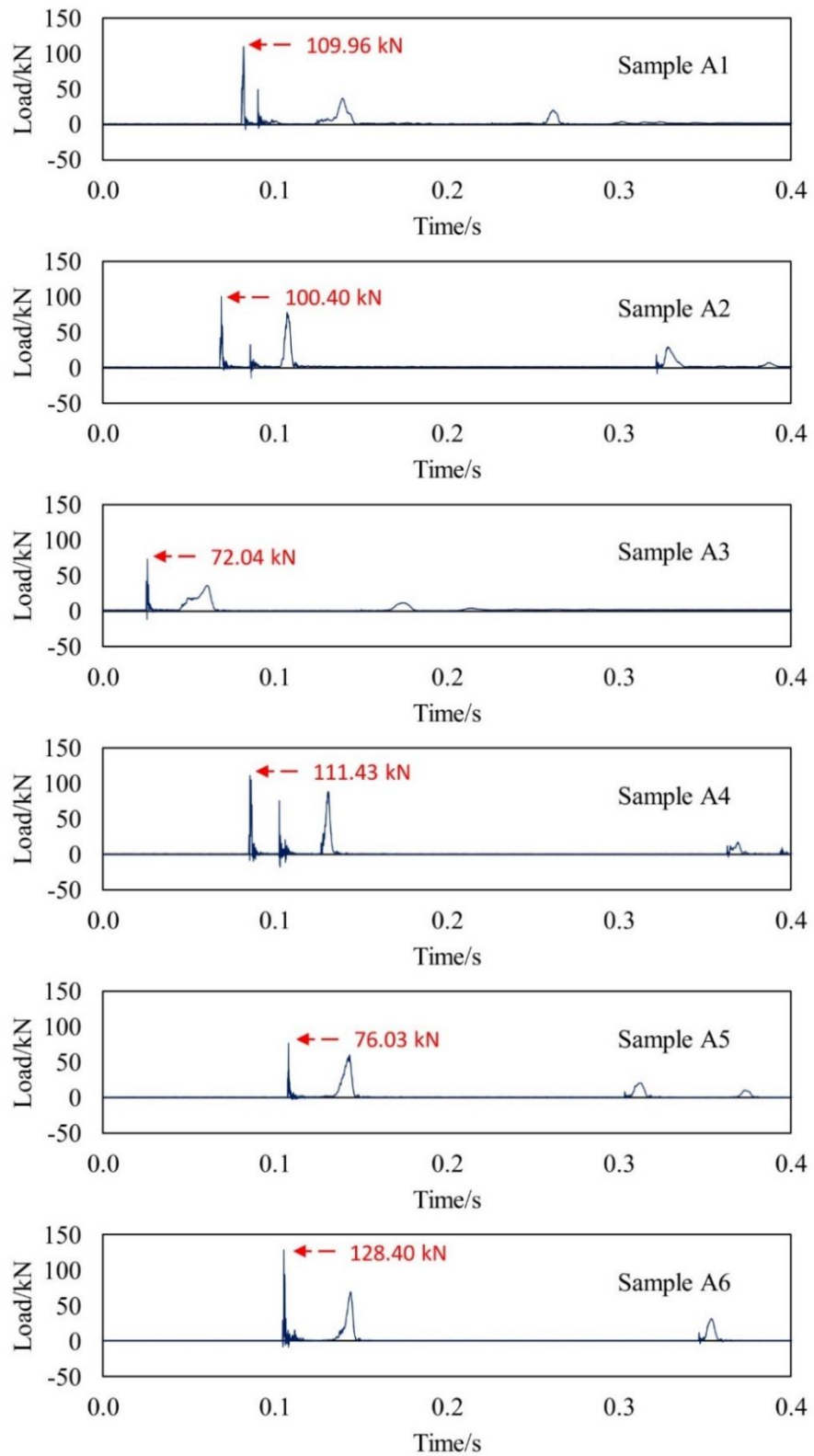
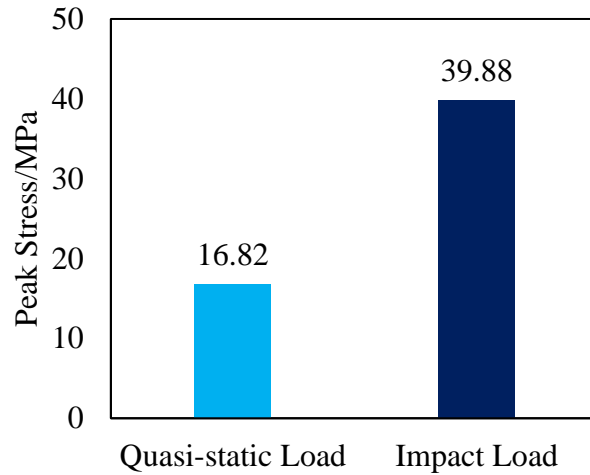


Figure 9. 5 Impact load of coal specimens



**Figure 9. 6 Average peak stress of coal specimens under quasi-static and impact loads**

The cumulative FSD of the coal specimens acquired by manual sieving and image processing is shown in Figure 9.7. It has been proven in previous research that the cumulative FSD of coal specimens subjected to uniaxial compression load (quasi-static load) can be characterised by the fractal model (Peng, Ju et al. 2015, Yang, Ren et al. 2020) :

$$F(d) = \left(\frac{d}{d_{max}}\right)^{3-n} \quad (8.4)$$

where  $F(d)$  is the cumulative mass fraction of the fragments smaller than size  $d$ ,  $d_{max}$  is the maximum size of the coal fragments and  $n$  is the fractal dimension of the fragment size distribution, which is related to coal properties.

The maximum fragment size of each specimen can be determined based on image processed data. Then the fractal dimension can be determined based on the fitting of manual sieving and image processing data. As shown in Figures 9.7, the fractal model also can be adopted to describe the FSD of coal specimens subject to impact load as the fitted curve is highly correlated to manual sieving and image processing data. The FSD of coal specimens subject to impact load has a relatively consistent distribution mode as the distribution curves of these 6 specimens are relatively similar, which can also be seen from Figure 9.8.

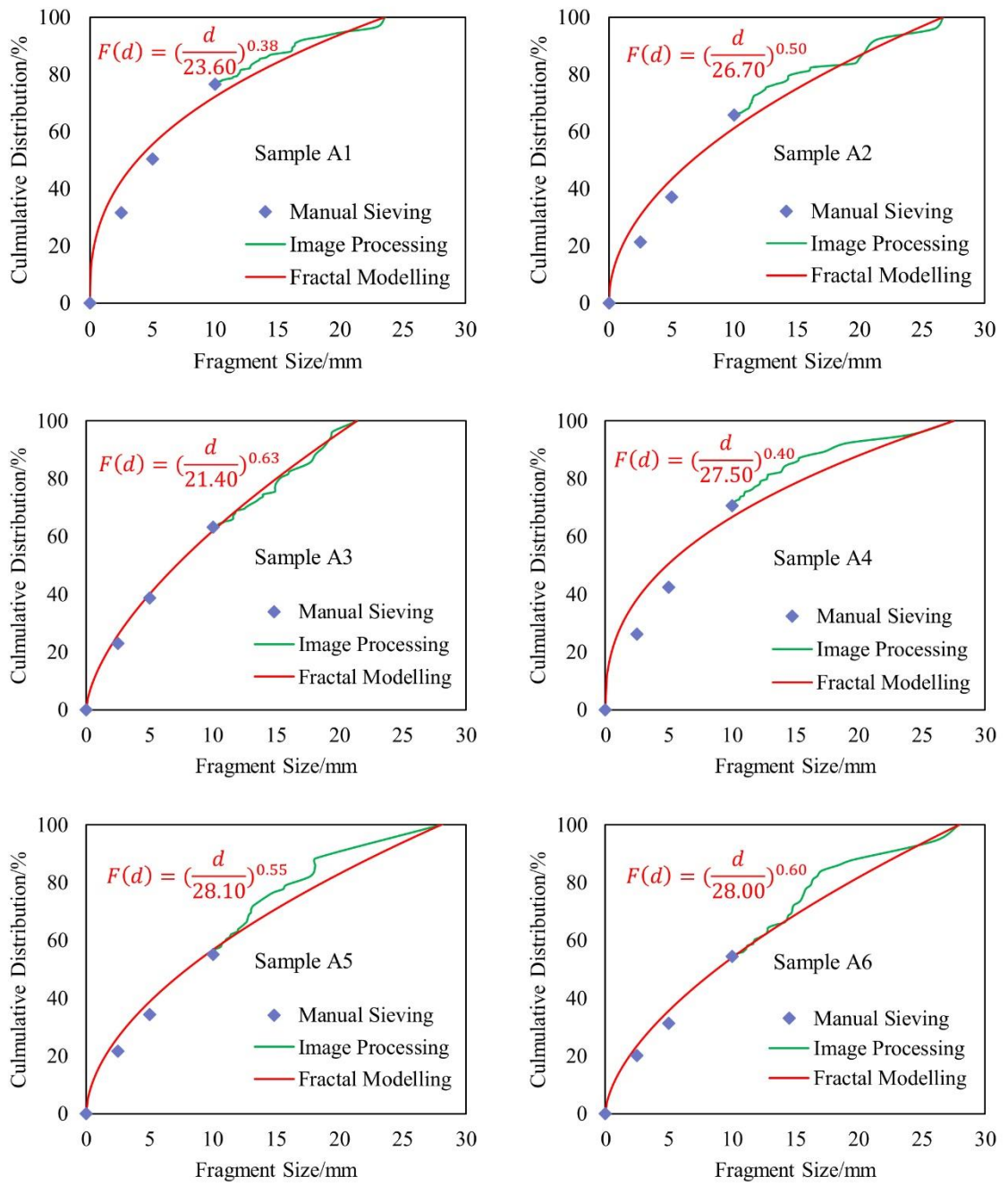
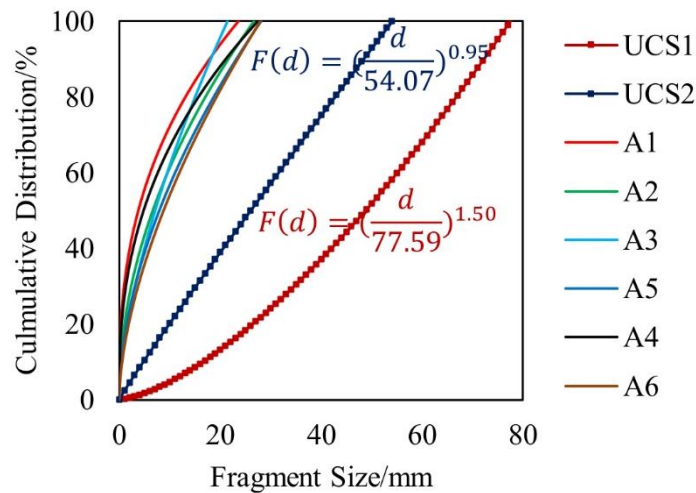


Figure 9. 7 FSD of specimen A1

Figure 9.8 shows the comparison of cumulative FSD of coal specimens subject to impact and quasi-static loads. UCS1 and UCS2 are FSD curves of two coal specimens tested by uniaxial compression load (quasi-static load). It is obvious that the fragmentation of coal under impact load is more pulverized. The maximum fragment size of coal under quasi-static load is over half the specimen length while under impact load it is only around 1/5 of the specimen length. This finding will be important for understanding the driving force of coal burst in underground coal mines according to its FSD data, hence, to adopt proper measures to maintain the stability of underground structures. Generally, the stress concentration induced by quasi-static load can be mitigated by water infusion (Frid 2000), de-stress drilling (Justine and Ian 2016) and de-stress blasting (Dou, Lu et al. 2004). However, the mitigation of coal burst induced by impact or dynamic loads needs the innovative design of roadways for example with strong-soft-strong structures (Dou, Mu et al. 2014) to absorb energy or specific solving techniques to eliminate the load pulse.



**Figure 9. 8 Comparison of cumulative FSD of coal specimens subject to impact and quasi-static**

The drop height for all impact tests is 0.5 m and the drop weight is 73.35 kg. Based on equation 9.3, the energy input by the impact load is 352.23 J. According to the fragmentation energy calculation equation proposed in Chapter 6, the energy consumed by fragmentation can be calculated based on the fractal FSD function of each of the

specimens. The burst energy can be calculated from equation 9.2. The values of burst and fragmentation energy for each coal specimen are shown in Figure 9.14. It has been proven by uniaxial compression testing of coal specimens that no more than 1% of the stored energy is dissipated in the form of burst energy for coal specimens subject to quasi-static load (Su, Jiang et al. 2016). However, for coal specimens subject to an impact load, the burst energy accounts for more than 99 % of the impact energy input while fragmentation energy only accounts for less than 1 %, which is distinctly different with quasi-static load tests. The burst severity and hazard are positively related to the burst energy scale (Rezaei, Hossaini et al. 2015, Yang, Ren et al. 2018). Hence, the burst of coal under an impact load will be more severe and instantaneous as more kinetic energy will be carried by burst coal.

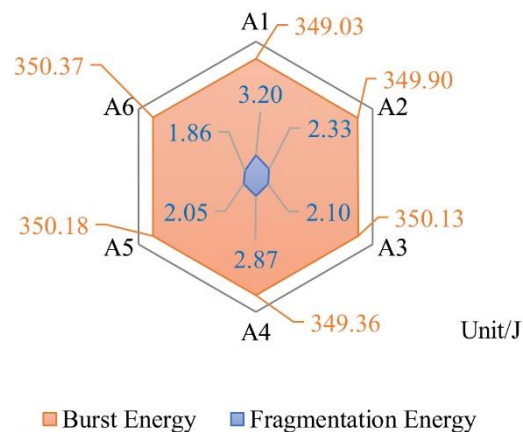


**Figure 9. 9 Burst and fragmentation energy of coal specimens under impact load**

## 9.4 Conclusions

The stability of coal is essential for the safety and efficiency of underground mining as the catastrophic failure of coal can cause personal casualties and economic losses. The coal body in a mine site is always under static, impact or dynamic loads induced by mining disturbances and the original stress. Research of the coal failure subject to impact load will contribute to the understanding of the fragmentation characteristics and burst behaviour of coal burst caused by impact load. In this chapter, the drop weight testing of

coal specimens was conducted in the laboratory to investigate the fragmentation characteristics and energy dissipation of coal under impact loading. Six coal specimens taken from a local coal seam were tested by a 0.72 kN weight dropped from 0.5 m height.

The main findings of this thesis include:

- (1) It is obvious that the impact load increases the peak stress of coal specimens. As shown in Figure 8.6, the average peak stress of coal specimens subjected to an impact load is 39.88 MPa, which is twice that of the average peak stress for coal specimens subject to a quasi-static load (16.82 MPa).
- (2) The FSD of coal specimens subject to an impact load has a relatively consistent distribution mode, which can be characterised by the fractal model. It is obvious that fragmentation of coal under an impact load is more pulverized.
- (3) For coal specimens subjected to an impact load, the burst energy accounts for more than 99 % of the impact energy input while fragmentation energy only accounts for less than 1 %, which is distinctly different with quasi-static load testing. That is, the burst of coal under an impact load will be more severe and instantaneous as more kinetic energy will be carried by the burst coal.

## CHAPTER 10 CONCLUSIONS AND RECOMMENDATIONS

### 10.1 Energy Accumulation and Dissipation of Coal Burst

- ❖ Generally, destruction and safety hazards are caused by ejection energy, as a result of the transformation of elastic energy. The accumulation of elastic energy in coal is dominated by geological conditions, such as mining depth, surrounding rock stiffness, seismicity events, and its mechanical properties. Mining depth and seismicity events are major contributors to the sources of energy by means of static and dynamic loads, respectively. The influence of these factors on the accumulation of elastic energy was established through energy analysis.
- ❖ According to the analysis of stiffness, energy transfers from the surrounding rock (high stiffness) to the coal (low stiffness). Hence, for coalmines with stiff roof and floor strata, the elastic energy tends to concentrate in the coal seam.
- ❖ The elasticity of coal is determined by its capacity and ability to store elastic energy. It is recommended from the laboratory tests that the ability of coal seams to store elastic energy should be evaluated using the coal burst propensity index prior to commencing the extraction of longwall faces or roadways. Australian coalmines can determine their potential risk of coal bursts according to the results of the coal burst propensity evaluation and other geological conditions.
- ❖ Some audible or visible phenomena, such as bulking and acoustic events, may appear prior to the occurrence of coal bursts. These phenomena indicate a concentration of high energy in the body of the coal, suggesting the possibility of coal bursts in the near future.

## 10.2 Evaluation and Prediction of Coal Burst

- ❖ It is demonstrated that the failure mode of coal seams is dominated by the mechanical properties of coal. The property that causes overstressed coal seams to violently burst is named coal burst propensity. A coal burst propensity index method for coal burst risk evaluation in Australian coal mines has been developed. The application feasibility of this method in Australia has also been verified by comprehensive experimental studies of 45 coal specimens taken from different coal seams.
- ❖ The differential analysis method for  $K_E$  and  $DT$  data and a preliminary four-level coal burst risk classification form are proposed. It has been demonstrated by the test results that the coal burst propensity index method is an effective way to evaluate the burst risk for coal mines.
- ❖ The improved method for  $W_{ET}$  testing including the volumetric strain indicator method and theoretical calculation method are discussed. The theoretical calculation result is dominated by fitting accuracy. The volumetric strain indicator method, although the test process is as complex as before, can provide an accurate estimation of the unloading point of the  $W_{ET}$  test. In future testing, these two methods can be used together to improve the test efficiency. After the  $R_C$  test, the theoretical calculation method can be adopted to get the fitting result. If the fitting result is unsatisfactory, the  $W_{ET}$  test with the application of the volumetric strain indicator method can be arranged.
- ❖ A brief review of the application of fractal theory and AE techniques in mining science has been provided. The mathematical formulas for the fractal dimension

calculation of AE spatial distribution are presented. The mathematical analysis process of fractal dimension of AE events is introduced in detail within section 6.3. Chapter 6 proposes the mathematical analysis method of fractal dimension based on the dimension calculation formula and MATLAB coding, which lays the ground work for real-time monitoring and automatic warning of coal burst risk by automatic analysis of data from the monitoring system.

- ❖ The loading rate has an obvious influence on the strength and failure behaviour of coal. Coal specimens tend to have high strength and brittle failure under high loading rates, which corresponds with the research results reported in other literature.
- ❖ Fractal dimension decrease of spatial distribution of AE is observed, which demonstrates the possibility of coal burst prediction through AE monitoring.

### **10.3 Fragmentation Characteristic and Energy Dissipation of Specimens Failure**

- ❖ The brittle failure of coal specimens can generate thousands of pieces of debris ranging from several millimetres to tens of millimetres during laboratory uniaxial compression testing. The application of image processing techniques in the measurement of coal fragments generated by uniaxial compression tests is developed. The acquisition setup, analysis step and coding process for image processing are introduced in detail. The watershed method is adopted for fragments segmentation.
- ❖ It has been demonstrated by comparing images before and after image processing that the image processing method proposed in Chapter 4 is suitable for coal fragments measurement. The fragment in the image can be taken as an ellipsoid

characterized by major axis, intermediate axis, and minor axis. The image processed cumulative distribution of coal specimens can be achieved based on image analysis results, the ellipsoid volume equation and the intermediate–minor axis value relationship. The size distribution of coal fragments demonstrates that the shape of coal fragments can be simplified into ellipsoid with intermediate/minor axis ratio of 1.

- ❖ Coal burst in the ribs of underground roadways is an important type of coal burst, which can result in very high ejection velocities of coal blocks or particles. The ejection velocity is a vital parameter not only for support and protection structural design but also coal burst scale estimation in burst-prone coal mines.
- ❖ Fractal model can be adopted to characterize the statistical distribution of coal fragments generated by uniaxial compression load. The fractal dimension can be calibrated based on the image processed data. The fragmentation theory and fractal size distribution are combined to derive the theoretical calculation model of fragment energy.
- ❖ The estimation method of ejection velocity was proposed based on the energy conservation equation and the fragmentation energy calculation model. The developed “coal ejection test” indicates the positive correlation between estimated velocity and measured velocity, which means the estimated velocity can indicate the ejection feature of coal specimens in the laboratory.
- ❖ The proposed ejection velocity estimation method is applied to a rib burst case in an underground roadway, and the estimated ejection velocity is highly correlated to the observations of rib burst damage and other research outcomes. The method

for assessing coal ejection velocity can be used as a basis for further research regarding proper roadway support and protective structure design for use in burst-prone coal mines.

- ❖ Fragment energy of rib burst case accounts for around 27% of the total elastic energy storage while this number for coal ejection tests is more than 90%. The percentage of fragment energy might be negatively correlated to burst scale as the volume of coal is negatively correlated to its specific surface area, which need to be further studied in the future research.

#### **10.4 Influence of Water Saturation and Impact Load**

- ❖ Sufficient water infusion can decrease the strength of coal specimens. However, the natural weaknesses and inhomogeneous properties of coal specimens can make the strength of some saturated specimens higher than un-saturated coal specimens.
- ❖ The magnitude of AE counts has been significantly decreased by water infusion, which indicates the low intensity of crack activities inside water saturated coal specimens during uniaxial loading process.
- ❖ Sufficient water saturation can make the fragmentation mode more stable while in-sufficient water saturation can make fragmentation patterns more random. This phenomenon might result from the uneven water distribution inside coal specimens when coal specimens are in-sufficiently saturated.
- ❖ Different with previous research, the burst propensity has not been mitigated by water infusion when the saturation time is 5 - 10 days. It is unclear whether this

phenomenon is caused by the individual difference between coal specimens. However the burst propensity of coal specimens is much lower than other groups as they are saturated for the longest time.

- ❖ It is obvious that impact load increases the peak stress of coal specimens. The average peak stress of coal specimens subjected to impact load is about 40 MPa, which is twice the average peak stress of coal specimens subjected to quasi-static load (16.82 MPa).
- ❖ The FSD of coal specimens subjected to impact load has a relatively consistent distribution mode, which can be characterized by the fractal model. It is obvious that fragmentation of coal under impact load is more pulverized.
- ❖ For coal specimens subjected to an impact load, the burst energy accounts for more than 99 % of the impact energy input while fragmentation energy only accounts for less than 1 %, which is distinctly different from quasi-static load testing. In other words, the burst of coal under an impact load will be more severe and instantaneous as more kinetic energy will be carried by the burst coal.

## **10.5 Recommendations for Future Studies**

The following topics are recommended for future studies based on the experimental and analytical studies mentioned in this thesis:

- ❖ The burst propensity index methodology for coal burst risk evaluation of Australian coal mines need more test results of specimens from different coal seams to establish the testing and data analysis standard. The preliminary risk classification form needs to be adjusted with the deep analysis of these tests data.

- ❖ The SHPB system has the capability of testing the specimens at an impact velocity up to 50 m/s, strain rate  $10^1$ - $10^2$  s<sup>-1</sup> at high in-situ stress conditions up to 50 MPa. The fragmentation characteristics and energy dissipation of coal under complex and superposition loads can be further studied with the application of SHPB test system to reveal the mechanism of other burst types.
- ❖ The water infusion effects on coal will change with coal properties, geological and geotechnical factors. Industrial water infusion trials can be carried out with proper borehole and water pressure parameters to develop a water infusion method for burst control. Thorough experimental and numerical research is still needed in this area.
- ❖ 3D X-Ray CT and high resolution SEM imaging of test specimens can be used for studying micro-damage evolution and dynamic failure of tested specimens under static/dynamic loading, and examining the changes of the microstructure and morphology of coal specimens before and after water infusion.
- ❖ Based on scale of the laboratory test specimens, a coupled fluid-solid numerical model, using DEM software, can be developed to simulate the water-coal interaction process for assessing stress redistribution and potential seam failure.
- ❖ The ejection energy and velocity estimation were based on the FSD data of failed specimens or burst cases. The stress and energy concentration zone can be identified by geophysical exploration such as passive seismic velocity tomography. Hence, the potential FSD model of coal burst can be established based on the volume of stress and the energy concentration zone. The application

of ejection energy and velocity estimation for burst scale prediction can be further explored.

- ❖ The image analysis was based on MATLAB coding and the data can be stored automatically in this thesis. But the code initiation, and human interaction when finalizing data analysis can be improved. It is very possible to make all these operations more intelligent by the application of programming, AI, and deep learning. The improved image analysis technique can provide a better method for fragmentation study of coal and rock.
- ❖ Micro seismicity monitoring is a widely used method for the early warning of coal burst in many countries. The locating principal for micro seismicity is the same with acoustic emission. The on-site early warning of coal burst through analysis of fractal spatial distribution of micro seismicity can be further studied.

## APPENDIX A IMAGE PROCESSING CODE

```
% fragment size with 2.5-10 mm
clc

clear

rgb = imread('file name')
I = rgb2gray(rgb)
imshow(I)
bw = imbinarize(I)
imshow(bw)
A=1-bw
Conn=8
[s1,s2]=size(A)
A=~bwmorph(A,'majority',10)
D=-bwdist(A,'cityblock')
B=medfilt2(D,[3 3])
B=watershed(B,Conn)
Pr=zeros(s1,s2)
for I=1:s1
    for J=1:s2
        if A(I,J)==0 && B(I,J)~=0
            Pr(I,J)=1
        end
    end
end

Pr=bwareaopen(Pr,9,Conn)
[Pr_L,Pr_n]=bwlabel(Pr,Conn)
s = regionprops(Pr_L, 'Orientation', 'MajorAxisLength', 'MinorAxisLength', 'Eccentricity',
'Centroid', 'Area')
RGB=label2rgb(Pr_L,'jet', 'w', 'shuffle')
imshow(RGB)
writetable(struct2table(s),'test.xlsx')
winopen test.xlsx
```

**% fragment size above 10 mm**

clc

clear

rgb = imread('file name')

I = rgb2gray(rgb)

imshow(I)

gmag = imgradient(I)

imshow(gmag,[])

L = watershed(gmag)

Lrgb = label2rgb(L)

imshow(Lrgb)

se = strel('disk',20)

Io = imopen(I,se)

imshow(Io)

Ie = imerode(I,se)

Iobr = imreconstruct(Ie,I)

imshow(Iobr)

Ioc = imclose(Io,se)

imshow(Ioc)

Iobrd = imdilate(Iobr,se)

Iobrcbr = imreconstruct(imcomplement(Iobrd),imcomplement(Iobr))

Iobrcbr = imcomplement(Iobrcbr)

imshow(Iobrcbr)

fgm = imregionalmax(Iobrcbr)

imshow(fgm)

I2 = labeloverlay(I,fgm)

imshow(I2)

se2 = strel(ones(5,5))

fgm2 = imclose(fgm,se2)

fgm3 = imerode(fgm2,se2)

fgm4 = bwareaopen(fgm3,20)

I3 = labeloverlay(I,fgm4)

```

imshow(I3)
bw = imbinarize(Iobrcbr)
imshow(bw)
A=1-bw
Conn=8
[s1,s2]=size(A)
A=~bwmorph(A,'majority',10)
D=-bwdist(A,'cityblock')
Pr=zeros(s1,s2)
for I=1:s1
    for J=1:s2
        if A(I,J)==0 && D(I,J)~=0
            Pr(I,J)=1
        end
    end
end
Pr=bwareaopen(Pr,9,Conn)
[Pr_L,Pr_n]=bwlabel(Pr,Conn)
s = regionprops(Pr_L, 'Orientation', 'MajorAxisLength', 'MinorAxisLength', 'Eccentricity',
'Centroid', 'Area')
RGB=label2rgb(Pr_L,'jet', 'w', 'shuffle')
imshow(RGB)
writetable(struct2table(s),'test.xlsx')

```

## APPENDIX B AE DIMENSION ANALYSIS CODE

### % Specimen A01

```
A=[-11.97, 13.62; -10.3, -14.77; 12.96, 16.09; -9.217, -20.93; -18.23, -10.94; -13.19, -20.46; 10.81, -10.2; -9.575, 0.5413; 0.2881, -25.07; -12.5, -16.09; -7.068, -18.57; 5.4, 10.37; 12.19, -1.263; -1.974, -2.054; -15.89, 11.59; 11.5, 7.311; 3.551, -20.47; -12, -19.54; 14.58, 3.752; 4.481, -18.59; 17.88, 18.01; 7.881, 17.21; -2.622, -2.942; -7.603, -19.49; 10.45, -19.35; -12.8, -6.774; -8.548, -12.53; 10.2, 17.1; 19.34, 6.47; -1.247, 10.32; -9.239, -10.7; 7.99, 17.7]
```

```
dismat=pdist(A)
```

```
B=squareform(dismat)
```

```
C=tril(b,-1)
```

### % Specimen A02

```
A=[-20.28 , 13.56; 5.424, -12.93; 0.3826, 9.889; 8.059, 12.72; 11.71, -13.84; -6.391, 20.2; 4.037, 17.66; 18.9, -13.89; 8.624, -20.84; -2.9, 17.4; 4.584, 7.986; 21.52, -5.783; -14.09, -12.35; -4.134, -15.43; 7.332, -18.26; -1.156, -19.41; -7.181, -9.385; -6.55, 6.219; 0.4814, -14.74; 8.055, 2.813; -18, -18.02; -11.34, 9.591; -10.43, 8.862; -9.188, 20.6; 15.35, 11.68; 17.4, -8.453; 11.1, 1.491; 14.44, 4.881; 14.61, -1.991; 7.314, 5.342; -19.67, -0.08542; -20.22, -7.457; 8.002, -19.72; -17.85, 1.934; -1.889, -14.7; -2.388, 1.45; -7.444, 22.85; -3.23, 25.28; 8.899, -6.789; 23.35, -3.486; 23.87, 8.615; 1.692, -3.448; 1.568, 22.79; -5.444, 3.812; -5.406, 2.221; 18.36, 12.71; -13.84, -14.63; -10.09, -6.751; -13.92, -2.768; 1.078, 1.167; -9.553, -4.823; -17.55, 6.533; -1.066, 1.176; 1.241, -9.329; 14.07, -3.917; -21.71, -9.601; -24.74, -4.57; -7.116, -9.535; 0.2468, 8.193; -24.07, -7.451; 2.513, 19.35; 2.706, 3.281; -15.69, 0.7535; -18.98, 9.308; -19.26, 3.012; -1.196, 19.23; 13.44, 16.57; 0.1917, -24.92; -8.948, -4.896; -2.442, -7.988; -6.804, 9.499; -4.921, -3.194; 12.87, 0.8312; -4.699, -10.37; -6.063, 7.586; 24.02, 3.826; -3.92, 17.38; -15.2, 11.51; 3.652, 1.358; -5.85, 12.92; -2.769, 17.2; -15.01, 1.874; -18.7, 0.6403; 11.03, -1.502; 15.01, -9.642; 5.216, 11.6; -14.17, 4.933; 0.822, -9.852; -19.44, 0.3211; -13.81, -18.91; 17.09, 3.362; -0.89, 20.47; 20.88, 7.712; 11.82, 3.431]
```

```
dismat=pdist(A)
```

```
B=squareform(dismat)
```

```
C=tril(b,-1)
```

### % Specimen B01

```
A=[17.48, 18.06; 7.74, -18.1; 11.27, -10.45; -5.766, -1.668; 18.29, -17.51; 17.03, -12.87; -8.46,
14.66; 11.26, 18.31; 18.2, -17.76; 14.29, 17.73; 16.12, -4.267; -17.2, -18.62; 3.132, 20.92; 17.49,
-18.32; 16.95, -17.9; -12.16, 3.739; 10.89, -16.41; -3.558, -24.75]
```

```
dismat=pdist(A)
```

```
B=squareform(dismat)
```

```
C=tril(b,-1)
```

```
% Specimen B02
```

```
A=[1.909, -17.35; 16.32, -18.24; 23.3, -4.854; 17.26, 18.73; 0.3929, -23.7; 7.67, 21.15; 5.67,
15.23; 12.78, 6.637; 17.03, -11.31; 4.717, 14.07; -4.249, 14.12; 16.86, -18.64; 20.13, 1.187; 18.26,
17.08; -18.5, -1.037; 1.98, 14.78; -18.07, 17.17; -0.386, 17.22; 18.46, -7.013; 0.7801, -10.96; -
6.512, -16.56; 15, -16.9; 7.913, -14.24; -6.912, -18.52; 7.685, -21.34; -8.341, -16.52; -18.42,
1.314; -2.801, 12.02; -14.59, 18.55; 14.57, 10.61; -16.47, 1.246; -17.21, -18.1; -5.188, 5.564;
8.956, 2.153; 18.04, 17.9; 15.28, -13.93; 19.91, 1.422]
```

```
dismat=pdist(A)
```

```
B=squareform(dismat)
```

```
C=tril(b,-1)
```

## REFERENCE

- [1] Aguado M. B. D. and Nicieza C. G. (2007). "Control and prevention of gas outbursts in coal mines, riosa–olloniego coalfield, spain." *International Journal of Coal Geology* 69(4): 253-266.
- [2] Ahn K. S., Zhang C. G. and Canbulat I. (2017). Study of seismic activities associated with australian underground coal mining. *Coal Operators' Conference*. Naj A. and Bob K. Wollongong: 275-282.
- [3] Al-Shayea N. A. (2005). "Crack propagation trajectories for rocks under mixed mode i–ii fracture." *Engineering Geology* 81(1): 84-97.
- [4] Amitrano D., Arattano M., Chiarle M., Mortara G., Occhiena C., Pirulli M. and Scavia C. (2010). "Microseismic activity analysis for the study of the rupture mechanisms in unstable rock masses." *Natural Hazards and Earth System Sciences* 10(4): 831-841.
- [5] Baghel A. S. (2009). Study of support system and strata behaviour analysis around underground workings in coal deposits.
- [6] Bailly P., Delvare F., Vial J., Hanus J. L., Biessy M. and Picart D. (2011). "Dynamic behavior of an aggregate material at simultaneous high pressure and strain rate: Shpb triaxial tests." *International journal of impact engineering* 38(2-3): 73-84.
- [7] Bieniawski Z. T. (1967). "Mechanism of brittle fracture of rock part i." *International Journal of Rock Mechanics and Mining Sciences & Geomechanics Abstracts* 4(4): 395-406.
- [8] Bieniawski Z. T. (1967). "Mechanism of brittle fracture of rock part ii." *International Journal of Rock Mechanics and Mining Sciences & Geomechanics Abstracts* 4(4): 407-423.
- [9] Bieniawski Z. T. (1967). "Mechanism of brittle fracture of rock part iii." *International Journal of Rock Mechanics and Mining Sciences & Geomechanics Abstracts* 4(4): 425-430.
- [10] Bieniawski Z. T., Denkhaus H. G. and Vogler U. W. (1969). "Failure of fractured rock." *International Journal of Rock Mechanics and Mining Sciences & Geomechanics Abstracts* 6(3): 323-341.
- [11] Borisov V. D. (2018). "Determining the parameters of microcracks from their electromagnetic radiation signals." *Journal of Applied Mechanics and Technical Physics* 59(1): 112-119.
- [12] Bowen P. (2002). "Particle size distribution measurement from millimeters to nanometers and from rods to platelets." *Journal of Dispersion Science and Technology* 23(5): 631-662.
- [13] Brace W. F. (1960). "An extension of the griffith theory of fracture to rocks." *Journal of Geophysical Research* 65(10): 3477-3480.
- [14] Braeuner G. (2017). *Rockbursts in coal mines and their prevention*. Netherlands, A. A. Balkema.
- [15] Brauner G. (1994). *Rockbursts in coal mines and their control*. Essen, Germany, Balkema, DMT,.
- [16] Bräuner G. (2017). *Rockbursts in coal mines and their prevention*, Routledge.
- [17] Brook M. S. (2016). Geomechanical behaviour and deformation of coal mine roof strata around faults: Toward an engineering geological model. Master Master's Thesis, University of New South Wales.
- [18] Bukowska M. (2012). "The rockbursts in the upper silesian coal basin in poland." *Journal of Mining Science* 48(3): 445-456.
- [19] Cai M. F. (2016). "Prediction and prevention of rockburst in metal mines – a case study of sanshandao gold mine." *Journal of Rock Mechanics and Geotechnical Engineering* 8(2): 204-211.
- [20] Cai W., Dou L. M., Han R. J., Zhang G. H. and Xu.Wei. L. (2011). "Bursting liability of coal based on damage statistical constitutive model." *Journal of China Coal Society* 36(s2): 346-352.
- [21] Cai W., Dou L. M., Si G. Y., Cao A. Y., He J. and Liu S. (2016). "A principal component analysis/fuzzy comprehensive evaluation model for coal burst liability assessment." *International Journal of Rock Mechanics and Mining Sciences* 81(Supplement C): 62-69.

- [22] Cai W., Dou L. M., Zhang M., Cao W. Z., Shi J. Q. and Feng L. F. (2018). "A fuzzy comprehensive evaluation methodology for rock burst forecasting using microseismic monitoring." *Tunnelling and Underground Space Technology* 80: 232-245.
- [23] Calleja J. and Nemcik J. (2016). Coalburst causes and mechanisms. *Coal Operators Conference*.
- [24] Casten U. and Fajklewicz Z. (1993). "Induced gravity anomalies and rock-burst risk in coal mines: A case history 1." *Geophysical prospecting* 41(1): 1-13.
- [25] Chen Q., Li R., Xiu W. Z., Zheng G., Zivkovic V. and Yang H. (2020). "Dynamics of irregular particles in the passive layer under the slumping regime." *Powder Technology*.
- [26] Chen X. H., Li W. Q. and Yan X. Y. (2012). "Analysis on rock burst danger when fully-mechanized caving coal face passed fault with deep mining." *Safety science* 50(4): 645-648.
- [27] Chen Z. M. (1994). *Analytical solution of surrounding rock stress distribution*. Beijing, China Coal Industry Publishing House
- [28] Chen Z. Y., Su G. S., Ju J. W. and Jiang J. Q. (2019). "Experimental study on energy dissipation of fragments during rockburst." *Bulletin of Engineering Geology and the Environment*: 1-18.
- [29] Cherepanov G. P., Balankin A. S. and Ivanova V. S. (1995). "Fractal fracture mechanics—a review." *Engineering Fracture Mechanics* 51(6): 997-1033.
- [30] Chouet B. A. (1996). "Long-period volcano seismicity: Its source and use in eruption forecasting." *Nature* 380(6572): 309.
- [31] Christopher M. (2016). "Coal bursts in the deep longwall mines of the united states." *International Journal of Coal Science & Technology* 3(1): 1-9.
- [32] Christopher M. (2017). "Coal bursts that occur during development: A rock mechanics enigma." *International Journal of Mining Science and Technology*.
- [33] Christopher M. and Gauna M. (2016). "Evaluating the risk of coal bursts in underground coal mines." *International Journal of Mining Science and Technology* 26(1): 47-52.
- [34] Číž R. and Růžek B. (1997). "Periodicity of mining and induced seismicity in the mayrau mine, czech republic." *Studia Geophysica et Geodaetica* 41(1): 29-44.
- [35] Colwell M. and Frith R. (2006). Why uniaxial compressive strength and young's modulus are commonly poor indicators of roadway roof stability—except in the tailgate. *Coal Operators' Conference*, Wollongong, University of Wollongong and the Australasian Institute of Mining and Metallurgy.
- [36] Cook N. G. W. (1965). "A note on rockbursts considered as a problem of stability." *Journal of the Southern African Institute of Mining and Metallurgy* 65(8): 437-446.
- [37] Czeceńska K. Z. and Zuo D. K. (1986). "The rockburst prevention in polish coal mines." *Mining Safety and Environmental Protection*(6): 58-63.
- [38] Demirdag S., Tufekci K., Kayacan R., Yavuz H. and Altindag R. (2010). "Dynamic mechanical behavior of some carbonate rocks." *International Journal of Rock Mechanics and Mining Sciences* 47(2): 307-312.
- [39] Deng Y., Chen M., Jin Y. and Zou D. W. (2016). "Theoretical analysis and experimental research on the energy dissipation of rock crushing based on fractal theory." *Journal of Natural Gas Science and Engineering* 33: 231-239.
- [40] Department of Planning and Environment. (2018). "Appin mine issued ban due to coal burst." Retrieved 25th June, 2018, from <https://www.resourcesandenergy.nsw.gov.au/about-us/news/2018/appin-mine-issued-ban-due-to-coal-burst>.
- [41] Department of Planning and Environment. (2018). "Coal burst leads to australian suspension." Retrieved 25th June, 2018, from <https://www.resourcesandenergy.nsw.gov.au/about-us/news/2018/coal-burst-leads-to-austar-suspension>.
- [42] Dou L. M., He J., Cao A. Y., Cai W., Li Z. L. and Zhang J. W. (2012). Mechanism and prevention methods discussion on coal mine rock burst induced by dynamic load. *High Level Academic Forum of Fifty Anniversary of China National Coal Association*, Beijing.

- [43] Dou L. M., He J., Cao A. Y., Gong S. Y. and Cai W. (2015). "Rock burst prevention methods based on theory of dynamic and static combined load induced in coal mine." *Journal of China Coal Society* 40(7): 1469-1476.
- [44] Dou L. M. and He X. Q. (2001). *Theory and technology of rock burst prevention*. Xuzhou, China University of Mining and Technology Press.
- [45] Dou L. M. and He X. Q. (2004). "Model for rock burst failure and its critical values of acoustic and electromagnetic emission." *Journal of China University of Mining and Technology* 33(5): 504-508.
- [46] Dou L. M., Lu C. P., Mou Z. L., Qin Y. H. and Yao J. H. (2004). "Intensity weakening theory for rockburst and its application." *Journal of China Coal Society* 30(6): 1-6.
- [47] Dou L. M., Lu C. P., Mou Z. L., Zhang X. T. and Li Z. H. (2006). "Rock burst tendency of coal rock combinations sample." *Journal of Mining and Safety Engineering* 23(1): 43-46.
- [48] Dou L. M., Lu C. P., Mu Z. L., Zhang X. T. and Li Z. H. (2006). "Rock burst tendency of coal-rock combinations sample." *Journal of Mining & Safety Engineering* 23(1): 43-46.
- [49] Dou L. M., Mu Z. L., Li Z. L., Cao A. Y. and Gong S. Y. (2014). "Research progress of monitoring, forecasting, and prevention of rockburst in underground coal mining in china." *International Journal of Coal Science & Technology* 1(3): 278-288.
- [50] Dou L. M., Zhao C. G., Yang S. G. and Wu X. R. (2006). *Prevention and control of rock burst in coal mine*. Xuzhou, China University of Mining and Technology Press.
- [51] Dvorsky P. and Konicek P. (2005). Systems of rock blasting as a rock burst measure in the czech part of upper silesian coal basin. *Proceedings of the Sixth International Symposium on Rockburst and Seismicity in Mines*.
- [52] Fakhimi A., Azhdari P. and Kimberley J. (2018). "Physical and numerical evaluation of rock strength in split hopkinson pressure bar testing." *Computers and Geotechnics* 102: 1-11.
- [53] Fan J., Dou L. M., He H., Du T. T., Zhang S. B., Gui B. and Sun X. L. (2012). "Directional hydraulic fracturing to control hard-roof rockburst in coal mines." *International Journal of Mining Science and Technology* 22(2): 177-181.
- [54] Fan X., Li K. H., Lai H. P., Xie Y. L., Cao R. H. and Zheng J. (2018). "Internal stress distribution and cracking around flaws and openings of rock block under uniaxial compression: A particle mechanics approach." *Computers and Geotechnics* 102: 28-38.
- [55] Fedotoval I., Kuznetcov N. and Kasparyan E. (2019). Estimating the rockburst hazard of hard rocks based on laboratory test results. *E3S Web of Conferences*, EDP Sciences.
- [56] Feng X. T., Yu Y., Feng G. L., Xiao Y. X., Chen B. R. and Jiang Q. (2016). "Fractal behaviour of the microseismic energy associated with immediate rockbursts in deep, hard rock tunnels." *Tunnelling & Underground Space Technology* 51: 98-107.
- [57] Fernlund J. M. R. (2005). "Image analysis method for determining 3-d shape of coarse aggregate." *Cement and Concrete Research* 35(8): 1629-1637.
- [58] Fernlund J. M. R. (2005). "Image analysis method for determining 3-d size distribution of coarse aggregates." *Bulletin of Engineering Geology and the Environment* 64(2): 159-166.
- [59] Frid V. (2000). "Electromagnetic radiation method water-infusion control in rockburst-prone strata." *Journal of Applied Geophysics* 43(1): 5-13.
- [60] Frid V. (2001). "Calculation of electromagnetic radiation criterion for rockburst hazard forecast in coal mines." *Pure and Applied Geophysics* 158(5-6): 931-944.
- [61] Frid V. and Vozoff K. (2005). "Electromagnetic radiation induced by mining rock failure." *International Journal of Coal Geology* 64(1-2): 57-65.
- [62] Frid V. and Vozoff K. S. (2005). "Electromagnetic radiation induced by mining rock failure." *International Journal of Coal Geology* 64(1-2): 57-65.
- [63] Frith R., Reed G. and Jones A. (2019). "A causation mechanism for coal bursts during roadway development based on the major horizontal stress in coal, very specific structural geology causing a localised loss of effective coal confinement and newtons' second law."

- [64] Frith R., Reed G. and Jones A. (2020). "A causation mechanism for coal bursts during roadway development based on the major horizontal stress in coal: Very specific structural geology causing a localised loss of effective coal confinement and newton's second law." *International Journal of Mining Science and Technology* 30(1): 39-47.
- [65] Ge M. C. (2005). "Efficient mine microseismic monitoring." *International Journal of Coal Geology* 64(1-2): 44-56.
- [66] Ge M. C. (2010). Microseismic monitoring in mines. *Extracting the science: A century of mining research*. Bruce J. Littleton, Colorado, USA, Society for Mining, Metallurgy, and Exploration.
- [67] Geoscience Australia and ABARE (2010). Australian energy resource assessment. Canberra.
- [68] Gombert P., Sracek O., Koukoulas N., Gzyl G., Valladares S. T., Frączek R., Klinger C., Bauerek A., Areces J. E. Á. and Chamberlain S. (2019). "An overview of priority pollutants in selected coal mine discharges in europe." *Mine Water and the Environment* 38(1): 16-23.
- [69] Goodman R. E. (1989). *Introduction to rock mechanics*. New York, Wiley.
- [70] Grady D. E. (2008). "Fragment size distributions from the dynamic fragmentation of brittle solids." *International Journal of Impact Engineering* 35(12): 1557-1562.
- [71] Gu S. T., Xiao Z. M., Huang R. F., Tan Y. L., Jiang B. Y. and Li W. S. (2014). Rock burst danger warning and large diameter drilling pressure-relief technology in fully mechanized caving island coal face. *Taishan Academic Forum—Project on Mine Disaster Prevention and Control*, Atlantis Press.
- [72] Guarino A., Garcimartin A. and Ciliberto S. (1998). "An experimental test of the critical behaviour of fracture precursors." *The European Physical Journal B-Condensed Matter and Complex Systems* 6(1): 13-24.
- [73] GuhaRoy D., Singh T. N., Kodikara J. and Das R. (2017). "Effect of water saturation on the fracture and mechanical properties of sedimentary rocks." *Rock Mechanics and Rock Engineering* 50(10): 2585-2600.
- [74] Guo W. Y., Tan Y. L., Yang Z. L., Zhao T. B. and Hu S. C. (2017). "Effect of saturation time on the coal burst liability indexes and its application for rock burst mitigation." *Geotechnical and Geological Engineering*.
- [75] Hainzl S. (2003). "Self-organization of earthquake swarms." *Journal of Geodynamics* 35(1): 157-172.
- [76] Hamzeloo E., Massinaei M. and Mehrshad N. (2014). "Estimation of particle size distribution on an industrial conveyor belt using image analysis and neural networks." *Powder Technology* 261: 185-190.
- [77] Hansen S. M. and Schmandt B. (2015). "Automated detection and location of microseismicity at mount st. Helens with a large - n geophone array." *Geophysical Research Letters* 42(18): 7390-7397.
- [78] Hardy H. R. and Mowrey G. L. (1976). "Study of microseismic activity associated with a longwall coal mining operation using a near-surface array." *Engineering Geology* 10(2): 263-281.
- [79] He H., Dou L. M., Fan J., Du T. T. and Sun X. L. (2012). "Deep-hole directional fracturing of thick hard roof for rockburst prevention." *Tunnelling and Underground Space Technology* 32: 34-43.
- [80] He H., Dou L. M., Gong S. Y., Zhou P., Xue Z. J. and He J. (2011). "Study of acoustic emission monitoring technology for rockburst." *Rock and Soil Mechanics* 32(4): 1262-1268.
- [81] He M. C., Jia X. N., Coli M., Livi E. and Luís S. (2012). "Experimental study of rockbursts in underground quarrying of carrara marble." *International Journal of Rock Mechanics and Mining Sciences* 52: 1-8.
- [82] He M. C., Miao J. L. and Feng J. L. (2010). "Rock burst process of limestone and its acoustic emission characteristics under true-triaxial unloading conditions." *International Journal of Rock Mechanics and Mining Sciences* 47(2): 286-298.

- [83] He M. C., Xia H. M., Jia X. N., Gong W. L., Zhao F. and Liang K. Y. (2012). "Studies on classification, criteria and control of rockbursts." *Journal of Rock Mechanics and Geotechnical Engineering* 4(2): 97-114.
- [84] Hebblewhite B. and Galvin J. (2017). "A review of the geomechanics aspects of a double fatality coal burst at austar colliery in nsw, australia in april 2014." *International Journal of Mining Science and Technology* 27(1): 3-7.
- [85] Hirata T., Satoh T. and Ito K. (1987). "Fractal structure of spatial distribution of microfracturing in rock." *Geophysical Journal International* 90(2): 369-374.
- [86] Hoek E. and Brown E. T. (1980). *Underground excavations in rock*.
- [87] Hogan J. D., Farbaniec L., Mallick D., Domnich V., Kuwelkar K., Sano T., McCauley J. W. and Ramesh K. T. (2017). "Fragmentation of an advanced ceramic under ballistic impact: Mechanisms and microstructure." *International Journal of Impact Engineering* 102: 47-54.
- [88] Hogan J. D., Rogers R. J., Spray J. G. and Boonsue S. (2012). "Dynamic fragmentation of granite for impact energies of 6–28j." *Engineering Fracture Mechanics* 79(Supplement C): 103-125.
- [89] Hou T. X., Xu Q., Yang X. G., Lu P. Y. and Zhou J. W. (2015). "Experimental study of the fragmentation characteristics of brittle rocks by the effect of a freefall round hammer." *International Journal of Fracture* 194(2): 169-185.
- [90] Hou T. x., Xu Q. and Zhou J. w. (2015). "Size distribution, morphology and fractal characteristics of brittle rock fragmentations by the impact loading effect." *Acta Mechanica* 226(11): 3623-3637.
- [91] Huang B. X., Li P. F., Ma J. and Chen S. L. (2014). "Experimental investigation on the basic law of hydraulic fracturing after water pressure control blasting." *Rock mechanics and rock engineering* 47(4): 1321-1334.
- [92] Huang B. X. and Liu J. W. (2013). "The effect of loading rate on the behavior of samples composed of coal and rock." *International Journal of Rock Mechanics and Mining Sciences* 61(10): 23-30.
- [93] Hukki R. T. (1961). Minerals beneficiation - proposal for a solomonic settlement between the theories of von rittinger, kick, and bond, The American Institute of Mining, Metallurgical, and Petroleum Engineers.
- [94] Hutton A. C. (2009). "Geological setting of australasian coal deposits."
- [95] Iannacchione A. T. and Tadolini S. (2008). Coal mine burst prevention controls. *27th International Conference on Ground Control in Mining*.
- [96] Iannacchione A. T. and Tadolini S. C. (2016). "Occurrence, predication, and control of coal burst events in the u.s." *International Journal of Mining Science and Technology* 26(1): 39-46.
- [97] Jankovic A., Dundar H. and Mehta R. (2010). "Relationships between comminution energy and product size for a magnetite ore." *Journal of the Southern African Institute of Mining and Metallurgy* 110(3): 141-146.
- [98] Jiang F. X., Wei Q. D., Yao S. L., Wang C. W. and Qu X. C. (2013). "Key theory and technical analysis on mine pressure bumping prevention and control [j]." *Coal Science and Technology* 6: 6-9.
- [99] Jiang Q., Su G. S., Feng X. T., Cui J., Pan P. Z. and Jiang J. Q. (2015). "Observation of rock fragment ejection in post-failure response." *International Journal of Rock Mechanics and Mining Sciences*(74): 30-37.
- [100] Jiang Y. D., Pan Y. S., Jiang F. X., DOU L. M. and Ju Y. (2014). "State of the art review on mechanism and prevention of coal bumps in china." *Journal of China Coal Society* 39(2): 205-213.
- [101] Jiang Y. D., Song H. H., Ma Z. Q., Ma B. J. and Gao L. T. (2018). "Optimization research on the width of narrow coal pillar along goaf tunnel in tectonic stress zone." *Journal of China Coal Society*.

- [102] Jin L. P. and Xian X. F. (1993). "The study on outburst-proneness of coal seam via experiments and fuzzy comprehensive judgement." *Journal of Chongqing University (Nature Science Edition)* 16(6): 114-119.
- [103] Justine C. and Ian P. (2016). Coalburst control methods. *Coal Operators' Conference*. Wollongong.
- [104] Kaiser P. K., MacCreath D. R. and Tannant D. D. (1996). *Canadian rockburst support handbook : Prepared for sponsors of the canadian rockburst research program 1990 - 1995*, Geomechanics Research Centre.
- [105] Karchevsky A. L. (2017). "Determination of the possibility of rock burst in a coal seam." *Journal of Applied and Industrial Mathematics* 11(4): 527-534.
- [106] Kidybiński A. (1981). "Bursting liability indices of coal." *International Journal of Rock Mechanics and Mining Sciences & Geomechanics Abstracts* 18(4): 295-304.
- [107] Kong X. G., Wang E. Y., Hu S. B., Shen R., Li X. L. and Zhan T. Q. (2016). "Fractal characteristics and acoustic emission of coal containing methane in triaxial compression failure." *Journal of Applied Geophysics* 124: 139-147.
- [108] Konicek P. and Holecko J. (2006). Impact assessment of induced seismicity on surface in conditions of czech part of upper silesian coal basin (okr). *IGSMiE Kraków, Warsztaty Górnicze*. 166.
- [109] Konicek P., Ptacek J., Waclawik P. and Kajzar V. (2019). "Long-term czech experiences with rockbursts with applicability to today's underground coal mines." *Rock Mechanics and Rock Engineering* 52(5): 1447-1458.
- [110] Konicek P., Soucek K., Stas L. and Przeczek A. (2013). "Rockbursts provoked by distress blasting in hard coal longwall mining."
- [111] Konicek P., Soucek K., Stas L. and Singh R. (2013). "Long-hole distress blasting for rockburst control during deep underground coal mining." *International Journal of Rock Mechanics and Mining Sciences* 61: 141-153.
- [112] Krishnan H., Priyadarshini K., Gowsic M., Mahesh N., Vijayananth S. and Sudhakar P. (2019). Plant disease analysis using image processing in matlab. *2019 IEEE International Conference on System, Computation, Automation and Networking (ICSCAN)*, IEEE.
- [113] Krzemień A., Sánchez A. S., Fernández P. R., Zimmermann K. and Coto F. G. (2016). "Towards sustainability in underground coal mine closure contexts: A methodology proposal for environmental risk management." *Journal of Cleaner Production* 139: 1044-1056.
- [114] Kumara G. H. A., Hayano K. and Ogiwara K. (2012). "Image analysis techniques on evaluation of particle size distribution of gravel." *Int. J. Geomate* 3(1): 290-297.
- [115] Kurita K. and Fujii N. (1979). "Stress memory of crystalline rocks in acoustic emission." *Geophysical Research Letters* 6(1): 9-12.
- [116] Labiouse V., Descoedres F. and Montani S. (1996). "Experimental study of rock sheds impacted by rock blocks." *Structural Engineering International* 6(3): 171-176.
- [117] Lama R. and Saghafi A. (2002). Overview of gas outbursts and unusual emissions. *Coal Operators' Conference*, Wollongong, University of Wollongong & the Australasian Institute of Mining and Metallurgy.
- [118] Landis E. N. and Lucie B. (2002). "Experiments to relate acoustic emission energy to fracture energy of concrete." *Journal of Engineering Mechanics* 128(6): 698-702.
- [119] Lei X., Qi M., Qin S. Q., Li G. L., Li P. and Wang M. M. (2015). "A potential strain indicator for brittle failure prediction of low-porosity rock: Part i—experimental studies based on the uniaxial compression test." *Rock Mechanics and Rock Engineering* 48(5): 1763-1772.
- [120] Li B. F., Liang X. H. and Qi L. W. (2011). "Research on the influence of coal's uniaxial compressive strength to impact energy index." *Procedia Engineering* 26: 863-868.
- [121] Li C. R., Kang L. J., Qi Q. X., Mao D. B., Liu Q. M. and Xu G. (2009). "The numerical analysis of borehole blasting and application in coal mine roof-weaken." *Procedia Earth and Planetary Science* 1(1): 451-459.

- [122] Li H., Zhou P., XUue Z. J. and Zhang Y. L. (2009). "Comprehensive prevention technology for rock-burst and application in huating colliery " *Coal Mining Technology* 3.
- [123] Li H. T., Zhou H. W., Jiang Y. D. and Wang. Hong. Wei (2016). "An evaluation method for the bursting characteristics of coal under the effect of loading rate." *Rock Mechanics and Rock Engineering* 49(8): 3281-3291.
- [124] Li H. Y. (2011). "Physical and mechanical property of coal and rock and its relationship with rockburst liability." *Coal Mining Technology* 16(3): 43-46.
- [125] Li X. B., Zhou Z. L., Lok T. S., Hong L. and Yin T. B. (2008). "Innovative testing technique of rock subjected to coupled static and dynamic loads." *International Journal of Rock Mechanics and Mining Sciences* 45(5): 739-748.
- [126] Li X. F., Li H. B., Zhang Q. B., Jiang J. L. and Zhao J. (2018). "Dynamic fragmentation of rock material: Characteristic size, fragment distribution and pulverization law." *Engineering Fracture Mechanics* 199: 739-759.
- [127] Li X. L., Wang E. Y., Li Z. H., Liu Z. T., Song D. Z. and Qiu L. M. (2016). "Rock burst monitoring by integrated microseismic and electromagnetic radiation methods." *Rock Mechanics and Rock Engineering* 49(11): 4393-4406.
- [128] Li Y. Y., Zhang S. C. and Zhang X. (2018). "Classification and fractal characteristics of coal rock fragments under uniaxial cyclic loading conditions." *Arabian Journal of Geosciences* 11(9): 201.
- [129] Li Z. L., Dou L. M., Wang G. F., Cai W., He J. and Ding Y. L. (2015). "Risk evaluation of rock burst through theory of static and dynamic stresses superposition." *Journal of Central South University* 22(2): 676-683.
- [130] Li Z. L., He X. Q., Dou L. M., Song D. Z., Wang G. F. and Xu X. L. (2019). "Investigating the mechanism and prevention of coal mine dynamic disasters by using dynamic cyclic loading tests." *Safety science* 115: 215-228.
- [131] Li Z. L., He X. Q., Dou L. M. and Wang G. F. (2018). "Rockburst occurrences and microseismicity in a longwall panel experiencing frequent rockbursts." *Geosciences Journal*: 1-17.
- [132] Lin C., Deng J. Q., Liu Y. R., Yang Q. and Duan H. F. (2016). "Experiment simulation of hydraulic fracture in colliery hard roof control." *Journal of Petroleum Science and Engineering* 138: 265-271.
- [133] Liu D. Q., Li D. J., Zhao F. and Wang C. C. (2014). "Fragmentation characteristics analysis of sandstone fragments based on impact rockburst test." *Journal of Rock Mechanics and Geotechnical Engineering* 6(3): 251-256.
- [134] Liu J., Wang E. Y., Song D. Z., Yang S. L. and Niu Y. (2014). "Effects of rock strength on mechanical behavior and acoustic emission characteristics of samples composed of coal and rock." *Journal of China Coal Society* 39(4): 685-691.
- [135] Liu J. X., Zhang H., Liu J. G. and Jiang X. M. (2016). "Comminution theory of superfine pulverized coal based on fractal analysis of aggregate structures." *Energy & Fuels* 30(12): 10244-10252.
- [136] Liu X., Xu G., Zhang C., Kong B., Qian J., Zhu D. and Wei M. (2017). "Time effect of water injection on the mechanical properties of coal and its application in rockburst prevention in mining." *Energies* 10(11): 1783.
- [137] Liu X. F., Xu G., Zhang C., Kong B., Qian J. F., Zhu D. and Wei M. Y. (2017). "Time effect of water injection on the mechanical properties of coal and its application in rockburst prevention in mining." *Energies* 10(11): 1783.
- [138] Liu X. H., Liu S. Y. and Tang P. (2015). "Coal fragment size model in cutting process." *Powder technology* 272: 282-289.
- [139] Liu X. M., Zhang M., Hu N., Yang H. R. and Lu J. F. (2016). "Calculation model of coal comminution energy consumption." *Minerals Engineering* 92: 21-27.

- [140] Liu Z. G., Cao A. Y., Zhu G. G. and Wang C. B. (2017). "Numerical simulation and engineering practice for optimal parameters of deep-hole blasting in sidewalls of roadway." *Arabian Journal for Science and Engineering* 42(9): 3809-3818.
- [141] Locat P., Couture R., Locat J. and Leroueil S. (2003). Assessment of the fragmentation energy in rock avalanches. *3rd Canadian conference on Geotechnique and Geohazards*, Citeseer.
- [142] Lockner D. (1993). "The role of acoustic emission in the study of rock fracture." *International Journal of Rock Mechanics and Mining Sciences & Geomechanics Abstracts* 30(7): 883-899.
- [143] Lockner D. A., Byerlee J. D., Kuksenko V., Ponomarev A. and Sidorin A. (1991). "Quasi-static fault growth and shear fracture energy in granite." *Nature* 350(6313): 39.
- [144] Lou Q., Song D. Z., He X. Q., Li Z. L., Qiu L. M., Wei M. H. and He S. Q. (2019). "Correlations between acoustic and electromagnetic emissions and stress drop induced by burst-prone coal and rock fracture." *Safety Science* 115: 310-319.
- [145] Lu C., Mai Y. W. and Xie H. (2005). "A sudden drop of fractal dimension: A likely precursor of catastrophic failure in disordered media." *Philosophical Magazine Letters* 85(1): 33-40.
- [146] Lu C. P., Liu G. J., Liu Y., Zhang N., Xue J. H. and Zhang L. (2015). "Microseismic multi-parameter characteristics of rockburst hazard induced by hard roof fall and high stress concentration." *International Journal of Rock Mechanics and Mining Sciences*(76): 18-32.
- [147] Macias-Garcia A., Cuerda-Correa E. M. and Diaz-Diez M. A. (2004). "Application of the rosin-rammler and gates-gaudin-schuhmann models to the particle size distribution analysis of agglomerated cork." *Materials Characterization* 52(2): 159-164.
- [148] Mandelbrot B. B. (1983). *The fractal geometry of nature*. New York, WH Freeman.
- [149] Mao X. B., Chen Z. Q., Xu S. and Li T. Z. (2001). "Experimental study on the relation between the burst tendency and water content in coal seam." *Chinese Journal of Rock Mechanics and Engineering* 20(1): 49-52.
- [150] Martin C. D. and Chandler N. A. (1994). "The progressive fracture of lac du bonnet granite." *International Journal of Rock Mechanics and Mining Sciences & Geomechanics Abstracts* 31(6): 643-659.
- [151] McGarr A. (1997). "A mechanism for high wall-rock velocities in rockbursts." *Pure and Applied Geophysics* 150(3-4): 381-391.
- [152] Meng Q. B., Han L. J., Li H. and Li H. (2015). "Experimental on the effect of strain rate and size on the energy accumulation and dissipation of rock." *Journal of China Coal Society* 40(10): 2386-2398.
- [153] Meng Z. P., Pan J. N., Liu L. L., Meng G. M. and Zhao Z. H. (2009). "Influence of moisture contents on mechanical properties of sedimentary rock and its bursting potential." *Chinese Journal of Rock Mechanics & Engineering* 28: 2637-2643.
- [154] Mine Safety (2016). Iir16-05 austar coal burst. Australia, NSW Department of Industry.
- [155] Mine Safety Investigation Unit (2016). Double fatality at austar coal mine on 15 april 2014 - extract of consultant's report Australia, NSW Department of Industry, Skills and Regional Developmen.
- [156] Mirośława B. (2015). "Post-critical mechanical properties of sedimentary rocks in the upper silesian coal basin (poland)." *Archives of Mining Sciences* 60.
- [157] Morrell S. (2008). "A method for predicting the specific energy requirement of comminution circuits and assessing their energy utilisation efficiency." *Minerals Engineering* 21(3): 224-233.
- [158] Mou Z. L., Dou L. M., Gong S. Y. and Wang Y. G. (2006). Study on surplus energy characteristic of coal bursting failure.
- [159] National Coal Mine Safety Administration (2018). Rules for prevention and controlling of coal burst in mines. (2018)8. National Coal Mine Safety Administration. Beijing, China.

- [160] National Standards of the People's Republic of China (2010). Methods for test, monitoring and prevention of rock burst. *Part 2 Classification and Laboratory Test Method on Bursting Liability of Coal*. Beijing, China Standards Press.
- [161] NSW Mine Safety Investigation Unit (2015). Investigation report: Report into the deaths of James Mitchell and Phillip Grant at the Austar coal mine. Paxton, NSW Dept of Industry (Resources & Energy).
- [162] NSW Resources Regulator (2018). Rib failures in underground coal mines. Department of Planning I. a. E. New South Wales, Division of Resources and Geoscience.
- [163] Numbi B. P. and Xia X. (2015). "Systems optimization model for energy management of a parallel hpgr crushing process." *Applied energy* 149: 133-147.
- [164] Numbi B. P. and Xia X. (2016). "Optimal energy control of a crushing process based on vertical shaft impactor." *Applied energy* 162: 1653-1661.
- [165] Obert L. and Duvall W. (1942). "Use of subaudible noises for the prediction of rock bursts." *Technical Report Archive & Image Library*.
- [166] Ohnaka M. and Mogi K. (1982). "Frequency characteristics of acoustic emission in rocks under uniaxial compression and its relation to the fracturing process to failure." *Journal of geophysical research: Solid Earth* 87(B5): 3873-3884.
- [167] Okubo S., Fukui K. and Qi Q. X. (2006). "Uniaxial compression and tension tests of anthracite and loading rate dependence of peak strength." *International Journal of Coal Geology* 68(3): 196-204.
- [168] Ouyang Z. H. (2012). Mechanism and experiment of hydraulic fracturing in rock burst prevention. *Proceedings of the 1st International Conference on Rock Dynamics and Applications (RocDyn-1'13)*.
- [169] Oye V., Aker E., Daley T. M., Kühn D., Bohloli B. and Korneev V. (2013). "Microseismic monitoring and interpretation of injection data from the In Salah CO<sub>2</sub> storage site (Krechba), Algeria." *Energy Procedia* 37: 4191-4198.
- [170] Pan Y. S. (1999). Research on coal burst formation of process Doctoral dissertation, Tsinghua University.
- [171] Pan Y. S. (1999). Study on rockburst initiation and failure propagation Doctoral Dissertation, Tsinghua University.
- [172] Pan Y. S., Geng L. and Li Z. H. (2010). "Research on evaluation indices for impact tendency and danger of coal seam." *Journal of China Coal Society* 35(12): 1975-1978.
- [173] Patynska R. and Kabiesz J. (2009). "Scale of seismic and rock burst hazard in the Silesian companies in Poland." *Mining Science and Technology (China)* 19(5): 604-608.
- [174] Peng R. D., Ju Y., Wang J. G., Xie H. P., Gao F. and Mao L. T. (2015). "Energy dissipation and release during coal failure under conventional triaxial compression." *Rock Mechanics and Rock Engineering* 48(2): 509-526.
- [175] Peperakis J. (1958). "Mountain bumps at the Sunnyside mines." *Mining Engineering* 211: 982-986.
- [176] Peregrina-Barreto H., Terol-Villalobos I. R., Rangel-Magdaleno J. J., Herrera-Navarro A. M., Morales-Hernández L. A. and Manríquez-Guerrero F. (2013). "Automatic grain size determination in microstructures using image processing." *Measurement* 46(1): 249-258.
- [177] Perera M. S. A., Ranjith P. G. and Peter M. (2011). "Effects of saturation medium and pressure on strength parameters of Latrobe Valley brown coal: Carbon dioxide, water and nitrogen saturations." *Energy* 36(12): 6941-6947.
- [178] Pimienta L. (2014). "Investigation of elastic weakening in limestone and sandstone samples from moisture adsorption." *Geophysical Journal International* 199(1): 335-347.
- [179] Potvin Y. and Hudyma M. R. (2001). Seismic monitoring in highly mechanized hardrock mines in Canada and Australia. *The Fifth International Symposium on Rockburst and Seismicity in Mines, South African Institute of Mining and Metallurgy*.

- [180] Qi Q. X., Peng Y. W., Li H. Y., Li J. Q., Wang Y. G. and Li C. R. (2011). "Study of bursting liability of coal and rock." *Chinese Journal of Rock Mechanics and Engineering* 30(s1): 2736-2742.
- [181] Qiu S. L., Feng X. T., Zhang C. Q. and Xiang T. B. (2014). "Estimation of rockburst wall-rock velocity invoked by slab flexure sources in deep tunnels." *Canadian Geotechnical Journal* 51(5): 520-539.
- [182] Rabbani A. and Ayatollahi S. (2015). "Comparing three image processing algorithms to estimate the grain-size distribution of porous rocks from binary 2d images and sensitivity analysis of the grain overlapping degree." *Special Topics & Reviews in Porous Media: An International Journal* 6(1).
- [183] Rahmani T., Kiani B., Shekarchi M. and Safari A. (2012). "Statistical and experimental analysis on the behavior of fiber reinforced concretes subjected to drop weight test." *Construction and Building Materials* 37: 360-369.
- [184] Rajput M. S., Burman M., Segalini A. and Hallström S. (2018). "Design and evaluation of a novel instrumented drop-weight rig for controlled impact testing of polymer composites." *Polymer Testing* 68: 446-455.
- [185] Ranjith P. G., Jasinge D., Choi S. K., Mehic M. and Shannon B. (2010). "The effect of co<sub>2</sub> saturation on mechanical properties of australian black coal using acoustic emission." *Fuel* 89(8): 2110-2117.
- [186] Reddish D. J., Stace L. R., Vanichkobchinda P. and Whittles D. N. (2005). "Numerical simulation of the dynamic impact breakage testing of rock." *International Journal of Rock Mechanics and Mining Sciences* 42(2): 167-176.
- [187] Remennikov A. and Kaewunruen S. (2007). Experimental determination of energy absorption capacity for prestressed concrete sleepers under impact loads. *The 4th International Conference on Structural Engineering and Construction* Melbourne, Taylor & Francis.
- [188] Ren T. X., Plush B. and Aziz N. I. (2011). "Dust controls and monitoring practices on australian longwalls."
- [189] Rezaei M., Hossaini M. F. and Majdi A. (2015). "Determination of longwall mining-induced stress using the strain energy method." *Rock Mechanics and Rock Engineering* 48(6): 2421-2433.
- [190] Rice G. S. (1935). *Bumps in coal mines of the cumberland field, kentucky and virginia: Causes and remedy*, United States Bureau of Mines.
- [191] Rosin P. and Rammler E. (1933). "Laws governing the fineness of powdered coal." *Journal of the Institute of Fuel* 7.
- [192] Saha M., Dally B. B., Medwell P. R. and Chinnici A. (2017). "Effect of particle size on the mild combustion characteristics of pulverised brown coal." *Fuel Processing Technology* 155: 74-87.
- [193] Saharan M. R. and Mitri H. (2011). "Destress blasting as a mines safety tool: Some fundamental challenges for successful applications." *Procedia Engineering* 26: 37-47.
- [194] Sam V. D., Joren P., Stijn D. P. and Wim V. P. (2014). "Experimental study on the dynamic behaviour of glass fitted with safety window film with a small-scale drop weight set-up." *International Journal of Impact Engineering* 73: 101-111.
- [195] Scholz C. H. (1968). "The frequency-magnitude relation of microfracturing in rock and its relation to earthquakes." *Journal of the Japanese Society of Internal Medicine* 96(9): 1909-1911.
- [196] Shadrin A. V. and Klishin V. I. (2018). Acoustic emission of rock mass under the constant-rate fluid injection. *IOP Conference Series: Earth and Environmental Science*, IOP Publishing.
- [197] Shehata H. M., Mohamed Y. S., Abdellatif M. and Awad T. H. (2018). "Depth estimation of steel cracks using laser and image processing techniques." *Alexandria engineering journal* 57(4): 2713-2718.
- [198] Shelly D. R. and Hill D. P. (2011). "Migrating swarms of brittle-failure earthquakes in the lower crust beneath mammoth mountain, california." *Geophysical Research Letters* 38(20).
- [199] Shen B. T. and Luo X. (2016). Review of chinese coal burst experience and analysis of microseismic data from australian mines. CSIRO, CSIRO Energy.

- [200] Shen B. T., Luo X., Moodie A. and McKay G. (2013). "Monitoring longwall weighting at australian mine using microseismic systems and stressmeters."
- [201] Shen W. (2011). "Fractal invariable distribution and its application in large-sized and super large-sized mineral deposits." *Geoscience Frontiers* 2(1): 87-91.
- [202] Shkuratnik V. L., Filimonov Y. L. and Kuchurin S. V. (2004). "Experimental investigations into acoustic emission in coal samples under uniaxial loading." *Journal of Mining Science* 40(5): 458-464.
- [203] Shkuratnik V. L., Filimonov Y. L. and Kuchurin S. V. (2005). "Regularities of acoustic emission in coal samples under triaxial compression." *Journal of Mining Science* 41(1): 44-52.
- [204] Sikorski W. (2012). *Acoustic emission*, InTech.
- [205] Singh S. P. (1988). "Burst energy release index." *Rock Mechanics and Rock Engineering* 21(2): 149-155.
- [206] Sirait B., Wattimena R. K. and Widodo N. P. (2013). "Rockburst prediction of a cut and fill mine by using energy balance and induced stress." *Procedia Earth and Planetary Science* 6: 426-434.
- [207] Skrzypkowski K. (2018). Laboratory testing of a long expansion rock bolt support for energy-absorbing applications. *E3S Web of Conferences*, EDP Sciences.
- [208] Song D. Z., Wang E. Y., Li N., Jin M. Y. and Xue S. P. (2012). "Rock burst prevention based on dissipative structure theory." *International Journal of Mining Science and Technology* 22(2): 159-163.
- [209] Song D. Z., Wang E. Y. and Liu J. (2012). "Relationship between emr and dissipated energy of coal rock mass during cyclic loading process." *Safety Science* 50(4): 751-760.
- [210] Soucek K., Konicek P., Stas L., Ptacek J. and Waclawik P. (2013). Experimental approach to measure stress and stress changes in rock ahead of longwall mining faces in czech coal mines. *13th Coal Operators' Conference*. Naj A. and Bob K. University of Wollongong, The Australasian Institute of Mining and Metallurgy & Mine Managers Association of Australia.
- [211] Stamboliadis E. T. (2007). "The energy distribution theory of comminution specific surface energy, mill efficiency and distribution mode." *Minerals engineering* 20(2): 140-145.
- [212] Su G. S., Jiang J. Q., Feng X. T., Mo C. and Jiang Q. (2016). "Experimental study of ejection process in rockburst." *Chinese Journal of Rock Mechanics and Engineering* 35(10): 1990-1999.
- [213] Tafesse S., Fernlund J. M. R. and Bergholm F. (2012). "Digital sieving-matlab based 3-d image analysis." *Engineering Geology* 137: 74-84.
- [214] Tan Y. A., Sun G. Z. and Guo Z. (1991). "A composite  $k_{rb}$  criterion for the ejection characteristics of the burst rock." *Scientia Geologica Sinica*(2): 193-200.
- [215] Tavares L. M. and King R. P. (1998). "Single-particle fracture under impact loading." *International Journal of Mineral Processing* 54(1): 1-28.
- [216] Thompson A. H. (1991). "Fractals in rock physics." *Annual Review of Earth and Planetary Sciences* 19(1): 237-262.
- [217] Tian B. Z., Liu S. J., Zhang Y. B. and Wang Z. L. (2016). "Analysis of fractal characteristic of fragments from rock burst tests under different loading rates." *Tehnički Vjesnik* 23(5): 1269-1276.
- [218] Trifu C. I. and Shumila V. (2010). "Microseismic monitoring of a controlled collapse in field ii at ocnele mari, romania." *Pure and Applied Geophysics* 167(1-2): 27-42.
- [219] Tu Q. Y., Cheng Y. P., Ren T., Wang Z. Y., Lin J. and Lei Y. (2019). "Role of tectonic coal in coal and gas outburst behavior during coal mining." *Rock Mechanics and Rock Engineering*: 1-17.
- [220] Tyler S. W. and Wheatcraft S. W. (1992). "Fractal scaling of soil particle-size distributions: Analysis and limitations." *Soil Science Society of America Journal* 56(2): 362-369.
- [221] Urbancic T. I., Shumila V., Rutledge J. T. and Zinno R. J. (1999). Determining hydraulic fracture behavior using microseismicity. *Vail Rocks 1999, The 37th US Symposium on Rock Mechanics (USRMS)*, American Rock Mechanics Association.

- [222] Vardar O., Tahmasebinia F., Zhang C., Canbulat I. and Saydam S. (2017). "A review of uncontrolled pillar failures." *Procedia engineering* 191: 631-637.
- [223] Varley F. and Whyatt J. (2008). Work practices to manage bump prone ground. *Proceedings of the 27th international conference on ground control in mining. West Virginia University, Morgantown.*
- [224] Verdon J. P., Kendall J. M., White D. J. and Angus D. A. (2011). "Linking microseismic event observations with geomechanical models to minimise the risks of storing co2 in geological formations." *Earth and Planetary Science Letters* 305(1-2): 143-152.
- [225] Voller V. R. (1983). "A note on energy-size reduction relationships in comminution." *Powder Technology* 36(2): 281-286.
- [226] Wan Z. J., Liu C. Y., Wei J. Q. and Liang G. F. (1999). "Study on burst propensity of coal seam and roof." *Journal of Mining and Safety Engineering* s1: 208-210.
- [227] Wang C. H., Cheng Y. P., He X. X., Yi M. H. and Wang Z. Y. (2019). "Size effect on uniaxial compressive strength of single coal particle under different failure conditions." *Powder technology* 345: 169-181.
- [228] Wang G. F., Gong S. Y., Li Z. L., Dou L. M., Cai W. and Mao Y. (2016). "Evolution of stress concentration and energy release before rock bursts: Two case studies from xingan coal mine, hegang, china." *Rock Mechanics and Rock Engineering* 49(8): 3393-3401.
- [229] Wang W. X., Pan C. L. and Feng T. (2000). "Fountain rockburst and inductive rockburst." *Journal of Central South University* 7(3): 129-132.
- [230] Wei M. Y., Wang E. Y., Liu X. F. and Wang C. (2011). "Numerical simulation of rockburst prevention effect by blasting pressure relief in deep coal seam." *Rock and Soil Mechanics* 32(8): 2539-2560.
- [231] Whittles D. N., Kingman S., Lowndes I. and Jackson K. (2006). "Laboratory and numerical investigation into the characteristics of rock fragmentation." *Minerals Engineering* 19(14): 1418-1429.
- [232] Whyatt J. (2008). Dynamic failure in deep coal: Recent trends and a path forward. *The 27th International Conference on Ground Control in Mining, Morgantown.*
- [233] Whyatt J., Blake W., Williams T. and White B. (1900). "60 years of rockbursting in the coeur d'alene district of northern idaho, USA: Lessons learned and remaining issues."
- [234] Wu L. C. and Yu C. (2012). Powder particle size measurement with digital image processing using matlab. *Advanced Materials Research*, Trans Tech Publ.
- [235] Xia B. W., Zhang X., Yu B. and Jia J. L. (2018). "Weakening effects of hydraulic fracture in hard roof under the influence of stress arch." *International Journal of Mining Science and Technology* 28(6): 951-958.
- [236] Xiao H. F., He X. Q. and Wang E. Y. (2006). "Research on transition law between eme and energy during deformation and fracture of coal or rock under compression." *Rock and Soil Mechanics* 27(7): 1097-1100.
- [237] Xie H. P. (1990). *Damage mechanics of rock and concrete*. Xuzhou, China University of Mining and Technology Press.
- [238] Xie H. P. (1996). *Introduction to fractal rock mechanics*. Beijing, Science Press.
- [239] Xie H. P., Ju Y. and Li L. Y. (2005). "Criteria for strength and structural failure of rocks based on energy dissipation and energy release principles." *Chinese Journal of Rock Mechanics & Engineering* 24(17): 3003-3010.
- [240] Xie H. P. and Pariseau W. G. (1993). "Fractal character and mechanism of rock bursts." *International Journal of Rock Mechanics and Mining Sciences & Geomechanics Abstracts* 30(4): 343-350.
- [241] Xie H. P., Peng R. D. and Ju Y. (2004). "Energy dissipation og rock deformation and fracture." *Chinese Journal of Rock Mechanics & Engineering* 23(21): 3565-3570.

- [242] Xiong D. G., Zhao Z. M., Su C. D. and Wang G. Y. (2011). "Experimental study of effect of water-saturated state on mechanical properties of rock in coal measure strata." *Chinese Journal of Rock Mechanics & Engineering* 30(5): 998-1006.
- [243] Xiong Z. Q. and He H. J. (2006). "Numerical simulation of rock burst stress and its control by stress-relief." *Journal of Mining & Safety Engineering* 4.
- [244] Xu T., Tang C. A., Zhang Z. and Zhang Y. B. (2003). "Theoretical , experimental and numerical studies on deformation and failure of brittle rock in uniaxial compression." *Journal of Northeastern University (Natural Science)* 24(1): 87-90.
- [245] Xu X. F., Dou L. M., Liu J., Cui X. H., Zhang Y. L. and Yao X. Y. (2010). "Research of reasons and controlling for floor burst in coal mine roadway." *Rock and Soil Mechanics* 31(6): 1977-1982.
- [246] Xue L., Qin S. Q., Sun Q., Wang Y. Y., Le M. L. and Li W. C. (2014). "A study on crack damage stress thresholds of different rock types based on uniaxial compression tests." *Rock Mechanics and Rock Engineering* 47(4): 1183-1195.
- [247] Yamada I., Masuda K. and Mizutani H. (1989). "Electromagnetic and acoustic emission associated with rock fracture." *Physics of the Earth and Planetary Interiors* 57(1): 157-168.
- [248] Yan P., Zhang J., Fang Q. and Zhang Y. (2018). "Numerical simulation of the effects of falling rock's shape and impact pose on impact force and response of rc slabs." *Construction and Building Materials* 160: 497-504.
- [249] Yang X. H., Ren T., He X. Q. and Tan L. H. (2019). A review of energy sources of coal burst in australian coal mines. *2019 Coal Operators Conference*. Naj A. and Bob K. Wollongong, University of Wollongong.
- [250] Yang X. H., Ren T., Remennikov A. M., He X. Q. and Tan L. H. (2018). "Analysis of energy accumulation and dissipation of coal bursts." *Energies* 11(7): 1816-1827.
- [251] Yang X. H., Ren T. and Tan L. H. (2020). "Estimation of average ejection velocity generated by rib burst under compression load." *International Journal of Rock Mechanics and Mining Sciences* 128: 104277.
- [252] Yang X. H., Ren T. and Tan L. H. (2020). "Size distribution measurement of coal fragments using digital imaging processing." *Measurement*: 107867.
- [253] Yang X. H., Ren T., Tan L. H., Remennikov A. and He X. Q. (2018). "Developing coal burst propensity index method for australian coal mines." *International Journal of Mining Science and Technology*.
- [254] Yang Z. D. (2012). The pressure relief control technology of the defects method on dynamic pressure area in zhaogezhuang coal mine. *Applied Mechanics and Materials*, Trans Tech Publ.
- [255] Yin G. Z., Zhang D. M., Dai G. F. and Wan L. (2002). "Damage model of rock and the damage energy index of rockburst." *Journal of Chongqing University (Nature Science Edition)* 25(9): 75-78.
- [256] Yu B., Liu C. Y., Yang J. X. and Liu J. R. (2013). "Research on the fracture instability and its control technique of hard and thick roof." *Journal of China University of Mining and Technology* 42(3): 342-348.
- [257] Zakupin A., Bogomolov L., Mubassarova V., Kachesova G. and Borovsky B. (2012). Acoustic emission and electromagnetic effects in loaded rocks. *Acoustic Emission*. Sikorski W., InTech.
- [258] Zhang C. G., Canbulat I., Hebblewhite B. and Ward C. R. (2017). "Assessing coal burst phenomena in mining and insights into directions for future research." *International Journal of Coal Geology* 179: 28-44.
- [259] Zhang C. G., Canbulat I., Tahmasebinia F. and Hebblewhite B. (2017). "Assessment of energy release mechanisms contributing to coal burst." *International Journal of Mining Science and Technology* 27: 43-47.
- [260] Zhang S. C., Li Y. Y., Shen B. T., Sun X. Z. and Gao L. Q. (2019). "Effective evaluation of pressure relief drilling for reducing rock bursts and its application in underground coal mines." *International Journal of Rock Mechanics and Mining Sciences* 114: 7-16.

- [261] Zhang W. B., Wang S. K., Wu Y. K. and Qu X. C. (1986). "To determine proneness of coal burst by dynamic failure time." *Coal Science and Technology* 14(3): 31-34.
- [262] Zhao J. (2000). "Applicability of mohr–coulomb and hoek–brown strength criteria to the dynamic strength of brittle rock." *International Journal of Rock Mechanics and Mining Sciences* 37(7): 1115-1121.
- [263] Zhao X. G., Wang J., Cai M., Cheng C., Ma L. K., Su R., Zhao F. and Li D. J. (2014). "Influence of unloading rate on the strainburst characteristics of beishan granite under true-triaxial unloading conditions." *Rock Mechanics and Rock Engineering* 47(2): 467-483.
- [264] Zhao Y. X. and Jiang Y. D. (2010). "Acoustic emission and thermal infrared precursors associated with bump-prone coal failure." *International Journal of Coal Geology* 83(1): 11-20.
- [265] Zhao Y. X., Jiang Y. D. and Han Z. R. (2007). "Experimental study on acoustic and thermal infrared characteristics of bump-prone coal." *Chinese Journal of Rock Mechanics and Engineering* 26(5): 965-971.
- [266] Zheng. W. and Zhang C. J. (1996). "Investigation of rock damage model and its mechanical behaviour." *Chinese Journal of Rock Mechanics and Engineering* 15(1): 55-61.
- [267] Zhou J. W., Liu Y., Du C. L. and Liu S. Y. (2017). "Effect of the particle shape and swirling intensity on the breakage of lump coal particle in pneumatic conveying." *Powder Technology* 317: 438-448.
- [268] Zhou J. W., Liu Y., Du C. L. and Wang F. R. (2016). "Experimental study on crushing characteristic of coal and gangue under impact load." *International Journal of Coal Preparation and Utilization* 36(5): 272-282.
- [269] Zhou J. W., Liu Y., Liu S. Y., Du C. L. and Li J. P. (2017). "Effects of particle shape and swirling intensity on elbow erosion in dilute-phase pneumatic conveying." *Wear* 380: 66-77.
- [270] Zhou X. J. and Xian X. F. (1998). "Research advance on rockburst theory and its engineering application in collieries." *Journal of Chongqing University (Nature Science Edition)* 21(1): 126-132.
- [271] Zhou Z. L., Cai X., Cao W. Z., Li X. B. and Xiong C. (2016). "Influence of water content on mechanical properties of rock in both saturation and drying processes." *Rock Mechanics and Rock Engineering* 49(8): 3009-3025.
- [272] Zhu Q. J., Feng Y., Cai M., Liu J. H. and Wang H. H. (2017). "Interpretation of the extent of hydraulic fracturing for rockburst prevention using microseismic monitoring data." *Journal of Natural Gas Science and Engineering* 38: 107-119.
- [273] Zmeskal O., Dzik P. and Vesely M. (2013). "Entropy of fractal systems." *Computers & Mathematics with Applications* 66(2): 135-146.